# Copyright Warning & Restrictions

The copyright law of the United States (Title 17, United States Code) governs the making of photocopies or other reproductions of copyrighted material.

Under certain conditions specified in the law, libraries and archives are authorized to furnish a photocopy or other reproduction. One of these specified conditions is that the photocopy or reproduction is not to be "used for any purpose other than private study, scholarship, or research." If a, user makes a request for, or later uses, a photocopy or reproduction for purposes in excess of "fair use" that user may be liable for copyright infringement,

This institution reserves the right to refuse to accept a copying order if, in its judgment, fulfillment of the order would involve violation of copyright law.

Please Note: The author retains the copyright while the New Jersey Institute of Technology reserves the right to distribute this thesis or dissertation

Printing note: If you do not wish to print this page, then select "Pages from: first page # to: last page #" on the print dialog screen

## ABSTRACT

## FLEXIBILITY VS CONSISTENCY: QUANTIFYING DIFFERENCES IN NEUROMODULATORY ELICITED PATTERNS OF ACTIVITY

**by**
**Elizabeth M. Cronin**

Central pattern generating circuits underly fundamental behaviors such as respiration or locomotion and are under the influence of neuromodulators. The presence of neuromodulators is thought to confer flexibility to these circuits to generate distinct patterns of activity to meet distinct behavioral needs. Network output flexibility can be achieved by distinct classes of neuromodulators, those which have convergent cellular actions but divergent circuit actions or by those which have divergent cellular actions but convergent circuit actions.

Both classes of neuromodulator exist in the stomatogastric nervous system of the crab *Cancer borealis* and influence the activity of a central pattern generating circuit in the stomatogastric ganglion, the pyloric network. The ability of both classes of neuromodulator, when applied individually, to generate qualitatively and quantitatively distinct patterns of activity has been demonstrated with respect to a baseline activity state. While it is assumed that each individual neuromodulator's activity pattern is distinct, there has yet to be a fully quantitative description of the degree of difference between two modulated activity patterns. It is also unlikely that any single circuit will be under the influence of only a single neuromodulator at any point. Therefore, the possibility of generating distinct network outputs increases with each distinct combination of neuromodulators. While the actions of individual neuromodulators have been explored, the consequences of co-modulation on the pyloric network's output are less understood.

Previous attempts at quantifying the effects of a neuromodulator on the pyloric network output relied on evaluating only a single, often multi-dimensional, attribute of activity at a time and statistically testing the dependent parameters of that attribute with statistics that assume independence. This dissertation uses a new approach to quantify and statistically test how different one neuromodulator elicited pattern of activity is from another, preserving the inherent multi-dimensional nature of the attributes evaluated. The results of this dissertation show that the pyloric network output is able to generate statistically distinct network outputs with individual neuromodulators; however, flexibility is lost in favor of consistency under co-modulatory conditions.

# FLEXIBILITY VS CONSISTENCY: QUANTIFYING DIFFERENCES IN NEUROMODULATORY ELICITED PATTERNS OF ACTIVITY

**by**
**Elizabeth M. Cronin**

**A Dissertation**
**Submitted to the Faculty of**
**New Jersey Institute of Technology**
**and Rutgers, The State University of New Jersey-Newark**
**in Partial Fulfillment of the Requirements for the Degree of**
**Doctor of Philosophy in Biology**

**Federated Biological Sciences Department**

**August 2022**

**APPROVAL PAGE**

**FLEXIBILITY VS CONSISTENCY: QUANTIFYING DIFFERENCES IN NEUROMODULATORY ELICITED PATTERNS OF ACTIVITY**

**Elizabeth M. Cronin**

| | |
|---|---|
| Dr. Dirk Bucher, Dissertation Co-Advisor<br>Associate Professor of Biology, NJIT | Date |
| Dr. Farzan Nadim, Dissertation Co-Advisor<br>Professor of Biology, NJIT | Date |
| Dr. Eric Fortune, Committee Member<br>Associate Professor of Biology, NJIT | Date |
| Dr. Kristen Severi, Committee Member<br>Assistant Professor of Biology, NJIT | Date |
| Dr. Dawn Blitz, Committee Member<br>Associate Professor of Biology, Miami University, Oxford, OH | Date |

## BIOGRAPHICAL SKETCH

**Author:** Elizabeth M. Cronin

**Degree:** Doctor of Philosophy

**Date:** August 2022

**Undergraduate and Graduate Education:**

- Doctor of Philosophy in Biology,
  New Jersey Institute of Technology, Newark, NJ, 2022

- Master of Science in Biology,
  New Jersey Institute of Technology, Newark, NJ, 2014

- Bachelor of Science in Biochemistry,
  Rowan University, Glassboro, NJ, 2012

**Major:** Biology

**Presentations and Publications:**

Gorur-Shandilya S, Cronin EM, Schneider AC, Haddad SA, Rosenbaum P, Bucher DM, Nadim F, Marder E (2022) Mapping circuit dynamics during function and dysfunction. Elife 11. E76579

Cronin E, Schneider AC, Nadim F, Bucher DM (2021) Quantifying differences in network output across neuromodulators. In: Dynamic Neural Networks Annual Meeting, Virtual.

Cronin E, Nadim F, Bucher DM (2019) Neuromodulation of circuit activity– How different is different enough? Small Circuits and Behavior Annual Meeting, University of Pennsylvania, Philadelphia, Pennsylvania.

Cronin E, Nadim F, Bucher DM (2019) How different is different enough: Quantifying difference across neuromodulators. Rutgers University Brain Health Institute Symposium, Bell Labs, New Providence, New Jersey

Cronin E, Nadim F, Bucher DM (2019) Does co-modulation produce consistent circuit activity? Society for Neuroscience Annual Meeting. Chicago, Illinois; 2019

C.-C. Yu, N. Barry, K. D. Piatkevich, S. Asano, G. Huynh, A. Kazatskaya, I. Nechipurenko, E. Cronin, I. Skvortsov, Z. Tanvir, S. W. Flavell, P. Sengupta, G. Haspel, M. B. Goodman, E. S. Boyden (2018) Expansion microscopy of *C. elegans* enables whole-organism *in situ* analysis with nanoscale spatial resolution**.** Society for Neuroscience Annual Meeting. San Diego, California

*I dedicate this dissertation to all the furs in my life: Chromium, Schrodinger, Tungsten, Zuzu, Fiona, Linux and McKenna. You all have been my source of wonder, happiness and strength through this journey. This dissertation is also dedicated to my greatest friends Michael Wagner and Omar Itani. Michael, you are my prairie vole forever and always and I can always count on you to deal with my silliness and have a glass of bourbon waiting for me at the end of the day. Omar, there are not enough words to express how grateful I am for your friendship. From our humble days as lab techs to our journeys through the program and our valent efforts to make our world a better place, in the simplest words I would not be the person I am today and would not have accomplished what I have done without your endless support. In times of trouble, I know I can always count on the n-dimensional connection as long as I have a towel and a trusty cardboard box.*

## ACKNOWLEDGMENT

My time at NJIT has led me to places I never would have imagined going and allowed me to do things I never would have considered doing. Facilitating that were my co-advisors Dr. Dirk Bucher and Dr. Farzan Nadim. Throughout the 10 years I've been at NJIT, I've learned not only the principals of neuroscience in the classroom but also how to think like a scientist outside of the classroom and keep questioning. You both allowed me the freedom to explore whatever questions I wanted to and shape the stories that I wanted to tell. This freedom pushed me to dive deeper into topics and analytical approaches that I never would have explored otherwise and shaped me into what I am today.

Thank you also to my committee chair, Dr. Eric Fortune. Being a teaching assistant for you will forever be my favorite teaching experience. You seamlessly balance being exceptionally brilliant with being unbearably funny. Thank you also to Dr. Kristen Severi and Dr. Dawn Blitz. Both of you agreed without hesitation to be on my committee and help me undertake this monumental task offering not only your own individual expertise but your unwavering support, especially when the light at the end of the tunnel was only a tiny flicker.

I thank NJIT for providing me with a teaching assistantship in the beginning of my Ph.D as well as the National Institutes of Health (Grant number: MH060605) for funding my research.

Thank you to Omar Itani for your unrivaled programming skills and for having the patience to sit and teach me Matlab all those years ago. The quantitative and statistical methods in this work would not have been possible without you.

I would also like to acknowledge all my wonderful lab mates over the years. The upside of being in one place for so long is that you have the opportunity to meet so many people that leave an indelible mark on your life. You have become so much more than just peers and collaborators; you have become my family. Teatime, yoga time, coffee breaks and talks about the n-dimensional feline network were my moments of calm and peace in what many times felt like a tumultuous sea.

## TABLE OF CONTENTS

**TABLE OF CONTENTS**
**(Continued)**

**TABLE OF CONTENTS**
**(Continued)**

**Chapter** **Page**

## LIST OF TABLES

## LIST OF FIGURES

## LIST OF FIGURES
## (Continued)

## LIST OF FIGURES
## (Continued)

**Figure** **Page**

# CHAPTER 1

# GENERAL INTRODUCTION

## 1.1 Central Pattern Generators and the Stomatogastric Nervous System

Central pattern generating circuits underly the generation of fundamental rhythmic behaviors such as locomotion, respiration and feeding (Marder and Bucher, 2001; Guertin, 2012; Katz, 2016). A prominent feature of central pattern generating circuits is the ability to generate rhythmic activity in the absence of sensory feedback. Because of the importance of these behaviors, it is necessary to understand how and under what circumstances these circuits generate their rhythmic outputs.

Central pattern generating circuits are found in both invertebrates and vertebrate species, though in vertebrates, these circuits are not well defined and likely contain a large number of neurons (MacKay-Lyons, 2002). Invertebrates, however, do have well defined central pattern generating circuits whose activity depends on a reasonably small number of neurons which can be easily identified, recorded and manipulated. One such invertebrate central pattern generating circuit is the pyloric network in the stomatogastric nervous system of decapods crustaceans.

The stomatogastric nervous system in decapod crustaceans consists of four ganglia: the paired commissural ganglia (CoGs), the unpaired esophageal ganglion (OG), and the stomatogastric ganglion (STG). The stomatogastric ganglion contains approximately 25 neurons, the absolute number differs across invertebrate species and can also vary across animals of the same species (Marder and Bucher, 2007). Of these 25 neurons, ~ 11 participate in pyloric rhythm generation which controls the filtering of food in the crustacean stomach while the others participate in the gastric mill rhythm which controls

the chewing of food in the stomach. The pyloric network is the faster of the two circuits (~1 Hz cycle frequency), pacemaker driven and is simpler than the gastric mill network which is significantly slower (~0.1 Hz cycle frequency) and is network driven (Nusbaum and Beenhakker, 2002). When isolated, the central pattern generators of the stomatogastric nervous system can generate fictive motor activity which can be recorded through extracellular motor nerve recordings and intracellular soma recordings.

The pyloric network can be reduced further to its core circuit. The core pyloric network is composed of the anterior burster (AB) which is the pacemaker neuron, the two pyloric dilator neurons (PD) which are electrically coupled to the AB neuron, the lateral pyloric (LP) neuron and the pyloric neurons (PY). The AB and PD neurons taken together are considered the pacemaker group while the LP and PY neurons do not have intrinsic oscillatory behavior and are considered follower neurons. All of the chemical synapses in this circuit are inhibitory and the sole feedback from the follower neurons to the pacemaker group comes from the chemical synapse from the LP neuron to the PD neuron. When recorded experimentally, extracellularly or intracellularly, the core pyloric network neurons generate rhythmic tri-phasic activity. The onset of pacemaker activity signals the start of a cycle of activity. While the pacemaker neurons are firing, the follow neurons are inhibited via the chemical synapses from the pacemaker neurons. Following the termination of pacemaker activity, the follower neurons LP and PY are able to fire in sequence, completing one cycle of activity (Figure 1.1).

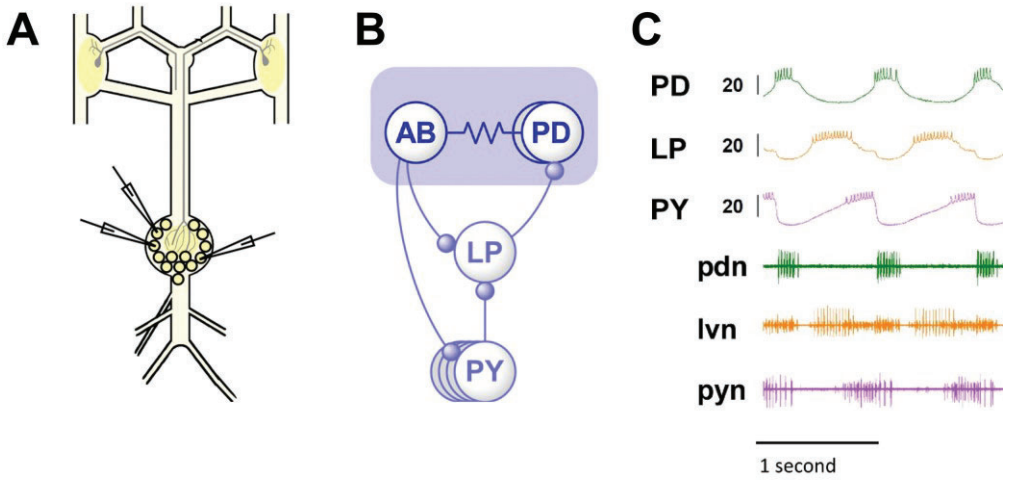


**Figure 1.1** The stomatogastric nervous system and the pyloric circuit. (A) Schematic of the stomatogastric nervous system (STNS) which contains the paired commissural ganglia (CoGs), the unpaired esophageal ganglion (OG), and the stomatogastric ganglion (STG). The STG contains two central pattern generating circuits, the pyloric network and the gastric mill network. (B) Connectivity diagram of the core pyloric neurons of the pyloric network. (C) Intracellular soma and extracellular motor nerve recordings of the PD, LP and PY neurons of the core pyloric network.

*Source : A and B adapted from (Daur et al., 2016).*

### 1.2 Neuromodulation of the Pyloric Network

While the pyloric circuit is pacemaker driven and can generate activity in the absence of sensory input, it requires neuromodulators to function. Neuromodulators are distinct from neurotransmitters and represent a class of neuroactive substance which operate on a slower time scale compared to classical neurotransmitters and signal through G-protein coupled receptors. When deprived of neuromodulators via experimental perturbation, the pyloric rhythm either stops completely or generates slow or disrupted activity (Hamood et al., 2015). In the stomatogastric nervous system approximately 100 distinct neuromodulators have been detected (Ma et al., 2009; Christie et al., 2010; Chen et al., 2014) though that number is likely higher.

The majority of the neuromodulators which influence the pyloric network can be broadly divided into two classes: neuropeptides and amines. Both neuropeptides and amines can be released by anterior ganglia in the stomatogastric nervous system and released into the hemolymph as neurohormones to modulate the activity of the neurons in the STG, though their mechanisms of modulation are distinct (Marder, 2012).

Neuropeptides, once bound to their receptors, have convergent cellular actions. Following receptor binding, each neuropeptide converges to activate the modulator activated inward current ($I_{MI}$), a mixed cation inward current that is calcium dependent (Golowasch and Marder, 1992b; Swensen and Marder, 2000). Although each neuropeptide converges to the same point cellularly, at the circuit level their actions diverge where distinct neuropeptides target distinct subsets of pyloric neurons (Swensen and Marder, 2001). This divergence in circuit activity helps to explain the apparent redundancy of their cellular convergence.

Unlike the relatively simple actions of the neuropeptides, the actions of amines on the neurons of the pyloric network are far more complex. Amines, such as dopamine, have cell type specific divergent actions cellularly. For example, dopamine can bind to distinct receptor subtypes on two different neurons. Even though dopamine is targeting both of these neurons, the cellular consequences of dopamine binding will be different. Countering the cellular level divergence of dopamine, at the circuit level, dopamine's actions are convergent (Figure 1.2). Even though dopamine will differentially affect each neuron in the circuit, all neurons have receptors for dopamine (Harris-Warrick and Johnson, 2010). Of the amines, dopamine is the best studied, but the general principal of divergent cellular and convergent circuit likely extends to other amines such as serotonin and octopamine

which also modify the activity pattern of the pyloric network (Flamm and Harris-Warrick, 1986a, b).

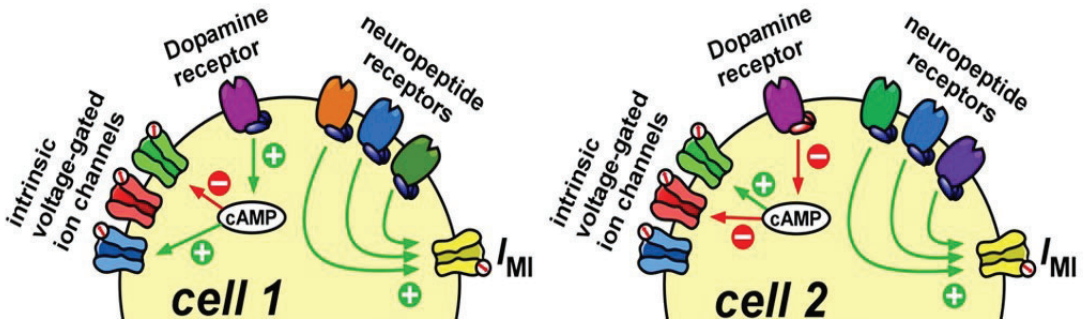


**Figure 1.2** Convergent and divergent actions of neuromodulators. Across distinct cell types, neuropeptides have the same cellular action, convergence to activate the modulator activated inward current $I_{MI}$ while monoamines such as dopamine have cell type specific cellular actions due to differences in receptor subtype.

### 1.3 The Necessity of Flexible Outputs and the Role of Neuromodulators

Regardless of the particular cellular or synaptic properties of central pattern generating circuits, a central pattern generating circuit is a collection of neurons and synaptic connections which are fixed and generate a pattern of activity. While we generalized these activities as respiration or locomotion and often think of them singularly, respiration, for example, is not a single pattern of activity (Viemari and Tryba, 2009). Because of the inflexibility in the composition of the circuit and the importance of the behaviors which are generated by these circuits, these circuits need to be able to modify the properties of their constituents to elicit distinct activity patterns.

Neuromodulators are thought to provide central pattern generating circuits the ability to reconfigure their circuits to generate distinct patterns of activity. In what is widely termed network output flexibility, a large number of neuromodulators which act distinctly can transform a static circuit into one which is capable of generating a wide range

of activity patterns which could signal for distinct behavioral outputs (Stein, 2009; Harris-Warrick, 2011). Extending this idea, if individual neuromodulators can generate distinct activity profiles which signal for distinct behavioral outputs, distinct combinations of neuromodulators should also provide flexibility to the network output and signal for distinct co-modulator based network outputs.

The flexibility of the pyloric network output across species under distinct modulatory conditions, both peptides and amines, has been shown (Flamm and Harris-Warrick, 1986b; Weimann et al., 1991; Weimann et al., 1993; Weimann et al., 1997; Swensen and Marder, 2000; Thirumalai and Marder, 2002; Goaillard et al., 2004; Haddad and Marder, 2018; Rosenbaum and Marder, 2018) though the effects of co-modulation on the network output are less understood. There are two common themes to these works: 1. the generation of qualitatively different rhythmic outputs in the presence of distinct neuromodulators and 2. some quantification demonstrating the effect of the neuromodulator on some aspect of network activity with respect to a baseline state.

The most commonly quantified attributes of activity are cycle frequency, phase, spike number and spike frequency. These can be generally thought of as attributes of excitability. If only the core pyloric network neurons of PD, LP and PY are considered, these four attributes have 12 individual parameters of activity. When quantified with respect to a baseline condition, often times the experimentally elicited decentralized state where the descending modulatory inputs from the upper end ganglia are removed, there are statistical differences when evaluated with parametric statistics such as t-tests or ANOVAs. When paired with a qualitative assessment, these results are often interpreted as

demonstrating the ability of individual neuromodulators to generate distinct network outputs. There are inherent issues with these approaches though.

While a neuromodulator elicited network output may be statistically different from a baseline state, there have been very few studies that have tried to quantify how different two neuromodulator elicited network outputs are from each other (Swensen and Marder, 2001; Thirumalai and Marder, 2002). The second inherent issue with these previous works is the statistical approach to quantifying how different one network output is from another. The phase, spike number and spike frequency attributes of excitability are comprised of five and three parameters each, respectively. When statistically tested, however, each parameter is considered individually. The issue with statistically testing individual parameters within one attribute of excitability is the dependence of each parameter within an attribute. The onset and offset phases of each neuron in the core pyloric network, for example, are determined in part by the synaptic connections among the three neurons, but when statistically tested they are treated as though they are independent. Outside of the statistical issues, these approaches only consider one parameter or one attribute of excitability as a proxy for the network output when in reality, the pyloric network output is a compilation of all of these individual parameters and outputs.

### 1.4 A New Approach to Fully Quantify Difference

To address the issues previously mentioned we took a new approach to quantifying the pyloric network output in the crab *Cancer borealis* under distinct neuromodulator conditions. Instead of considering each parameter of the phase attribute, for example, individually, we combined all five parameters of the phase attribute together to create

distinct 5-dimensional vectors for each modulatory condition. The difference between two modulatory conditions can be quantified with these five dimensional vectors using the Euclidean distance measurement. The Euclidean distance is the sum of differences between each parameter in the attribute. This collapses, in this example, a 5-dimensional difference into a single number which can be interpreted intuitively. Two vectors which are identical in each parameter will have a Euclidean distance of zero and any deviation from zero represents a degree of difference. To statistically test whether the distance between two modulatory conditions is sufficient to consider them different, we used a modified version of a multi-variate permutation test (Anderson, 2001; Nichols and Holmes, 2002). Unlike the multivariate analysis of variance (MANOVA), the multi-variate permutation test is non-parametric statistical test and does not force us to make any assumption about the underlying structure of our data, namely that they are normally distributed and are equally variant.

### 1.5 Questions Addressed in this Dissertation

In this dissertation we used the pyloric network output of the crab *C. borealis* to ask a set of related questions about whether distinct neuromodulator elicited network outputs are in fact different from each other and if they are different, how different are they?

In Chapter 2 we ask whether the individually applied neuropeptides proctolin, CCAP and RPCH generate distinct patterns of activity using the cycle frequency, phase, spike number and spike frequency attributes as a proxy for network output activity. We quantify the exact degree of difference between these neuropeptides in each n-dimensional attribute individually as well as in a combined 12-dimensional network output space.

In Chapter 3 we build on the work quantifying differences across individual neuropeptides and ask whether distinct combinations of neuropeptides generate distinct network outputs and whether those co-modulated network outputs are distinct from their constituent neuromodulators. We use the 12-dimensional network output space to quantify the degree of difference between these co-modulated network outputs. We asked this question using pairs of co-modulators (proctolin + CCAP, CCAP + RPCH, RPCH + proctolin) as well as triplet combinations of co-modulators (proctolin + CCAP + RPCH and CCAP + proctolin + oxotremorine).

In Chapter 4 we explore the effects of dopamine, octopamine and serotonin on the pyloric network output and statistically test whether distinct amines generate statistically different outputs. Unlike peptides which have been widely characterized at the network, cellular and synaptic levels in the crab pyloric circuit, the effects of amines are largely unknown. We quantify the effects of dopamine and octopamine on both the full pyloric network output using the excitability metrics as well their effects on the PD neuron's slow wave oscillation and spiking behavior.

In Chapter 5 we explore the consequences of peptide and amine co-modulation on the attributes of excitability and PD's individual activity. Though both peptides and amines exist in this system, there has yet to be any qualitative or quantitative description of their combined effects. We combine the peptides CCAP and RPCH with either dopamine, octopamine or serotonin to statistically test, across these six distinct combinations, how different peptide and amine co-modulated outputs are from each other.

# CHAPTER 2

# INDIVIDUAL PEPTIDE MODULATION GENERATES BOTH FLEXIBLE AND CONSISTENT PYLORIC NETWORK OUTPUTS

## 2.1 Introduction

Neuromodulators are ubiquitous and help to shape fundamental behaviors such as feeding (Blitz et al., 1999; Nusbaum and Beenhakker, 2002; Jing et al., 2007; Eriksson et al., 2017), respiration (Pena and Ramirez, 2002, 2004; Viemari and Ramirez, 2006), locomotion (Sawin et al., 2000; Gabriel et al., 2009) and behavioral states such as sleep and attention (Noudoost and Moore, 2011; Griffith, 2013). In some cases, the number of neuromodulators identified in a system can seem disproportionate to its size or function. The stomatogastric nervous system in crustaceans, for example, has >100 identified peptide neuromodulators (Ma et al., 2009; Christie et al., 2010; Chen et al., 2014) and the genome of the small nematode *C.elegans* encodes for > 200 peptides (Bargmann, 2012). At first pass, the large number of neuromodulators in these small circuits seems puzzling but can be understood in the context of network output flexibility.

Owing to the small number of neurons and synapses in these circuits, the ability to modify intrinsic and synaptic properties to ultimately alter an output is crucial. The idea that individual modulators transform static networks into flexible entities capable of generating behaviorally relevant and distinct outputs is well documented (Katz, 1995; Nusbaum and Beenhakker, 2002; Viemari and Tryba, 2009; Harris-Warrick, 2011; Miles and Sillar, 2011; McCormick and Nusbaum, 2014). This is most apparent when looking at recordings during ongoing activity (Marder and Weimann, 1992; Swensen and Marder, 2001; Lane et al., 2018). The outputs look different under distinct modulatory conditions,

so we assume that individual neuromodulators are in fact generating distinct activity patterns.

When a population is considered, approaches to quantifying the effects of a neuromodulator rely on isolating a single, often multi-dimensional, attribute, plotting those data as individual bar plots and performing a basic parametric statistic such as an ANOVA or a t-test. When evaluated in this way, the most salient feature or features of a modulated output can be found (Dickinson et al., 2001; Goaillard et al., 2004; Lane et al., 2018). While useful, the determination of salient features can only state particular places within a multi-dimensional attribute where outputs are different but cannot provide a measure of how different two outputs are from each other when an attribute is considered holistically.

Additionally, while we hold the belief that different neuromodulators generate distinct activity profiles, there have been very few studies that have tried to quantify the difference between two modulated states (Swensen and Marder, 2001; Thirumalai and Marder, 2002; Lane et al., 2018). Almost exclusively, the comparison is made with respect to a baseline state. What is missing from our understanding of how neuromodulators act on a network output is a rigorous comparison across modulators and a fully quantitative metric of difference which preserves the inherently multi-dimensional nature of these data. This would allow us to make an unambiguous statement not only about whether one network output is statistically different from another, but also allows us to state the exact degree of difference between these outputs. Here we quantify the effects of three distinct neuropeptides on four attributes of excitability which represent a proxy of the pyloric network output. By taking a new approach to the quantification and statistical testing of

these data we not only ask whether one neuropeptide elicited network output is different from another but also how different they are.

## 2.2 Materials and Methods

**Animals.** All experiments were performed on male *Cancer borealis* crab obtained from local fish markets and maintained in recirculating saltwater tanks at 12°C. Crabs were anesthetized in ice for ~30 minutes prior to dissection. The dissection of the stomatogastric nervous system (STNS) was performed according to standard procedure and the isolated nervous system was pinned down on Sylgard coated petri dishes (Selverston et al., 1976).

**Electrophysiology.** During experiments, the stomatogastric ganglion (STG) was continuously superfused with *Cancer borealis* saline composed of 11 mM KCl, 440 mM NaCl, 13 mM $CaCl_2$, 26 mM $MgCl_2$, 11.2 mM Trizma base and 5.1 mM maleic acid with pH of 7.4. Superfused saline was maintained at 11-13°C and to facilitate modulator application, a large petroleum jelly well was made around the STG. Extracellular recordings were made by electrically isolating motor nerves of interest with small petroleum jelly wells. Stainless steel electrodes were then place both inside and outside of the well to record activity and the signals were amplified with differential AC amplifiers (A-M systems). Intracellular recordings were performed on the desheathed ganglion using sharp microelectrodes with resistance of 20-30 MΩ. Electrodes were filled with a 0.6M $K_2SO_4$ and 20mM KCl solution and mounted on Scientifica motorized microelectrode manipulators. Neurons of interest were identified by their stereotyped waveforms along with matching the intracellular activity pattern to the extracellular motor nerve recordings. All intracellular recordings were obtained in current clamp with Axoclamp 900A and 2B

intracellular amplifiers (Molecular Devices). Both intracellular and extracellular activity was recorded using a Micro1401 digitizer and Spike2 data acquisition software (Cambridge Electronic Design).

**The pyloric network and attribute extraction.** The STNS contains four ganglia: the paired commissural ganglia (CoGs), the unpaired esophageal ganglion (OG), and the STG (Figure 2.1 A). The STG contains two distinct but overlapping central pattern generating circuits, the pyloric network and the gastric mill network. The pyloric network is made up of approximately 11 neurons and the pyloric dilator (PD), lateral pyloric (LP) and pyloric (PY) neurons form the core pyloric network. The two PD neurons are electrically coupled to the anterior burster (AB) neuron and taken together form the pacemaker group. While the pacemaker neurons are active, they inhibit both the LP and PY neurons. Following inhibition, the LP and PY neurons fire in sequence to generate a tri-phasic activity pattern. In addition to intracellular soma recordings, the activity of the PD and PY neurons can be measured by recording the pyloric dilator nerve (*pdn*) and pyloric nerve (*pyn*) extracellularly while the activity of the LP neuron can be measured extracellularly on the lateral ventricular nerve (*lvn*) (Figure 2.1 B).

All initial attribute extraction was done in Spike2 with custom written scripts. Measurements for the phase and cycle frequency attributes were obtained from the extracellular motor nerve recordings. The cycle frequency is the reciprocal of the cycle period which is defined as the time from the onset of PD bursting in one cycle to the next onset of PD bursting. There are five phases of activity which characterize the three core pyloric neurons in the pyloric network. The individual phases were calculated as the delay to each neurons burst onset or offset (latency) with respect to PD burst start divided by the

cycle period. The number of spikes and intraburst spike frequency measurements were obtained from the intracellular soma recordings for the PD and PY neurons and from both intracellular and extracellular recordings for the LP neuron. The intraburst spike frequency was calculated as the number of spikes per burst minus 1 divided by the duration of the burst and is referred to as spike frequency (Figure 2.1 B).

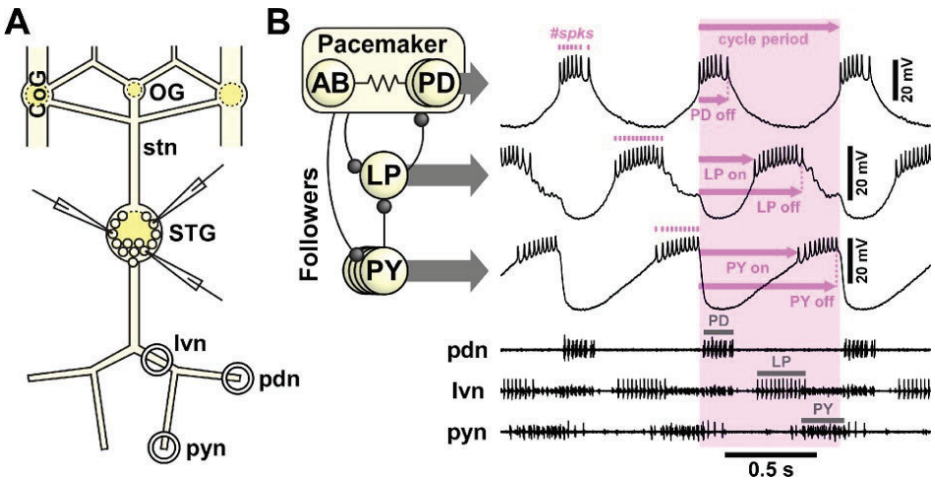


**Figure 2.1** The pyloric circuit and excitability attribute extraction. (A) Schematic of the stomatogastric nervous system (STNS). The STNS is composed of four sets of ganglia: the paired commissural ganglia (CoGs), the unpaired esophageal ganglion (OG), and the stomatogastric ganglion (STG). To record activity from the motor nerves within the STG, the STG can be desheathed and the individual motor neurons impaled with sharp microelectrodes. (B) Schematic of the core pyloric neurons. The core pyloric circuit, one of the central pattern generating circuits in the STG, is made up of the pacemaker group, the anterior burster (AB) and two pyloric dilator (PD) neurons. These neurons, when active, inhibit the activity of the two follower neurons, the lateral pyloric (LP) and pyloric (PY) neurons. Following inhibition, these follower neurons rebound to fire sequentially generating the tri-phasic motor pattern of PD-LP-PY activity. The activity of the core pyloric network can be recorded via intracellular soma recordings or extracellularly with motor nerve recordings. PD neuron activity can be recorded from the pyloric dilator nerve (pdn) motor nerve, LP activity can be recorded from the lateral ventricular nerve (lvn) nerve and PY activity can be recorded from the pyloric nerve (pyn). With a combination of intracellular and extracellular recordings, attributes describing the pyloric network's activity can be extracted. These attributes include the cycle period or frequency, the phases, the number of spikes per burst and the intraburst spike frequency.

**Modulators and experimental protocol.** To block descending modulatory inputs from upper end ganglia (decentralization) the stomatogastric nerve (stn) was blocked with a $10^{-7}$ M TTX (Biotium) + 750 mM sucrose (Sigma) solution. Proctolin (RS synthesis) and CCAP (Bachem) were initially dissolved in distilled water as a stock solution at $10^{-3}$M,

aliquoted and held at -20°C until needed. RPCH (Bachem) was dissolved in DMSO (Sigma) to a stock solution concentration of $10^{-3}$M, aliquoted and stored at -20°C until needed. Final dilution of modulators to the experimental concentration of $10^{-6}$ M occurred immediately before application in chilled *Cancer borealis* saline. Modulators were bath applied via peristaltic pump for 5 minutes and when multiple modulators were applied to the same preparation, each modulator was washed out for a minimum of 30 minutes. Sample size for each condition (N): 43 intact, 46 decentralized, 15 proctolin, 18 CCAP, 19 RPCH.

**Statistics:** Basic statistical analysis was performed using SigmaPlot (SigmaStat). One or two way ANOVA were performed along with post-hoc Holm–Sidak pairwise comparisons. Statistical significance is noted as follows: * $p < 0.05$, ** $p < 0.01$, *** $p < 0.001$. See Table A.1 for complete statistical results. The Euclidean distance and principle component analysis were performed using Matlab (Mathworks) built in functions. The multi-variate permutation test was performed using custom written scripts in Matlab.

**Euclidean distance and multi-variate permutation test calculation:** The Euclidean distance is a pairwise distance measurement between two conditions. It was calculated by taking the difference of each parameter within a multi-dimensional attribute under two test conditions. The Euclidean distance in the phase attribute ($\Delta\ \phi$) is a 5-dimensional difference calculated by taking the difference between the PD off, LP on, LP off, PY on and PY off phase vectors between each test conditions. The Euclidean distances in the spike number attribute ($\Delta$ #spikes) and spike frequency attribute ($\Delta F_{spk}$) are 3-dimensional differences calculated by taking the difference between the PD, LP and PY spike number or spike frequency vectors between two test conditions. The Euclidean

distance in the network output space (Δ z-score) is a 12-dimensional difference calculated by first combining the four attributes of activity into condition specific vectors. All vectors across the five conditions evaluated were combined and z-score standardized. Pairwise distances were then calculated using the z-scored vectors. All distance values reported are means from individual distance measurements between single vectors.

The multi-variate permutation test used here is a modified version of a permutation test and uses the Euclidean distance measurements as a test statistic (Anderson, 2001; Nichols and Holmes, 2002). Following the calculation of the mean Euclidean distance value between two conditions, the vectors from both test conditions were combined and then permuted by column with replacement ($n^p$) to create a single matrix which holds all possible combinations of values. Following this, vectors from the permuted matrix were randomly reassigned into two new matrices of the same size as the initial condition matrices. The Euclidean distance measurements were calculated on the two new permuted matrices in the same way as the non-permuted data, each vector against all other vectors. Following that, the mean Euclidean distance was calculated. The permuted Euclidean distance calculation was performed a total of 9,999 times.

The single Euclidean distance measurement from the non-permuted data and the 9,999 permuted Euclidean distance measurements were combined to form a 10,000 x 1 matrix and ranked in descending order. The index corresponding to the Euclidean distance measurement of the non-permuted data was divided by 10,000 to provide the p-value. The determination of statistical difference was made with a 0.05 alpha value. Statistical significance is noted as follows: * $p < 0.05$, ** $p < 0.01$, *** $p < 0.001$.

**Machine Learning.** The machine learning implementation, methods and results sections were performed and written by Dr. Anna C. Schneider.

In order to see whether our findings were affected by the particular methodology we had used and by the specific attributes we had chosen for circuit activity, we also analyzed our datasets using supervised machine learning algorithms. We used two different supervised machine learning approaches. For the first approach, we used a pattern recognition network that was trained and tested on the exact same data as for the Euclidean distance analysis. This method allowed for an objective comparison of our distance metric without changing the input data. In the second approach, we used a minimally analyzed dataset based on the raw measurements of spike times of circuit neurons as the input for the time series classification algorithm. In this dataset, all circuit activity that included periodic activity of the PD neuron was included, even if there was no triphasic pyloric rhythm such as when the follower neurons were silent or aperiodic.

All networks were created using Matlab (Deep Learning Toolbox version 14.2; Parallel Computing Toolbox version 7.4) with default settings, unless otherwise noted, and custom written functions for data preprocessing.

The training outcome partially depends on the initial values of the network parameters. In addition, our available datasets are relatively small. Therefore, we used a bootstrapping approach to sample the distribution of network accuracy based on network initialization and dataset splitting in training and test data. For each experimental condition (intact, decentralized, proctolin, CCAP, RPCH) the corresponding dataset was randomly split into 70% training data and 30% test data. We then randomly initialized 50 networks, trained them, and kept the most accurate one. On the next run, we again split the dataset

randomly into training and test data, randomly initialized 50 networks, and kept the most accurate network of that run. We repeated this process for 100 runs, ending up with 100 networks of varying accuracy. We then classified the test data with the corresponding networks and calculated the percentage of correct and false positive classifications across the 100 networks for each modulatory condition.

**Pattern recognition.** The shallow pattern recognition network was created with the Matlab function "patternnet". It consists of one input layer, one hidden layer with 50 units, and one output layer. Of the training data, 70% was used for the actual network training, the other 30% were used for validation. We used the same dataset as for the vector length analysis. After splitting and bootstrapping the dataset, the networks were tested with a total of 1300 intact, 1400 decentralized, 400 proctolin, 600 CCAP, and 600 RPCH.

**Time series classification.** The core pyloric rhythm consists of the sequential bursting of three types of neurons. For the pattern recognition network, we had to choose and extract attributes from the raw data that were available in all experimental conditions. In this second machine learning approach, we wanted to use the information of the sequential bursting to classify the data with a deep network suitable for time series classification.

This network consisted of the following layers: A sequence input layer with three channels (PD, LP, PY), a bi-directional long short-term memory layer with 50 hidden units and the 'OutputMode' set to 'last', a fully connected layer with five channels (one for each experimental condition), a softmax layer, and the classification layer. In contrast to Matlab's default settings, we used the Adam optimizer with a denominator offset of $10^{-6}$, set the mini-batch size to accommodate all input data in one batch, allowed a maximum of

1000 epochs for training, validated the network at every other iteration with the test data and set the patience of validation stopping to 25.

We preprocessed the raw data in the following way to compress the data and obtain uniform input matrices: We took 30 seconds of data from each experiment and condition 24 intact, 24 decentralized, 11 proctolin, 12 CCAP, 9 RPCH; some experiments had sequential application of modulators after a thorough wash with normal saline. In these 30 seconds, we identified pyloric cycles from the beginning of one PD burst to the next. Each cycle was divided into 20 bins, and we calculated the average spike number for PD, LP and PY per bin across the number of cycles present in the 30 seconds of data.

While the binning has the advantage that the inputs are the same size for all experiments, regardless of the cycle frequency, the important information of cycle frequency is not included. Therefore, we z-scored each individual cycle frequency based on the decentralized cycle frequencies and added the z-score to each bin of an individual experiment. We used all of the training data for training and the test data for validation. After splitting and bootstrapping the dataset, the networks were tested with 700 intact, 700 decentralized, 300 proctolin, 400 CCAP, and 300 RPCH experiments.

## 2.3 Results

**Neuromodulators transform a single circuit into visually distinct outputs.** The PD, LP and PY neurons form the core pyloric network within the stomatogastric nervous system. These neurons are also individually targeted by peptide modulators, albeit to varying degrees (Swensen and Marder, 2001). Mechanistically, peptides in this system have convergent cellular actions, targeting the modulator activated inward current ($I_{MI}$) through

GPCR signaling and divergent circuit actions (Golowasch and Marder, 1992b; Swensen and Marder, 2000, 2001). These previous works, highlighting the differential modulation and cellular and circuit actions of these peptides, aids in our understanding of how multiple outputs could be generated given a single set of neurons and connections. Previous work has evaluated the effect of applying individual neuropeptides during ongoing activity (Marder and Weimann, 1992; Weimann et al., 1993). When qualified, under distinct modulatory conditions, these outputs appear to differ (Figure 2.2 A).

To quantify the degree of difference between these peptide outputs, we chose four attributes of excitability: cycle frequency, phase, spike number and spike frequency. These attributes were chosen because they have been widely used to describe the effects of neuropeptides on the pyloric network.

Proctolin targets each of the core pyloric neurons and due to proctolin's ubiquitous actions, we expect the responses of proctolin to be different than the responses of CCAP or RPCH in these attributes. Because CCAP and RPCH target the same subset of neurons in the pyloric network, any differences found could be attributed to a difference in peptide receptor number on the neurons they target or an effect on the synapses. The mRNA copy number of CCAP receptors among the core pyloric neurons has been previously quantified (Garcia et al., 2015) but is not known for RPCH. Additionally, we expect the decentralized response in these attributes to be different from both the intact and peptide modulated conditions. The intact state is one that is multiply modulated where it is assumed that $I_{MI}$ is active in all pyloric neurons. Because proctolin activates $I_{MI}$ in each of the core pyloric neurons, proctolin may be able to recapitulate the intact state while we expect the intact responses across these attributes to be distinct from those of CCAP or RPCH.

**There are no statistical differences across peptides in the cycle frequency attribute.** Under intact conditions, the pyloric network cycles at ~ 1 to 2 Hz and once decentralized, the cycle frequency drops. The application of neuropeptides has been shown to restore the cycle frequency, but the degree of change is state dependent (Nusbaum and Marder, 1989; Weimann et al., 1997). In these data, when the preparations were decentralized there was a significant drop in cycle frequency compared to the intact. Neuropeptide application, however, did not restore the cycle frequency to its initial intact state and all peptide conditions were statistically different from the intact condition. While not restored to the intact state, the pyloric cycle frequency with proctolin or RPCH was statistically different compared to the decentralized, but CCAP was not statistically different from decentralized. Additionally, the cycle frequency of the CCAP preparations was statistically different than the RPCH preparations (One way ANOVA: $F_{(4,136)} = 101.308$, $p < 0.001$) (Figure 2.2 B).

**There are no statistical differences across peptides in the phase attribute.** The phases of the three pyloric neurons are influenced by both the inhibitory synapses between the neurons as well as intrinsic currents, specifically the A-type potassium current and the hyperpolarized activated inward current. Once decentralized, the duty cycle of PD was reduced and LP activity was weakened, advancing its off phase. As a consequence of LP's activity weakening, the onset of PY activity advanced. Following decentralization, application of proctolin, CCAP or RPCH shifted the phase relationships of the three neurons back towards the intact state. When statistically tested there was one difference between intact and CCAP in the LP on phase and differences between the decentralized and peptide conditions in the LP off and PY on phases (Two way ANOVA interaction: $F_{(16,680)} = 15.639$, $p < 0.001$).

Between the three peptides there were small differences in their specific phase responses though none were statistically meaningful. The duty cycle of PD was shortened compared to proctolin or RPCH and the onset of LP activity was also slightly advanced whereas the phase responses of both proctolin and RPCH were similar. Both the shortening of PD duty cycle and LP on phase advance with CCAP compared to proctolin have been reported previously (Swensen and Marder, 2001) (Figure 2.2 C).

**Peptide responses can be separated in LP spike number but not PD or PY spike number.** All three peptides used target the LP neuron but only proctolin targets the PD and PY neurons. Because the peptides activate an inward current, they act to enhance the excitability of the neurons they target. It has been previously shown that both proctolin and CCAP increase LP spike number, though the effect of CCAP application is greater. Additionally, proctolin increases the number of PD and PY spikes, although this was evaluated with extracellular recordings and included spikes from multiple neurons (Swensen and Marder, 2001).

Quantification of our data indicated similar trends compared to the results of previous studies. In the PD spike number parameter, proctolin increased the mean spike number compared to CCAP or RPCH although this was not statistically significant. Additionally, there were no statistical differences between the intact and the peptide modulated states, although the intact response was statistically different from decentralized. In LP spike number, CCAP had the largest effect and was statistically different from both proctolin and RPCH, while the proctolin and RPCH responses were not statistically different from each other. The intact and decentralized conditions were both statistically different from each peptide as well in LP spike number. Lastly, proctolin

enhanced PY spiking compared to CCAP or RPCH and was statistically different from both. The intact PY spike number response was also statistically different from the decentralized, proctolin, and RPCH responses but not the CCAP response. Additionally, the decentralized response was statistically different from both the CCAP and RPCH responses but not the proctolin response (Two way ANOVA interaction: $F_{(8,408)} = 26.097$, $p < 0.001$) (Figure 2.2 D).

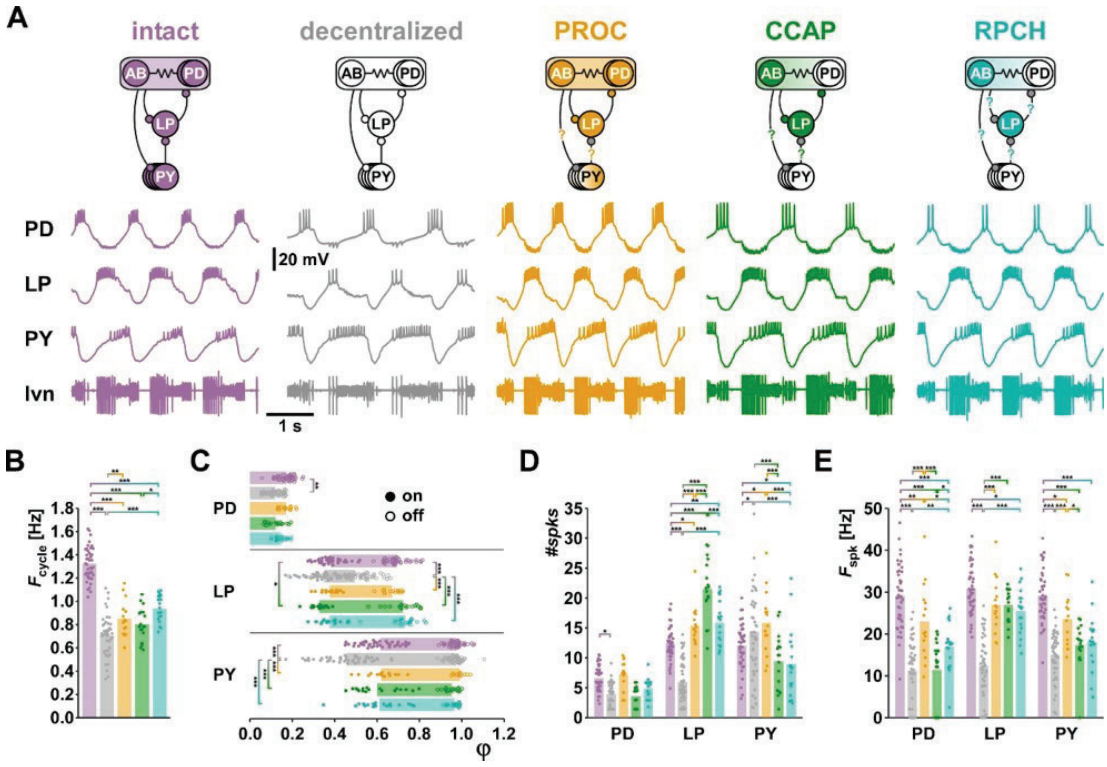


**Figure 2.2**: The cellular targets of neuropeptides in the core pyloric circuit and the qualitative and quantitative responses to individual neuropeptide application. (A) The cellular targets and responses of individual neuropeptides application to the pyloric circuit. (B) Cycle frequency response across intact, decentralized and three neuropeptide conditions. Bars represent mean cycle frequency responses and points represent individual animal responses. (C) Phase responses of the PD, LP and PY responses during the intact, decentralized and neuropeptide conditions. Bars represent mean phase on and off values. Filled in circles represent individual animal phase on values and empty circles represent individual animal phase off values. (D) Spike number responses of the PD, LP and PY neurons across distinct neuromodulatory conditions. Bars represent mean spike number responses across the five modulatory conditions while the individual points represent individual animal responses. (E) Spike frequency responses of the PD, LP and PY neurons. Bars represent mean spike frequency responses across all modulatory conditions and individual points represent individual animal responses.

**Peptide responses can be separated in the PD and PY spike frequency attributes.** Spike frequency is related to spike number attribute and is the ratio of the number of spikes to burst duration. The pyloric network, when decentralized, not only slows down but the individual neurons within the network also show a reduction in burst frequency. Neuropeptide application acts to shorten the duration of bursting for each neuron thereby increasing each neurons spike frequency. Because spike frequency is a ratio, there can be changes in frequency without a change in the number of spikes and may allow for separation between peptide conditions which were not different in spike number.

When quantified, both the intact and decentralized responses were statistically different from all peptide conditions in PD spike frequency. All three peptide conditions were also statistically different from each other. In LP spike frequency, the intact response was statistically different from the decentralized response and RPCH but not proctolin or CCAP while the decentralized was statistically different from all three peptide conditions. There were also no statistical differences between the peptide conditions. Lastly, in PY spike frequency, the intact response was statistically different from the decentralized response and all three peptide conditions and the decentralized was statistically different from proctolin. Additionally, proctolin was statistically different from CCAP (Two way ANOVA interaction: $F_{(8,408)} = 6.388$, $p < 0.001$) (Figure 2.2 E).

**Individual attribute statistical testing is necessary but not sufficient to quantify differences across distinct neuromodulatory conditions.** When these metrics of excitability were evaluated individually, there were differences across the neuropeptide conditions and differences between the modulated states and the decentralized matching our initial expectations. Additionally, there were several differences between the intact

responses across these attributes and the responses of CCAP and RPCH but a reduced number of differences between intact and proctolin. Taken together, these results suggest that the actions of individual peptides on these attributes of excitability are distinct and application of proctolin to the pyloric network may recapitulate the intact network output. While these individual attributes and statistical tests allow us to highlight specific parameters where the actions of individual peptides are distinct, there are inherent problems with this approach.

The first problem is the interpretation of what individual differences within an attribute mean when the entire attribute is considered holistically. The phase attribute, for example, is 5-dimensional. Differences in individual phases between two conditions allows us to say specifically where in the 5-dimensional attribute differences are found. This is not equivalent to saying one condition is statistically different from another in the phase attribute though because we are not considering all five dimensions together. The second issue is with the statistical tests used. Individual statistical tests, such as ANOVA's, assume independence across the parameters within an attribute however the activity of the PD, LP and PY neurons are not independent.

To make unambiguous statements about differences across conditions in a multi-dimensional attribute, we need to preserve the multi-dimensional nature of these attributes. This requires a new approach to the quantification and statistical testing of these data. Therefore, we used Euclidean distance measurements to quantify the exact distance between two conditions in an n-dimensional space and a multi-variate permutation test to statistically test whether the distance measured was large enough to consider two conditions statistically different from one another. The Euclidean distance allows for the

maintenance of an attribute's n-dimensional nature while the multi-variate permutation test is non-parametric and does not make any assumptions about the normality or independence of the data.

**The phase attribute cannot distinguish across individual peptides or between peptides and the intact state but can distinguish between peptide elicited and decentralized outputs.** Specific differences in the phases between a modulated condition and the decentralized state have been widely reported along with a small number of studies evaluating how different one modulated output is from another in phase (Weimann et al., 1997; Swensen and Marder, 2001; Thirumalai and Marder, 2002; Goaillard et al., 2004). While these previous studies highlight specific phases that are different between two conditions, there has not been a fully quantified measure of difference between modulated conditions in phase. Here we quantify the degree of difference in the 5-dimensional phase output across neuropeptide conditions, between the intact state and modulated states and the decentralized and modulated states.

To visualize these data, the 5-dimensional phase attribute can be represented in a lower dimensional space by plotting 3-dimesional permutations of the phases. In the first permutation of LP on, LP off and PY on, when all five conditions were plotted together and only the means were considered, there was a clear shift from the intact state to the decentralized. When the neuropeptides were reintroduced, there was a shift back towards the intact state with the proctolin output moving closest (Figure 2.3 A).

While plotting the mean coordinates of all five conditions together provided an outline of how these modulated conditions shift in phase, only evaluating the mean distance between the conditions fails to provide the context of whether that distance is statistically

meaningful. To visualize the distribution in phase of these modulated conditions, all individual data points were plotted and fit with a convex hull.

When all five conditions were plotted together in the LP on, LP off and PY on phase space and fit with a convex hill, there was overlap between the peptide modulated states and the intact. In this permutation, the distribution of the proctolin outputs occupied a space within the intact distribution while the decentralized outputs occupied a distinct area in the phase space. There was overlap between the modulated outputs and the decentralized responses as well, though this overlap was confined to one tail of the decentralized distribution. When only the modulators were considered in the LP on, LP off and PY on phase space, there was overlap between the distributions of all of them (Figure 2.3 A).

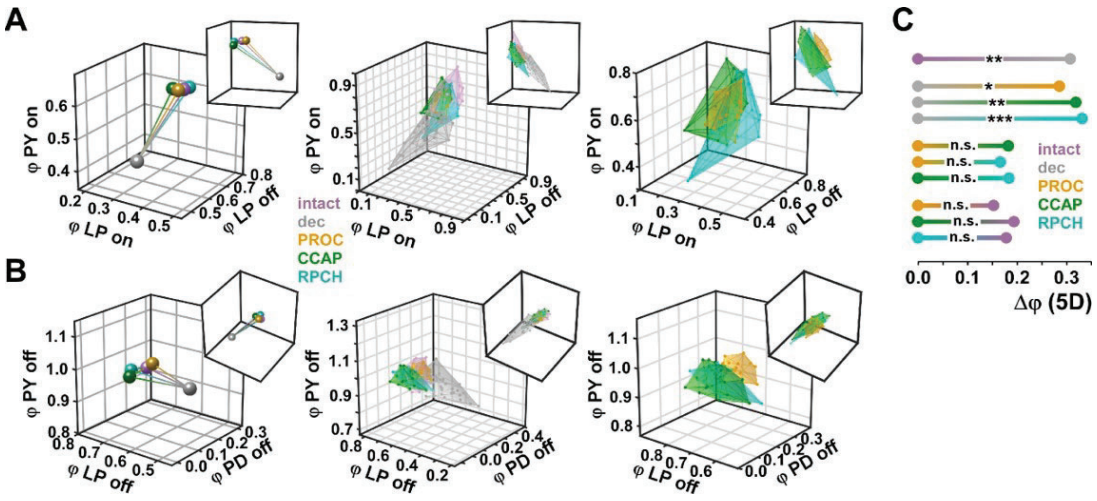


**Figure 2.3** Quantification of five dimensional phase difference across distinct modulatory conditions. (A) The effect of peptide neuromodulation on the 3-dimensional phase permutation of LP on, LP off and PY on. The intact, decentralized and three peptide responses in the reduced phase space plotted as either means, as individual animal responses fit with a convex hull or when only the individual neuropeptide responses are considered (B) The effect of peptide neuromodulation on the 3-dimensional phase permutation of PD off, LP off and PY off. The effects of neuropeptide modulation relative to each other and the intact and decentralized baseline conditions on the phase attribute when only the means are considered, when all five conditions are plotted as individual animal responses and fit with a convex hull or when only the modulated conditions are considered. (C) Euclidean distance measurement and statistical result in the 5-dimensional phase space.

The means in the second permutation of PD off, LP off and PY off showed a similar trajectory for the intact, decentralized and peptide modulated outputs previously visualized. Starting in the intact state, decentralization moved the mean phase response to a distinct space and the reintroduction of peptide modulators shifted the means back towards the intact with proctolin shifting closest (Figure 2.3 B). When the distributions were considered, all three peptide modulators shared space with the intact distribution, with the proctolin outputs sharing the most. The decentralized distribution also overlapped with the peptide modulated distributions, but like the previous permutation, this overlap was

confined to one tail of the distribution. When only the peptide modulators were considered, there was overlap between the three distributions however the proctolin distribution projected away from the CCAP and RPCH distributions along the axis of PD off.

While we were limited visually to three dimensions, the mean Euclidean distances and p-values reported reflect the evaluation of the full 5-dimensional attribute. In the 5-dimensional phase space, the mean decentralized phase response was statistically different from the intact as well as the three peptide conditions. The mean phase responses of the three peptides were not statistically different from each other and no peptide response was statistically different from the intact (Figure 2.3 C). The mean Euclidean distance between the intact and proctolin was also the smallest measured. This indicated that in the 5-dimensional phase space, the intact and proctolin distributions were closest to each other and consequently the most similar.

**Quantifying the effects of peptides on the spike number and spike frequency attributes.** As with phase, the effects of peptide neuromodulators on the number of spikes and spike frequency have been widely reported. Once decentralized, the number of spikes for the PD and LP neurons drops but increases for the PY neuron. Spike frequency also drops for all neurons following decentralization. The three peptides used here have been shown to strongly enhance the number of LP spikes and the LP spike frequency while proctolin has also been shown to enhance bursting in the PD and PY neurons (Nusbaum and Marder, 1988; Weimann et al., 1997; Dickinson et al., 2001; Swensen and Marder, 2001). While the effects of peptide modulators on a decentralized preparation on spike number and frequency have been reported, there have been fewer studies quantifying the

effect of peptide application with respect to the intact condition or across peptide conditions.

**Spike number can distinguish peptide outputs from each other and from both baseline conditions.** When the mean coordinates for all five conditions were plotted together in the 3-dimensional spike number space, the mean decentralized values shifted away from the intact like the phase response. When the neuropeptides were reintroduced, the mean values for all three peptides shifted away from the decentralized state, most notably along the LP spike number axis. Unlike in phase, however, the peptide modulators did not cluster around intact condition and were more distinguished (Figure 2.4 A). This was most notable for CCAP, which enhanced LP spiking, and proctolin, which enhanced PY spiking, compared to the intact. There was also more separation among the three peptide conditions, with CCAP enhancing the number of LP spikes compared to proctolin or RPCH and proctolin enhancing the number of PY spikes compared to CCAP or RPCH.

When the distributions were plotted, the intact, proctolin and RPCH distributions overlapped with the decentralized, though the overlap was limited. The intact distribution also overlapped with the three peptide modulated conditions thought the overlap between CCAP and intact was limited. When only the neuropeptide distributions were plotted, the three conditions overlapped though there were distinguishing features among them. CCAP enhanced the number of LP spikes beyond that of proctolin or RPCH while proctolin enhanced the number of PD and PY spikes compared to CCAP. The distribution of RPCH however bisected the distributions of both CCAP and proctolin (Figure 2.4 A).

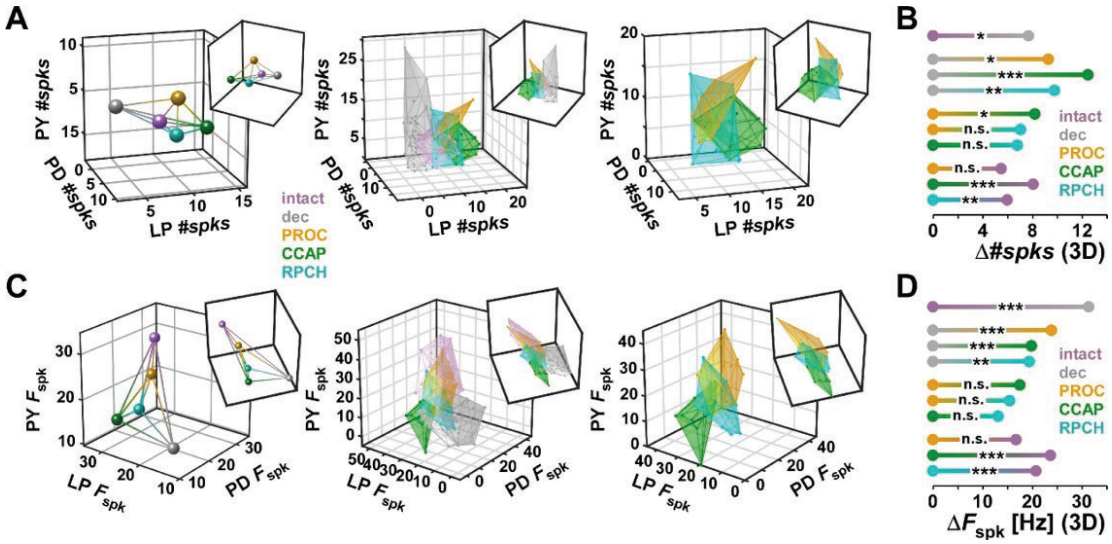


**Figure 2.4** Quantification of three dimensional spike number and frequency differences across distinct modulatory conditions. (A) Visualization of the intact, decentralized and three neuropeptide responses in the 3-dimensional spike number space. The intact, decentralized and three peptide responses visualized as means, distributions or only the peptide responses visualized as distribution. (B) Euclidean distance quantification and statistical testing of difference across distinct modulatory conditions in the 3-dimensional spike number space. (C) Visualization of the intact, decentralized and three neuropeptide responses in the 3-dimensional spike frequency space. The intact, decentralized and three peptide responses visualized as means, distributions or only the peptide responses visualized as distribution. (D) Euclidean distance quantification and statistical testing of difference across distinct modulatory conditions in the 3-dimensional spike frequency space.

When quantified and statistically tested in the 3-dimensional spike number space, the decentralized spike number response was statistically different from the intact and the three neuropeptide conditions. The intact spike number response was statistically different from both the CCAP and RPCH responses but not proctolin and the distance between the intact and proctolin distributions was the smallest. This indicated that the intact and proctolin responses were most similar in this space. Across the peptide conditions, the CCAP spike number response was statistically different from the proctolin response, but

neither the CCAP nor proctolin spike number responses were statistically different from RPCH (Figure 2.4 B).

**Spike frequency cannot distinguish peptide outputs from each other but can distinguish peptide outputs from both baseline conditions.** Similar to the effect with phase and spike number, the process of decentralization shifted the mean spike frequency values to a new space compared to intact. The subsequent addition of neuropeptides then shifted the mean spike frequency responses away from the decentralized albeit to different degrees. In all three cases, the mean LP spike frequency was enhanced compared to decentralized however only proctolin increased the mean PD and PY spike frequencies compared to decentralized (Figure 2.4 C).

The mean proctolin response best recapitulated the intact response though the response of proctolin along the axes of PD and PY spike frequency was attenuated compared to intact. This attenuation of PD and PY activity was also apparent when the mean values for CCAP or RPCH were compared to the intact. Among the three neuropeptide conditions, the CCAP and RPCH mean spike frequency responses were similar along the axes of LP and PY spike frequency but diverged along the axis of PD spike frequency. Proctolin enhanced the LP spike frequency comparably to the other two neuropeptide conditions but also enhanced PD and PY spike frequency, causing the mean proctolin response to diverge along those two axes compared to CCAP and RPCH (Figure 2.4 C).

When the distributions of all five conditions were plotted together, the intact and decentralized distributions shared minimal overlap. The distributions for the three neuropeptide conditions overlapped with the intact distribution though the CCAP

distribution did so minimally. The three peptide distributions also overlapped with the decentralized distribution though the overlap was confined to one tail. When only the peptide distributions were considered, the CCAP and proctolin distributions were the most distinct, diverging along the PD and PY spike frequency axes while the RPCH distribution overlapped with both proctolin and CCAP (Figure 2.4 C).

When quantified, the decentralized response in spike frequency space was statistically different from the intact, proctolin, CCAP and RPCH responses while the intact spike frequency response was statistically different from the CCAP and RPCH responses but not the proctolin response. Across the peptide conditions, there were no statistical differences with the distance between the CCAP and RPCH distributions being the smallest (Figure 2.4 D).

**Redundancies and dependencies across the chosen metrics of excitability.** Quantifying the effects of a neuropeptide on the pyloric network output requires the extraction of attributes from both the intracellular and extracellular recordings. In total, there are 22 possible attributes that could be used to quantify a neuropeptides effect on the network output. Due to the derived nature of some of these measurements, using all of them would include redundant information and some attributes have been shown to have strong correlations.

It has been previously shown in the intact preparation that the delay to burst onset and offset of the pyloric neurons, the latencies, scale with cycle period while the phases of each neuron do not scale with cycle frequency (Bucher et al., 2005; Goaillard et al., 2009). This scaling makes latency an unreliable measure because any change in burst onset or offset could be explained by a change in how fast the network is cycling. It is not known,

however, if neuropeptide modulated latencies also scale with cycle period while the phases remain consistent across cycle frequency. When the latencies of the PD, LP and PY neurons following proctolin, CCAP or RPCH application were plotted, the modulated latencies scaled with cycle period while the phases did not scale with cycle frequency (Figure 2.5 A).

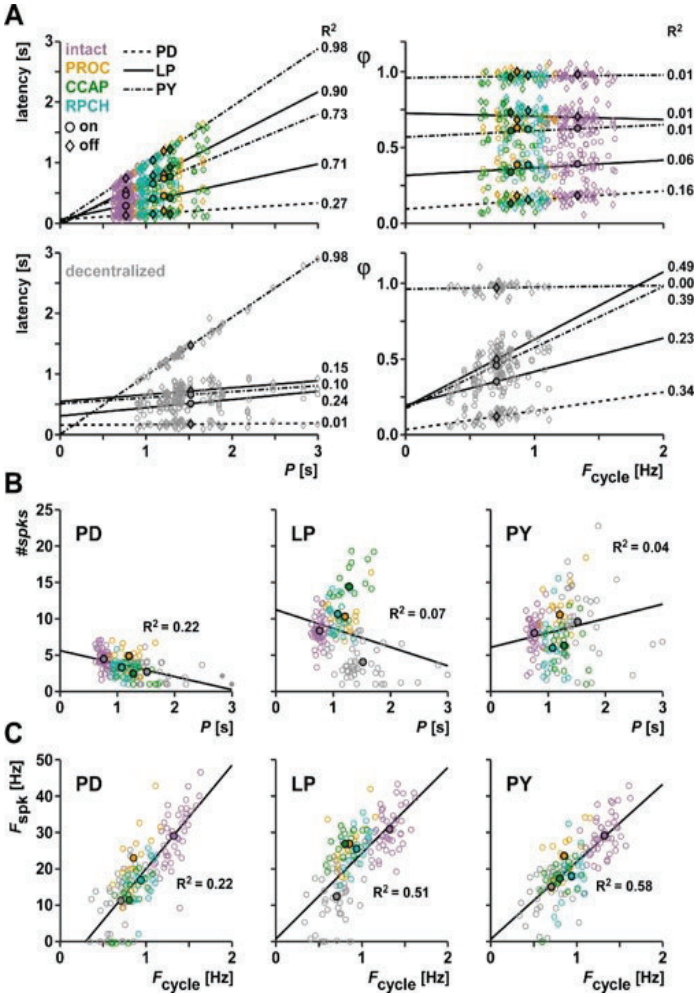


**Figure 2.5** Correlations across the attributes of excitability. (A) Latencies under modulated conditions scale with cycle period while phases do not scale with cycle frequency. The decentralized latencies do not scale as well with cycle period compared to the modulated conditions but the decentralized phases scale better with cycle frequency with the exception of PY off latency and phase. (B) The number of spikes per burst of each core pyloric neuron is weakly correlated with cycle period. (C) The spike frequencies of the core pyloric neurons show correlations with cycle frequency.

It is also not known whether the decentralized latencies and phases scale or remain constant across cycle period or frequency. When plotted, the decentralized latencies did not scale appreciably with cycle period like the intact or peptide conditions did, with the exception of the burst offset of PY. The decentralized phases did, however, scale better with cycle frequency unlike the intact or peptide responses, with the exception of PY off phase. While not tested directly, a linear relationship between frequency and phase has been shown previously during pyloric network recovery following decentralization (Luther et al., 2003) though it is not clear why this occurs (Figure 2.5 A).

When the number of spikes per burst for each condition was plotted against cycle period across all three neurons, there were correlations particularly between number of PD spikes and cycle period (Figure 2.5 B). This indicated that any difference in spike number across conditions was influenced but not solely due to a change in period across conditions. Correlations were also found between spike frequency and cycle frequency (Figure 2.5 C).

**Multi-dimensional quantification preserves apparent differences while additional differences emerge.** Evaluating individual attributes of a network output, either with traditional plots and statistics or, more holistically in a multi-dimensional space, can identify individual places in the network output where there are differences. However, a network output is not the result of a singular parameter or attribute, it is the combination of all attributes working in conjunction. Additionally, knowing the degree of interdependence across the attributes previously evaluated undermines any conclusion of difference that may have been drawn. To fully address whether one neuropeptide elicited pattern is quantitatively different from another and to resolve any issues of interdependency, all four attributes need to be considered together.

The 5-dimensional phase, 3-dimensional spike number, 3-dimensional spike frequency and the unidimensional cycle frequency attributes were combined into condition specific 12-dimensional network output vectors. Due to differences in units across the four attributes, all 12-dimensional vectors were z-score standardized prior to Euclidean distance calculation and statistical testing (Figure 2.6 A).

When statistically tested in the 12-dimensional z-scored network output space, the decentralized network outputs were statistically different from the intact, proctolin, CCAP and RPCH network outputs. The intact network outputs were also statistically different from all three peptide conditions. Across the neuropeptides, the proctolin network outputs were statistically different from both the CCAP and RPCH network outputs but the CCAP and RPCH network outputs were not statistically different from each other. The mean distance between the CCAP and RPCH network outputs was also the smallest, indicating their closeness in this space (Figure 2.6 B).

The 12-dimensional space was visualized using the scores in the first three principal components following principal component analysis (PCA). When the mean PCA scores for each condition were plotted in the first three principal components, there was clear separation between the intact and decentralized mean scores. With proctolin application, the mean PCA scores shifted back towards the intact mean. There was also a shift away from the decentralized with CCAP and RPCH application though these two conditions did not cluster around the intact or proctolin mean values (Figure 2.6 C).

To visually see what a change in each of the three principal components meant to the pyloric network output, a reference tri-phasic rhythm was created based on the intact condition. The reference rhythm values for the 12 parameters were scaled based on the

coefficients from the principal component analysis. The scaled intact parameters values in the first three principal components were then plotted. This visualization allowed us to see which parameters of the network output were strongly influencing the first three principal components.

In each individual PC space, the reference rhythm was shifted by two standard deviations in both directions along the PC axis (Figure 2.6 D). When the reference rhythm was shifted in PC 1, the largest change seen was in cycle frequency with secondary effects in PY spike number and LP spike frequency. In PC 2, the largest change seen was in LP spike number. In PC 3, the changes were more subtle, with small changes in PY spike frequency but an opposite effect of cycle frequency seen in PC 1.

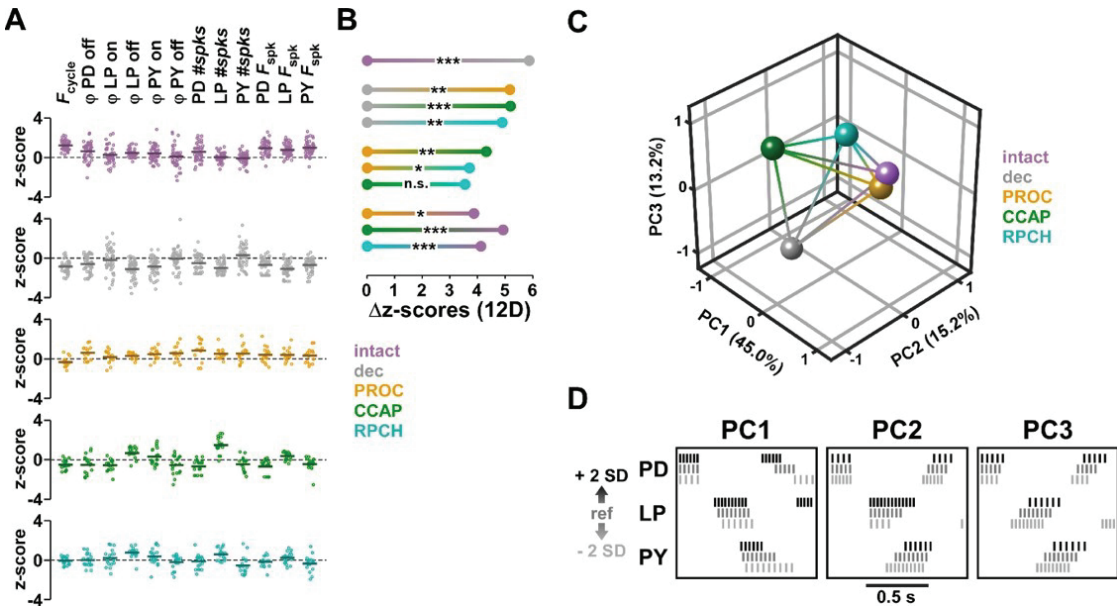


**Figure 2.6** Differences in the 12D pyloric network output across neuropeptide conditions. (A) Z-scores for all condition in each of the 12 parameters which were statistically tested. The black lines represent the mean z-score value. (B) Euclidean distance quantification and statistical testing of difference across all modulatory conditions in the 12-dimensional network output space. (C) Mean scores of all five conditions in a reduced 3-dimensional principal component space. (D) A reference intact rhythm shifted along the axes of the first three principal components. An intact rhythm was generated with the raw values for each of the 12 network output parameters. Those values were transformed using the coefficients from the principal component analysis and then plotted. The transformations of that rhythm within two standard deviations are equivalent to moving along the axes of each principal component from C.

**Pattern recognition and time series machine learning classification.** The previous analyses of the pyloric rhythm depend on which attributes were chosen and could be extracted from the raw data by the experimenter. In this study, we only included experiments with triphasic rhythms present in all modulatory conditions. However, individual or even all neurons may stop spiking upon decentralization and/or rhythms can become irregular. Therefore, we took a machine learning approach to 1) try to replicate key results of the Euclidean distance and permutation analysis with the already existing

features, and 2) use minimally processed data that only required a rhythmically active PD neuron to define cycle period and relative spike times (phases) of the follower neurons. While it would have been possible for this second approach to use unprocessed data, i.e., the raw voltage measurements, the preprocessing compressed the data and minimized computation time.

**Pattern recognition network.** For the first step, we used the existing 12-D data matrix as input to a shallow network for pattern recognition (Figure 2.7 A). After training and bootstrapping, the average accuracy for the 100 pattern recognition algorithms was 82.7% (range: 72.1% - 93.1%). Intact and decentralized experiments were correctly classified in 91.6% and 94.3% of the two conditions, respectively. Correct classification for proctolin experiments was 64.5%. Proctolin was mostly misclassified as intact (12.6%) or RPCH (14.0%). Correct classification for CCAP experiments was 73.3%. CCAP was mostly misclassified as RPCH (13.5%). Correct classification for RPCH experiments was 57.8%. RPCH was mostly misclassified as CCAP (20.3%). Overall, these results match the observation of the Euclidean distance and multi-variate permutation test in that intact and decentralized states are different from the modulated states, and that RPCH experiments share features with CCAP experiments (Figure 2.7 B).

**Time series classification network.** The pattern recognition network has only one input layer, which constrains the inputs to a vector of preselected features that largely loses the temporal relationships between multiple neurons. This requires that the experimenter chooses and measures the same features in each experimental condition. Therefore, analysis is limited to experiments that fit the input template; in the case of this study the fully triphasic pyloric rhythm. However, perturbations, such as the removal of

neuromodulators, can have disruptive effects on that rhythm, and the selection of features gives rise to the possibility of missing information. Hence, we wanted to work with minimally processed data (Figure 2.7 C) and used distinct but overlapping experiments for a second machine learning approach using a deep bi-directional long short-term memory network for time series classification with one input layer per neuron (3 input layers total) (Figure 2.7 D).

In each experiment, we separated each cycle into 20 bins and averaged the number of spikes per bin per neuron across all cycles for each condition (Figure 2.7 C, left y-axis). This preserves the overall spike structure while keeping the time steps limited to 20 bins to reduce computational time. Furthermore, neurons that fall silent during some experimental conditions can be included as empty (= 0) bins.

After training and bootstrapping, the average accuracy for the 100 time series classification algorithms was 68.3% (range: 54.2.1% - 79.2%), much lower than that of the pattern recognition network. Intact and decentralized experiments were correctly classified in 86.0% and 83.3% of the two conditions, respectively. While 73.5% of CCAP experiments were correctly classified, the majority of proctolin (27.7% correct) and RPCH (25.7% correct) experiments were misclassified. The most common misclassification of proctolin was as decentralized (39.0%) or intact (17.0%), and RPCH as intact (45.3%) or CCAP (25.7%) (Figure 2.7 E). Overall, this algorithm was able to differentiate between unmodulated and modulated conditions, however, it largely failed to correctly classify pyloric activity in the presence of a single neuromodulator.

Removing neuromodulatory input to the STG can lead to dramatic changes in the rhythmic activity; most commonly observed is a decrease in cycle frequency (Hamood et

al., 2015). Application of neuromodulators can, at least partially, restore rhythmic activity and increase cycle frequency. While we could obtain the same input structure for all experiments with our minimal preprocessing, information about cycle frequencies was lost in this process. Therefore, to include a measure of cycle frequency, we added the z-scored cycle frequency, based on the distribution of decentralized cycle frequencies, as offset to each bin (Figure 2.7 C, right y-axis).

After training and bootstrapping with these data, the average accuracy for the 100 time series classification algorithms increased to 75.5% (range: 58.3% - 87.5%). Correct classification of intact experiments increased to 97.0%. Furthermore, intact experiments were never misclassified as RPCH and < 1% as CCAP. Consistent with this result, CCAP and RPCH were never misclassified as intact, indicating that there are differences between the intact network activity, which is most likely influenced by multiple neuromodulators of unknown concentrations at any given time, and the network activity that is generated when single neuromodulators are applied individually. Adding the z-scored cycle frequency increased the correct classification of proctolin to 44.0%. However, a large proportion of proctolin data was still misclassified as decentralized (31.7%) or intact (12.7%). CCAP and RPCH were correctly classified in 64.8% and 56.7% of cases, respectively. Most commonly, CCAP was misclassified as RPCH (17.5%), and RPCH as CCAP (35.0%) (Figure 2.7 F). With the exception of proctolin, the general results from Euclidean distance and pattern recognition classification are comparable with the results obtained from the time series classification.

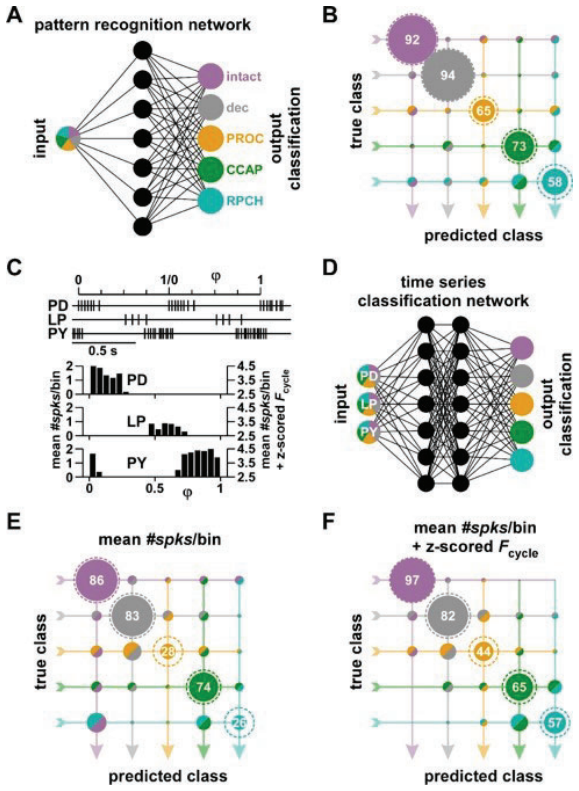


**Figure 2.7** Rhythm classification with machine learning. (A) Schematic representation of a shallow pattern recognition network with one input layer (multicolored circle), one hidden layer (black circle), and output layer (colored circles). (B) Transition matrix between the true (known) modulatory conditions and the conditions predicted by the pattern recognition network. Dot sizes at the nodes scale with the probability across the whole dataset. Hatched circles along the diagonal represent 100% of each true class, Numbers in the circles represent the percentage of correct classification for each modulatory condition. (C) Spike raster of three pyloric neurons (top) that was normalized to cycle period on a cycle-by-cycle basis. These were used to create histograms of the average spike count per bin per cycle (bottom, left y-axis), which was offset by the z-scored cycle period for that experiment (right y-axis). These histogram data were used as input for a time series classification network. (D) Schematic representation of a deep time series classification network with one input layer per neuron (multicolored circles), multiple hidden layers for feature extraction and classification (black circles), and output layer (colored circles). (E) Transition matrix between the true modulatory conditions and the conditions predicted by the time series classification network for the histograms without the z-scored cycle frequency. (F) Transition matrix between the true modulatory conditions and the conditions predicted by the time series classification network for the histograms with the added z-scored cycle frequency.

## 2.4 Discussion

The hypothesis that individual neuromodulators generate distinct patterns of activity provides a solution as to how network output flexibility could be achieved in central pattern generating circuits (Marder and Weimann, 1992; Marder and Thirumalai, 2002). Given different circumstances or needs, an animal must have the flexibility to change the behavior governed by a static neural network. With recordings of the same activity pattern under distinct modulatory conditions and traditional quantifications, these outputs do appear different in both form and presumably function. However, due to the complex nature of the activity being quantified, the previously utilized statistics could only make statements about differences in individual parameters, not across n-dimensional attributes or the network output. Therefore, the true degree of difference, or lack thereof, could not be determined. By taking a new approach to the analysis of four attributes of excitability, we sought not only to ask whether one output is different from another but went further to address: if they are different, how different are they?

**Modulated phase outputs are not different.** The first metric evaluated was the phase response across the individual neuropeptides and between the neuropeptides and the baseline conditions of intact and decentralized. When traditionally quantified with phase plots there were statistical difference between the modulated conditions and the decentralized but there no statistical differences across the peptide conditions and a single difference between CCAP and intact. The differences between the decentralized and modulated phases were not surprising but the lack of differences across the peptide conditions were. The only other direct peptide comparison in phase showed a statistical difference between proctolin and CCAP in the phases of PD off and PY off (Swensen and

Marder, 2001) however those differences were not replicated here, though the duty cycle of PD with CCAP is reduced compared to proctolin. This is mostly likely due to the difference in concentration of CCAP used.

The lack of differences in phase across the intact and peptide conditions can be understood by evaluating the slope of the fit line after plotting the latencies of each neuron against cycle period. The latencies under each modulated condition scale with the same slope meaning that each modulated condition is having the same effect. A mechanistic explanation for the similar activity of the modulated conditions in phase is the similar activation of $I_{MI}$ in the AB neuron. The AB neuron is the main pacemaker of the pyloric network and each of the three neuropeptides target this neuron. While we do not know the composition of the neuromodulatory environment in the intact animal, it is likely that neuropeptides are present and sufficiently activating this neuron. We are currently testing the hypothesis that $I_{MI}$ activation in the pacemaker is sufficient to maintain phase across distinct neuromodulatory conditions while $I_{MI}$ activation in the follower neurons LP and PY will not affect the phase attribute but instead modulates each follower neurons excitability. Neuropeptides operate unidirectionally, converging to activate $I_{MI}$, and do not modulate other intrinsic currents like the A-type potassium current and the hyperpolarized activated inward current, which are known to influence the phasing of the pyloric neuron (Harris-Warrick et al., 1995a; Harris-Warrick et al., 1995b). It is this unidirectional action by neuropeptides which may prevent differences in phase while monoamines like dopamine do modulate these currents and may allow the phases to shift in a statistically meaningful manner.

**Spike number reveals small differences within and across peptides and baseline conditions.** In the 3-dimensional spike number attribute the only statistical difference across the peptide conditions was between proctolin and CCAP. This difference arose from the distinct actions of proctolin in the PY neuron and the distinct actions of CCAP in the LP neuron.

Underlying a change in spike number is the activation of $I_{MI}$ following peptide receptor binding. It has been previously shown that the PD and PY neurons do not express CCAP receptor mRNA and $I_{MI}$ is not activated in these neurons during CCAP application (Swensen and Marder, 2001; Garcia et al., 2015). Of the pyloric neurons which do express CCAP receptor mRNA, the LP neuron had the highest expression level. Additionally, CCAP maximally elicited $I_{MI}$ in LP with $10^{-6}$ M while the same concentration of proctolin did not (Garcia et al., 2015). While we do not know the expression levels of proctolin receptors in any pyloric neurons, proctolin has been shown to activate $I_{MI}$ in the PD, LP and PY neurons and increases PD and PY spike number (Swensen and Marder, 2001). These differences in $I_{MI}$ activation in response to CCAP or proctolin application in the three pyloric neurons is sufficient to explain the individual differences found and the statistical difference in the combined 3-dimensional spike number space.

Like proctolin, the expression levels of RPCH receptors are not known in pyloric neurons however RPCH was shown to only activate $I_{MI}$ in the AB and LP neurons. These are the same pyloric neuron targets of CCAP. While the RPCH elicited increase in LP spike number was statistically lower than the CCAP mediated increase, the lack of difference between CCAP and RPCH in PD and PY spike number is sufficient to explain the lack of difference between them in the combined 3-dimensional space.

While RPCH targets the same pyloric neurons as CCAP, when quantified, the spike number responses in the 3-dimensional space with RPCH and proctolin were not statistically different. Within the individual neurons, there was a single statistical difference between RPCH and proctolin, in PY spike number. While both peptides activate $I_{MI}$ in LP and increase its excitability, they do so similarly which could suggest a similar number of proctolin and RPCH receptors on the LP neuron. This is in contrast to the more profound effect of CCAP application. Taken together, the single statistical difference in the number of PY spikes and the similar increase in excitability of the LP neuron was not sufficient to statistically differentiate the RPCH and proctolin responses.

All of the modulated conditions were statistically different from the decentralized response in the 3-dimensional spike number space which was not surprising. The decentralized state is one which lacks the influence of neuromodulators. Unlike the decentralized response, the intact spike number response was not statistically different from proctolin but was statistically different from both CCAP and RPCH. The simplest explanation for this is the known neuron targets for each of the three peptides. Both CCAP and RPCH only target a subset of neurons in the circuit while proctolin targets almost all of them. While we do not know what the modulatory environment is for the intact preparation, peptides are present (Chen et al., 2014). This distinct targeting of pyloric neurons by CCAP and RPCH compared to the multiply modulated intact state explains the difference found while the similarity in targeting between proctolin and intact explains the lack of difference found.

**Spike frequency reveals no differences across peptides but reveals differences from baseline conditions.** The differences and lack of differences across the five conditions in

spike number space were largely preserved in spike frequency space. When quantified the intact, proctolin, CCAP and RPCH spike frequency responses were all statistically different from the decentralized response. The intact spike frequency response was also statistically different from the CCAP and RPCH spike frequency responses but not different from the proctolin response.

Interestingly, the statistical difference between proctolin and CCAP in spike number space was lost in spike frequency space. The intraburst spike frequency is the ratio of the number of spikes per burst and the burst duration. For the proctolin and CCAP spike number responses, the largest individual difference was in LP spike number but when evaluated as individual parameters, there was no difference in LP spike frequency between proctolin and CCAP. This indicates that the duration of the LP burst with CCAP is extending compared to proctolin. While there were individual differences between proctolin and CCAP in PD and PY spike frequency, their distributions overlapped more in spike frequency space compared to spike number space. The loss of LP spike frequency difference and the increase in PD and PY spike frequency overlap is sufficient to explain the lack of difference found.

The lack of difference between the spike frequency responses of CCAP and RPCH, however, is not surprising. In the 3-dimensional spike number space, these outputs were not different statistically though there was an increase in mean LP spike number with CCAP compared to RPCH. The reduction in LP spike frequency with CCAP, indicating a change in burst duration, coupled with no statistical differences in PY or PD spike frequency makes the lack of overall statistical difference in the 3-dimensional space reasonable. The lack of difference between RPCH and proctolin in spike frequency space

is also not surprising given the large amount of overlap between them in all three dimensions.

**Why do differences or the lack of differences emerge in the 12D space?** While evaluating individual attributes of the network output provides insight as to where a particular peptide modulators effects are strongest, a network output is not the result of a single attribute. Our expectation was that these individual peptide responses were different, but the exact degree of difference was not known. Additionally, we expected the decentralized network outputs to be distinct from the network outputs of individually applied peptides and the intact to be different from minimally the CCAP and RPCH network outputs. To fully quantify how different one peptide elicited network output was from another, a profile of each modulators effects on the network output was constructed and tested.

The four attributes of excitability chosen for this analysis are a proxy for the entire network output but are also meaningful features that the animal may use to discriminate between patterns and generate specific behaviors. By combining these features and building condition specific network output profiles for each peptide we found that only the proctolin network outputs were distinct, they were distinguishable from the CCAP network outputs as well as the RPCH network outputs. Additionally, the proctolin network outputs could be distinguished from the decentralized and intact states in the combined space though in almost all of the individual attributes, the proctolin outputs were not different from the intact.

The emergence of difference between the proctolin and intact network outputs came from the inclusion of the cycle frequency attribute. In these data, the proctolin cycle

frequency was statistically slower than the intact and this was sufficient to render these outputs distinct in the network output space. This highlights the importance of evaluating a multitude of attributes in the same space.

Like the emergence of statistical difference between the intact and proctolin network outputs, the lack of difference between the CCAP and RPCH network outputs was also surprising and unexpected. When the attributes of excitability were evaluated individually there was a single difference in cycle frequency and when evaluated in the 12-dimensional network output space, the CCAP and RPCH network outputs were not statistically different. While they both activate $I_{MI}$ in the same subset of pyloric neurons, each of the levels underlying a network output including but not limited to the intrinsic currents are subject to neuromodulation (Marder and Thirumalai, 2002; Katz and Calin-Jageman, 2009; Nadim and Bucher, 2014). For these modulator outputs to not be different they could either bridge those levels in the same way or find different solutions to end up at the same output.

**Caveats to the detection of difference in the network output space.** There are two caveats to the detection of differences or the lack of differences in this 12-dimensional network output space. One is the experimental approach. Traditionally, experiments in this system use bath application of neuromodulators. This results in the exposure of the entire network to a neuromodulator. Bath application is a simpler experimental approach which allows for insights into the general principals of peptide neuromodulation. Biologically, however, the circuit is likely experiencing more precise effect of neuropeptides. The presence of peptidases and targeted local release of neuromodulators to particular subsets of neurons within the circuit allows for a high degree of fine tuning of

what an output could be (Blitz and Nusbaum, 1999; Nusbaum, 2002). This fine tuning could allow for distinct and obvious differences between neuropeptide outputs which were not captured here. The second caveat is the choice of attributes. While the quantification of multiple attributes together is an improvement over the previous approaches to quantification, we are only sampling from a portion of the available attributes which describe the output of the pyloric network. While we did not find differences in the network output between CCAP and RPCH with these attributes, these outputs may still be quantitatively distinct from one another but in attributes that we did not evaluate such as the structure of the burst or cycle to cycle variability.

**Two different approaches for distinguishing neuropeptide elicited pyloric network outputs reach the same conclusion.** The results from the Euclidean distance and multi-variate permutation testing indicated that a proctolin network output was statistically distinct from a CCAP and RPCH network output but the network outputs of CCAP and RPCH were not distinguishable statistically. This assessment came after the extraction of four specific attributes and explicit testing for statistical difference between two conditions. One possibility was that the statistical power of our initial approach was not high enough to find statistical differences across these distinct conditions. Additionally, because we were intentionally choosing the attributes we evaluated, we may have biased our data set. Therefore, we also tested our data using two distinct machine learning approaches. While the Euclidean distance/multi-variate permutation test and machine learning approaches were complementary, they also addressed distinct questions. In the Euclidean distance approach, we asked statistically how different two conditions were while with the machine learning approach we asked, given a pattern of activity, how accurately can it be classified?

The main conclusions from both machine learning approaches were that a CCAP network output, when misclassified, is often mistaken for an RPCH network output and vice versa and that cycle frequency represents an important attribute for classification. When the cycle frequency was included in the time series classification network, the accuracy of classification was improved across all conditions, most notably with proctolin and RPCH. Both of these conclusions match the main results from the Euclidean distance and multi-variate permutation test approach.

There are caveats with using machine learning on these data, most apparent is the sample size. Data sets for machine learning classification typically are larger than the data set used here which may have contributed to accuracy issues. Additionally, the sample sizes for each condition were unbalanced specifically with respect to the peptide conditions which may have also contributed to accuracy issues. Taken together, both approaches reach the same conclusion: individual peptide modulated network outputs are difficult to distinguish.

**How different is different enough and does it matter?** By taking a new approach to the analysis of these network outputs we found differences across peptide elicited network outputs which support the hypothesis of network output flexibility but also a lack of difference which challenges this hypothesis. The natural extension of these results is: what do these differences mean outside of what we evaluate in an experimental setting?

This preparation can generate fictive motor activity in a petri dish which we use as a proxy for what the fully intact animal is experiencing, and it is tempting to bridge these levels to make higher order statements about what a particular output pattern may mean (Marder and Bucher, 2001; Carandini, 2012; Gao and Ganguli, 2015). However, the results

here do not necessarily translate downstream to the level of the neuromuscular junction or ultimately behavior (Feldman and Kam, 2015). The differences we report here may not be different enough to matter to the animal in a behavioral sense.

The functional consequences of peptide neuromodulation, at least measured experimentally, are largely protective or stabilizing in nature. This ranges from the regulation or stabilization of the cycle frequency (Nusbaum and Marder, 1989; Dickinson et al., 2001) to robustness in the face of temperature perturbation (Haddad and Marder, 2018) and maintenance of ionic current correlations (Khorkova and Golowasch, 2007). The hallmark of peptide application though is the generation of a reliable tri-phasic output where one did not previously exist or was significantly slower or less functional. It may be that the large number of neuropeptides available simply generate a functional tri-phasic rhythm which is good enough.

The fact that neuropeptides, signaling through G-protein coupled receptors, converge cellularly allows for multiple solutions to the same problem to ensure that a needed behavior can persist regardless of the flux in the neuromodulatory environment (Kitano, 2004). It could be that the functioning animal only cares that a tri-phasic rhythm, which fits into some expected range of parameter boundaries, is present rather than the statistical nuances reported here. In the behaving animal, the pyloric network acts to control the pylorus to filter food (Selverston, 2017). From the perspective of the animal, it may evaluate these differentially single modulated outputs as all being good enough to accomplish the behavior needed. Additionally, neuromodulators like dopamine have more complex and cell type specific effects compared to neuropeptides in the pyloric network (Flamm and Harris-Warrick, 1986b, a; Harris-Warrick and Johnson, 2010). It may be that

the peptides are necessary to generate a baseline tri-phasic rhythm while neuromodulators with more complex actions can generate network outputs which are distinct to the animal.

On the other hand, the neuromuscular junction and muscle may care a great deal about these differences. These peptide modulators could, in a way, be fine tuning specific features of the network output to allow for differentiation (Brezina, 2010). It has recently been shown that two distinct muscles innervated by the same pyloric nerve respond differently to changes in spike number, burst frequency and burst duration (Daur et al., 2021). While we consider differences evaluated that meet a certain p-value to be meaningful, the intact animal may respond to more subtle changes. It may be that effective communication of the need for a proctolin output would require an obvious change in spike number to ensure that downstream from the circuit, a proctolin message does not get mistaken for a CCAP message. Instead of a large and obvious change, the distinguishing of a proctolin rhythm from an RPCH rhythm might be more subtle and require smaller differences across a larger number of parameters in different attributes while CCAP and RPCH could be degenerate peptides that can substitute for one another. At this point though, we do not appreciably understand the coding and decoding mechanisms which transform an activity pattern into a behavioral output to know which of these possibilities is occurring.

# CHAPTER 3

# CONVERGENT PEPTIDE CO-MODULATION PROMOTES CONSISTENCY OVER FLEXIBILITY IN THE PYLORIC NETWORK OUTPUT

## 3.1 Introduction

In Chapter 2 we sought to fully quantify the degree of statistical difference between individual peptide elicited network outputs. The result of that quantification showed that when the four chosen attributes of excitability were tested holistically, the proctolin network outputs were statistically different from the CCAP network outputs and the RPCH network outputs. However, the CCAP elicited network outputs were not statistically different from the RPCH network outputs. These results indicated that there was a degree of flexibility within the circuit to generate distinct outputs but that individually applied neuropeptides do not guarantee a flexible network output. It is unlikely, though, that any circuit is under the effects of only a single neuromodulator (Marder, 2012).

Unlike single peptide neuromodulators, the effects of peptide co-modulation on a network output are less understood. Co-modulation can occur through the release of different neuroactive substances from distinct vesicles like dense core vesicles for neuropeptides and small, clear synaptic vesicles for small molecule transmitters or two or more neuroactive substances can be co-localized within the same vesicle (Vaaga et al., 2014; Svensson et al., 2019). Additionally, co-modulator interactions can occur through multiple circulating hormones and/or intrinsically released neuromodulators (Christie et al., 1995; Swensen and Marder, 2001). Regardless of the mechanism of release or interaction, co-modulation is likely the dominant influence on every aspect of a network output.

The large number of neuromodulators present in many small circuits is rationalized through the context of network output flexibility and the need for static circuits to generate multiple patterns of activity to meet different behavioral needs (Doi and Ramirez, 2008; Stein, 2009; Marder, 2012; McCormick and Nusbaum, 2014). From this perspective, a large number of individual neuromodulators would allow for an even larger number of co-modulator combinations leading to a seemingly endless number of distinct network outputs.

Trying to predict the outcome of co-modulation at any level is complicated due to the large number of ways that neuromodulators can interact with each other. The simplest type of interaction is a linear one where the individual effects of each modulator sum together when co-applied. While this can happen (Li et al., 2018) there are mechanisms which result in non-linear interactions between two or more modulators. In some cases, the combination of modulators modify a common target in a way which is distinct from the actions of either constituent (Dickinson et al., 1997; Thirumalai and Marder, 2002; Brezina et al., 2003; Brezina, 2010; Brewer et al., 2019). In other cases, the presence of one neuroactive substance can directly affect the actions of another (Matsumoto et al., 1999; Djokaj et al., 2001; Doyon et al., 2013). The potential for non-linear interactions at each level that underlies a network output makes predicting the outcome of co-modulation challenging. While non-linear interactions suggest the generation of distinct network outputs, flexibility, may not be the only outcome of interactions across all types of neuromodulators.

If we consider co-modulation in terms of neuropeptides, an alternative hypothesis for co-modulation of the network output is a reduction in flexibility. Neuropeptides in the stomatogastric nervous system have convergent cellular actions, targeting the modulator activated inward current ($I_{MI}$), but divergent circuit actions where each modulator targets distinct yet overlapping subsets of neurons in the circuit (Golowasch and Marder, 1992b; Swensen and Marder, 2000, 2001).

Despite the non-linearities that may be present, particularly at the intrinsic current level, if convergence is the dominant consequence of neuropeptide interactions, then co-modulation may reduce network output flexibility in favor of an increase in consistency. Flexibility in this context means that network outputs are different from each other in the presence of different combinations of neuromodulators or that distinct combinations allow for precise fine tuning of the network output. Consistency means that network outputs are similar to each other despite the presence of different combinations of neuromodulators and that the identity of any particular neuromodulator becomes less important the more neuromodulators present.

Mechanistically, the combination of multiple peptides together could lead to more consistent activation of the entire circuit due to the overlapping of their individual modulator cellular targets. A more consistent activation of the entire circuit could then lead to a reduction in flexibility between distinct pairs of co-modulators in their network outputs. If co-modulated outputs are not different from each other, this would add to the idea that neuropeptides function largely to produce a tri-phasic rhythm and individual neuromodulators may be able to substitute for one another in a co-modulated situation to maintain necessary behavior.

Here we quantify how different three distinct peptide co-modulatory pairs and two distinct peptide co-modulatory triplets are in their network outputs to test the hypothesis that convergent peptide co-modulation promotes consistency, not flexibility, at the level of the network output.

## 3.2 Materials and Methods

The animals, electrophysiological approach, attribute extraction, primary statistics, Euclidean distance and multi-variate permutation test calculation were the same as reported in Chapter 2. See Table A.2 for paired peptide co-modulation statistical tests and results and Table A.3 for triplet peptide co-modulation statistical results and results.

**Modulators and experimental protocol:** The stomatogastric nervous system was decentralized by blocking the stomatogastric nerve with a $10^{-7}$ M TTX (Biotium) + 750 mM sucrose (Sigma) solution. Proctolin (RS synthesis), CCAP (Bachem) and RPCH (Bachem) were diluted, aliquoted and stored as previously mentioned until needed. Final dilution of co-modulator pairs or triplets to the experimental concentration of $10^{-6}$ M occurred immediately before application in chilled *Cancer borealis* saline. For all co-modulator experiments, the total concentration of peptide used was $10^{-6}$ M and each combination of peptides was bath applied via peristaltic pump for 5 minutes. In the cases of repeated application of co-modulators to the same preparation, the first application was washed out in chilled *Cancer borealis* saline for a minimum of 45 minutes.

**N for paired peptide co-modulation:** 27 intact, 28 decentralized, 11 proctolin + CCAP, 11 CCAP + RPCH, 11 RPCH + proctolin.

**N for triplet peptide co-modulation:** 10 intact, 5 decentralized, 5 proctolin + CCAP + RPCH, 5 CCAP + proctolin + oxotremorine.

**N for constituent versus co-modulator condition analysis:** 80 intact, 79 decentralized, 15 proctolin, 18 CCAP, 19 RPCH, 11 proctolin + CCAP, 11 CCAP + RPCH, 11 RPCH + proctolin, 5 proctolin + CCAP + RPCH, 5 CCAP +proctolin + oxotremorine. Individual peptide responses in the 12 parameters of excitability were the same as reported in Chapter 2.

## 3.3 Results

**Paired peptide co-modulation reduces differences in four attributes of pyloric network excitability.** While there are limited reports examining qualitative and quantitative differences on individual attributes of a network output under co-modulatory conditions (Blitz et al., 1999; Thirumalai and Marder, 2002; Lane et al., 2018), there has yet to be a full qualitative and quantitative description of the effects of peptide co-modulation on the pyloric network output To first test the hypothesis that convergent co-modulation promotes consistency in the network output, we qualified and quantified the effects of three peptide co-modulator pairs on four attributes of excitability in the pyloric network. The three individual peptide neuromodulators used for the single peptide comparison previously were combined to form three distinct co-modulator pairs. These pairs were proctolin + CCAP, CCAP + RPCH, and RPCH + proctolin.

When the network outputs were qualified during ongoing activity, there was a clear shift in activity and appearance between the intact and decentralized states. Following decentralized, the distinct peptide co-modulator network outputs appeared similar (Figure

3.1 A). To quantify the degree of apparent similarity between the co-modulated conditions we evaluated the effects of each condition on the pyloric network cycle frequency, the phase responses, the number of spikes per burst and the spike frequency.

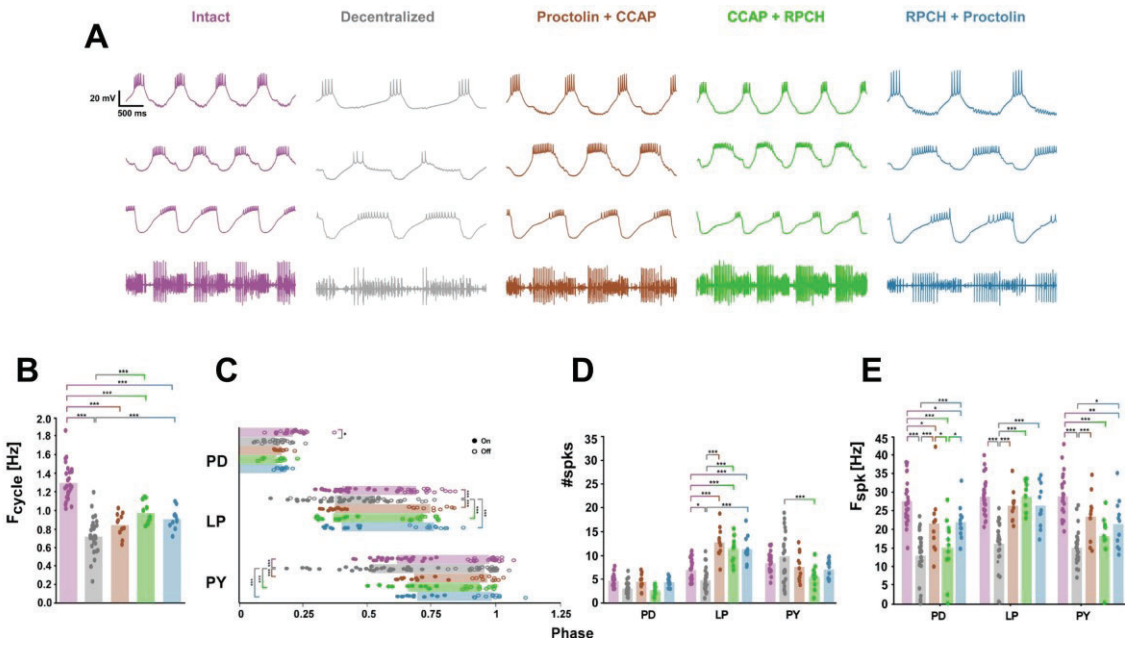


**Figure 3.1** Qualitative and quantitative response of the core pyloric neurons to paired peptide co-modulation. (A) The qualitative response of the core pyloric neurons to $10^{-6}$ M total concentration paired peptide application. (B) Cycle frequency response across intact, decentralized and three paired peptide conditions. Bars represent mean cycle frequency responses and points represent individual animal responses. (C) Phase responses of the PD, LP and PY responses under intact, decentralized and paired peptide conditions. Bars represent mean phase on and off values. Filled in circles represent individual animal phase on values and empty circles represent individual animal phase off values. (D) Spike number responses of the core pyloric neurons under intact, decentralized and paired peptide conditions. Bars represent mean spike number responses across the five modulatory conditions while the individual points represent individual animal responses. (E) Spike frequency responses of the core pyloric neurons under intact, decentralized and paired peptide conditions. Bars represent mean spike frequency responses across all modulatory conditions and individual points represent individual animal responses.

We expected differences between the co-modulated network outputs and the decentralized outputs in each of these attributes when quantified, as well as differences between the intact and decentralized states. Based on our hypothesis, we do not expect

differences between the co-modulated network outputs in any of these individual attributes. Additionally, if the combination of two peptides sufficiently targets the pyloric circuit, then we would also expect to see no differences between the co-modulated and the intact responses across these attributes.

**Cycle frequency**. In the cycle frequency attribute, the intact response was statistically faster compared to the decentralized and co-modulated responses. The decentralized response was also statistically slower than the CCAP + RPCH and RPCH + proctolin responses however there were no statistical differences between the co-modulated cycle frequency responses (One way ANOVA: $F_{(4,83)} = 41.429$, $p < 0.001$) (Figure 3.1 B).

**Phase.** In the phase of PD off, the intact response was statistically larger than the decentralized. There were no statistical differences across any condition in the phase of LP on while the decentralized off phase of LP was statistically different compared to all modulated conditions. The decentralized response was also statistically different compared to all modulated conditions in the on phase of PY but there were no statistical differences in the PY off phase (Two way ANOVA interaction: $F_{(16,415)} = 6.118$, $p < 0.001$) (Figure 3.1 C).

**Spike number**. In the PD spike number parameter, there were no statistical difference across any condition. In LP spike number the decentralized response was statistically lower compared to all the modulated conditions and the intact response was statistically lower than all three co-modulated responses. Lastly in PY spike number, the decentralized response was statistically higher than the CCAP + RPCH response but there were no statistical differences between any modulated state (Two way ANOVA interaction: $F_{(8,249)} = 11.916$, $p < 0.001$) (Figure 3.1 D).

**Spike frequency.** In PD spike frequency, the intact response was statistically higher compared to the decentralized and all three co-modulated conditions. The decentralized response was statistically lower than the proctolin + CCAP and RPCH + proctolin responses but not different from the CCAP + RPCH response. Additionally, the CCAP + RPCH response was statistically lower than the proctolin + CCAP and RPCH + proctolin responses. In LP spike frequency, the decentralized response was statistically lower than all modulated conditions, but there were no differences across the modulated conditions. Lastly in PY spike frequency, the intact response was statistically higher than the decentralized, CCAP + RPCH and RPCH + proctolin responses. The decentralized response was also statistically lower than the proctolin + CCAP and RPCH + proctolin responses but not statistically different from the CCAP + RPCH responses. There were also no statistical differences between the three co-modulated responses (Two way ANOVA interaction: $F_{(8,249)} = 2.815$, $p = 0.005$) (Figure 3.1 E).

**The co-modulator peptide pairs are not different in the combined 12D network output space but are different compared to the intact state.** We expected differences across the attributes of excitability between the decentralized and co-modulator pairs, however, the lack of differences across the three co-modulator pairs suggested that convergent co-modulation is promoting consistency in the network output. However, we cannot make a reasoned quantitative assessment about the network output by looking at the attributes individually. Due to the dependences both within and across attributes, we cannot evaluate each attribute individually. Therefore, we quantified how different one co-modulated output was from another in the 12-dimensional network output space. The complete 12-

dimensional matrix with all five conditions was z-score standardized prior to quantification and statistical testing (Figure 3.2 A) and visualized in a reduced principal component space.

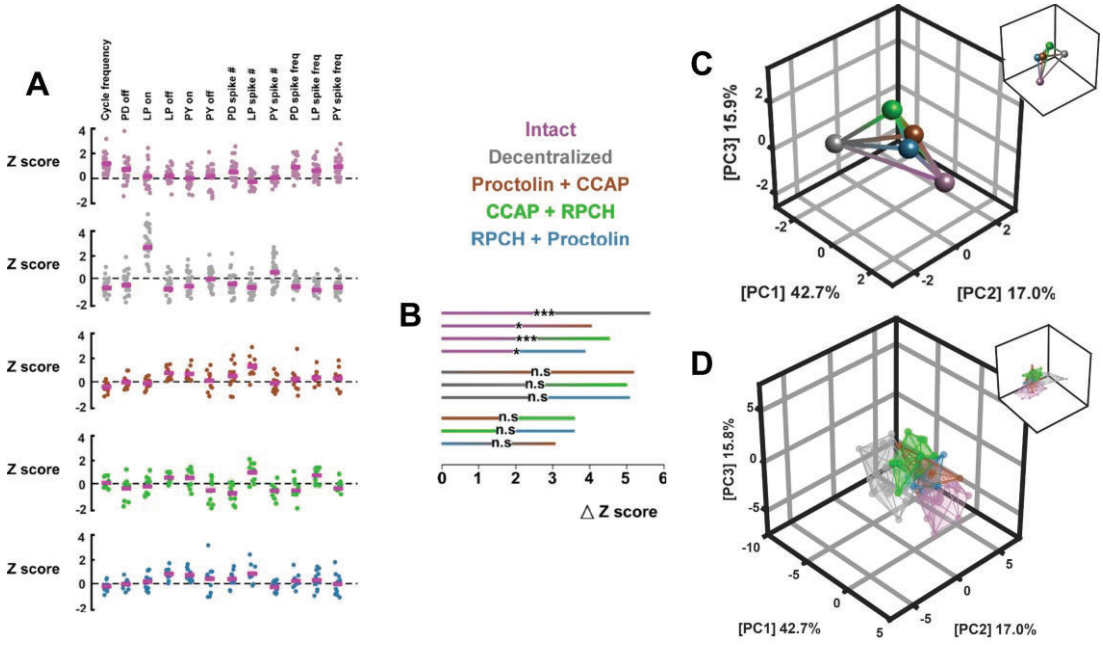


**Figure 3.2** Quantification and statistical testing of difference between paired co-modulated network outputs. (A) All 12 parameters from all five test conditions were initially combined and z-score standardized. Magenta lines represent the mean z-score value. (B) Euclidean distance measurement between each pairwise comparison and determination of statistical significance in the 12-dimensional space. (C) Visualization of the mean network output space across all five conditions in a reduced 3-dimensional principal component space. (D) Visualization of the network output distributions of all five conditions in the reduced principal component space.

When the z-scores were quantified and statistically tested in the 12-dimensional space, the peptide co-modulator pairs were not statistically different from each other. The proctolin + CCAP versus RPCH + proctolin comparison also resulted in the smallest distance measurement, indicating their closeness in this space. Compared to the intact state, the peptide co-modulator pairs were all statistically different. Compared to the decentralized state, however, the co-modulator pairs were not statistically different (Figure 3.2 B).

To visualize these data, we used principal component analysis and plotted the scores for each condition in the first three principal components as means as well as distributions which were fit with a convex hull. In the reduced principal component space, when only the means were considered, there was a clear separation between the intact and decentralized conditions with the peptide co-modulation pairs occupying the space in between (Figure 3.2 C). The separation of the intact and decentralized conditions along with the closeness of the co-modulated peptide means was also seen when the distributions were plotted (Figure 3.2 D). Here the distributions of the three peptide pairs overlapped with the RPCH + proctolin distribution bisecting the proctolin + CCAP and CCAP + RPCH distributions. All three co-modulator distributions also overlapped with the decentralized and intact distributions, occupying the space in between them.

**Triplet co-modulation further reduces differences in the four metrics of excitability.** The results with the paired peptide co-modulators suggested that peptide co-modulation was promoting consistency in the network output over flexibility. There was a single statistical difference in PD spike frequency across the three peptide pairs tested but no statistical differences between any pair when quantified in the network output space. While the peptide co-modulators were not different from each other, the network outputs of the co-modulator pairs were all statistically different from the intact. We next wanted to ask whether combining three modulators together would further reduce the degree of difference between these co-modulated outputs and whether combinations of three modulators could recapitulate the multiply modulated intact network output. Two modulator triplets were used in this evaluation: proctolin + CCAP + RPCH and CCAP + proctolin + oxotremorine. Oxotremorine, a muscarinic agonist, also activates $I_{MI}$ (Rosenbaum and Marder, 2018).

When qualified, the network output of CCAP + proctolin + oxotremorine appears similar to the network output of proctolin + CCAP + RPCH and both triplet network outputs qualitatively recapitulate the intact network output (Figure 3.3 A). As expected, there was also a clear qualitative difference between the modulated states and the decentralized.

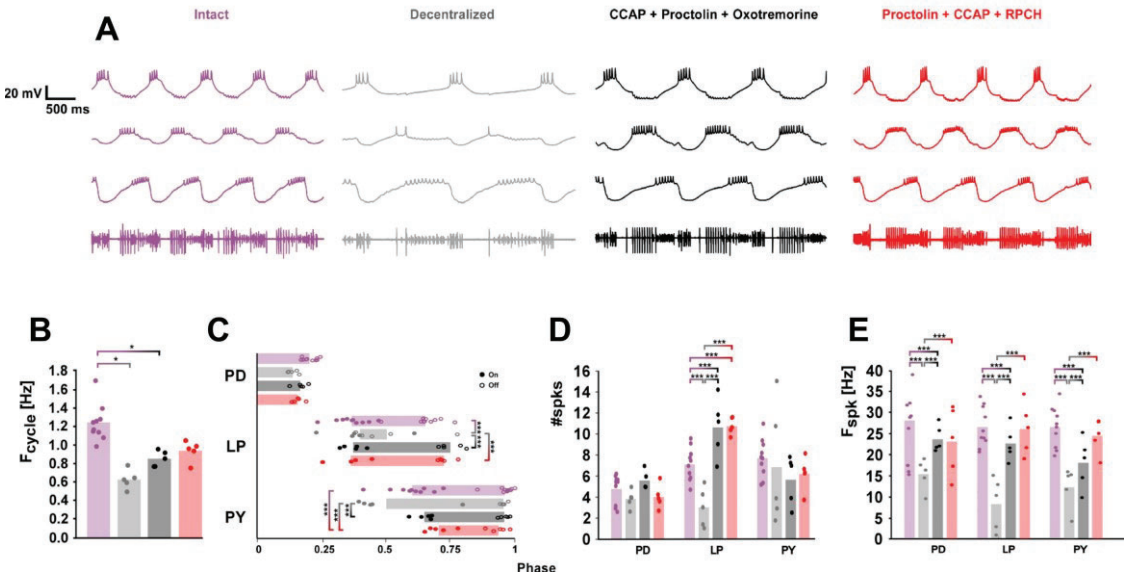


**Figure 3.3** Qualitative and quantitative response of the core pyloric neurons to triplet co-modulation. (A) The qualitative response of the core pyloric neurons to $10^{-6}$ M total concentration triplet co-modulator application. (B) Cycle frequency response across intact, decentralized and triplet co-modulator conditions. Bars represent mean cycle frequency responses and points represent individual animal responses. (C) Phase responses of the PD, LP and PY responses under intact, decentralized and triplet co-modulator conditions. Bars represent mean phase on and off values. Filled in circles represent individual animal phase on values and empty circles represent individual animal phase off values. (D) Spike number responses of the core pyloric neurons under intact, decentralized and triplet co-modulator conditions. Bars represent mean spike number responses across the five modulatory conditions while the individual points represent individual animal responses. (E) Spike frequency responses of the core pyloric neurons under intact, decentralized and triplet co-modulator conditions. Bars represent mean spike frequency responses across all modulatory conditions and individual points represent individual animal responses.

From the qualitative result we expected no differences between the triplet modulated states in any attribute and limited to no difference between the triplet modulated states and the intact. We did, however, expect differences between the modulated states and the decentralized state.

**Cycle frequency.** In the cycle frequency attribute, the intact response was statistically faster compared to the decentralized and CCAP + proctolin + oxotremorine response but there were no statistical differences between the decentralized and peptide triplet responses and no statistical differences between the peptide modulated responses themselves (One way ANOVA on ranks: $H_{(3)} = 19.715$, $p < 0.001$) (Figure 3.3 B).

**Phase.** There were no statistical differences in the phases of PD off or LP on. In the off phase of LP, the decentralized response was statistically different from the intact and both triple peptides. In the PY on phase, the intact response was statistically different from the proctolin + CCAP + RPCH triplet and the decentralized response was statistically different both triple peptide response. Lastly there were no statistical differences in the off phase of PY (Two way ANOVA interaction: $F_{(12,105)} = 2.925$, $p = 0.002$) (Figure 3.3C).

**Spike number**. There were no statistical differences in the PD spike number parameter. In the LP spike number parameter, the intact response was statistically lower than either triplet peptide combination and the decentralized response was statistically lower than the intact and both triplet peptide combinations. There were also no statistical differences in the PY spike number response (Two way ANOVA interaction: $F_{(6,63)} = 5.756$, $p < 0.001$) (Figure 3.3 D).

**Spike frequency.** A two way ANOVA with neuron type and modulator condition as factors did not reveal an interaction between these factors (Two way ANOVA

Factor = neuron type: $F_{(2,63)} = 0.859$, $p = 0.429$, Two way ANOVA Factor = modulatory condition: $F_{(3,63)} = 20.865$, $p < 0.001$, Two way ANOVA Interaction: $F_{(6,63)} = 0.869$, $p = 0.523$) but revealed a statistically significant effect of modulatory condition. Across the three neuron types in spike frequency, the intact response was statistically higher than the CCAP + proctolin + oxotremorine triplet but not the proctolin + CCAP + RPCH triplet. The decentralized response was also statistically lower than the intact and both triplet combinations (Figure 3.3 E).

**The triplet co-modulators are not different in the combined 12D network output space and are not different from the intact condition.** The lack of individual differences between the two triple modulator combinations suggested a further promotion of consistency in the pyloric network output while the network outputs were still different from the intact across some individual parameters. To fully quantify whether the two triplet modulator network outputs were holistically different from one another as well as the degree of difference between each triplet and the intact, we evaluated their z-scored differences in the 12-dimensional network output space (Figure 3.4 A) and visualized the distance in a reduced principal component space.

When quantified and statistically tested in the 12-dimensional space, the triplet of proctolin + CCAP + RPCH was not statistically different from the triplet of CCAP + proctolin + oxotremorine. The distance between the pair of triplets in the 12-dimensional space was not reduced in all cases, however, compared to paired co-modulator evaluations. This indicated that the combination of three modulators does not necessarily make the network output more similar compared to a combination of two peptides at the same total concentration. Interestingly, both triplets were not statistically different from the intact

condition but were different compared to the decentralized network output (Figure 3.4 B). This contrasted with the result from both the single modulators and peptide co-modulator pairs and suggested that the presence of three or more peptides was sufficient to capture the activity of the intact preparation though there are caveats to that suggestion.

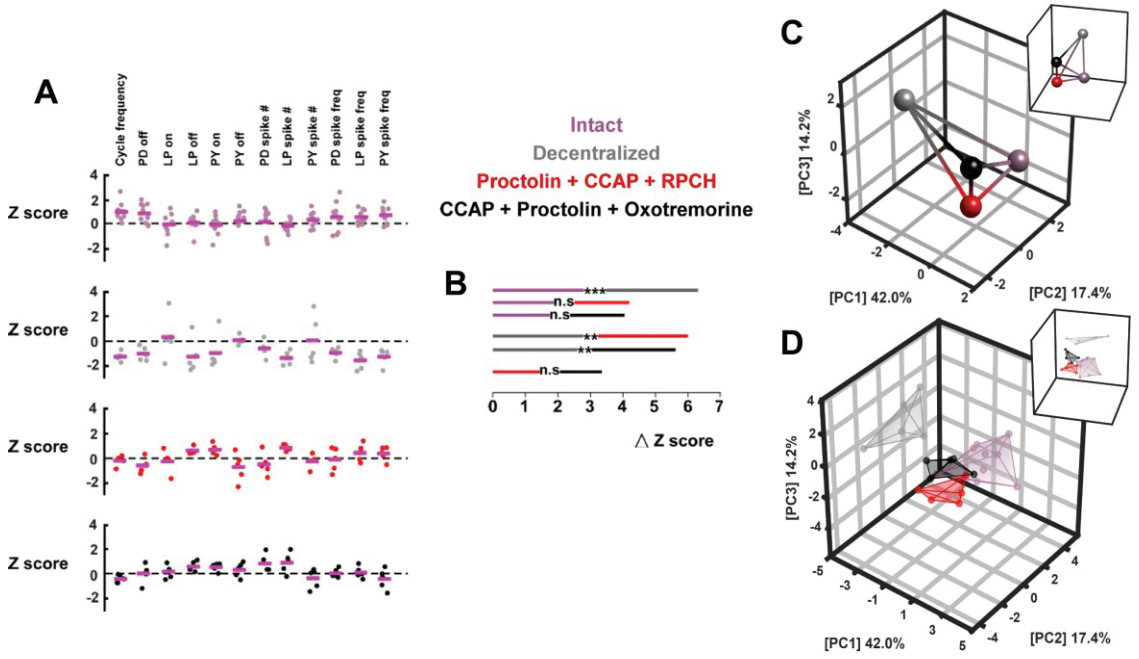


**Figure 3.4** Quantification and statistical testing of difference between triplet co-modulated network outputs. (A) All 12 parameters from the intact, decentralized and two triplet conditions were combined and z-score standardized prior to statistical testing. Magenta lines represent the mean z-score values. (B) Euclidean distance measurement between each pairwise comparison and determination of statistical significance in the 12-dimensional space. (C) Visualization of the mean network output space across all four conditions in a reduced 3-dimensional principal component space. (D) Visualization of the network output distributions of all four conditions in the reduced principal component space.

When the mean scores were visualized in the reduced principal component space, the separation between the intact and decentralized responses was apparent. Following triplet modulator application, the mean scores for both combinations shifted away similarly from the decentralized mean towards the intact mean (Figure 3.4 C). When the individual

observations were plotted and fit with a convex hull, the separation between the intact and decentralized responses seen with the means was recapitulated. These two conditions occupied distinct areas in the principal component space. The distributions of both triplet combinations, while not overlapping (Figure 3.4 D), were close to one another and were close to the intact distribution as well.

**Are co-modulated network outputs distinct from their constituent neuromodulator network outputs?** In the combined network output space, the co-modulator peptide pairs were not statistically different from each other nor were the co-modulator triplets. While these results suggest a convergence in the network output and a loss of flexibility, it is not known whether the co-modulated peptide outputs are different from the outputs of their constituent neuromodulators.

It has been previously shown that the individual effects of two peptides, RPCH and Cab-TRP, on the phases of the pyloric network of the American lobster, *Homarus americanus*, differ significantly. The co-applied rhythm, however, also differs significantly from either of the rhythms generated by its constituent neuromodulators (Thirumalai and Marder, 2002). The interplay of both peptides here creates a new niche in the network output space that is distinct from the single modulator conditions. This has also been shown in the prefrontal cortex with serotonin and dopamine, where changes in cortical neuron excitability during co-modulator application were distinct from changes during individual modulator application (Di Pietro and Seamans, 2011). While the co-modulated conditions considered here converge to the same network output space, rendering them not statistically different, the newly defined co-modulated network output

space may be distinct from the individual peptide output space. In this way, both flexibility and consistency can play distinct roles in transforming the network output.

To address this question, we statistically tested the 12-dimensional network outputs of each co-modulator peptide pair and triplet against the network outputs of each of their constituent peptides. We did not evaluate the effects of oxotremorine singularly therefore the triplet of CCAP + proctolin + oxotremorine was only compared to the network outputs of CCAP and proctolin. Before statistical testing all experiments from the single, co-modulator pairs and co-modulator triplets were combined, and z-score standardized. The z-scored 12-dimensional vectors were used to evaluated difference and the distributions were visualized by plotting the scores of each condition in the first three principal components and fitting the observations with a convex hull.

**Co-modulator peptide pairs are not different from their constituent modulators in network output space.** When the distribution of the proctolin + CCAP network outputs were plotted with the distributions of both constituent neuropeptides, the co-modulated network outputs bisected the individual neuropeptide distributions (Figure 3.5 A). The distribution of the CCAP + RPCH network outputs and RPCH + proctolin network outputs also bisected the individual distributions of their constituent neuromodulators (Figure 3.5 B and C). When statistically tested, there were no differences between any constituent and co-modulated network output in the 12-dimensional network output space (Figure 3.5 D).

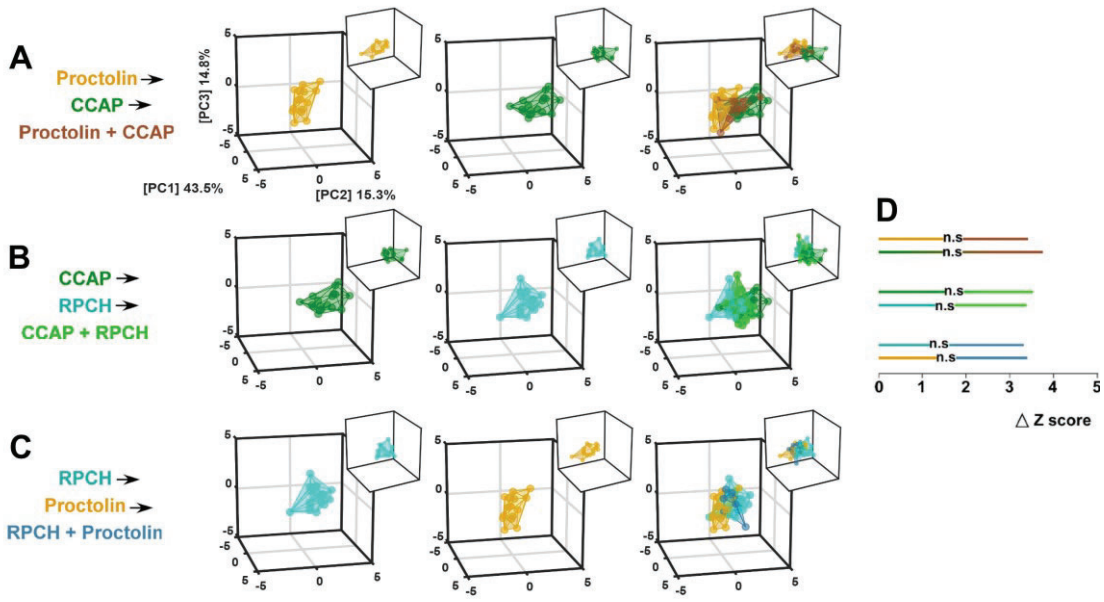


**Figure 3.5** Visualization of constituent and paired peptide co-modulated network outputs in principal component space. All data from the single modulator, paired peptide co-modulator and triplet peptide co-modulator conditions, including all intact and decentralized were initially combined and z-score standardized. Following standardization, principal component analysis was run and the scores were plotted and fit with convex hulls. To facilitate the visualization of the modulated distributions, the distributions of the intact and decentralized are not shown. (A) Individual distributions of proctolin, CCAP and the merged distributions of both constituent peptide modulators and proctolin + CCAP. (B) Individual distributions of CCAP, RPCH and the merged distributions of both constituent peptide modulators and CCAP + RPCH. (C) Individual distributions of RPCH, proctolin and the merged distributions of both constituent peptide modulators and RPCH + proctolin. (D) Euclidean distance measurement between each constituent peptide modulator and co-modulated condition and determination of statistical significance in the 12-dimensional network output space.

**The individual CCAP network output is statistically different from both the proctolin + CCAP + RPCH and CCAP + proctolin + oxotremorine network outputs.**

Lastly, each modulator triplet was statistically tested against its constituent modulators. When the individual distributions of proctolin, CCAP and RPCH were plotted with the distribution of the proctolin + CCAP + RPCH triplet, the triplet network outputs intersected

the three constituent network outputs (Figure 3.6 A). When the network outputs of both proctolin and RPCH were tested against the proctolin + CCAP + RPCH triplet, neither were statistically different. The CCAP network output, however, was statistically different from the triplet network output and had the largest mean distance out of the three individual peptides tested (Figure 3.6 C). When the individual proctolin and CCAP distributions were plotted with the CCAP + proctolin + oxotremorine distribution, the triplet distribution also overlapped with both constituents (Figure 3.6 B). When statistically tested, the proctolin network outputs were not different compared to the triplet network outputs. The CCAP network outputs, however, were statistically different from the triplet network outputs and resulted in a larger distance value compared to proctolin (Figure 3.6 C).

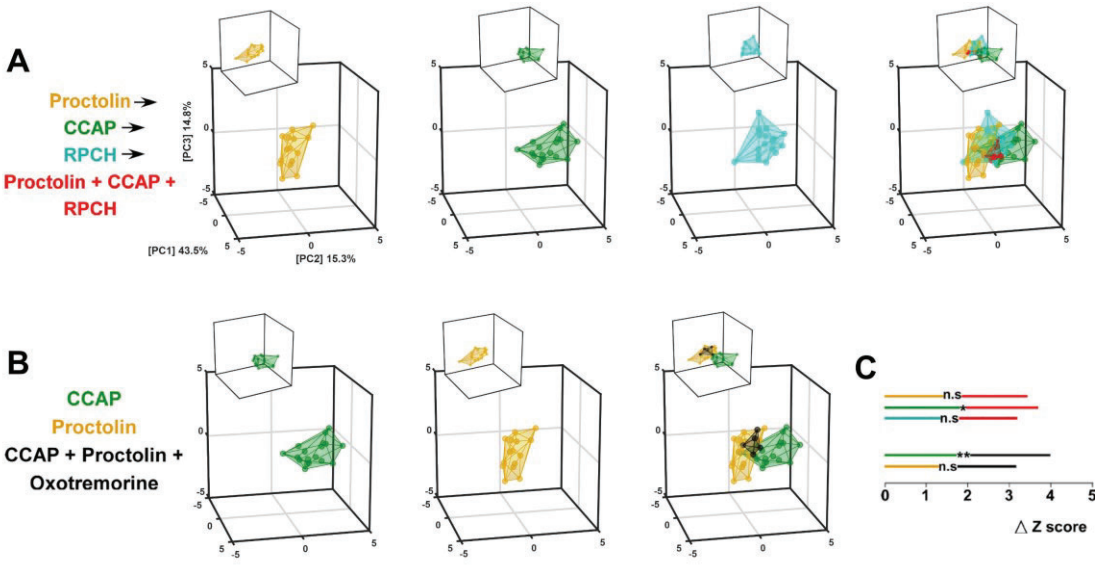


**Figure 3.6** Visualization of constituent and triplet modulator co-modulated network outputs in principal component space. Scores from principal component analysis were obtained from description in Figure 3.5. (A) Individual distributions of proctolin, CCAP, RPCH and the merged distributions of the three constituent peptide modulators and the proctolin + CCAP + RPCH triplet. (B) Individual distributions of CCAP, proctolin and the merged distributions of both constituent peptide modulators and the CCAP + proctolin + oxotremorine triplet. (C) Euclidean distance measurement between each constituent peptide modulator and the triplet co-modulated conditions and determination of statistical significance in the 12-dimensional network output

## 3.4 Discussion

**Convergent co-modulation with peptide pairs promotes consistency over flexibility at the level of the network output.** There are two general possibilities for the network output under co-modulatory conditions with two peptides: an increase in flexibility leading to distinct co-modulator network outputs or an increase in consistency leading to co-modulator network outputs that are not distinct from each other. When the co-modulator pairs were evaluated within the individual metrics of excitability, the number of differences decreased when compared to number of differences across the single modulator responses. The simplest explanation for this decrease in difference is a more complete and consistent

activation of the circuit components which generate these outputs. This decreases the importance of the individual peptide's identity.

Each neuropeptide targets a distinct but overlapping set of neurons in the circuit, leading to the differences seen when those single modulator outputs are evaluated quantitively. Proctolin in the pyloric network targets all neurons in the circuit while CCAP and RPCH target the same subset of neurons (Swensen and Marder, 2001). In this analysis, the peptide pairs of proctolin + CCAP and RPCH + proctolin were not statistically different in any individual attribute and were not statistically different in the 12-dimensional network output space. With these two pairs of co-modulators, we are combining the complete activation of the circuit by proctolin, adding one of two additional peptides which were not different individually and applying each modulator at half of the concentration used to evaluate its individual effects. The reduction in concentration reduces any signature effect, like CCAP's strong enhancement of LP spiking (Weimann et al., 1997). These three factors combined lead to a more blended effect and a lack of statistical difference. This, however, does not fully explain the result when both proctolin containing pairs were tested against the CCAP + RPCH pair.

The CCAP + RPCH pair was the only one to have any statistical difference across the co-modulator conditions, in PD spike frequency. While not activating the whole circuit, the lack of individual differences between both proctolin containing pairs and the CCAP + RPCH pair could be due to the lower concentration of proctolin used. While proctolin was present, it was used at a half saturating concentration. It may be that the circuit components targeted by proctolin alone, the PD and PY neurons, were not sufficiently activated. This reduced influence of proctolin may not have been enough to

allow for any proctolin specific differences to emerge which lead to a more consistent level of excitability across all pairs. Additionally, when visualized in the reduced principal component space, the co-modulated pairs also appear to be more tightly clustered compared to the single modulators. This suggests that not only are the network outputs across distinct co-modulator conditions becoming more consistent but the response to distinct co-modulator application across animals is becoming more consistent.

**Convergent co-modulation with peptide pairs is not different from the decentralized state but is different from the intact.** The co-modulated pairs evaluated here were not different from the decentralized network outputs when quantified in the 12-dimensional network output space which was surprising. Decentralization can produce a wide range of effects from no perceptible difference in network activity to a complete loss of activity (Hamood et al., 2015). In these co-modulator experiments, the decentralization process did not consistently result in substantial differences to the network output. Despite the individual statistical differences found throughout the individual parameters, the inconsistent decentralization process resulted in a large degree of overlap between the decentralized distributions and the paired peptide co-modulation distributions. The lack of statistical difference in the 12-dimensional space is a direct result of this overlap.

The intact state is often imagined as a state with any number of individual modulators present leading to complete activation of the circuit across animals. One possibility of paired co-modulation, at least with the pairs containing proctolin, is the generation of a pattern that replicates the activity profile of the intact state. When evaluated, however, these peptide pairs were still statistically different from the intact.

This indicates that two peptides alone, even at a combined saturating concentration, is not sufficient to mimic the complex neuromodulatory environment of the intact circuit output. **Convergent triplet co-modulation further promotes consistency at the level of the network output.** To test whether the pyloric network output could be pushed into a state that is even more consistent across peptide co-modulatory conditions we evaluated how different two triplet combinations were. Across the individual attributes as well as in the combined 12-dimensional space, there were no differences between the sets of triplet co-modulators. There were also no statistical differences in the 12-dimensional network output space between the two triplets and the intact network outputs. This suggests that combining three modulators does allow the network to reach a state where there are no individual statistical differences, further reducing the importance of peptide identity, and that combinations of three peptides can replicate the intact state. However, there are caveats to these suggestions.

The first caveat is the sample size. Compared to the analysis with both the single peptide modulators and the co-modulator pairs, the number of animals tested was lower. The lower sample size here could be masking differences that would be revealed with a larger sample size. The second caveat is the number and composition of triplets used. In previous analyses, three different groups were evaluated. Due to issues obtaining reliable peptides we could not test whether an additional triplet combination resulted in the same degree of similarity reported here. Additionally, a triplet should be tested which does not share a peptide with another combination. This would act as a control to ensure that the results seen here are not just a result of proctolin and/or CCAP being present.

**Paired peptide co-modulation does not result in a new niche within the network output space.** The co-modulated peptide pairs not being statistically different from each other suggests a mechanism of consistency over flexibility with respect to the network output. A role for flexibility could still exist in terms of distinct niches in network output space when moving from single to co-modulation. There is evidence of this in the stomatogastric nervous system although in a different species (Thirumalai and Marder, 2002). In this previously published work, the individually applied peptides generated non-triphasic rhythms but the combined effected restored the full rhythm in the American lobster, *Homarus americanus*. This suggests the idea that the sum of two peptides is greater than the individual effects and each peptide elicited output, whether single or co-modulated, occupies a distinct place in network output space.

The result with single versus paired co-modulators here does not support that suggestion. Here, the paired co-modulated outputs were not statistically different from any of their constituent neuromodulators. This suggests instead that paired peptide co-modulation at this concentration acts to average out the individual effects of each peptide to generate a blended network output. This can be seen clearly with the sequential PCA's where the co-modulated outputs occupied the space directly in between the individual peptide distributions. The difference in result between the previously published work and this current work could come from a difference in species, a difference in the approach to analysis or a combination of both.

**CCAP's dominating effects on the network output distinguish it from both triplet co-modulated network outputs.** Unlike the co-modulator pairs, both modulator triplets were statistically different from the individual CCAP network outputs but not from proctolin or

RPCH. In visualizing the distributions of the first triplet of proctolin + CCAP + RPCH and each of the constituents, there is clear overlap between the triplet and the proctolin and RPCH distributions. The distribution of CCAP, however, occupies a more distinct space particularly along the axes of PC 2 and PC 3. Unlike proctolin or RPCH, CCAP does have a signature effect when applied at a high concentration, highly exciting the LP neuron. The difference found between the proctolin + CCAP + RPCH triplet and CCAP on its own could be from the difference in concentration used. The individual CCAP observations were recorded at a concentration of $10^{-6}$ M, whereas the triplet observations were recorded using a total concentration of $10^{-6}$ M. Reducing the CCAP concentration by 1/3 in the triplet case could sufficiently dampen CCAP's strong effect in LP spike number leading to the difference found. Additionally, the difference found could be a result of a large sample size for the CCAP distribution and a low sample size for the proctolin + CCAP + RPCH triplet.

The same result was seen with the CCAP + proctolin + oxotremorine triplet. It is likely that the difference found with this triplet and CCAP is a result of the concentration difference and a smaller sample size for the triplet condition. Additionally, the individual effects of oxotremorine are missing. Oxotremorine is known to strongly activate the pyloric network following decentralization and is thought to be similar to proctolin in terms of its receptor distribution across the core pyloric neurons (Haddad and Marder, 2018; Rosenbaum and Marder, 2018). Qualitatively and to some extent quantitatively, the effects of oxotremorine on the network output are also similar to proctolin however in these previous studies, oxotremorine was applied at $10^{-5}$ M concentration. The concentration of oxotremorine used in this current work was lower therefore, it is hard to assume whether

individually applied oxotremorine would result in a new niche like CCAP or occupy the same general space as proctolin. However, given the similarity in network output generation compared to proctolin, a first pass assumption would be that it occupies a similar space to proctolin and would not be statistically different from the CCAP + proctolin + oxotremorine triplet.

**Is it possible to make the circuit flexible?** Central pattern generating circuits underly many important rhythmic motor behaviors which are fundamental to survival (Dickinson, 2006). With the static nature of these circuits, the necessity to generate distinct patterns of activity is thought to be facilitated by the presence of neuromodulators and it is highly unlikely that any circuit will be singularly modulated. The idea of network output flexibility suggests that a large population of individual neuromodulators can combine to form an even larger number of co-modulator combinations. Each of these combinations could then generate distinct patterns of activity.

While combinations of co-modulators with distinct cellular actions may generate distinct patterns, the convergent cellular mechanism of neuropeptides in the neurons of the pyloric network suggests an alternative possibility. Because the actions of peptides are convergent and consequently unidirectional, combining multiple peptides may instead generate more consistent network outputs as opposed to distinct and flexible ones.

The results presented here evaluating the effects of peptide co-modulation on the pyloric network output support the hypothesis that convergent co-modulation promotes consistency in the network output as opposed to flexibility. Co-modulation with neuropeptides in the pyloric network may function as a stabilizing feature to provide the circuit with multiple ways to achieve the same goal (Kitano, 2004). The requirement for

stable function over flexibility is not isolated to the pyloric circuit (Beliez et al., 2014) and may serve as a general principal for central pattern generators. While network output flexibility under co-modulatory conditions is lost in terms of the generation of distinct outputs, it could be look at as a different form of flexibility afforded to the circuit. Flexibility here comes from the ability to combine different combinations of peptides and still generate meaningful and functional outputs (Werner and Mitterauer, 2013).

The largest caveat to this finding, however, is the use of bath application to elicit a network output. Practically, this approach is much simpler but may not recapitulate what the intact animal is experiencing (Blitz et al., 1999). Additionally, the co-applied peptides used here combined both intrinsically released neuromodulators as well as ones that exist as circulating hormones. It is likely that these two classes of neuropeptide are released or circulate at different concentrations that the ones used here, particularly with CCAP (Weimann et al., 1997). The generation of distinct co-modulated peptide outputs may be achieved by adjusting the concentrations of both or all three peptides used to mimic more closely those of the intact animal, however, at this point we do not know what those concentrations are. Additionally, circulating neuromodulators have the ability to influence multiple aspects of a system whereas neuronally released neuromodulators, restricted by peptidases for example, may only influence a local neighborhood (Katz and Frost, 1996; Wood and Nusbaum, 2002). Knowing where each neuromodulator exerts its influences may uncover distinct actions on the circuit underlying a network output and consequently a difference in that network output.

# CHAPTER 4

# DISTINCT MONOAMINES DIFFERENTIALLY MODULATE ASPECTS OF THE PYLORIC NETWORK OUTPUT

## 4.1 Introduction

Monoamines such as dopamine and serotonin are pervasive in all systems and act to influence behavioral states such as sleep and wakefulness (Brown et al., 2012), locomotion (Gabriel et al., 2009; Brown et al., 2012; Slawinska et al., 2014), respiration (Viemari and Tryba, 2009), reward (Grace et al., 2007; Vaaga et al., 2014) and psychiatric disorders (Conio et al., 2020). Octopamine, also a monoamine, is derived from the same precursor as dopamine (Cole et al., 2005) and is structurally similar to noradrenaline in vertebrate systems (Roeder, 1999). Octopamine is a prevalent modulator in invertebrate systems and, like dopamine and serotonin, influences behaviors such as learning (Sabandal et al., 2020), locomotion, muscle contraction and modulation of the neuromuscular junction (Djokaj et al., 2001; Selcho et al., 2012; Ormerod et al., 2013).

In the stomatogastric nervous system, dopamine, octopamine and serotonin can reach the stomatogastric ganglion in multiple ways. Octopamine is released from descending modulatory inputs but does not circulate as a hormone (Barker et al., 1979). Dopamine can be released via descending modulatory inputs from upper end ganglia (Barker et al., 1979) or circulate as a neurohormone (Clark et al., 2008). Serotonin can be locally released via ascending sensory inputs as well as circulate hormonally (Beltz et al., 1984; Katz et al., 1989). Neurohormones typically circulate at much lower concentrations than locally released neuromodulators. This affords amines that operate in both domains a wide range of concentrations where they can exert influence.

Neuromodulators in the stomatogastric nervous system can be broadly divided into two classes: those with convergent cellular effects but divergent circuit effects and those with divergent cellular effects but convergent circuit effects. Neuropeptides converge cellularly to target a single inward current in distinct subsets of neurons. Amines, however, divergent cellularly to affect multiple currents within each neuron but converge by targeting most or all neurons within the circuit. It has been shown previously that all neurons in the pyloric network in the spiny lobster *Panulirus interruptus* respond to dopamine, octopamine and a subset of neurons respond to serotonin application (Flamm and Harris-Warrick, 1986a). Cellularly, dopamine and octopamine modulate a substantial number of intrinsic currents and synapses in a cell type specific manner which is receptor subtype mediated (Zhang and Harris-Warrick, 1994; Peck et al., 2001; Peck et al., 2006; Harris-Warrick and Johnson, 2010; Zhang et al., 2010; Johnson et al., 2011).

The effects of amine application in the crab *Cancer borealis*, however, are far less understood. Their cellular actions have not been investigated but their effects on the pyloric network output have been qualified and minimally quantified. What has been reported is a loss of rhythmic activity with dopamine application (Marder and Weimann, 1992), a variable version of the triphasic rhythm with serotonin application (Haddad and Marder, 2018) and a fully tri-phasic activity pattern following octopamine application (Goaillard et al., 2004).

Despite the caveats when quantifying the effects of single and co-applied peptides, flexibility does not appear to be the default effect of individual peptide neuromodulation and is lost with peptide co-modulation. The inflexibility with peptides is likely due to their convergence to a target which can only operate unidirectionally. If the activation of only

the modulator activated inward current ($I_{MI}$) is driving these peptide network outputs towards an inflexible state, the presence of an amine which does not act unidirectionally cellularly could allow for greater flexibility in pyloric network output.

Here we quantify the effects of three amines, dopamine, octopamine and serotonin, on the pyloric network output of the crab *C. borealis*. This will serve as the first fully quantitative description of these amines on this species pyloric network output. Additionally, this will allow for the continued testing of the network output flexibility hypothesis with a different class of neuromodulator and provide a baseline expectation as to the consequences of amine and peptide co-modulation.

## 4.2 Materials and Methods

**Methods.** The animals, electrophysiological approach, excitability attribute extraction, Euclidean distance and multi-variate permutation test calculation were the same as reported in Chapter 2.

**Statistical evaluation.** All initial statistical tests were performed in SigmaPlot. All statistical tests performed were one way ANOVAs except for the slow wave oscillation analyses which were either t-tests or paired t-tests. In all cases, following one way ANOVA testing, a Holm-Sidak post hoc test was performed. If the data initially failed a test for normality or equal variance, a one way ANOVA on ranks was performed. If the slow wave oscillation data initially failed a test for normality or equal variance a Mann-Whitney Rank Sum Test was performed instead of a t-test. Table A.4 summarizes all statistical tests and results for the excitability attribute analysis. Table A.5 summarizes all

statistical tests and results for the slow wave oscillation analysis. Statistical significance was determined as follows: * $p < 0.05$, ** $p < 0.01$, *** $p < 0.001$.

**Modulators and experimental protocol:** The preparation was decentralized by blocking the stomatogastric nerve (STN) with a $10^{-7}$ M TTX (Biotium) + 750 mM sucrose (Sigma) solution. Dopamine hydrochloride (Sigma) was prepared right before application by dissolving in distilled water to an initial concentration of $10^{-2}$ M. Dopamine was further diluted to the experimental concentration of $10^{-6}$ M in chilled *Cancer borealis* saline. Dopamine is highly light sensitive and care was taken to minimize exposure to light. CCAP (Bachem), serotonin hydrochloride (Sigma) and octopamine hydrochloride (Sigma) were diluted with distilled water, initially aliquoted to a concentration of $10^{-3}$ M and stored until needed. Final dilution of CCAP, serotonin and octopamine to the experimental concentration of $10^{-6}$ M occurred immediately before application in chilled *Cancer borealis* saline. Each neuromodulator was bath applied via peristaltic pump for 5 minutes. In cases of repeated application of amine, the first application was washed out in chilled *Cancer borealis* saline for a minimum of 30 minutes.

**Slow wave oscillation parameter extraction.** All Matlab code for the extraction of the slow wave oscillation attributes was written by Omar Itani.

All parameter extraction and analysis for the slow wave oscillation analysis of PD was performed in Matlab with custom written scripts. The attributes extracted and quantified were the amplitude, half-width, spike prominence, inter-spike interval, area of synaptic input from the LP neuron to the PD neuron and the trough voltage (see Figure 4.4 A). A minimum of 15 cycles of activity were analyzed and the individual points plotted represent the mean for each animal.

Briefly, the amplitude of the slow wave oscillation was measured by low pass filtering the PD waveform to remove the spikes and the smoothed peak voltage was subtracted from the trough voltage. The half width was calculated by initially finding the half prominence of the oscillation amplitude. From the half prominence voltage, the start and end of the oscillation in time was determined by when the rising or falling slopes of the oscillation crossed the half prominence voltage. The half width reported was the difference of the end and start times. The spike prominences were determined by signal detection. The reported mean value for each animal was the mean spike prominence for all spikes detected across all cycles analyzed. The mean inter-spike interval was calculated by taking the difference in time between each spike detected and then averaging all inter-spike intervals across all cycles of activity. The mean synaptic area was calculated by initially taking the start of the presynaptic neuron's burst in time (the LP neuron) and finding the voltage of the postsynaptic neuron (the PD neuron) at that time. This voltage represented the threshold of synaptic area. The area of the trough under that threshold voltage was then calculated. Lastly the trough voltage was extracted from the amplitude measurement.

**N for excitability bar plots.** Intact: 29 phase and cycle frequency, 24 spike number and spike frequency. Decentralized: 33 phase and cycle frequency, 28 spike number and spike frequency. Modulators: 8 dopamine, 4 octopamine, 5 serotonin (only for phase and cycle frequency analysis) and 18 CCAP. Serotonin was only evaluated with extracellular recordings and was not included in the 12-dimensional analysis. Serotonin's intact and decentralized values were included only for the individual phase and cycle frequency analyses. The CCAP experiments were the same used in Chapter 2.

**N for 12-dimensional network output analysis:** 24 intact, 28 decentralized, 8 dopamine, 4 octopamine, 18 CCAP.

**N for PD slow wave oscillation analysis not including paired trough analysis:** 8 decentralized, 8 dopamine.

**N for paired PD trough analysis:** 7 decentralized and dopamine. In one experiment there was no quantifiable decentralized response forcing the exclusion of the dopamine response from the paired trough analysis.

## 4.3 Results

**Dopamine network outputs recapitulate the decentralized state whereas octopamine and serotonin generate network outputs which resemble a peptide modulated state.** The effects of dopamine, octopamine and serotonin on the core pyloric neurons in crab are not well described. What has been reported is a loss of tri-phasic activity under dopamine conditions, a retention of tri-phasic activity under octopamine conditions and a highly variable response to serotonin. Though acting as a starting point, the effects of dopamine and octopamine have not been thoroughly quantified for all neurons of the core pyloric network using both intracellular and extracellular recordings. Therefore, we sought to both qualify and quantify the effects of these amines on the same attributes of excitability evaluated under the peptide conditions. The serotonin experiments only used extracellular recordings and could not be included in the quantitative description outside of cycle frequency and phase. We included the effects of CCAP as well to test whether a peptide elicited network output differs from an amine generate network output, given their distinct cellular mechanisms.

The effects of CCAP on the network output were evaluated in Chapter 2, therefore we have an expectation as to its actions. It is more difficult to have an expectation as to the effects of the amines on these attributes of excitability. At a minimum we expect differences in phase between the amine responses and the intact and CCAP responses. From the hypothesis presented in Chapter 2, the intact and CCAP phase responses are not statistically different due to $I_{MI}$ activation solely in the pacemaker neuron. Neuropeptides do not modulate other intrinsic currents like the A-type potassium current or the hyperpolarized activated inward current (h current), both of which can shift the phase responses of the pyloric neurons, but dopamine does (Harris-Warrick et al., 1995a; Harris-Warrick et al., 1995b). If we assume a similar modulation of these currents by dopamine in the pyloric neurons of *C. borealis* then we would expect differences in phase between dopamine, CCAP and the intact state. It is not known whether octopamine and serotonin also modulate the A-type potassium current and h current but if they do, there should be a statistical difference in phase between octopamine, serotonin and the intact and CCAP.

Qualitatively, dopamine, octopamine and serotonin generated tri-phasic activity though the activity profile of dopamine resembled the decentralized state while octopamine and serotonin's activity profile resembled that of the reference peptide CCAP or the intact state (Figure 4.1 A). When quantified, there were no differences between the decentralized state, the three amines and CCAP in the cycle frequency attribute, though all were different from the intact (One way ANOVA: $F_{(5,91)} = 47.527$, $p < 0.001$) (Figure 4.1 B).

In the phase attribute, the decentralized and CCAP responses were statistically different from both the intact and dopamine responses in PD off (One way ANOVA on ranks: $H_{(5)} = 27.758$, $p < 0.001$). In the LP on phase only CCAP was statistically different

from serotonin (One way ANOVA on ranks: $H_{(5)} = 21.067$, $p < 0.001$). In LP off, the decentralized response was statistically different from serotonin and CCAP (One way ANOVA on ranks: $H_{(3)} = 47.362$ $p < 0.001$). In the PY on phase, the decentralized response was statistically different from the intact and CCAP conditions (One way ANOVA: $F_{(5,91)} = 7.852$, $p < 0.001$) while there were no statistical differences in PY off phase (One way ANOVA on ranks: $H_{(5)} = 5.844$, $p = 0.322$). Interestingly, the three amines themselves were not statistically different from each other in any phase (Figure 4.1 C).

In PD spike number, the intact responses were statistically larger than the decentralized or CCAP responses (One way ANOVA on ranks: $H_{(4)} = 14.095$, $p = 0.007$). In LP spike number, the CCAP responses were statistically higher from all other conditions and the intact response was statistically larger than the decentralized and dopamine responses (One way ANOVA: $F_{(4,69)} = 45.824$, $p < 0.001$). In PY spike number the only statistical difference was between the decentralized response and the octopamine and CCAP responses (One way ANOVA on ranks: $H_{(4)} = 16.574$, $p = 0.002$) (Figure 4.1 D).

Lastly, the intact response was statistically different from all conditions except octopamine in PD spike frequency (One way ANOVA on ranks: $H_{(4)} = 43.076$, $p < 0.001$). In LP spike frequency, the intact response was statistically different from all conditions except CCAP and CCAP was statistically different from the decentralized, dopamine and octopamine responses (One way ANOVA: $F_{(4,77)} = 41.932$, $p < 0.001$). In PY spike frequency, the intact response was statistically different from all other responses (One way ANOVA on ranks: $H_{(4)} = 48.209$, $p < 0.001$) (Figure 4.1 E). Like with cycle frequency, phase and spike number, there were no statistical differences across the individual amine responses.

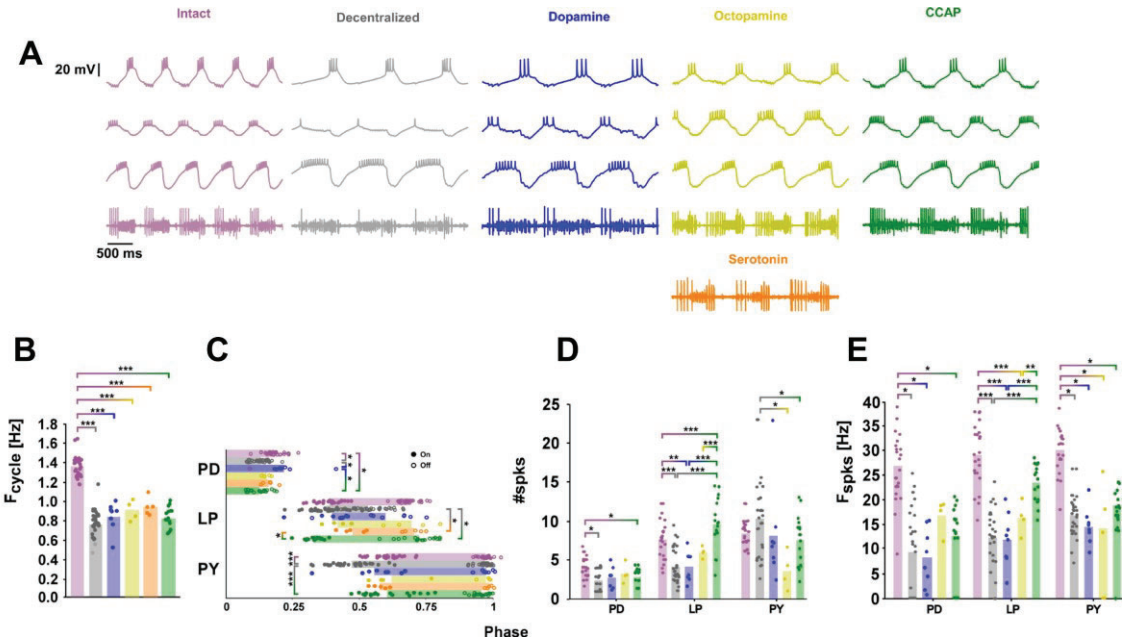


**Figure 4.1** Qualitative and quantitative pyloric network response to amine modulation. (A) Qualitative response of the core pyloric neurons under intact conditions, decentralized, dopamine, octopamine, serotonin and CCAP. All modulators were applied at $10^{-6}$ M concentration. (B) Cycle frequency response following distinct amine and peptide application. Bars represent means and individual points represent individual animal responses. (C) Phase response following distinct amine and peptide application. Bars represent mean phase values and individual points represent individual animal responses. Closed circles indicate the phase onset of each neuron, open circles indicate phase offset of each neuron. (D) Individual pyloric neuron spike number response following distinct amine and peptide application. Bars represent means, individual points represent individual animal responses. (E) Individual pyloric neuron spike frequency responses following distinct amine and peptide application. Bars represent means, individual points represent individual animal responses.

**Dopamine is not different from decentralized or octopamine in the combined 12D space but is different from a peptide response**. The qualitative observation that dopamine's activity profile matches the decentralized activity profile while octopamine's matches to different degrees intact and CCAP is supported quantitatively in the attributes of excitability. Due to the dependencies across these attributes, individual statistical tests are not sufficient to assess the actual degree of difference across these modulatory states. We, therefore, combined all 12 parameters of activity across the four attributes of

excitability into condition specific vectors, z-score standardized all values (Figure 4.2 A) and ran the Euclidean distance and multi-variate permutation test analysis. Because the serotonin experiment did not include intracellular recordings, those data were excluded from this analysis.

In the 12-dimensional network output space, the intact network outputs were statistically different from all other conditions tested with the intact verses decentralized comparison having the largest distance measured, indicating the greatest difference. The decentralized network outputs were not statistically different from the dopamine network outputs but were statistically different from the octopamine and CCAP network outputs. Like the intact, the CCAP network outputs were also statistically different from the decentralized, dopamine and octopamine network outputs while the dopamine and octopamine network outputs were not statistically different from each other. The dopamine and octopamine comparison also resulted in the smallest distance value among all the comparisons in this analysis, indicating their similarity in this space (Figure 4.2 B).

These statistical results were visualized in a reduced 3-dimensional principal component space. When the mean scores were plotted, there was a clear shift in mean score between the intact and decentralized conditions. When dopamine, octopamine or CCAP were applied, all three modulated conditions shifted away, in varying degrees, from the decentralized, with the dopamine response remaining the closest (Figure 4.2 C). When the distributions were plotted and fit with convex hulls, the intact distribution occupied a distinct space from all other conditions. The octopamine and CCAP distributions overlapped and both shared space with the dopamine distribution. The dopamine

distribution also shared the most overlap with the decentralized distribution in the principal component space (Figure 4.2 D).

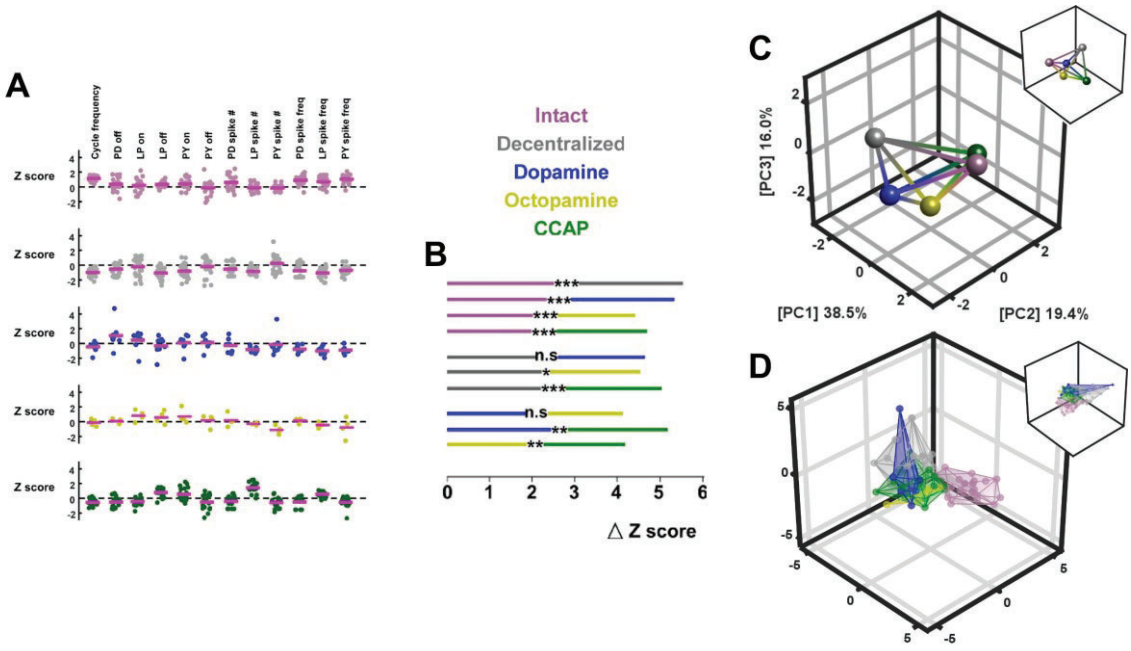


**Figure 4.2** Euclidean distance measurements and statistical testing of the 12D network outputs across distinct modulatory conditions. (A) Z-scored values for all conditions tested. Magenta line represents the z-score mean. (B) Euclidean distance measurements between all pairwise comparisons. (C) Projection of the 12-dimensional network outputs means in the first three principal components. (D) Projection of 12-dimensional network outputs distributions in the same principal component space as the means. Each individual point represents an individual animal. All distributions were fit with a convex hull.

**Dopamine application can generate a gradient of responses in the network output from tri-phasic functional to non-functional or quantifiable.** Our basic assumption in quantifying the effect of a neuromodulator on the pyloric network output is a difference between each modulator's effects and the baseline decentralized state. When statistically tested, either as individual attributes or in the combined 12-dimensional network output space, there were no differences between dopamine and decentralized. This would suggest that dopamine has no effect on the pyloric network output.

Unlike the peptides or octopamine, the application of dopamine to the pyloric network generated inconsistent responses. While some dopamine elicited rhythms were tri-phasic, others were either abnormal looking or showed a complete loss of tri-phasic activity (Figure 4.3 A-B). These abnormal or non-functional rhythms were the direct result of dopamine application because full tri-phasic activity resumed once dopamine was washed out. Unlike dopamine, octopamine never resulted in a non-functional network output. Because of the requirement of tri-phasic activity for the multi-variate statistical analysis, we could not include those abnormal or non-functional dopamine responses. By losing those dopamine network outputs, we were not able to fully profile the effects of dopamine on the pyloric network and were intentionally testing rhythms generated from only a subset of dopamine's network output space.

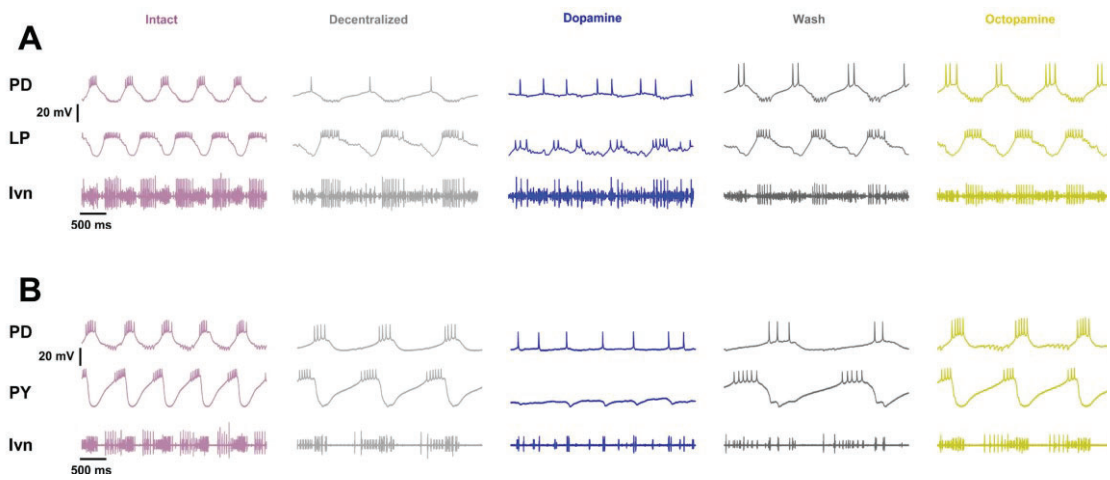


**Figure 4.3** Abnormal and non-functional dopamine elicited pyloric network outputs. (A) Following decentralization, $10^{-6}$ M dopamine application resulted in an abnormal pyloric network output. Notably, dopamine application resulted in a loss of stereotyped oscillatory activity of the PD and LP neurons. Activity was restored following a wash in saline and $10^{-6}$ M octopamine application resulted in quantifiable tri-phasic activity. (B) In a separate experiment, $10^{-6}$ M dopamine application resulted in a loss of pyloric activity. In addition to a loss of oscillatory activity, the PD neuron tonically fired, the PY neuron stopped firing completely and the extracellular recording showed no rhythmicity. A normal pyloric network was restored following a wash in saline and octopamine generated a quantifiable tri-phasic pyloric network output.

**The quantification of PD's slow wave oscillation and spiking attributes allows for an emergence of differences between decentralized and dopamine**. The example traces of both the abnormal and non-functional dopamine network outputs indicated that dopamine did have an effect on the pyloric network, but its effects were not always quantifiable with our previous approach. Outside of dopamine inconsistent effects on the excitability attributes evaluated, when quantifiable, dopamine application often resulted in changes to the slow wave oscillations of the pyloric neurons.

Dopamine modulates potassium, calcium, leak and synaptic currents in the pyloric neurons in *P. interruptus* (Harris-Warrick et al., 1995b; Kloppenburg et al., 1999; Peck et

al., 2001; Harris-Warrick and Johnson, 2010) and presumably does so in the pyloric neurons of *C. borealis*. These currents help to shape aspects of the underlying slow wave oscillation such as the inter-spike interval and half width. Conversely and importantly, peptides do not modulate these intrinsic currents.

Therefore, we quantified the effects of dopamine on attributes of PD's slow wave oscillation and spiking behavior not captured with the previous analysis (Figure 4.4 A). The choice to use PD came from its role as part of the pacemaker ensemble, its simpler waveform compared to LP and PD does not typically lose all activity under decentralized and dopamine conditions like the PY neuron. It may be that dopamine's effect can be differentiated from decentralized outside of the four attributes of excitability evaluated previously.

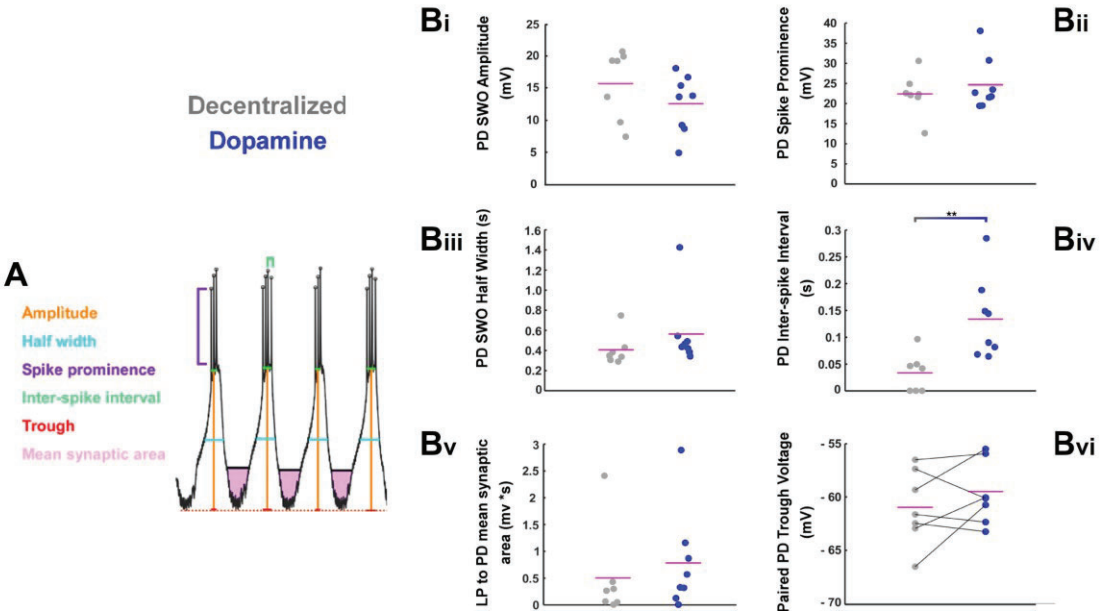


**Figure 4.4** Quantification and statistical testing of the PD neuron's slow wave oscillation (SWO) and spiking attributes. (A) Attributes extracted from the PD waveform. (Bi – Bvi) Individual attributes of PD's activity under decentralized or dopamine conditions. Magenta line represents the mean, and each individual point represents an individual animal's response. For the trough voltage analysis, each animal's modulated response was paired with its initial decentralized state.

**Amplitude of PD's slow wave oscillation.** It has previously been shown that the negative slope region of $I_{MI}$, which can be approximated as a linear leak conductance, is sufficient to restore oscillations in the PD neuron during ongoing activity in the absence of neuropeptides (Zhao et al., 2010). Dopamine modulates leak current in the anterior burster (AB) in *P. interruptus* (Harris-Warrick and Johnson, 2010) but it is unknown if dopamine modulates leak current in the PD neuron of *C. borealis*.

When quantified, the amplitude of PD's slow wave oscillation following dopamine application was not statistically lower compared to the decentralized, though there was a decrease in the mean value (two tailed t-test: t= 1.223, p = 0.243) (Figure 4.4 Bi).

**Mean spike prominence.** The height of the action potentials riding on top of the slow wave oscillation is related to the concentration of sodium. In *P. interruptus* dopamine modulates the persistent sodium current in the AB neuron which is electrically coupled to the PD neuron and makes up the pacemaker group (Harris-Warrick and Johnson, 2010). We therefore wanted to quantify whether dopamine or octopamine application modulated this attribute via a presumed modulation of sodium current in the pacemaker group. When statistically tested, there were no differences between any condition in mean spike prominence (two tailed t-test: t= -0.732, p = 0.477) (Figure 4.4 Bii).

**PD's slow wave oscillation half width.** The half width of the slow wave oscillation is dependent on both calcium currents for the depolarizing portion of the oscillation and calcium dependent potassium currents for the termination of the oscillation (Franklin et al., 2010). In *P. interruptus* dopamine decreases calcium currents in the PD neuron while increasing the calcium dependent potassium current (Johnson et al., 2003; Harris-Warrick and Johnson, 2010). The effect of this modulation would be a reduction in the PD's half

width compared to an unmodulated state. When quantified, there was no statistical difference between the decentralized and dopamine responses (Mann-Whitney Rank Sum Test: U = 12.00, p = 0.072) (Figure 4.4 Biii).

**PD's inter-spike interval.** Spiking activity, including the inter-spike interval, is a form of communication and information (Stein et al., 2005) and distinct alteration to spiking activity under specific modulatory conditions may signal to downstream areas the need for a particular behavior. The minimum inter-spike interval is limited by the refractory period but changes in potassium currents can alter the inter-spike interval (Zakharov et al., 2016; Ha and Cheong, 2017). In the cases where PD fired only a single spike per cycle or was not spiking, the inter-spike interval was 0 for that animal. There was a statistical difference in inter-spike interval between the dopamine response and decentralized (two tailed t-test: t= -3.197, p = 0.007) (Figure 4.4 Biv).

**LP to PD mean synaptic area.** The LP neuron provides the sole feedback via chemical synapse to the pacemaker group and this synapse is modulated by dopamine in *P. interruptus* (Johnson and Harris-Warrick, 1997; Ayali et al., 1998) though it is not known if dopamine modulates this synapse in *C.borealis*. When statistically tested, the dopamine response was not statistically different from the decentralized responses (Mann-Whitney Rank Sum Test: U = 17.50, p = 0.232) (Figure 4.4 Bv).

**PD's Trough voltage**. The voltage at the trough of an oscillation is primarily dependent on synaptic strength. The LP to PD synapse is glutamatergic and has a reversal potential of approximately -70 mV (Goaillard et al., 2009). Therefore, if a modulator was strengthening the synapse between the LP and PD neurons, the trough voltage of PD would shift towards the reversal potential of the synapse. In addition to being dependent on the

properties of the synapse, the measured trough voltage is also dependent on the impalement of the neuron. Therefore, the modulated responses were paired with their initial decentralized state and statistically tested with paired t-tests. When statistically tested, there was no significant change in the trough voltage in the presence of dopamine (two tailed paired t-test: $t = -1.106$ , $p = 0.311$) and its respective decentralized state (Figure 4.4 Bvi).

## 4.4 Discussion

The pyloric network output is a result of the combined effects of neuropeptides and amines. While the effects of peptides have been well described and quantified, the effects of amines have not been widely studied. We were interested in exploring the effects of amines on the pyloric network output for two primary reasons: to fully qualify and quantify the effects of amines on the *C. borealis* pyloric network which have not been reported and to test the hypothesis that non $I_{MI}$ activating neuromodulators also generate distinct network outputs.

Here we show the first fully quantitative exploration of the effects of dopamine and octopamine in this system in four metrics of excitability as well as in PD's slow wave oscillation. We also show, briefly, the effects, of serotonin on two attributes of the network output.

**When tri-phasic, dopamine recapitulates a decentralized network output while octopamine generates peptide like behavior**. The effects of amines have been explored widely in the spiny lobster *P. interruptus*, with the effects of dopamine being best characterized. Not only has the effect on the network output been qualified (Flamm and Harris-Warrick, 1986b) but the intrinsic currents which are modified by dopamine (Harris-Warrick and Johnson, 2010) and the receptor subtypes which mediate this modulation have

been characterized (Clark et al., 2008; Oginsky et al., 2010; Zhang et al., 2010). The effects of serotonin application have also been reported along with the identification of two serotonin receptors (Clark et al., 2004; Spitzer et al., 2008). Unlike dopamine and serotonin, the cellular mechanism of octopamine signaling is not known in *P. interruptus* but octopamine receptors in other species such as *D. melanogaster* are similar to vertebrate adrenergic receptors (Evans and Maqueira, 2005; Perez, 2006; Farooqui, 2012).

Conversely, the effects of these amines have not been well characterized in the pyloric network of the Jonah crab *C. borealis* outside of a qualitative assessment of both dopamine and serotonins actions and a qualitative and minimally quantitative assessment of octopamine's actions. These works showed a loss of functional activity with $10^{-6}$ M dopamine application (Marder and Weimann, 1992), a functional network output which strongly activates the pacemaker and the PY neurons without strong activation of the LP neuron with $10^{-4}$ M octopamine application (Goaillard et al., 2004) and a variable but sometimes functional network output with $10^{-5}$ M serotonin (Haddad and Marder, 2018) but irregular pyloric neuron activity with $10^{-4}$ M serotonin application in a related crab species (Beltz et al., 1984).

The lack of information regarding receptor subtype, cellular targets and a difference in concentration used between those previous works and this current work, which used $10^{-6}$ M amine application, makes predicting the consequence of amine modulation of the pyloric network output challenging. However, we can use those works as a starting point. Keeping the concentration of amine used here in mind, we would expect to see a similar loss of functional activity with dopamine application, a functional output with octopamine but with less robust pacemaker and PY activity and limited LP activity and a tri-phasic

serotonin network output if the higher concentration used is leading to the inconsistency in output previously reported. Additionally, the concentrations used here, while lower, are not biologically unrealistic. It is likely that the concentrations used previously are far higher than what would be found in the fully intact animal.

When evaluated qualitatively, the dopamine elicited network output appears similar to the decentralized baseline state whereas the octopamine network output resembles a peptide or intact baseline state. For octopamine, the results presented here met our expectations while the network responses following dopamine were somewhat contrary to our expectation. Important to note though was the state of the network before the application of these modulators.

In the previous work examining the effects of dopamine on the network output, the decentralized state before dopamine application was quiescent. In the example traces used here, the state of the network before amine application was slow but still functional. The response to decentralization today is distinct from the response in the past and preparations rarely cease activity and instead slow down and/or have a loss of LP activity. The effect of neuromodulators is highly state dependent (Nusbaum and Marder, 1989). This departure from the traditional response to decentralization may explain why these recordings did not consistently match the expectations we had for the dopamine response.

With serotonin, the previous work in *C. borealis* reported a highly variable responses to $10^{-5}$ M application. However, when qualified at 11°C, similar to the temperature used in these experiments, a fully functional tri-phasic rhythm was generated in the majority of cases (Haddad and Marder, 2018). While there was a degree of variability in those responses, other published work which used a higher concentration of

serotonin reported a loss of consistent tri-phasic activity in a related crab species (Beltz et al., 1984). Taken together, the highly variable response to serotonin appears to be both a function of temperature as well as concentration. Here, the expectation for serotonin application at lower concentration and at a more typical experimental temperature was met.

**Quantitively, dopamine's modulation of the four metrics of excitability is not different from the decentralized response while octopamine generates a potentially unique pattern of activity.** When quantified with traditional statistics there were a number of differences between the intact state and the amines and peptide used which was not unexpected. The intact state is a multiply modulated one so it was not surprising that a single amine or peptide could not replicate it. Primarily, these differences were found in the cycle frequency and spike frequency attributes. What was surprising though was octopamine's response in phase compared to the intact state. Out of the three amines tested, octopamine most closely replicated the intact phase response though we do not know how octopamine modulates this circuit cellularly.

Unlike the intact state, there were fewer quantitative differences between the amine modulated states and the decentralized. The primary differences between decentralized and dopamine, serotonin and octopamine responses were the PD off and LP off phases and PY spike number respectively. The lack of additional statistical differences in the phase and spiking attributes between the amine modulated conditions and the decentralized state could be due to an insufficient concentration of amine used. The effects of amines have been shown to be highly concentration dependent (Flamm and Harris-Warrick, 1986b) though the statistically significant effects in the PD off phase and PY spike number

attributes by dopamine and octopamine suggest that at $10^{-6}$ M concentration these amines did have some effect.

Among the modulators, there were statistical differences between the amine responses and CCAP in the phases of PD off, LP on, LP spike number and LP spike frequency. CCAP, through $I_{MI}$ activation, is known to have profound effects on LP spike number and frequency (Weimann et al., 1997) while the effects of dopamine and octopamine are limited in these parameters and do not differ from the decentralized. The differences in phase between the peptide and amine modulated states are more interesting though.

The hypothesis presented in Chapter 2 suggests that phase maintenance with peptide application is a direct result of $I_{MI}$ activation in the AB neuron while $I_{MI}$ activation in the follower neurons only modulates individual parameters of excitability like spike number and frequency. This hypothesis explains the lack of differences between the intact and CCAP states in the phase attribute. Additionally, peptides do not modulate intrinsic currents like the A-type potassium current or the h current which can advance or delay phase, but dopamine does in *P. interruptus* (Harris-Warrick et al., 1995a; Harris-Warrick et al., 1995b; Martinez et al., 2019). We do not know if dopamine similarly modulates these currents in the pyloric neurons of *C. borealis* and we do not know the cellular effects of serotonin or octopamine modulation. However, the phase shifts presented here suggest that these amines may be modulating these currents and possibly in conjunction with the synaptic currents to shift the phases of the pyloric neurons in ways that are not possible with peptides.

It was surprising that there were no statistical differences between dopamine and octopamine, though the mean values of several of the parameters were different between them. This is likely related to the sample size of octopamine, and differences between these two amine states may become statistically meaningful with additional experiments. Additionally, because the effects of amines are concentration dependent (Flamm and Harris-Warrick, 1986b), the lack of differences across the amine network outputs would likely change if they were applied at a higher concentration. Using the results presented here, as well as what has been previously published, we would expect an abnormal and potential loss of tri-phasic activity with a higher concentration of serotonin, a complete loss of tri-phasic activity with a higher concentration of dopamine but a retention of functional activity with higher octopamine concentration. While these network outputs would be qualitatively distinct, it is unclear how those activity patterns could be quantified and tested against each other.

**In the 12D network output space dopamine does not positively modulate the excitability metrics but octopamine may be acting as a bridge across distinct conditions**. Due to the dependent nature of these attributes, evaluating them holistically in a combined 12-dimensional space is necessary. When the intact network outputs were tested against the decentralized and modulator network outputs, the intact was statistically different from all. This matches our expectation from the individual attribute quantifications. What was surprising was octopamine's closeness in both distance as well as mean principal component score to the intact. While not able to completely replicate the intact state, an octopamine modulated pyloric network output can generate a rhythm which is more similar to the intact state than a peptide. This consistent generation of tri-

phasic activity by octopamine provides the network with an opportunity to generate what we would consider functional activity without solely relying on $I_{MI}$ activation via neuropeptides.

When the modulated states were tested against the decentralized, both CCAP and octopamine were statistically different. This was not surprising for CCAP and indicated that, despite the small number of individual statistical differences between decentralized and octopamine, an octopamine network output is a distinct state. The dopamine network outputs, however, were not statistically different from the decentralized network outputs. From the qualification and quantification of dopamine's effects on the pyloric network this result was not surprising. This would also suggest that dopamine had no effect on the network output, though from what was reported here, dopamine's actions are more complex than what was quantified in that analysis.

From the qualitative assessment as well as the statistical analyses, it was apparent that dopamine did not function like a peptide in this system. When the network outputs of dopamine and CCAP were statistically tested in the 12-dimensional network output space, they were different. The CCAP network output response was also statistically different than octopamine. Unlike the result with dopamine, the statistical difference between CCAP and octopamine represented flexibility, distinct cellular mechanisms which generate tri-phasic pyloric activity. The lack of statistical difference in the 12-dimensional space between dopamine and octopamine was surprising, though, like the lack of statistical differences when the attributes were evaluated individually, this is likely due to the low sample size of octopamine.

A general principal that can be taken from the results comparing the network outputs between amines and CCAP is that neuromodulation in the pyloric network is not unidirectional. The action of applying any single neuromodulator, whether peptide or monoamine, does not automatically push the network into an excitable state and can instead result in a gradient of effects. Dopamine application, when a tri-phasic rhythm is maintained, can minimally alter the phases of the pyloric network but not do much else. Dopamine can also completely disrupt or shut down the rhythm. Octopamine, on the other hand, functions as an intermediary modulator, one whose actions are distinct, functional but not hyperexcitable.

**The highly restrictive nature of the 12D excitability analysis intentionally excludes experiments with strong dopamine responses.** Dopamine application to the pyloric network was unpredictable. In total, 20 experiments were done using dopamine, however six of those experiments were not usable due to a complete loss of functional activity. In addition to a complete loss of functional activity, the requirement of simultaneous intracellular recordings of the PD and PY neurons forced the exclusion of six additional experiments. Intracellularly recorded PD and PY activity is necessary because these neurons exist in multiple copies in the ganglion and their activity can summate. This makes extracting reliable spike number or frequency information from extracellular recordings difficult. In three experiments which were excluded because a PD or PY neuron could not be recorded intracellularly, a clear effect of dopamine was present.

This intentional exclusion of experiments creates a very narrow window into the wider range of outputs dopamine can generate. With this approach, we are intentionally reducing the possibly of finding differences between the dopamine and decentralized and

dopamine and octopamine network outputs. The only dopamine experiments which could be used had to meet the most minimal requirement, which was tri-phasic activity. Because of that, it is not surprising that the dopamine results that we quantified were not different from the decentralized network outputs because the decentralized state is the most minimally active state.

This variable response to dopamine application is likely a result of concentration used and the state of the network before dopamine application. It is possible that $10^{-6}$ M represents a threshold concentration where anything below that will consistently generate a quantifiable tri-phasic rhythm, likely one that is not different from the decentralized state, and anything higher will result in a completely disrupted and not quantifiable rhythm. Additionally, the state of the decentralized network likely plays a large role in dictating the type of dopamine output generated. If decentralization results in a quiescent activity pattern, $10^{-6}$ M dopamine application can result in a non-quantifiable rhythm while dopamine will have little effect on a decentralized rhythm which is still cycling. Taken together, the multiple types of activity that dopamine can generate, both quantifiable and not quantifiable, suggest minimally that dopamine is not positively modulating the attributes of excitability.

**Dopamine can be distinguished from the decentralized state in the inter-spike interval attribute.** Exploring the effects of dopamine and octopamine on the attributes of excitability was a reasonable place to start qualifying and quantifying their effects on the pyloric circuit of *C. borealis*. Given the vast amount of literature describing their effects in lobster and the limited literature in crab, at a minimum, we would have expected some change in the excitability attributes under these amine conditions. While there were some

statistical differences with octopamine application, there were no differences qualitatively or quantitatively between dopamine and the decentralized state. This was surprising, but in evaluating the wide range of effects of dopamine, it was clear that focusing only on excitability attributes and using a rigorous and restrictive analytical approach would not allow the diverse nature of dopamine to present itself.

When looking at the example dopamine recordings, both the functional and abnormal, what stands out are the changes in waveform of each of the pyloric neurons. Based on this qualitative observation, we explored how dopamine was modulating attributes of the underlying slow wave oscillation in the PD neuron.

The attributes of the slow wave oscillation that we evaluated are largely under the control of potassium, calcium and leak currents, all of which have been reported to be modulated by dopamine in pyloric neurons (Harris-Warrick and Johnson, 2010). While suggestive, the results presented here are not intended as a proposal of any mechanism for dopamine modulation. Instead, the differences in these attributes of the slow wave oscillation may serve as a starting point to further explore how these amines may be modulating these intrinsic currents leading to the modulation of the slow wave oscillation attributes reported here.

The effects of dopamine on aspects of PD's slow wave oscillation including trough potential, amplitude and spike prominence have been previously described (Flamm and Harris-Warrick, 1986b). This current work evaluated the same attributes which had been previously reported in addition to the inter-spike interval, half width and LP to PD mean synaptic area to capture more holistically where these amines may be exerting an effect.

**Amplitude.** When quantified and statistically tested, the dopamine oscillation amplitude was not statistically smaller compared to the decentralized but there was a reduction in the mean value. Because a reduction of leak current can recapitulate the effects of peptide activated $I_{MI}$ (Zhao et al., 2010), these results suggest that dopamine may be reducing the amplitude of oscillation by increasing the amount of leak current. We only included the dopamine experiments which were used in the 12-dimensional analysis so a difference between decentralized and dopamine may become apparent with an increase in sample size.

**Mean spike prominence.** Any increase in spike prominence could suggest a modulation of sodium current by either dopamine. When statistically tested, there was no difference between dopamine and decentralized. This result suggests that either dopamine is not modulating this current at this concentration.

**Half width.** Underlying the half with of the oscillation are calcium currents which initiate the oscillation and calcium dependent potassium currents which terminate the oscillation. When plotted as individual experimental means, there was a single dopamine response which had a significantly higher half width value and is likely an outlier. When statistically tested, the effect of dopamine was not statistically different compared to decentralized.

When dopamine application results in a loss of tri-phasic activity, there is no appreciable PD neuron oscillation meaning there is no measurable half width. While dopamine may be modulating these currents in the PD neuron, its effect could only be seen if there was still a baseline level of activity. How dopamine is modulating these currents and under what conditions an increase in half width or a loss of rhythmic activity leading

to a loss of measurable half width occurs is beyond the scope of this work but leaves many future directions to explore.

**Inter-spike interval.** The inter-spike interval is shaped by two main factors, the refractory period as well as potassium currents, specifically the A-type potassium current (Falk et al., 2003). The calcium dependent potassium current can also contribute to a change in inter-spike interval during spike frequency adaptation (Ha and Cheong, 2017). While not direct, any statistical increase in this attribute by a modulator would suggest a modulation of these currents in the crab PD neuron.

When plotted as individual animal means, the dopamine responses were highly distributed compared to the decentralized responses. When statistically tested, there was a significant difference between the dopamine response and decentralized. This result with dopamine suggests a modulation of the A-type potassium current. While the calcium dependent potassium current may also be playing a role, these neurons were not spiking rapidly so spike frequency adaptation is not likely to be a mechanism here. A higher concentration of dopamine would likely increase the consistency in response across animals though the effect of a higher concentration would be different than the results presented here. When dopamine application results in a complete loss of rhythmic activity, the PD neuron often fires only a single spike per burst. This would consistently result in an inter-spike interval of 0.

**Mean synaptic area.** The effect of dopamine was not statistically different compared to the decentralized state in the synaptic area attribute. Dopamine reportedly enhances the LP to PD synapse in spiny lobster and although not statistically meaningful, there was an increase in the mean synaptic area when dopamine is compared to the decentralized. This

may suggest a potential enhancement of this synapse which is obscured by the variable dopamine response. An increase in concentration may reduce the degree of variability but would not lead to statistical difference between decentralized and dopamine.

This assessment comes from the qualitative observation of the range of outputs dopamine can generate. When dopamine application results in a loss of rhythmic activity, the LP neuron either stops spiking completely or fires tonically and its oscillatory activity becomes significantly dampened (see Figure 4.3 B). Both the spike mediated and graded components of this synapse are subject to neuromodulation (Zhao et al., 2011) and when dopamine application results in a loss of functional activity, the synaptic input is effectively non-existent. This outcome is similar to decentralization and most of the dopamine observations are clustered in the same range of values as the decentralized.

There are a few observations that show an enhancement of this synapse. One possibility for this mixed response is a differential effect of dopamine on the spike mediated and graded components of this synapse. It has been previously reported that dopamine differentially modulates the spike mediated and graded components of the LP to PD synapse (Ayali et al., 1998). Here dopamine reduced the LP to PD spike mediated component of the synapse by reducing the input resistance in the PD neuron. The graded component of this synapse, however, was enhanced by dopamine application (Johnson et al., 1995). If dopamine also differentially modulates the two components of this synapse in crab, it is possible that the state of the LP neuron before dopamine application could result in an enhancement of this synapse if, for example, LP was not spiking but regularly oscillating. Additionally, an incomplete inhibition of PD activity with no or limited decrease in input resistance could result in an overall enhancement of this synapse.

**Paired trough voltage.** The LP to PD synapse is glutamatergic with a reversal potential of about -70 mV. A strongly enhanced modulated synapse will move the trough voltage towards its reversal potential whereas a weakly nor non-existent modulated synapse would result in no change compared to the baseline decentralized state. When quantified, the trough voltage following dopamine application was not statistically different compared to the decentralized but in many cases was unpredictable.

The response to dopamine application in this attribute lead to a depolarization of the trough, a hyperpolarization or in some cases no appreciable change. Because of the inconsistency in response, it is hard to make any statement about what may be happening with dopamine application and this attribute.

From the synaptic area comparison, dopamine may not modulate this synapse or may have state dependent effects. Statistically, though, the decentralized and dopamine responses were not different. Outside of the synaptic influence, intrinsic currents may also be playing a role in setting the trough voltage, specifically the hyperpolarized activated inward current. This current is most strongly activated at highly hyperpolarized potentials, is subject to modulation by amines in pyloric neurons and can contribute to setting the membrane potential (Golowasch and Marder, 1992a; Lupica et al., 2001; Peck et al., 2006). Considering the membrane potential at the trough, other intrinsic currents are likely not participating in the shaping of this attribute. The caveat to this is the low level of h current in PD neurons (Temporal et al., 2012). The h current is also temperature sensitive where the amount measured can increase significantly at elevated temperatures (Peck et al., 2006). At the temperature used in these experiments, it is unlikely that the h current was

contributing largely. It still remains possible though that dopamine is modulating this current, leading to the slight depolarization of the trough voltage of PD.

**Balancing flexibility and function in pyloric network output**. Our initial expectation was that the application of distinct amines would generate distinct pyloric network outputs, adding another layer to the idea of network output flexibility. This is the same expectation that we had when applying individual peptide neuromodulators to the pyloric network. Unlike the results with the peptide modulated network outputs, there were no statistical differences between any amine in any attributes evaluated here. If only the statistical results are considered, it would suggest that network output flexibility is not achievable with amine application.

The general idea of network output flexibility is the generation of identifiable network outputs with distinct neuromodulator application. While the results presented here do not support that, distinct network outputs would likely be generated with an increase in amine concentration. However, these distinct network outputs may or may not be quantifiable in the excitability or slow wave oscillation spaces. From a functional perspective though, the generation of qualitatively and quantitatively distinct amine network outputs with increased concentration may not be meaningful or functional to the intact animal. While quantitative nuances in tri-phasic activity have been shown to elicit distinct muscle responses downstream from the ganglion (Daur et al., 2021), it is unlikely that a dopamine elicited rhythm which has lost all tri-phasic activity would signal for any meaningful behavior. This brings up an important distinction between the need to generate flexible outputs and the need to generate functional outputs. Distinct network outputs can

easily be elicited but distinct experimentally generated network outputs are not necessarily meaningful to the behaving animal.

While not distinct on their own, a more robust or obvious effect of these amines may be found when they are combined with other modulators, specifically neuropeptides. The presence of peptides, which are functionally excitatory, can provide a different canvas for the amines to act on compared to the canvas provided here which was the decentralized state. Given how important the state of the network is for evaluating a modulator's action, it would be particularly interesting to evaluate how a seemingly non-functional amine responds when the network is shifted towards a more functional and excitatory starting point.

# CHAPTER 5

# PEPTIDE AND AMINE CO-MODULATION DOES NOT RESTORE FLEXIBILITY TO THE PYLORIC NETWORK OUTPUT

## 5.1 Introduction

From the previous analyses, the neuropeptides present in the stomatogastric nervous system strongly modulate attributes related to excitability. Octopamine, an amine, also functions in this space while dopamine does not positively modulate these attributes when quantifiable and can be strongly inhibitory. While not investigated completely, serotonin may also function in a space similar to octopamine, where it provides the network another solution to generate functional activity.

Like the peptides, however, evaluating the effects of dopamine, octopamine or serotonin on their own is necessary but not sufficient to understand how these neuromodulators are shaping the network output. It is unlikely that any one amine will be acting in isolation. In particular, it is unlikely that any single amine will be operating in a space which is not influenced by the presence of peptides.

Complements of neuroactive substances can be co-localized at shared synaptic terminals and may package into the same vesicle or occupy distinct vesicles, as in the case of small molecule transmitters and neuropeptides. Classic small molecule transmission can act locally while neuropeptides can diffuse to modulate targets away from the local release at anatomical synapses, acting in a volume transmission capacity. In complex circuits, these types of release can act together to generate outputs which are distinct from either neuromodulator acting individually (Fuxe et al., 2010). Co-transmitters can modulate their own release or the release of their co-localized modulator partners

(Malcangio and Bowery, 1999; Salio et al., 2006) and can also act separately to suppress or promote distinct patterns of activity (Blitz and Nusbaum, 1997, 1999).

Distinct neuromodulators can also interact and influence each other's individual actions outside of a co-transmission capacity. In the stomatogastric nervous system, neuromodulators such as dopamine can be released into the hemolymph in addition to directed release into the ganglion (Marder, 2012). These circulating neuromodulators operate in the nanomolar range and have been thought to set a baseline modulatory tone (Rodgers et al., 2011). Another opportunity for circuit flexibility arises from the interaction of an endogenously released neuromodulator into a space that is already under nanomolar modulatory influence. It is reasonable to assume that the circuit outputs achieved in the presence of either a sufficiently concentrated endogenously released modulator or nanomolar concentration circulating modulator will be different than a circuit output achieved in the presence of both. A low-level modulatory tone may also represent a priming effect. It is known that the effects of neuromodulators are state dependent and the presence of a circulating modulator at lower concentration may act to prime the circuit to respond in a particular way when an additional modulator is introduced (Nusbaum and Marder, 1989; Dickinson et al., 1997; Svensson et al., 2001)

Neuromodulators signal through G-protein coupled receptors and these receptors have multi-step second messenger systems (Lopez and Brown, 1992). Multiple neuromodulators acting on the same neuron, whether it be in a divergent manner where each neuromodulator signals through a distinct G-protein mediated signaling cascade or a convergent manner where both neuromodulators signal through presumably the same G-protein, can result in cross-talk (Ramirez et al., 2012). In mouse taste cells, increased

cAMP levels have been linked to an increase in calcium indicating an interaction between protein kinase A and protein kinase C, the downstream effectors of $G_s$ and $G_q$ receptor activation (Roberts et al., 2009). Cross-talk between $G_i$ and $G_s$ G proteins in the rat amygdala has also been reported with the point of interaction occurring downstream from cAMP production (Wang et al., 1999). In rat hippocampus, $GABA_B$ and cannabinoid $CB_1$ receptors are both coupled to $G_i$ G-proteins and act to inhibit each other's signaling (Cinar et al., 2008). The ultimate consequence of cross-talk between pathways is a modification of output which cannot be recapitulated by the activation of only one signaling pathway.

In the stomatogastric nervous system, the consequences of co-modulation with neuropeptides has been investigated at the level of intrinsic and synaptic currents in the PD and LP neurons of the pyloric network (Li et al., 2018). Peptides all converge to target the same effector, though the intracellular signaling pathway mediating this is not known. When quantified, the effect of peptide co-modulation is sub-linear at the intrinsic current level but additive at the synaptic current level. This indicates, at the intrinsic current level, a point of interaction within the activated signaling pathways which is mutually inhibitory and distinct from the type of interaction mediating the change in synaptic current. The consequences of co-modulation with two amines is not known in the pyloric network, though the cell type receptor identities and signaling pathways for dopamine and serotonin are known, at least in part, and cross-talk between these signaling pathways is likely.

These distinct classes of neuromodulators, the convergent peptides and divergent amines, are likely interacting with each other in the stomatogastric nervous system but we do not know the consequences of this interaction. Therefore, we combined dopamine, octopamine or serotonin with either crustacean cardioactive peptide (CCAP) or red

pigment concentrating hormone (RPCH), both peptides, and evaluated their combined effects on the pyloric network output. We specifically chose CCAP and RPCH because of their high degree of similarity when evaluated individually but, while not statistically different, were not identical. This inflexibility represents an interesting place to test whether their network outputs can be separated from each other in the presence of an amine. If not, then the assessment that they are degenerate neuropeptides from Chapter 2 may still hold.

This work represents the first quantitative and qualitative exploration of the effects of peptide and amine co-modulation and allows for a number of first pass questions to be tested. In particular, we can test again the idea of network output flexibility. With peptide co-modulation, combining multiple peptides together decreased flexibility in the type of pyloric network output that could be generated due to $I_{MI}$ convergence. While a loss of one type of flexibility, the pyloric network also gained flexibility by having multiple solutions which could generate the same output. Unlike the peptides which function unidirectionally, the amines can effect multiple opposing currents at the same time. The combination of a unidirectional peptide with a bidirectional amine may allow the network output to move into novel spaces which were not accessible with only peptides.

Here we test whether dopamine, octopamine and serotonin contribute to shaping the network output when combined with a peptide and whether distinct combinations of peptides and amines regain flexibility in the network output that was lost with peptide co-modulation.

## 5.2 Materials and Methods

The animals, electrophysiological approach, excitability attribute extraction, Euclidean distance and multi-variate permutation test calculation were the same as reported in Chapter 2.

**Modulators and experimental protocol:** The preparation was decentralized by blocking the STN with a $10^{-7}$ M TTX (Biotium) + 750 mM sucrose (Sigma) solution. Dopamine hydrochloride (Sigma) was prepared right before application by dissolving in distilled water to an initial concentration of $10^{-2}$ M. Care was taken to avoid unnecessary exposure to light. CCAP (Bachem), RPCH (Bachem), serotonin hydrochloride (Sigma) and octopamine hydrochloride (Sigma) were diluted with distilled water and initially aliquoted to a concentration of $10^{-3}$ M and stored until needed. Final dilution of CCAP or RPCH + dopamine, CCAP or RPCH + octopamine and CCAP or RPCH + serotonin occurred immediately before application in chilled *Cancer borealis* saline. Each co-modulator pair was prepared at $10^{-6}$ M total concentration.

Initially, either CCAP or RPCH was applied to the preparation at $10^{-6}$ M for 5 minutes via peristaltic pump. Following the initial peptide application, the peptide + amine combination was immediately applied for 5 minutes. In cases of repeated application, the first co-modulator application was washed out in chilled $10^{-6}$ M peptide for a minimum of 30 minutes.

**N for excitability attribute comparison**. CCAP/CCAP + dopamine = 9, RPCH/RPCH + dopamine = 9, CCAP/CCAP + serotonin = 6, RPCH/RPCH + serotonin = 4, CCAP/CCAP + octopamine = 7 and RPCH/RPCH + octopamine = 5.

**Statistical evaluation:** All initial statistical tests were either paired t-tests or One Way ANOVA's and were performed in SigmaPlot. For the One Way ANOVA tests, if the data failed a test for normality or variance, a One Way ANOVA on ranks was performed instead. In all cases a post hoc test was performed following the initial ANOVA test. Table A.6 summarizes all ANOVA statistical tests for Figure 5.8. Statistical significance was determined as follows: * $p < 0.05$, ** $p < 0.01$, *** $p < 0.001$.

## 5.3 Results

Building on the previous work evaluating the effects of single peptide and amine neuromodulators on the pyloric network output, we next asked the consequences of combining individual peptides and amines together on the network output. We first wanted to ask whether the presence of an amine had a qualitative or quantitative effect compared to a singularly applied peptide response. Therefore, we qualified the effects of each co-modulated network output with respect to its peptide constituent and quantified their effects on the four attributes of activity previously evaluated.

Because the full effects of both CCAP and RPCH were previously shown in Chapter 2, we did not quantify the effects of either the peptide or the peptide and amine co-modulated conditions with respect to either the intact or decentralized baseline state. In Chapter 2, both peptides positively modulated the cycle frequency, spike number and spike frequency attributes whereas in Chapter 4, dopamine and octopamine had limited to no effect on these attributes. Because of that, we do not expect the presence of any amine to have any appreciable effect in those attributes compared to the peptide alone.

It is more difficult to form an expectation for the phase attribute. The hypothesis presented in Chapter 2 suggests that the neuropeptides maintain phase through activation of $I_{MI}$ in the pacemaker neuron and any activation of $I_{MI}$ in the follower neurons can modulate aspects of that neuron's excitability, spike number and frequency, but do not modulate phase. The amines, however, presumably modulate intrinsic currents such as the A-type potassium current and h current. Both of these currents are known to modulate the phasing of the pyloric neurons in the spiny lobster. By combining these two classes of modulator together, it is unclear if the presence of the peptide through $I_{MI}$ activation in the pacemaker will dominate and maintain the phase of these neurons in the co-modulated condition or if the presence of the amine will dominate and shift the phases relative to the peptide control.

**Co-application of CCAP and dopamine does result in statistical differences in phase, spike number and spike frequency compared to CCAP.** When evaluated qualitatively, the addition of dopamine did not generate an appreciably distinct rhythm compared to CCAP alone outside of a decrease in both LP and PY spiking activity (Figure 5.1 A).

Because there was a slight change in some of the attributes of activity when qualified, we quantified the effect of CCAP + dopamine co-modulation on the cycle frequency, phases, spike number and spike frequency parameters of the pyloric network. When quantified, there were no statistical differences between CCAP and CCAP + dopamine in cycle frequency (Figure 5.1 B). In phase, there was a statistical difference between CCAP and CCAP + dopamine in the PD off phase (paired t-test: $t_8 = -3.075$, p-value = 0.015) and the LP on phase (paired t-test: $t_8 = -2.370$, p-value = 0.045) (Figure 5.1 C). There were also statistical differences in the PY spike number parameter (paired t-test:

$t_8$ = 3.663, p-value = 0.006) (Figure 5.1 D), PD spike frequency (paired t-test: $t_8$ = 3.966, p-value = 0.0041) and PY spike frequency (paired t-test: $t_8$ = 8.504, p-value = <0.001) (Figure 5.1 E).

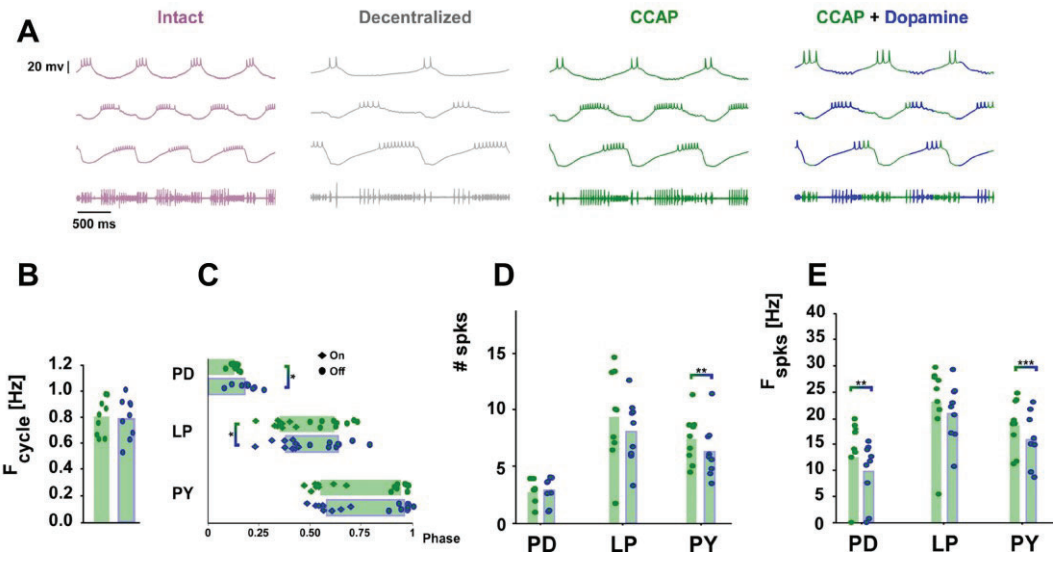


**Figure 5.1** Qualitative and quantitative response of the core pyloric neurons to CCAP and CCAP + dopamine co-modulator application. (A) Example trace of pyloric network response to sequential application of CCAP and CCAP + dopamine. (B) Quantitative response in cycle frequency to CCAP and CCAP + dopamine application. Bars represent means, individual points represent individual animal responses. Color of bars and filled points indicates the peptide used and outline of bars and points represent amine used. (C) Quantitative response in phase to CCAP and CCAP + dopamine application. Color of bars and filled points indicates the peptide used and outline of bars and points represent amine used. The filled circles indicate the off phase of each neuron while the filled diamonds indicate the on phase of each neuron. (D) Quantitative response in spike number to CCAP and CCAP + dopamine application. Bars and points are the same as described in B. (E) Quantitative response in spike frequency to CCAP and CCAP + dopamine application. Bars and points are the same as described in B.

**Co-application of RPCH and dopamine does result in statistical differences in phase, spike number and spike frequency compared to RPCH.** When evaluated qualitatively, the activity of the PD and LP neurons with RPCH + dopamine looked qualitatively similar to the RPCH elicited activity. The PY neuron, however, did appear to change qualitatively. In the presence of the co-modulated condition, there was an apparent change in the duration

of PY bursting and a decrease in the spiking activity with no apparent change to any of the pyloric waveforms (Figure 5.2 A). When the cycle frequency was quantified, there was no statistical difference (Figure 5.2 B). In phase, the RPCH + dopamine co-modulated condition was statistically different from RPCH in the phase of PD off (Wilcox Signed Rank Test: $Z = 2.66$, p-value = 0.004), LP on (paired t-test: $t_8 = 2.55$, p-value = 0.033) and PY on (paired t-test: $t_8 = -3.067$, p-value = 0.015) (Figure 5.2 C). In the spike number attribute, the LP (paired t-test: $t_8 = 2.376$, p-value = 0.045) and PY (Wilcox Signed Rank Test: $Z = -2.547$, p-value = 0.008) spike numbers under the co-modulated condition were statistically lower compared to the RPCH response alone (Figure 5.2 D). Lastly, in spike frequency, the RPCH + dopamine response was statistically lower compared to the RPCH response in PY spike frequency (paired t-test: $t_8 = 3.363$, p-value = 0.010) (Figure 5.2 E).

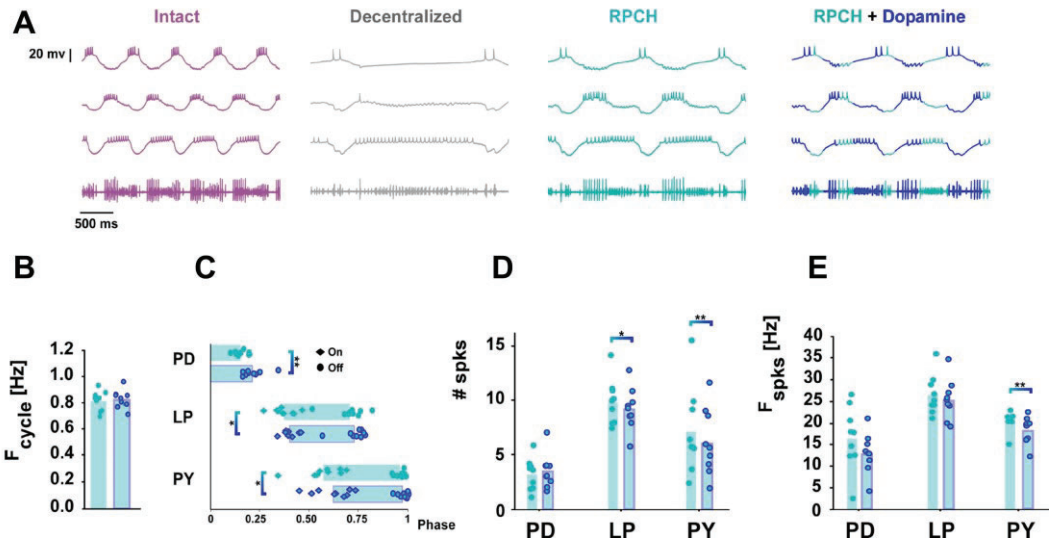


**Figure 5.2** Qualitative and quantitative response of the core pyloric neurons to RPCH and RPCH + dopamine co-modulator application. (A) Example trace of pyloric network response to sequential application of RPCH and RPCH + dopamine. (B) Quantitative response in cycle frequency to RPCH and RPCH + dopamine application. Bars represent means, individual points represent individual animal responses. Color of bars and filled points indicates the peptide used and outline of bars and points represent amine used. (C) Quantitative response in phase to RPCH and RPCH + dopamine application. Color of bars and filled points indicates the peptide used and outline of bars and points represent amine used. The filled circles indicate the off phase of each neuron while the filled diamonds indicate the on phase of each neuron. (D) Quantitative response in spike number to RPCH and RPCH + dopamine application. Bars and points are the same as described in B. (E) Quantitative response in spike frequency to RPCH and RPCH + dopamine application. Bars and points are the same as described in B.

**Co-application of peptide and dopamine does not generate a distinct network output in the 12D network output space compared to the individual peptides.** In the six peptide and amine comparisons, the co-modulated network outputs with dopamine had a number of statistical differences compared to their peptide constituents. We therefore asked whether the CCAP network outputs were statistically different from the CCAP + dopamine network outputs and whether the RPCH network outputs were statistically different from the RPCH + dopamine network outputs in the 12-dimensional network output space. To do this, we combined the network outputs of CCAP, RPCH, CCAP +

dopamine and RPCH + dopamine and z-score standardized them (Figure 5.3 A) before running the Euclidean distance and multi-variate permutation test.

When quantified, there was no statistical difference between the CCAP and CCAP + dopamine network outputs or between the RPCH and RPCH + dopamine network outputs (Figure 5.3 B), though the distance between RPCH and RPCH + dopamine was smaller indicating more similarity. We then visualized the network outputs of all four conditions in a reduced principal component space (Figure 5.3 C). In this space, there was a large amount of overlap between each co-modulated condition and its peptide constituent, leading to the lack of difference detected when quantified.

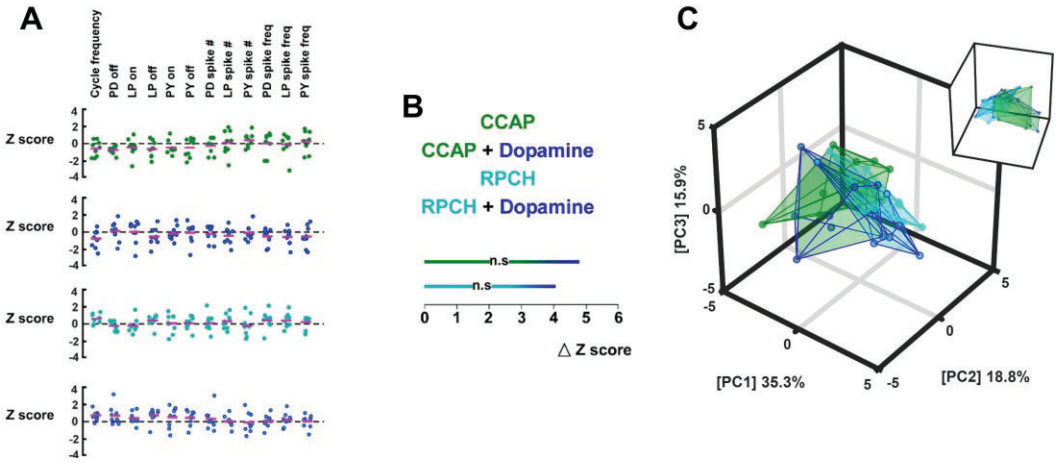


**Figure 5.3** 12D statistical testing of difference between CCAP versus CCAP + dopamine and RPCH versus RPCH+ dopamine network outputs. (A) Euclidean distance measurements and statistical assessment of difference between each peptide and peptide and amine co-modulated network output. The outline of each individual point represents the presence of dopamine while the fill represents the peptide used. (B) Euclidean distance measurements and statistical assessment between each individual peptide and its co-modulated network outputs. (C) Projection of all observations from all conditions in a 3-dimensional principal component space. Each distribution of scores was fit with a convex hull.

**Co-application of CCAP and serotonin does result in statistical differences in cycle frequency and the PY on phase compared to CCAP.** When qualified, there was no obvious difference between the CCAP elicited network output and the co-applied CCAP + serotonin network output (Figure 5.4 A). When quantified, the co-applied CCAP + serotonin cycle frequency was statistically higher compared to CCAP alone (paired t-test: $t_5 = -3.369$, p-value = 0.02) (Figure 5.4 B). In the phase attribute, the phase onset of PY was statistically delayed under the co-modulated condition compared to the peptide alone (paired t-test: $t_5 = -2.607$, p-value = 0.047) but there were no other differences in phase (Figure 5.4 C). Additionally, there were no differences between the single peptide and co-modulated responses in the spike number or spike frequency attributes (Figure 5.4 D and E).

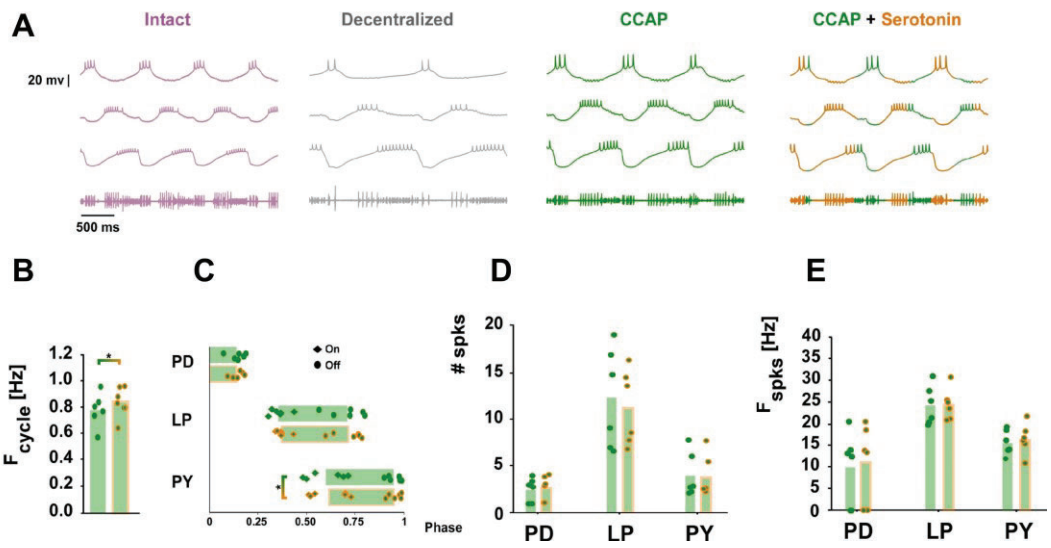


**Figure 5.4** Qualitative and quantitative response of the core pyloric neurons to CCAP and CCAP + serotonin co-modulator application. (A) Example trace of pyloric network response to sequential application of CCAP and CCAP + serotonin. (B) Quantitative response in cycle frequency to CCAP and CCAP + serotonin application. Bars represent means, individual points represent individual animal responses. Color of bars and filled points indicates the peptide used and outline of bars and points represent amine used. (C) Quantitative response in phase to CCAP and CCAP + serotonin application. Color of bars and filled points indicates the peptide used and outline of bars and points represent amine used. The filled circles indicate the off phase of each neuron while the filled diamonds indicate the on phase of each neuron. (D) Quantitative response in spike number to CCAP and CCAP + serotonin application. Bars and points are the same as described in B. (E) Quantitative response in spike frequency to CCAP and CCAP + serotonin application. Bars and points are the same as described in B.

**Co-application of RPCH and serotonin does not result in any statistical differences in the four attributes quantified compared to RPCH alone.** Qualitatively, the only apparent difference between the RPCH elicited network output and the RPCH + serotonin network output was a change in the spiking behavior of the LP neuron (Figure 5.5 A). When quantified, however, there were no statistical differences across any of the attributes evaluated (Figure 5.5 B-E).

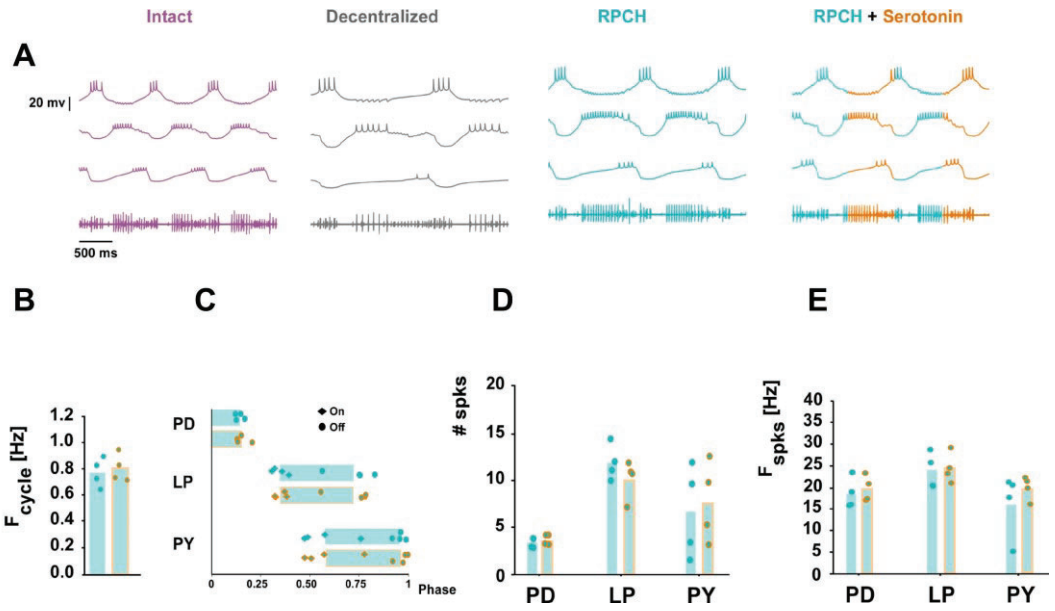


**Figure 5.5** Qualitative and quantitative response of the core pyloric neurons to RPCH and RPCH + serotonin co-modulator application. (A) Example trace of pyloric network response to sequential application of RPCH and RPCH + serotonin. (B) Quantitative response in cycle frequency to RPCH and RPCH + serotonin application. Bars represent means, individual points represent individual animal responses. Color of bars and filled points indicates the peptide used and outline of bars and points represent amine used. (C) Quantitative response in phase to RPCH and RPCH + serotonin application. Color of bars and filled points indicates the peptide used and outline of bars and points represent amine used. The filled circles indicate the off phase of each neuron while the filled diamonds indicate the on phase of each neuron. (D) Quantitative response in spike number to RPCH and RPCH + serotonin application. Bars and points are the same as described in B. (E) Quantitative response in spike frequency to RPCH and RPCH + serotonin application. Bars and points are the same as described in B.

**Co-application of CCAP and octopamine does result in statistical differences in cycle frequency and LP spike number compared to CCAP.** There were no apparent differences between the CCAP elicited network output and the CCAP + octopamine network output. Out of the three amines tested, octopamine appeared to have the smallest effect and the CCAP + octopamine network output appeared to completely mirror the individual CCAP effect on the network output (Figure 5.6 A).

When quantified, the effect of CCAP + octopamine was statistically different from the CCAP response in cycle frequency (paired t-test: $t_6 = -2.544$, p-value = 0.043) (Figure 5.6 B). In the phase attribute, there were no statistical differences between CCAP and CCAP + octopamine (Figure 5.6 C). In the spike number attribute, the CCAP + octopamine response was statistically different from CCAP in PD spike number (paired t-test: $t_6 = -3.678$, p-value = 0.010) (Figure 5.6 D) and in LP spike number (Wilcox Signed Rank Test: Z = -2.028, p-value = 0.047) (Figure 5.6 E).

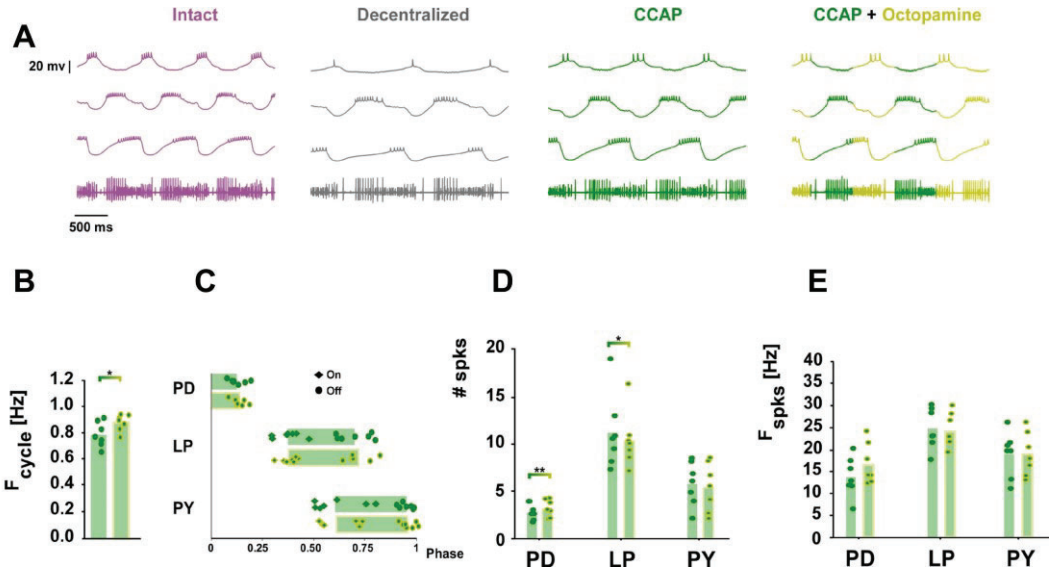


**Figure 5.6** Qualitative and quantitative response of the core pyloric neurons to CCAP and CCAP + octopamine co-modulator application. (A) Example trace of pyloric network response to sequential application of CCAP and CCAP + octopamine. (B) Quantitative response in cycle frequency to CCAP and CCAP + octopamine application. Bars represent means, individual points represent individual animal responses. Color of bars and filled points indicates the peptide used and outline of bars and points represent amine used. (C) Quantitative response in phase to CCAP and CCAP + octopamine application. Color of bars and filled points indicates the peptide used and outline of bars and points represent amine used. The filled circles indicate the off phase of each neuron while the filled diamonds indicate the on phase of each neuron. (D) Quantitative response in spike number to CCAP and CCAP + octopamine application. Bars and points are the same as described in B. (E) Quantitative response in spike frequency to CCAP and CCAP + octopamine application. Bars and points are the same as described in B.

**Co-application of RPCH and octopamine does not result in a qualitatively or quantitatively distinct network output compared to RPCH.** Lastly, we qualified and quantified the effects of RPCH and RPCH + octopamine. When qualified, there was no apparent difference between the individual peptide elicited response and the co-applied RPCH + octopamine response (Figure 5.7 A). When quantified, there were no statistical differences between RPCH and RPCH + octopamine in the four attributes evaluated (Figure 5.7 B-E).

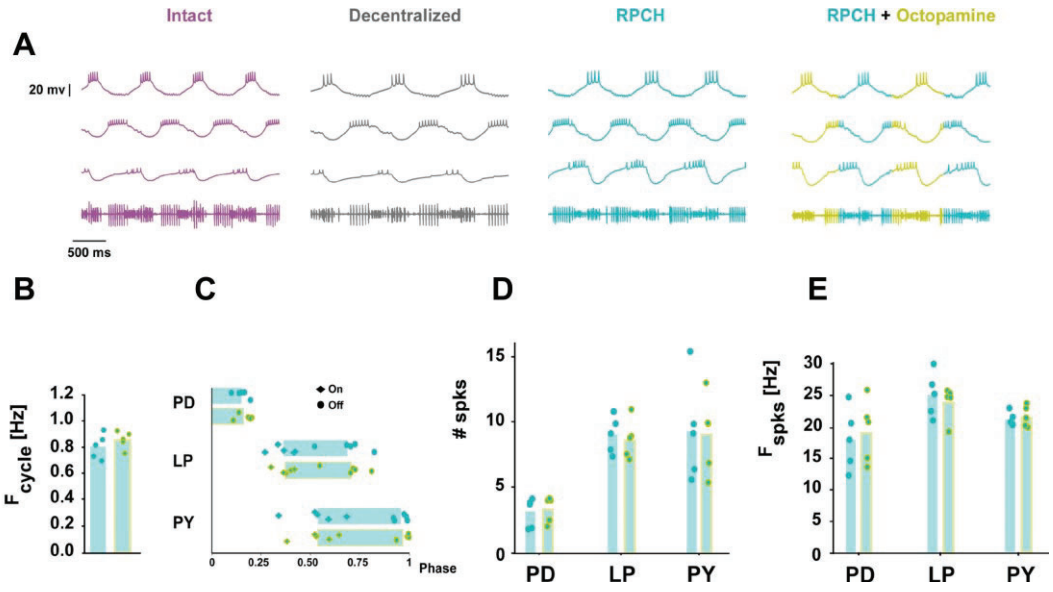


**Figure 5.7** Qualitative and quantitative response of the core pyloric neurons to RPCH and RPCH + octopamine co-modulator application. (A) Example trace of pyloric network response to sequential application of RPCH and RPCH + octopamine. (B) Quantitative response in cycle frequency to RPCH and RPCH + octopamine application. Bars represent means, individual points represent individual animal responses. Color of bars and filled points indicates the peptide used and outline of bars and points represent amine used. (C) Quantitative response in phase to RPCH and RPCH + octopamine application. Color of bars and filled points indicates the peptide used and outline of bars and points represent amine used. The filled circles indicate the off phase of each neuron while the filled diamonds indicate the on phase of each neuron. (D) Quantitative response in spike number to RPCH and RPCH + octopamine application. Bars and points are the same as described in B. (E) Quantitative response in spike frequency to RPCH and RPCH + octopamine application. Bars and points are the same as described in B.

**Distinct combinations of peptides and amines are quantitatively distinct from each other across the four attributes of excitability.** Lastly, we wanted to quantify whether distinct combination of peptide and amines were distinct from each other across the four attributes of excitability. When evaluated individually, there were differences between individual co-modulated pairs and their peptide constituents and it is likely that each individual amine is signaling through its own distinct cellular pathway. Therefore, it is possible that when the co-modulated conditions are compared to each other, there will be differences in their actions across these attributes.

We can combine the results from the previous three chapters to form a set of expectations for this analysis. In Chapter 2 the CCAP and RPCH cycle frequency responses were statistically different but in Chapter 4 there were no statistical differences between the three amines tested. Therefore, we do not expect a difference between the co-modulated pairs which share the same peptide but there may be differences across co-modulated pairs which differ in their peptide.

The spike number and spike frequency attributes were strongly modulated by the individual peptides in Chapter 2 and the CCAP and RPCH responses were statistically different in LP spike number and PD spike frequency. Dopamine did not modulate these attributes when quantifiable and octopamine did not appreciably modulate these attributes outside of a statistical decrease in PY spike number in Chapter 4. Therefore, it is possible that the co-modulated pairs with CCAP may be different in some parameters of the spike number and frequency attributes compared to the RPCH co-modulated pairs. Additionally, the presence of octopamine may inhibit the spiking activity of the PY neuron when

combined with either peptide allowing the pairs with octopamine to be differentiated from the dopamine and serotonin co-modulated pairs.

The expectation with phase is unclear for the same reason as previously mentioned. Because the amines used here presumably modulate the intrinsic currents which can shift the phases of the pyloric neurons, it is possible that their effects will dominate over the activation of $I_{MI}$ in the pacemaker neuron by the peptides. If the presence of the amines dominates over the peptides in this attribute, it is unlikely that all three amines would be modulating these currents in the same way, leading to potential differences across the distinct co-modulated conditions.

We also tested each peptide and amine co-modulated pair against the intact and decentralized conditions. Our expectation in all cases is that there will be differences across the four attributes between the co-modulated pairs and the baseline states.

**Cycle frequency.** In the cycle frequency attribute, the intact response was statistically different from all other conditions tested while the decentralized response was statistically different from all co-modulated conditions which contained RPCH. Across the co-modulators, the CCAP + dopamine response was statistically different from the RPCH + dopamine and RPCH + octopamine responses (One way ANOVA: $F_{(7,86)} = 41.34$, $p < 0.001$) (Figure 5.8 A).

**Phase.** In the phase attribute the decentralized response in PD off was statistically different than the intact, CCAP + dopamine and RPCH + dopamine while RPCH + dopamine was statistically different from CCAP + serotonin and CCAP + octopamine (One way ANOVA: $F_{(7,86)} = 6.718$, $p < 0.001$). There were no statistical differences in the phase of LP on (One way ANOVA on Ranks: $H = 12.383$, $p = 0.089$) and in the phase of LP off, the

decentralized response was statistically different from all conditions except CCAP + dopamine (One way ANOVA on Ranks: $H = 52.635$, $p < 0.001$). In the PY on phase, the decentralized response was statistically different from the intact, all three CCAP co-modulated pairs and RPCH + dopamine (One way ANOVA: $F_{(7,86)} = 7.003$, $p < 0.001$) while there were no differences in the PY off phase (Figure 5.8 B).

**Spike number.** In the spike number attribute, a one way ANOVA on ranks indicated a statistical difference in PD spike number (One way ANOVA on Ranks: $H = 20.822$, $p = 0.004$) and PY spike number (One way ANOVA on Ranks: $H = 17.672$, $p = 0.014$) but a post hoc analysis did not indicate any condition specific effects in either case. In LP spike number, the decentralized response was statistically different compared to all other conditions (One way ANOVA: $F_{(7,86)} = 11.459$, $p < 0.001$) (Figure 5.8 C).

**Spike frequency.** Lastly, in the spike frequency attribute, the intact response was statistically different from both co-modulator pairs with dopamine and CCAP + serotonin in the PD spike frequency parameter (One way ANOVA on Ranks: $H = 57.076$, $p < 0.001$). In LP spike frequency, the decentralized response was statistically different from all other comparisons and the intact response was statistically different compared to the CCAP + dopamine response (One way ANOVA: $F_{(7,86)} = 19.007$, $p < 0.001$). In PY spike frequency, the intact response was statistically different from all other conditions (One way ANOVA: $F_{(7,86)} = 18.262$, $p < 0.001$).

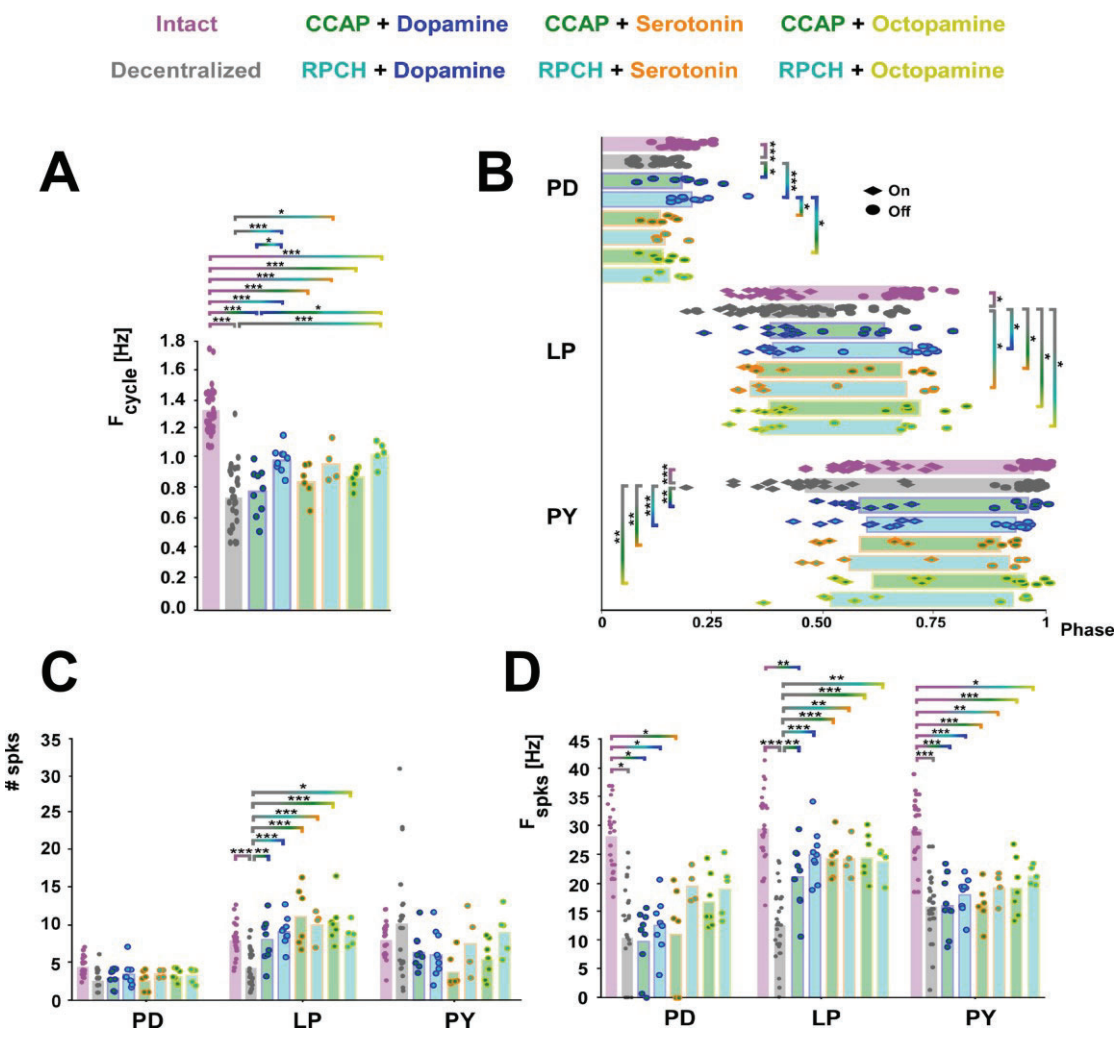


**Figure 5.8** Quantitative response of the core pyloric neurons to peptide and amine co-modulator application. In all panels, the color of the bars and the fill of the individual points indicate the peptide used and the outline of the bars and individual points indicate the amine used. (A) Cycle frequency response following peptide and amine application. Bars represent means and individual points represent individual animal responses. (B) Phase response following peptide and amine application. Bars represent means and individual points represent individual animal responses. The filled circles indicate the off phase of each neuron while the filled diamonds indicate the on phase of each neuron.

**Dopamine may be priming the pyloric circuit differently than a peptide.** While there were limited statistical differences across the peptide and amine co-modulator comparisons, these results suggested that the presence of an amine in combination with a peptide was not contributing significantly to the pyloric network output. The design of these experiments utilized sequential application of neuromodulators. In the experiments

used for this analysis, the peptide was applied first at $10^{-6}$ M concentration and then the co-modulator pair was applied immediately after but in some experiments the order was reversed, and the amine was applied first. When $10^{-6}$ M CCAP was applied first instead of the peptide, a quantifiable tri-phasic network output was reliably generated in all cases. When the same concentration of dopamine was applied first and followed with co-application of CCAP + dopamine, a quantifiable rhythm was not always generated (Figure 5.9 A-B). In two experiments, an obviously perturbed rhythm was generated. Features of these rhythms included a cycle period of ~10 seconds, dramatic shifts in phase between the LP and PY neurons where the PY neuron fired completely in LP time, and a combination of bursting and tonic firing of the PD neuron. This effect was clearly a result of the presence of dopamine and washed out completely. While inconsistent, this difference in response depending on which modulator was applied first could represent a priming effect of the circuit by dopamine. Interestingly, a perturbed response never occurred when RPCH + dopamine followed dopamine application.

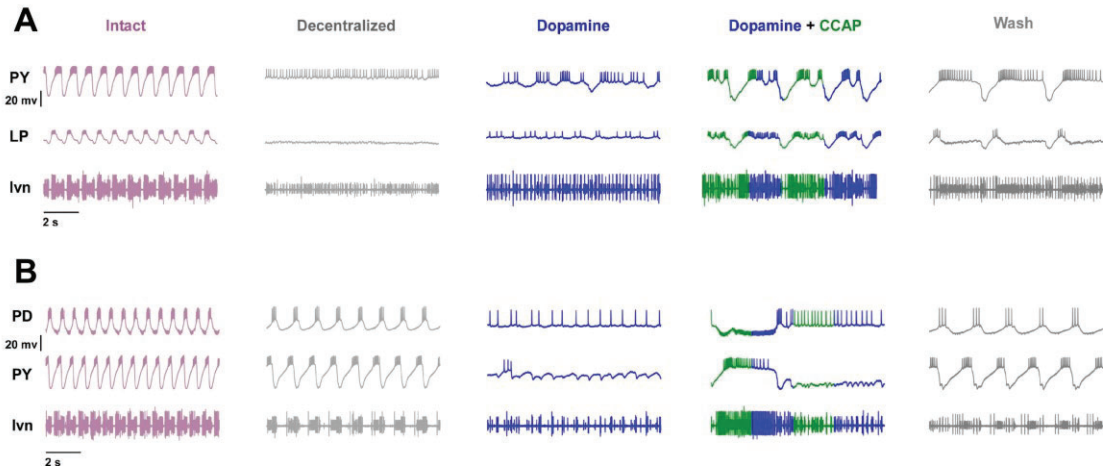


**Figure 5.9** Perturbed response of the core pyloric neurons to CCAP and dopamine co-modulator application when dopamine was applied first. Each panel represents a single animal. (A) Following decentralization where the pyloric rhythm ceased activity application of $10^{-6}$ M dopamine resulted in a loss of functional activity. When $10^{-6}$ M total concentration of CCAP + dopamine was then applied, an abnormal pyloric rhythm was generated. Regular pyloric activity was restored following a wash in saline. (B) In a separate experiment where decentralization did not result in a loss of pyloric activity, application of $10^{-6}$ M dopamine resulted in a tonic activity. When $10^{-6}$ M total concentration of CCAP + dopamine was then applied, an abnormal pyloric rhythm was generated which was distinct from the abnormal behavior in the previous panel. This effect also washed out.

## 5.4 Discussion

Evaluating a network under the influence of both a peptide and an amine represents an interesting opportunity to both test and speculate as to the consequences of combining two distinct classes of neuromodulators. From the previous chapters, we have an understanding about the base effects of single peptides and amines as well as co-modulation with peptides on the pyloric network output. The results presented here represent the culmination of those works where we can test if the addition of an amine modulates an existing peptide elicited network output and whether network output flexibility can be regained through peptide and amine co-modulation. The largest caveat to the results testing whether the presence of an amine modulates an existing peptide network output is the concentration of

modulators used in those analyses. The individual peptides were applied at $10^{-6}$ M concentration whereas the co-applied modulators were applied at a total concentration of $10^{-6}$ M concentration. Therefore, while we can speculate as to the actions of the amines on the pyloric network responses reported here, it is important to note that we cannot make a clear one to one comparison and any differences found may be the result of the difference in concentration of peptide used.

**The presence of dopamine does modulate an existing peptide network output across the attributes of excitability but does not persist in the 12-dimensional space.** While the effects of individual peptides and amines were evaluated in previous chapters, it was unclear if the addition of an amine would appreciably modify an existing peptide network output. Therefore, as a first step, we qualified and statistically tested the four attributes of excitability in the presence of the peptide alone and in combination with dopamine. When the CCAP elicited rhythms were tested against the CCAP + dopamine elicited rhythms, there were a number of statistical differences between the two. In the phase attribute, there were statistical differences in the PD off phase and LP on phase where the presence of dopamine extended the duty cycle of PD and delayed the onset of LP phase. In both cases, the presence of dopamine in this co-modulated pair recapitulated the effects of dopamine evaluated in isolation in Chapter 4. In that analysis, the duty cycle of PD was statistically larger than CCAP and the on phase of LP was delayed, though not significantly. The difference between that work and these current results is the concentration of dopamine used. In the previous chapter, both dopamine and CCAP were applied at $10^{-6}$ M concentration. In these results, CCAP was still applied at $10^{-6}$ M concentration, but the

concentration of dopamine is half of that. Despite being at half the concentration, the changes in phase suggest that dopamine is having an effect at this reduced concentration.

Across the four attributes evaluated, we expected the possibility of statistical differences in phase due to dopamine's presumed modulation of intrinsic currents which can shift the phases which the peptides cannot do. While suggestive, the caveat to this result is the concentration of dopamine used.

In the spike number and spike frequency attributes, the co-modulated CCAP + dopamine response was also statistically different compared to the CCAP response in PY spike number, PD spike frequency and PY spike frequency. Initially, we did not expect the presence of dopamine to have any effect in these attributes because when evaluated individually, dopamine did not modulate these attributes. The statistical differences presented here may suggest that the presence of dopamine, likely signaling through $D_2$ receptors, in combination with CCAP is inhibiting the activity of these neurons. An alternative explanation for the statistical differences between the individual peptide and the co-modulated condition, however, is the difference in concentration used.

The comparison between RPCH and RPCH + dopamine also resulted in a number of statistical differences in phase, spike number and spike frequency. Notably again, the increase in PD duty cycle and delay in LP and PY on phase in the dopamine co-modulated condition. Additionally, the differences in the spike number and frequency attributes may also indicate an activation of $D_2$ receptors which may be slightly inhibiting the activity of these neurons . While these decreases may also reflect the reduced concentration of RPCH used in the co-modulated condition, out of the three co-modulated comparisons tested, the

pairing with dopamine was the only one where there were statistical differences in these attributes.

Due to the number of differences found when either CCAP or RPCH were tested against their respective dopamine co-modulated responses across the four attributes of excitability, we then asked whether those differences persisted in the 12-dimensional network output space. Neither the CCAP network outputs nor the RPCH network outputs were statistically different compared to their dopamine co-modulated network outputs. While there were not different, when visualized in the reduced principal component space, the distributions of each individual peptide compared to their respective co-modulated distributions were not identical. In both the CCAP and RPCH co-modulated distributions, there was a shift relative to the distributions of only the peptide. This could be indicative of dopamine's actions, or it could simply be due to a difference in the concentration of the peptide used in both cases.

**The presence of serotonin modulates some aspects of an existing CCAP network output but not an existing RPCH network output across the attributes of excitability.** The effects of serotonin were briefly evaluated in Chapter 4. In those results, the cycle frequency following serotonin application was slightly higher than that of CCAP but not statistically different and there was a significant delay in on phase of LP compared to CCAP. The results presented here showed a statistical difference in cycle frequency with CCAP + serotonin compared to CCAP alone. Because the concentration of peptide used in the co-modulated condition was half of the peptide alone, it is unlikely that the increase in cycle frequency was related to the presence of the peptide. This result suggests that the presence of serotonin in combination with CCAP is acting to speed the pyloric rhythm up,

though it is marginal. Additionally, the single statistical difference between CCAP and serotonin when both were evaluated individually, in LP on phase, was lost when CCAP was compared to the co-applied CCAP + serotonin response. This result suggests that in this phase, the phase modulation by serotonin was overshadowed by the presence of CCAP. There was, however, a statistical difference in the on phase of PY, though the delay following CCAP + serotonin application was marginal. It is likely that this statistical difference would be lost with an increase in sample size.

Our initial expectation was that the amines would have limited to no effect on the spike number or spike frequency attributes when combined with a peptide. In this comparison, there were no statistical differences between CCAP and CCAP + serotonin. While we did not evaluate the effects of serotonin alone on these attributes, these results suggest that serotonin is having no effect at this concentration.

When the RPCH + serotonin co-modulated network outputs were compared to RPCH alone, there were no statistical differences in any attribute evaluated. When qualified, the addition of serotonin did not appear to have any significant effect either with the exception of a change in the example LP neuron's burst duration. Both the qualification and quantification suggest that serotonin is having no effect at this concentration on an RPCH elicited network output.

**The presence of octopamine modulates an existing CCAP network output but not an existing RPCH network output across the attributes of excitability.** When qualified, the CCAP and CCAP + octopamine network outputs looked indistinguishable. This was interesting because of the difference in concentration used for the single peptide and co-applied condition. This strong recapitulation of a CCAP network output by CCAP +

octopamine could indicate the octopamine works synergistically with CCAP to maintain the pyloric network output. When qualified on its own in Chapter 4, octopamine also generated a pyloric network output which strongly resembled that of CCAP or the intact state.

When quantified, there was a statistical difference between CCAP and CCAP + octopamine in cycle frequency. Like the increase in cycle frequency with CCAP + serotonin compared to CCAP alone, this increase is unlikely related to the concentration of peptide used. When quantified individually in Chapter 4, the cycle frequency under octopamine conditions was marginally higher though not statistically higher compared to CCAP. The result presented in this work suggests that the combination of CCAP and octopamine are working synergistically to increase the cycle frequency.

There were no differences in the phase attribute between CCAP and CCAP + octopamine. This result is not surprising considering the lack of statistical differences between these two conditions in the phase attribute when evaluated individually which indicated that octopamine was either not modulating the intrinsic currents which could shift the phases or was not at a high enough concentration when evaluated individually. In this current work, that concentration was halved so it is not surprising that there were no differences. There were statistical differences in the PD and LP spike number parameters between CCAP and CCAP + octopamine, however, but both were marginal. The difference in PD spike number is likely a reflection of a slight increase in mean value. The difference in LP spike number likely comes from the single CCAP experiment which would likely be considered an outlier and shifted the mean value enough for a statistical difference to emerge. We initially expected a difference in PY spike number between

CCAP and CCAP + octopamine due to octopamine's inhibitory effect on the PY neuron when evaluated individually. When tested though, there was no statistical difference between the two modulated conditions. This may be the result of octopamine not being at a high enough concentration to sufficiently inhibit PY's activity.

Lastly, like CCAP, the application of RPCH + octopamine strongly recapitulated the RPCH network output when qualified. When statistically tested, there were no differences between RPCH and RPCH + octopamine. These results indicated that octopamine was not contributing to shaping the pyloric network output when combined with RPCH. When evaluated individually in Chapter 2, the network outputs of CCAP and RPCH were not statistically different, but they were not identical. The statistical differences found between CCAP and CCAP + octopamine and the lack of differences found when octopamine was combined with RPCH may reflect the slight differences in each individual peptide's response that the presence of octopamine was acting on. This may be what lead to the detection of difference in some cases but not all. This may also be the reason for the differences found in the CCAP + serotonin network outputs but not the RPCH + serotonin network outputs.

**Peptide and amine co-modulation does not restore flexibility to the pyloric network output.** Following our initial testing to determine if adding an amine in combination with a peptide had any effect on the pyloric network, we next wanted to ask whether distinct pyloric networks could be generated in the presence of distinct combinations of peptide and amine co-modulators. It is likely that each amine is signaling through a distinct pathway intracellularly and there may be differences in the response of the pyloric neurons to the activation of an amine specific signaling pathway and $I_{MI}$ activation by the peptide.

We therefore wanted to ask whether the six co-modulator pairs tested individually were statistically different from each other.

In all four attributes we expected statistical differences between the co-modulators and the intact and decentralized states and there were differences in all four attributes tested. With respect to the co-modulators themselves, there were far fewer differences. The CCAP + dopamine cycle frequency response was statistically lower than the RPCH + dopamine and RPCH + octopamine responses and the duty cycle of PD following RPCH + dopamine application was statistically larger than CCAP + serotonin and CCAP + octopamine.

The statistical difference between CCAP + dopamine and RPCH + dopamine and octopamine in cycle frequency is likely an initial reflection of the difference in cycle frequency between CCAP and RPCH which may be bolstered by the presence of dopamine. When evaluated individually in Chapter 2, the CCAP cycle frequency was statistically slower compared to RPCH and in Chapter 4 the dopamine cycle frequency was slower compared to octopamine though not statistically. Dopamine may be having a stronger effect when coupled with CCAP compared to RPCH and may be acting to further slow the cycle frequency compared to the RPCH co-modulated comparisons and the lack of statistical difference between RPCH + serotonin is likely a reflection of sample size.

The increase in PD duty cycle following RPCH + dopamine application was comparable to that of CCAP + dopamine but the RPCH + dopamine experiments had a single point that shifted its mean further and allowed for the difference to be found.

This increase in PD duty cycle, is interesting because this may represent dopamine's influence in the RPCH + dopamine co-modulated pair. From the previous

chapter evaluating the effects of single amines on the excitability attributes of the network output, the only statistical difference between dopamine and the decentralized and other modulated states was in the PD off phase. There, the duty cycle of PD with dopamine was also significantly delayed compared to decentralized and CCAP. Unlike the increase in PD duty cycle which was captured when dopamine was co-applied with a peptide, the individual action of serotonin in phase, in particular the delay in LP on phase, was not recapitulated when combined with either peptide.

We initially expected a greater number of differences in phase due to the presumed ability of the amines to modulate intrinsic currents which can shift the phases. The lack of differences found, however, could mean either that $I_{MI}$ activation in the pacemaker by the peptide is the dominant effect in controlling the phase response or that the concentration of amine used was not sufficient. To distinguish between these two possibilities, these experiments would need to be repeated using a higher concentration of amine.

We expected there to be no differences across the co-modulated conditions in spike number and spike frequency because dopamine and octopamine did not appreciably modulate those attributes. The only exception being octopamine's inhibitory effect on PY spike number. When combined with a peptide, this drop may have been statistically significant. When evaluated individually, however, there were no differences across the distinct co-modulated conditions in either spike number or frequency.

**At $10^{-6}$ M total concentration, the signaling pathways of peptides and amines do not appear to interact though dopamine may be priming the pyloric network output distinctly.** While we cannot make any absolute statements about the interactions between the peptides and amines at the cellular level, the lack of statistical differences between these

distinct pairs of co-modulators, outside of dopamine's effect on phase and cycle frequency, suggests that there are no appreciable interactions between the cellular pathways of peptides and amine. Dopamine, however, may be priming the pyloric network distinctly from the peptides.

In the results presented here, the peptide was always applied first before co-application of peptide and amine. In five additional experiments not included in these results where CCAP + dopamine was applied, dopamine instead was applied at $10^{-6}$ M concentration. In two of those experiments an obviously perturbed rhythm was generated. This effect did not happen when octopamine was applied first, did not happen when CCAP was applied first and did not happen when RPCH was involved.

The generation of perturbed rhythms following dopamine application only happened twice and this low sample size may be related to an inconsistent response of dopamine at $10^{-6}$ M which may resolve with higher concentration. Because this phenomenon only occurred when dopamine was applied first and when dopamine generated a disrupted rhythm, a first pass assumption is that dopamine is priming the network differently compared to a peptide or octopamine. If this type of activity is able to be generated more consistently, a next step could be to explore whether this network priming effect extends to the intrinsic currents underlying network output generation.

A possible explanation for the difference in activity pattern between CCAP + dopamine and RPCH + dopamine, when dopamine was applied first, is a recruitment of the gastric mill rhythm. The gastric mill rhythm is elicited by a distinct but overlapping set of neurons in the stomatogastric ganglion and has a cycle period of ~ 10 seconds (Nusbaum et al., 2001; Hooper and DiCaprio, 2004). CCAP, in addition to activating $I_{MI}$ in the AB

and LP neurons, also activates $I_{MI}$ in the IC neuron which can participate in both the pyloric and gastric motor patterns (Weimann et al., 1991) while RPCH does not modulate the IC neuron. CCAP can also directly modulate gastric mill neurons (Kirby and Nusbaum, 2007). It is possible that this perturbation in activity represents an enhanced gastric mill rhythm elicited by CCAP but made possible by an initial change in state by dopamine.

**Network output flexibility is not easy to achieve.** Taken together, these results suggest that the pyloric network output cannot become flexible in the presence of both a peptide and an amine. It is likely that distinct network outputs, at least across different amines, can be achieved if the concentration of amine is increased. Similar to the individual amine analysis though, the generation of distinct network outputs statistically may not be meaningful to the intact animal.

Instead of obvious qualitative and quantitative differences across peptide and amine conditions, the slight differences which are not statistically significant may be signaling for distinct behavioral outputs. Until we have a better understanding of coding and decoding mechanisms, we cannot know if these slight differences are meaningful and instead have to rely on statistical measures. The most salient message of this work, coupled with the previous chapters, is that the pyloric network output is remarkable resilient to changes. Despite changes in concentration and combining distinct classes of neuromodulators, the pyloric network is remarkably good at maintaining its output.

# CHAPTER 6
# GENERAL DISCUSSION

## 6.1 Goals

The primary goal of this dissertation was to test under what conditions the pyloric network generates flexible activity or consistent activity. This primary goal was divided into four aims which explored the consequences of peptide modulation, peptide co-modulation, amine modulation and peptide and amine co-modulation.

Our baseline expectation for the first aim was the generation of peptide specific network outputs due to their divergent circuit actions on the pyloric network. We then expected those peptide specific network outputs, representing network output flexibility, to be lost with peptide co-modulation in the second aim. We hypothesized that the combination of multiple peptides, all converging to the same point cellularly and overlapping in their target neurons would activate the pyloric circuit more consistently. This would represent network output consistency instead of flexibility.

We expected in the third aim to also generate modulator specific network outputs by applying individual amines to the pyloric network. Amines, unlike peptides, do not converge cellularly but instead operate bidirectionally to modulate a diverse set of currents, often times in opposing ways within the same neuron. Lastly, in the fourth aim, we expected the generation of distinct pyloric network outputs in the presence of different combinations of peptides and amines. While network output flexibility was lost with convergent peptide co-modulation, the combination of two neuromodulators which do not have the same cellular mechanism could restore flexibility in the network output.

## 6.2 Main Results

The results presented in this dissertation suggest that the generation of statistically distinct pyloric network outputs is possible but difficult to do. The main findings of the four aims are discussed below.

### 6.2.1 Chapter 2: Individual peptide modulation generates both flexible and consistent pyloric network outputs

In Chapter 2, we sought to explore how different individually applied peptide network outputs were from each other, testing the most basic assumption of network output flexibility. Individual peptides have convergent cellular actions and divergent circuit actions which strongly suggest the ability to generate distinct network outputs when applied individually. While the effects of peptides have been widely studied in the pyloric network, there have been fewer studies quantifying how different one peptide elicited output was from another. Additionally, the statistical assessments used did not consider the network output as a whole but instead tested for statistical differences in individual parameters which are highly dependent.

The results presented here, on the one hand, do support the idea of network output flexibility. When fully quantified, a proctolin network output was statistically different from a CCAP network output and an RPCH network output. On the other hand, the results also demonstrate that the network is not as flexible in its output as we initially thought. Outside of the expectation of greater differences between the network outputs of proctolin and CCAP or RPCH, the CCAP and RPCH network outputs were not different from each other in any of the individual attributes or in the combined network output space. This result can be understood by these two peptides targeting the same core pyloric neurons but

represents a place of inflexibility for the pyloric network. It may be that these two peptides are degenerate and can substitute for one another.

### 6.2.2 Chapter 3: Convergent peptide co-modulation promotes consistency over flexibility in the pyloric network output

In Chapter 3, we explored the consequences of convergent co-modulation on the pyloric network output and sought to test another assumption about network output flexibility. The specific hypothesis we tested was that convergent co-modulation promotes consistency in the network output and the results of this chapter support that hypothesis. The neuropeptides in this circuit all converge to activate a single excitable current. This unidirectional convergence bottlenecks the network output resulting in a loss of flexibility and a promotion of consistency. The application of three peptides together did not further promote consistency in any substantial way indicating that the pyloric network output can lose flexibility with only two peptides.

While the network outputs of the co-modulators were not different from each other, the individual peptides constituents could still occupy a distinct place in network output space compared to the peptide combinations. When quantified though there was only a single difference between a constituent and the triplet peptide combinations, and this difference was likely the result of sample size and difference in concentration used. This result indicates that a co-modulated network output does not shift into a new place in network output space but instead occupies the space in between its constituents.

### 6.2.3 Chapter 4: Distinct monoamines differentially modulate aspects of the pyloric network output

We were next interested in evaluating the effects of amines on the pyloric network output with the expectation of flexibility in the network output. Amines, unlike peptides, do not operate unidirectionally towards excitability, at least in various lobster species. We assumed that the amines would have a similar bidirectional effect on the pyloric network in the crab and our expectation was the generation of amine specific network outputs. The results of this chapter, however, were surprising in many ways.

The first surprise was the vastly different activity profiles that dopamine could generate. When quantifiable, a dopamine network output was not different from the decentralized state but when not quantifiable the effect of dopamine was complete disruption of the pyloric network and a loss of tri-phasic activity. This result indicated minimally that dopamine, when quantifiable, does not positively modulate the attributes of excitability. While there were no appreciable effects in the excitability metrics, dopamine application did result in changes to the slow wave oscillations of the pyloric neurons. When attributes of PD's slow wave oscillation were evaluated, differences emerged with dopamine application between the decentralized state, though not all were statistically meaningful.

Octopamine, on the other hand, functioned mostly like a peptide in the excitability space and points to another area of flexibility for the pyloric network output. A fully functional tri-phasic network output can be achieved outside of peptide modulation.

The results of both dopamine and octopamine's actions on the excitability attributes and dopamine's actions on PD's activity indicated that these two amines operate in distinct

spaces and that evaluating only a single group of attributes is not sufficient to capture each neuromodulator's unique actions.

### 6.2.4 Chapter 5: Peptide and amine co-modulation does not restore flexibility to the pyloric network output

Lastly, we wanted to explore the consequences of peptide and amine co-modulation on the pyloric network. Combining the results of the previous three chapters, that CCAP and RPCH elicited network outputs were not statistically different but not identical, that peptide co-modulation does not result in network output flexibility and that individual amines operate in distinct spaces, we asked whether the network output flexibility that was lost with peptide co-modulation could be restored with peptide and amine co-modulation.

As a first step, we evaluated whether a peptide and amine co-modulated network output was statistically different from the peptide response alone. In these evaluations, the only statistical differences were found between the co-modulated pairs with dopamine and their respective peptides. When evaluated in the 12-dimensional network output space, however, the individual differences found between CCAP versus CCAP + dopamine and RPCH versus RPCH + dopamine did not lead a statistical difference.

Taken together, these results suggest that dopamine's actions are fundamentally distinct from octopamine and serotonin. Additionally, even at a concentration of $5x10^{-7}$ M, dopamine is still able to exert an effect on the pyloric network, though it is not as dramatic as a higher concentration can be. Unlike dopamine, octopamine and serotonin may instead be acting synergistically with the peptide to bolster the peptide effect, but this synergistic effect may be concentration dependent where a higher concentration may shift the response from cooperative to disruptive, particularly with serotonin.

When the co-modulated conditions are tested against each other, there were a limited number of differences between them. The statistical differences found were isolated to the cycle frequency and the PD off phase parameter. The differences in the cycle frequency attribute may be related to the inherent differences in cycle frequency between CCAP and RPCH while the difference in the phase of PD off may be related to the presence of dopamine. The phase attribute in general is an interesting attribute to evaluate because of the amines presumed modulation of the intrinsic currents which can shift the phases. The increase in PD duty cycle with both dopamine containing co-modulator pairs suggests that even at a reduced concentration, dopamine is still able to exert an effect, which may be enhanced at a higher concentration.

## 6.3 General Conclusions

The results presented in this dissertation represent the first fully quantitative description of how different two neuromodulator elicited patterns of activity are. This was accomplished by taking a new approach to the quantification of difference and statistical testing, with the express purpose of evaluating an entire pattern of activity not just a single parameter or attribute. From this quantification of difference, we could then probe the idea of network output flexibility. In particular we were interested in testing whether individual neuromodulator elicited patterns of activity represented flexibility in the network output and what the consequences to network output flexibility were under distinct co-modulatory conditions.

The most salient point from this collection of results is that the pyloric network output is remarkably resilient. The pyloric network was presented with four distinct

challenges to see under which circumstances flexibility could arise. Outside of the statistically distinct effects of one peptide, proctolin, and the loss of activity with dopamine, all other neuromodulator elicited network outputs evaluated were not statistically different from each other. Additionally, when not completely disrupted like with dopamine, these outputs qualitatively look similar to one another.

The lack of flexibility in the network output of a central pattern generating circuit, while unexpected, could act as a stabilizing mechanism. This circuit, like other central pattern generating circuits, generates a fundamental pattern of activity. It may be that these circuits are not able to deviate appreciably in their output under any particular neuromodulator condition to ensure that a functional output can always be generated. This lack of flexibility, however, is a lack of flexibility from a statistical perspective in the particular attributes of activity we evaluated. As much as this work is an improvement on the previous methods of quantifying and statistically testing difference, a network output is more than just the four attributes of excitability and PD's slow wave oscillation evaluated here. It may be that these individual neuromodulator network outputs, and even the co-modulated network outputs, are in fact distinct from each other but those differences are held in attributes or parameters that we did not explicitly evaluate. The dopamine result also highlights the necessity to explore a wide range of attributes because differences can arise in places not initially considered.

Additionally, we define difference in terms of a p-value however these network outputs, while not statistically different according to their p-values, were not identical. The smaller changes in the network output elicited by each distinct neuromodulator and combination of neuromodulators may be more important downstream of the ganglion then

we can appreciate.  While not meaningful enough for our statistics, these smaller changes may be what is signaling for distinct patters of activity.

# APPENDIX A

# STATISTICAL TABLES

In Chapters 2-5 a brief statistical result was included in the text. In Appendix A we provide the full statistical results for those analyses. In all tables, df indicates degrees of freedom and S.E.M. indicates standard error of the mean. If the data were not normally distributed, the median along with the 25th and 75th percentiles is given instead. Number in parentheses below or next to each condition indicates the sample size per condition.

In Table A.2, P & C indicates proctolin + CCAP, C & R indicates CCAP + RPCH, R & P indicates RPCH + proctolin. In Table A.3, P & C & R indicates proctolin + CCAP + RPCH, C & P & O indicates CCAP + proctolin + oxotremorine.

# A.1 Single Peptide Excitability Attributes

**Table A.1** Statistical Results of Single Peptide Excitability Attributes

| parameter | normality | variance | statistical test | test statistic | df | residuals | p value | intact: mean ± S.E.M (43) | decentralized: mean ± S.E.M (46) | proctolin: mean ± S.E.M (15) | CCAP: mean ± S.E.M (18) | RPCH: mean ± S.E.M (19) |
|---|---|---|---|---|---|---|---|---|---|---|---|---|
| cycle frequency | passed | passed | One way ANOVA | F = 101.308 | 4 | 136 | **< 0.001** | 1.323 ± 0.021 | 0.705 ± 0.025 | 0.854 ± 0.040 | 0.804 ± 0.033 | 0.94 ± 0.026 |
| phase | failed | failed | Two way ANOVA | $F_{phase}$ = 2415.25<br>$F_{modulator}$ = 62.660<br>$F_{interaction}$ = 15.639 | 4<br>4<br>16 | 680<br>680<br>680 | **< 0.001**<br>**< 0.001**<br>**< 0.001** | PD off: 0.183 ± 0.005 | PD off: 0.1264 ± 0.005 | PD off: 0.1726 ± 0.007 | PD off: 0.1272 ± 0.009 | PD off: 0.1418 ± 0.006 |
| | | | | | | | | LP on: 0.402 ± 0.008 | LP on: 0.3608 ± 0.011 | LP on: 0.3929 ± 0.011 | LP on: 0.3332 ± 0.008 | LP on: 0.3874 ± 0.012 |
| | | | | | | | | LP off: 0.710 ± 0.008 | LP off: 0.5023 ± 0.016 | LP off: 0.6806 ± 0.010 | LP off: 0.7036 ± 0.016 | LP off: 0.7347 ± 0.015 |
| | | | | | | | | PY on: 0.666 ± 0.014 | PY on: 0.4840 ± 0.016 | PY on: 0.6260 ± 0.017 | PY on: 0.6396 ± 0.025 | PY on: 0.6651 ± 0.023 |
| | | | | | | | | PY off: 0.980 ± 0.005 | PY off: 0.9707 ± 0.005 | PY off: 0.9941 ± 0.006 | PY off: 0.9554 ± 0.007 | PY off: 0.9616 ± 0.005 |
| spike number | failed | failed | Two way ANOVA | $F_{neuron}$ = 139.49<br>$F_{modulator}$ = 13.765<br>$F_{ineraction}$ = 26.097 | 2<br>4<br>8 | 408<br>408<br>408 | **< 0.001**<br>**< 0.001**<br>**< 0.001** | PD: 4.46 ± 0.207 | PD: 2.71 ± 0.196 | PD: 4.88 ± 0.407 | PD: 2.47 ± 0.257 | PD: 3.31 ± 0.261 |
| | | | | | | | | LP: 8.36 ± 0.288 | LP: 4.05 ± 0.345 | LP: 10.30 ± 0.562 | LP: 14.40 ± 0.755 | LP: 10.65 ± 0.559 |
| | | | | | | | | PY: 8.10 ± 0.3715 | PY: 9.64 ± 0.832 | PY: 10.61 ± 0.918 | PY: 6.36 ± 0.730 | PY: 6.05 ± 0.862 |
| spike frequency | passed | passed | Two way ANOVA | $F_{neuron}$ = 26.04<br>$F_{modulator}$ = 115.02<br>$F_{ineraction}$ = 6.388 | 2<br>4<br>8 | 408<br>408<br>408 | **< 0.001**<br>**< 0.001**<br>**< 0.001** | PD: 29.05 ± 1.153 | PD: 11.26 ± 1.121 | PD: 23.01 ± 2.295 | PD: 11.38 ± 1.803 | PD: 16.89 ± 1.266 |
| | | | | | | | | LP: 30.87 ± 0.903 | LP: 12.41 ± 1.052 | LP: 26.90 ± 1.681 | LP: 26.88 ± 0.9240 | LP: 25.51 ± 1.251 |
| | | | | | | | | PY: 29.16 ± 0.916 | PY: 15.07 ± 0.824 | PY: 23.59 ± 1.596 | PY: 17.31 ± 1.2345 | PY: 18.05 ± 1.460 |

## A.2 Paired Peptide Co-modulation Excitability Attributes

**Table A.2** Statistical Results of Paired Peptide Co-modulation Excitability Attributes

| parameter | normality | variance | statistical test | test statistic | df | residuals | p value | intact: mean ± S.E.M (27) | decentralized: mean ± S.E.M (28) | P & C: mean ± S.E.M (11) | C & R: mean ± S.E.M (11) | R & P: mean ± S.E.M (11) |
|---|---|---|---|---|---|---|---|---|---|---|---|---|
| cycle frequency | passed | passed | One way ANOVA | F = 41.429 | 4 | 83 | **< 0.001** | 1.291 ± 0.037 | 0.715 ± 0.037 | 0.839 ± 0.037 | 0.967 ± 0.035 | 0.902 ± 0.033 |
| phase | failed | failed | Two way ANOVA | $F_{phase}$ = 1051.426<br>$F_{modulator}$ = 25.098<br>$F_{interaction}$ = 6.118 | 4<br>4<br>16 | 415<br>415<br>415 | **<0.001**<br>**<0.001**<br>**<0.001** | PD off: 0.2076 ± 0.010 | PD off: 0.1376 ± 0.009 | PD off: 0.1640 ± 0.008 | PD off: 0.1454 ± 0.013 | PD off: 0.1660 ± 0.006 |
| | | | | | | | | LP on: 0.3987 ± 0.012 | LP on: 0.3704 ± 0.021 | LP on: 0.3699 ± 0.010 | LP on: 0.3626 ± 0.016 | LP on: 0.3963 ± 0.016 |
| | | | | | | | | LP off: 0.6869 ± 0.014 | LP off: 0.5250 ± 0.026 | LP off: 0.7402 ± 0.019 | LP off: 0.7119 ± 0.014 | LP off: 0.7548 ± 0.017 |
| | | | | | | | | PY on: 0.6106 ± 0.016 | PY on: 0.5094 ± 0.028 | PY on: 0.6771 ± 0.019 | PY on: 0.6550 ± 0.027 | PY on: 0.6892 ± 0.018 |
| | | | | | | | | PY off: 0.9695 ± 0.008 | PY off: 0.9506 ± 0.009 | PY off: 0.9616 ± 0.011 | PY off: 0.9316 ± 0.014 | PY off: 0.9782 ± 0.017 |
| spike number | failed | failed | Two way ANOVA | $F_{neuron}$ = 63.476<br>$F_{modulator}$ = 4.439<br>$F_{interaction}$ = 141.916 | 2<br>4<br>8 | 249<br>249<br>249 | **<0.001**<br>**0.002**<br>**<0.001** | PD: 4.70 ± 0.251 | PD: 3.04 ± 0.254 | PD: 4.53 ± 0.495 | PD: 2.65 ± 0.311 | PD: 4.44 ± 0.281 |
| | | | | | | | | LP: 6.96 ± 0.429 | LP: 4.81 ± 0.457 | LP: 12.77 ± 0.945 | LP: 11.45 ± 0.856 | LP: 11.33 ± 0.828 |
| | | | | | | | | PY: 8.41 ± 0.391 | PY: 9.88 ± 1.333 | PY: 7.62 ± 0.894 | PY: 5.52 ± 0.739 | PY: 7.08 ± 0.592 |
| spike frequency | passed | passed | Two way ANOVA | $F_{neuron}$ = 16.016<br>$F_{modulator}$ = 55.613<br>$F_{interaction}$ = 2.815 | 2<br>4<br>8 | 249<br>249<br>249 | **<0.001**<br>**<0.001**<br>**0.005** | PD: 27.32 ± 1.116 | PD: 12.91 ± 1.190 | PD: 21.31 ± 2.529 | PD: 14.80 ± 2.484 | PD: 21.77 ± 1.443 |
| | | | | | | | | LP: 28.46 ± 0.933 | LP: 16.05 ± 1.178 | LP: 26.08 ± 1.242 | LP: 28.46 ± 1.236 | LP: 26.05 ± 1.765 |
| | | | | | | | | PY: 28.55 ± 1.134 | PY: 14.97 ± 0.845 | PY: 23.21 ± 1.903 | PY: 18.06 ± 2.063 | PY: 21.22 ± 2.004 |

## A.3 Triplet Co-modulation Excitability Attributes

**Table A.3** Statistical Results of Triplet Co-modulation Excitability Attributes

| parameter | normality | variance | statistical test | test statistic | df | residuals | p value | intact: median [25%, 75%] (10) | decentralized: median [25%, 75%] (5) | P & C & R: median [25%, 75%] (5) | C & P & O: median [25%, 75%] (5) |
|---|---|---|---|---|---|---|---|---|---|---|---|
| cycle frequency | passed | passed | One way ANOVA on Ranks | H = 19.715 | 3 | | **<0.001** | 1.209 [1.126, 1.311] | 0.652 [0.543, 0.713] | 0.962 [0.844, 1.019] | 0.849 [0.768, 0.937] |
| phase | failed | passed | Two way ANOVA | $F_{phase}$ = 378.869<br>$F_{modulator}$ = 7.104<br>$F_{interaction}$ = 2.925 | 4<br>3<br>12 | 105<br>105<br>105 | **<0.001**<br>**<0.001**<br>**0.002** | PD off: 0.2056 ± 0.008 | PD off: 0.1404 ± 0.008 | PD off: 0.1579 ± 0.009 | PD off: 0.1759 ± 0.011 |
| | | | | | | | | LP on: 0.3698 ± 0.021 | LP on: 0.4011 ± 0.061 | LP on: 0.3618 ± 0.030 | LP on: 0.3892 ± 0.018 |
| | | | | | | | | LP off: 0.6559 ± 0.023 | LP off: 0.5065 ± 0.071 | LP off: 0.7243 ± 0.013 | LP off: 0.7132 ± 0.021 |
| | | | | | | | | PY on: 0.6042 ± 0.027 | PY on: 0.5032 ± 0.075 | PY on: 0.7034 ± 0.022 | PY on: 0.6781 ± 0.016 |
| | | | | | | | | PY off: 0.9639 ± 0.012 | PY off: 0.9597 ± 0.005 | PY off: 0.9363 ± 0.016 | PY off: 1.00 ± 0.008 |
| spike number | failed | failed | Two way ANOVA | $F_{nueron}$ = 13.922<br>$F_{modulator}$ = 4.866<br>$F_{interaction}$ = 5.756 | 2<br>3<br>6 | 63<br>63<br>63 | **<0.001**<br>**0.004**<br>**<0.001** | PD: 4.79 ± 0.434 | PD: 3.84 ± 0.377 | PD: 4.04 ± 0.506 | PD: 5.60 ± 0.398 |
| | | | | | | | | LP: 7.13 ± 0.491 | LP: 3.05 ± 0.830 | LP: 10.76 ± 0.363 | LP: 10.64 ± 1.249 |
| | | | | | | | | PY: 7.73 ± 0.570 | PY: 6.88 ± 2.577 | PY: 6.24 ± 0.713 | PY: 5.67 ± 1.048 |
| spike frequency | passed | passed | Two way ANOVA | $F_{nueron}$ = 0.859<br>$F_{modulator}$ = 20.865<br>$F_{interaction}$ = 0.869 | 2<br>3<br>6 | 63<br>63<br>63 | 0.426<br>**<0.001**<br>0.523 | PD: 27.87 ± 3.121 | PD: 15.32 ± 1.631 | PD: 22.94 ± 3.608 | PD: 23.52 ± 1.396 |
| | | | | | | | | LP: 26.26 ± 1.484 | LP: 8.24 ± 2.771 | LP: 25.93 ± 2.713 | LP: 22.52 ± 1.823 |
| | | | | | | | | PY: 26.13 ± 1.522 | PY: 12.20 ± 2.174 | PY: 24.32 ± 1.812 | PY: 17.98 ± 2.665 |

## A.4 Single Monoamine Excitability Attributes

**Table A.4** Statistical Results of Single Monoamine Excitability Attributes

| parameter | normality | variance | statistical test | test statistic | df | residuals | p value | intact: mean ± S.E.M (29) | decentralized: mean ± S.E.M (33) | Dopamine: mean ± S.E.M (8) | Octopamine: mean ± S.E.M (4) | CCAP: mean ± S.E.M (18) | Serotonin: mean ± S.E.M (5) |
|---|---|---|---|---|---|---|---|---|---|---|---|---|---|
| cycle frequency | passed | passed | One way ANOVA | F = 47.527 | 5 | 91 | **< 0.001** | 1.356 ± 0.0292 | 0.749 ± 0.0319 | 0.831 ± 0.073 | 0.897 ± 0.072 | 0.804 ± 0.033 | 0.928 ± 0.057 |

| parameter | normality | variance | statistical test | test statistic | df | residuals | p value | intact: median [25%, 75%] / mean ± S.E.M (29) | decentralized: median [25%, 75%] / mean ± S.E.M (33) | Dopamine: median [25%, 75%] / mean ± S.E.M (8) | Octopamine: median [25%, 75%] / mean ± S.E.M (4) | CCAP: median [25%, 75%] / mean ± S.E.M (18) | Serotonin: median [25%, 75%] / mean ± S.E.M (5) |
|---|---|---|---|---|---|---|---|---|---|---|---|---|---|
| PD off phase | failed | | One way ANOVA on ranks | H = 27.758 | 5 | | **< 0.001** | 0.172 [0.154, 0.208] | 0.136 [0.0976, 0.163] | 0.201 [0.179, 0.235] | 0.151 [0.132, 0.168] | 0.127 [0.083, 0.150] | 0.164 [0.130, 0.183] |
| LP on phase | passed | failed | One way ANOVA on ranks | H = 21.067 | 5 | | **< 0.001** | 0.377 [0.337, 0.427] | 0.379 [0.315, 0.432] | 0.434 [0.365,0.450] | 0.418 [0.362, 0.463] | 0.333 [0.298, 0.354] | 0.462 [0.425, 0.524] |
| LP off phase | failed | | One way ANOVA on ranks | H = 47.362 | 5 | | **< 0.001** | 0.675[0.646, 0.704] | 0.534 [0.456, 0.604] | 0.629 [0.541, 0.694] | 0.690 [0.593, 0.793] | 0.725 [0.694, 0.783] | 0.708 [0.660, 0.742] |
| PY on phase | passed | passed | One way ANOVA | F = 7.852 | 5 | 91 | **< 0.001** | 0.601 ± 0.0135 | 0.469 ± 0.0182 | 0.554 ± 0.0429 | 0.617 ± 0.057 | 0.601 ± 0.025 | 0.573 ± 0.015 |
| PY off phase | failed | | One way ANOVA on ranks | H = 5.844 | 5 | | 0.322 | 0.976 [0.959, 0.985] | 0.978 [0.955, 0.985] | 0.975 [0.962, 0.999] | 0.982 [0.942 0.986] | 0.955 [0.926, 0.983] | 0.983 [0.972, 0.998] |



| parameter | normality | variance | statistical test | test statistic | df | residuals | p value | intact: median [25%, 75%] / mean ± S.E.M (24) | decentralized: median [25%, 75%] / mean ± S.E.M (20) | Dopamine: median [25%, 75%] / mean ± S.E.M (8) | Octopamine: median [25%, 75%] / mean ± S.E.M (4) | CCAP: median [25%, 75%] / mean ± S.E.M (18) |
|---|---|---|---|---|---|---|---|---|---|---|---|---|
| PD spike num. | failed | | One way ANOVA on ranks | H = 14.095 | 4 | | **0.007** | 3.94 [3.00, 5.00] | 2.43 [1.00, 4.00] | 3.00 [1.27, 3.75] | 3.04 [2.25, 4.52] | 3.00 [1.00, 3.18] |
| LP spike num. | passed | passed | One way ANOVA | F = 45.824 | 4 | 69 | **< 0.001** | 7.61 ± 0.497 | 4.12 ± 0.519 | 4.19 ± 0.689 | 6.01 ± 0.353 | 14.40 ± 0.755 |
| PY spike num. | failed | | One way ANOVA on ranks | H = 16.574 | 4 | | **0.002** | 8.50 [7.17, 9.48] | 11.18 [5.14, 13.89] | 6.92 [4.79, 8.72] | 3.40 [1.38, 6.04] | 7.02 [3.04, 8.12] |

| parameter | normality | variance | statistical test | test statistic | df | residuals | p value | intact: median [25%, 75%] / mean ± S.E.M (24) | decentralized: median [25%, 75%] / mean ± S.E.M (20) | Dopamine: median [25%, 75%] / mean ± S.E.M (8) | Octopamine: median [25%, 75%] / mean ± S.E.M (4) | CCAP: median [25%, 75%] / mean ± S.E.M (18) |
|---|---|---|---|---|---|---|---|---|---|---|---|---|
| PD spike freq. | failed | | One way ANOVA on ranks | H = 43.07 | 4 | | **< 0.001** | 27.35 [22.87, 31.86] | 10.69 [0, 17.10] | 7.84 [1.65, 14.73] | 18.40 [13.20, 19.07] | 13.56 [0, 16.50] |
| LP spike freq. | passed | passed | One way ANOVA | F = 41.932 | 4 | 77 | **< 0.001** | 29.15 ± 1.27 | 12.43 ± 1.092 | 11.98 ± 1.926 | 16.41 ± 1.664 | 26.88 ± 0.924 |
| PY spike freq. | failed | | One way ANOVA on ranks | H = 48.209 | 4 | | **< 0.001** | 31.35 [28.25, 33.00] | 17.51 [13.99, 19.34] | 14.40 [12.05, 16.21] | 15.73 [3.34, 23.83] | 18.08 [15.66, 20.45] |

.

## A.5 Single Monoamine Slow Wave Oscillation and Spiking Attributes

**Table A.5** Statistical Results of Single Monoamine Slow Wave Oscillation and Spiking Attributes

| parameter | normality | variance | statistical test | test statistic | df | p value | decentralized: median [25%, 75%] / mean ± S.E.M (7) | Dopamine: median [25%, 75%] / mean ± S.E.M (8) |
|---|---|---|---|---|---|---|---|---|
| Amplitude | passed | passed | t-test | t = 1.223 | 13 | 0.243 | 15.710 ± 2.049 | 12.575 ± 1.594 |
| Half width | failed | | Mann-Whitney Rank Sum Test | U = 40.000 | | 0.072 | 0.340 [0.299, 0.423] | 0.444 [0.388, 0.524] |
| Spike prominence | passed | passed | t-test | t = -0.732 | 13 | 0.477 | 22.613 ± 2.013 | 24.876 ± 2.292 |
| Inter-spike interval | passed | passed | t-test | t = -3.197 | 13 | **0.007** | 0.0334 ± 0.0136 | 0.1330 ± 0.0267 |
| Synaptic area | failed | | Mann-Whitney Rank Sum Test | U = 17.500 | | 0.232 | 0.259 [0.0443, 0.425] | 0.443 [0.168, 1.080] |

| parameter | normality | variance | statistical test | test statistic | df | p value | decentralized: mean ± S.E.M (14) | Dopamine: mean ± S.E.M (14) |
|---|---|---|---|---|---|---|---|---|
| Paired trough voltage | passed | | Paired t-test | t = -1.106 | 6 | 0.311 | -61.016 ± 1.312 | -59.762 ± 1.115 |

## A.6 Peptide and Amine Co-modulation Excitability Attributes

**Table A.6** Statistical Results of Peptide and Peptide + Amine Co-modulation Excitability Attributes

| parameter | normality | variance | statistical test | test statistic | df | residuals | p value | intact: median [25%, 75%] / mean ± S.E.M (27) | decentralized: median [25%, 75%] / mean ± S.E.M (27) | CCAP + Dopamine: median [25%, 75%] / mean ± S.E.M (9) | RPCH + Dopamine: median [25%, 75%] / mean ± S.E.M (9) | CCAP + Octopamine: median [25%, 75%] / mean ± S.E.M (7) | RPCH + Octopamine: median [25%, 75%] / mean ± S.E.M (5) | CCAP + Serotonin: median [25%, 75%] / mean ± S.E.M (6) | RPCH + Serotonin: median [25%, 75%] / mean ± S.E.M (4) |
|---|---|---|---|---|---|---|---|---|---|---|---|---|---|---|---|
| cycle frequency | passed | passed | One way ANOVA | F = 41.340 | 7 | 86 | **< 0.001** | 1.316 ± 0.0234 | 0.715 ± 0.0339 | 0.792 ± 0.0525 | 0.999 ± 0.0281 | 0.889 ± 0.0240 | 1.034 ± 0.0355 | 0.856 ± 0.0487 | 0.975 ± 0.0674 |
| PD off phase | passed | passed | One way ANOVA | F = 6.718 | 7 | 86 | **< 0.001** | 0.184 ± 0.007 | 0.126 ± 0.007 | 0.180 ± 0.0196 | 0.212 ± 0.0188 | 0.137 ± 0.0125 | 0.160 ± 0.0181 | 0.138 ± 0.0134 | 0.150 ± 0.0176 |
| LP on phase | passed | failed | One way ANOVA on ranks | H = 12.383 | 7 | | 0.089 | 0.372 [0.348, 0.391] | 0.340 [0.272, 0.379] | 0.414 [0.344, 0.430] | 0.397 [0.385, 0.435] | 0.392 [0.351, 0.409] | 0.377 [0.333, 0.411] | 0.368 [0.347, 0.385] | 0.349 [0.324, 0.380] |
| LP off phase | failed | | One way ANOVA on ranks | H = 52.635 | 7 | | **< 0.001** | 0.679 [0.647, 0.703] | 0.513 [0.411, 0.590] | 0.630 [0.586, 0.701] | 0.754 [0.716, 0.771] | 0.698 [0.692, 0.781] | 0.723 [0.632, 0.776] | 0.753 [0.628, 0.772] | 0.771 [0.608, 0.783] |
| PY on phase | passed | passed | One way ANOVA | F = 7.003 | 7 | 86 | **< 0.001** | 0.587 ± 0.015 | 0.440 ± 0.022 | 0.582 ± 0.021 | 0.625 ± 0.031 | 0.613 ± 0.037 | 0.538 ± 0.044 | 0.616 ± 0.041 | 0.585 ± 0.067 |
| PY off phase | failed | | One way ANOVA on ranks | H = 4.737 | 7 | | 0.69 | 0.977 [0.961, 0.989] | 0.978 [0.940, 0.982] | 0.978 [0.940, 0.981] | 0.982 [0.955, 0.996] | 0.950 [0.933, 0.997] | 0.990 [0.935, 0.997] | 0.961 [0.914, 0.981] | 0.974 [0.929, 0.989] |
| PD spike num. | failed | | One way ANOVA on ranks | H = 20.822 | 7 | | **0.004** | 4.00 [3.41, 5.00] | 2.00 [1.00, 4.00] | 3.60 [1.84, 4.00] | 3.03 [2.28, 3.98] | 3.00 [2.08, 4.13] | 4.00 [2.23, 4.07] | 2.89 [1.00, 3.83] | 3.54 [3.02, 4.00] |
| LP spike num. | passed | passed | One way ANOVA | F = 11.459 | 7 | 86 | **< 0.001** | 7.93 ± 0.419 | 4.30 ± 0.453 | 8.12 ± 0.948 | 9.16 ± 0.642 | 10.44 ± 1.110 | 8.62 ± 0.673 | 11.16 ± 1.639 | 10.04 ± 1.046 |
| PY spike num. | failed | | One way ANOVA on ranks | H = 17.672 | 7 | | **0.014** | 7.35 [6.03, 9.51] | 9.60 [4.83, 12.66] | 5.89 [4.62, 7.74] | 5.54 [3.72, 8.68] | 5.60 [2.69, 8.26] | 9.93 [6.16, 11.53] | 2.48 [2.34, 5.90] | 7.39 [3.50, 11.77] |
| PD spike freq. | failed | | One way ANOVA on ranks | H = 57.076 | 7 | | **< 0.001** | 28.76 [22.87, 32.51] | 10.90 [0, 16.49] | 11.76 [4.15, 14.18] | 12.50 [10.07, 15.23] | 14.07 [12.59, 21.53] | 20.23 [13.98, 23.05] | 13.50 [0, 18.94] | 18.86 [16.90, 22.45] |
| LP spike freq. | passed | passed | One way ANOVA | F = 19.007 | 7 | 86 | **< 0.001** | 29.23 ± 1.17 | 12.57 ± 1.17 | 20.99 ± 1.848 | 24.85 ± 1.517 | 24.29 ± 1.489 | 23.64 ± 1.16 | 24.15 ± 1.48 | 24.12 ± 1.71 |
| PY spike freq. | passed | passed | One way ANOVA | F = 18.262 | 7 | 86 | **< 0.001** | 29.11 ± 1.00 | 15.83 ± 1.06 | 16.00 ± 1.64 | 17.83 ± 1.01 | 19.07 ± 1.88 | 21.08 ± 0.72 | 16.08 ± 1.44 | 19.08 ± 1.35 |

# APPENDIX B

# MAPPING CIRCUIT DYNAMICS DURING FUNCTION AND DYSFUNCTION

This work has been published in eLife. Author contributions are as follows: Srinivas Gorur-Shandilya, Conceptualization, Data curation, Formal analysis, Investigation, Methodology, Software, Validation, Visualization, Writing – original draft, Writing – review and editing; Elizabeth M. Cronin, Investigation, Methodology, Writing – review and editing; Anna C. Schneider, Investigation, Methodology, Resources, Writing – review and editing; Sara Ann Haddad, Conceptualization, Investigation, Methodology, Writing – review and editing; Philipp Rosenbaum, Investigation, Methodology; Dirk Bucher, Project administration, Software, Supervision, Writing – original draft, Writing – review and editing; Farzan Nadim, Project administration, Supervision, Writing – original draft, Writing – review and editing; Eve Marder, Conceptualization, Funding acquisition, Project administration, Supervision, Writing – original draft, Writing – review and editing.

## B.1 Introduction

Neural circuits can generate a wide variety of spiking dynamics, but must constrain their dynamics to function appropriately. Cortical circuits maintain irregular spiking patterns through a balance of excitatory and inhibitory inputs (van Vreeswijk and Sompolinsky, 1996; Mariño et al., 2005; Brunel and Wang, 2003) and the loss of canonical dynamics is associated with neural diseases like channelopathies and epilepsy (Marbán, 2002; Staley, 2015). Preserving functional dynamics can be a challenge for neural circuits for the following reasons. The same spike pattern can be generated by diverse circuits with many

different topologies and broadly distributed synaptic and cellular parameters (Prinz et al., 2004; Golowasch et al., 2002; Alonso and Marder, 2019; Memmesheimer and Timme, 2006). Furthermore, neural circuits are constantly being reconfigured, with ion channel protein turnover, and homeostatic feedback mechanisms modifying conductance and synapse strengths continuously (Turrigiano et al., 1994; Turrigiano et al., 1995; O'Leary et al., 2014; Franci et al., 2020). The problem of maintaining functional activity patterns is aggravated by the fact that functional circuit dynamics tend to lie within a low-dimensional subspace within the high-dimensional state space: of the numerous possible solutions, only a few are functional and are found in animals (Cunningham and Yu, 2014; Pang et al., 2016). How do neural circuits preserve functional dynamics despite these obstacles?

Answering this question requires, as a prerequisite, a quantitative description of the dynamics of neural circuits during function and dysfunction. When rhythms are regular, this is relatively simple, but when rhythms become irregular, classifying them becomes hard (Haddad and Marder, 2018; Tang et al., 2012; Haley et al., 2018). In this article, we study the dynamics of a well-studied central pattern generator, the pyloric circuit in the stomatogastric ganglion (STG) in Cancer borealis (Marder and Bucher, 2007). The pyloric circuit is small, in crabs consisting of 13 neurons coupled by inhibitory and electrical synapses. Its topology and cellular dynamics are well understood, and the circuit generates a clearly defined 'functional' collective behavior where bursts of spikes from three different cell types alternate rhythmically to generate a triphasic motor pattern. The stereotypy and periodicity of the motor pattern suggest that the baseline dynamics of the pyloric circuit are fundamentally low dimensional. This has allowed for the effective parameterization of the rhythm by a small number of ad hoc descriptors such as the burst

period, duty cycles, and phase of each neuron (Hartline and Maynard, 1975; Eisen and Marder, 1984; Miller and Selverston, 1982).

In response to perturbations that span many cycles, pyloric circuit dynamics are not always periodic, and descriptors that work well to characterize the canonical rhythm are inadequate to describe these atypical dynamic states. Efforts to study circuit dynamics under these regimes, and to characterize how the circuit responds to, and recovers from perturbations, have been frustrated by the inability to quantitatively describe irregular and non-stationary dynamics (Haddad and Marder, 2018; Tang et al., 2012; Haley et al., 2018).

In this article, we set out to address the problem of quantitatively describing neural circuit dynamics under a variety of conditions. We reasoned that circuit dynamics lie on some lower-dimensional set within the full high-dimensional space of possible dynamics, even when circuits exhibit atypical and nonfunctional behavior, because even circuits generating dysfunctional dynamics are still constrained by cellular parameters and network topology. We therefore set out to find and visualize this subset of spike patterns using an unsupervised machine learning approach to visualize patterns in the high-dimensional data in two dimensions. This method allows us to visualize the totality of a large and complex dataset of spike patterns, while being explicit about the assumptions and biases in the analysis. Using this method, we found nontrivial features in the distribution of the data that hinted at diverse, stereotyped responses to perturbations. Using this compact representation allowed us to efficiently manually classify these patterns and measure transitions between these patterns. We were thus able to characterize the diversity of circuit dynamics under baseline and perturbed conditions, and identify anecdotally observed atypical states within the full repertoire of spiking patterns for many hundreds of animals.

## B.2 Results

**Perturbations can destabilize the triphasic pyloric rhythm.** Studies that measure the pyloric rhythm commonly involve recording from nerves from the STG in ex vivo preparations. Preparations typically also include the stomatogastric nerve (stn) that carries the axons of descending neuromodulatory neurons from the esophageal and commissural ganglia that project into the STG. Under baseline conditions (11°C, with the stn intact, Figure B.1a), the periodic triphasic oscillation of the pyloric circuit can be measured by extracellular recordings of the lateral pyloric, pyloric dilator, and pyloric nerves (lpn, pdn, and pyn) (Figure B.1a). Bursts of spikes from the pyloric dilator (PD) neurons on the pdn are followed by bursts of spikes from the lateral pyloric neuron (LP) on lpn and bursts of spikes from the pyloric neurons (PY) on pyn. Spikes from lateral posterior gastric (LPG) neurons are also found on the pyn nerve in these recordings and can be differentiated from PY spikes by their shape and timing (LPG is active during PD bursts). Under these control conditions, where the rhythm is robust and spikes from these neurons are easily identifiable both by their location on the nerve and their phase in the cycle, the dual problems of identifying spikes from raw extracellular recordings and meaningfully describing circuit dynamics are easily resolvable.

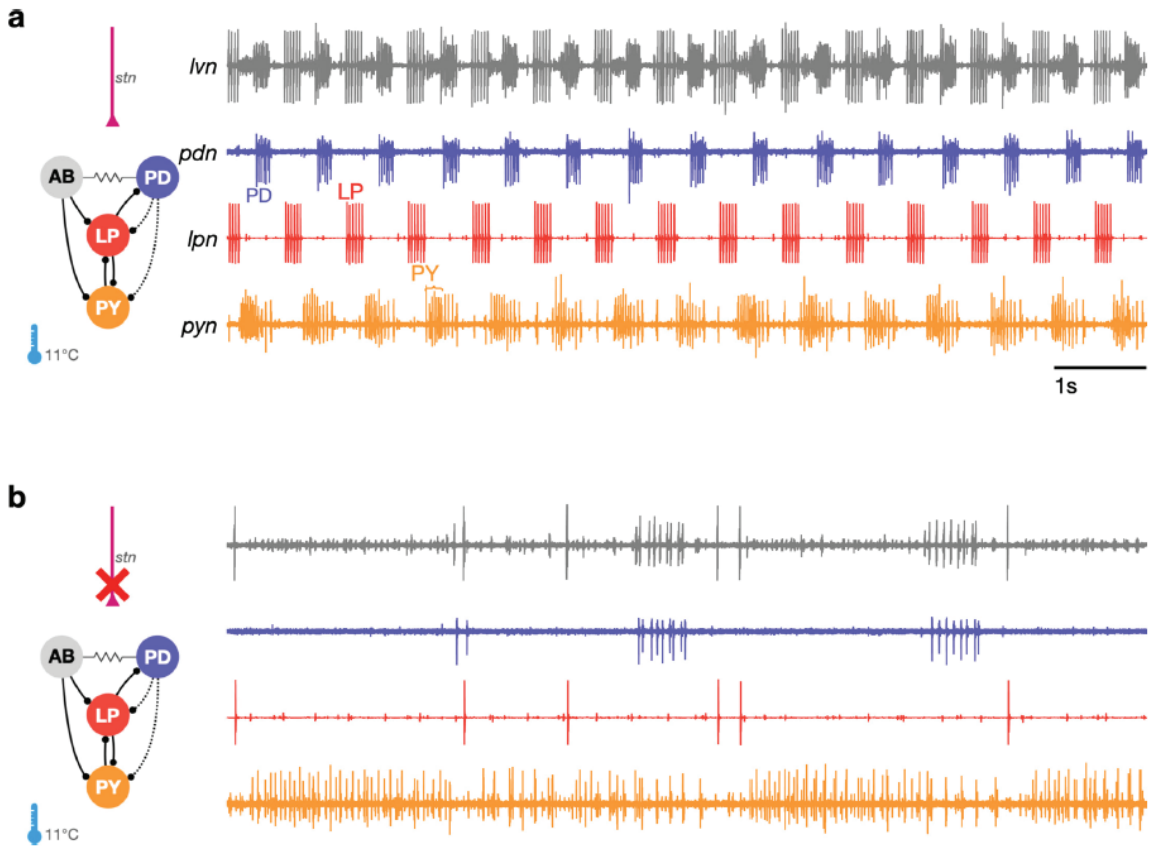


**Figure B.1** The triphasic pyloric rhythm can become irregular and hard to characterize under perturbation. (a) Simplified schematic of part of the pyloric circuit (left). Filled circles indicate inhibitory synapses, solid lines are glutamatergic synapses, and dotted lines are cholinergic synapses. Resistor symbol indicates electrical coupling. The pyloric circuit is subject to descending neuromodulatory control from the stomatogastric nerve (stn). Right: simultaneous extracellular recordings from the lvn, lpn, pdn, and pyn motor nerves. Action potentials from lateral pyloric (LP), pyloric dilator (PD), and pyloric (PY) are visible on lpn, pdn, and pyn. Under these baseline conditions, PD, LP, and PY neurons burst in a triphasic pattern. The anterior burster (AB) neuron is an endogenous burster and is electrically coupled to PD neurons. (b) When the stn is cut, neuromodulatory input is removed and the circuit is 'decentralized.' In this case, the pyloric rhythm can become irregular and hard to characterize. In addition, spikes from multiple PY neurons can become harder to reliably identify on pyn.

In studies that characterize the changes in circuit dynamics to prolonged perturbations, spike identification and circuit dynamics characterization are less straightforward. For example, when descending neuromodulatory projections from the stn are cut (i.e., when the STG is decentralized, Figure B.1b), the collective dynamics of the

pyloric circuit can become less regular. This loss of regularity is concomitant with spikes being harder to reliably identify in extracellular recordings. While PD and LP neuron spikes can still be typically easily identified on the pdn and lpn nerves (Figure B.1b), identifying PY on the pyn in the absence of a regular rhythm can be challenging. This problem is aggravated by the fact that spikes from the LPG neuron are frequently found on pyn, and because there are several copies of the PY neuron, whose spikes can range from perfect coincidence to slight offsets that can unpredictably change the amplitude and shape of PY spikes due to partial summation. For these reasons, some previous works studying the response of pyloric circuits to perturbations have consistently recorded from the lpn and pdn nerves, but not from the pyn (Hamood et al., 2015; Haley et al., 2018; Haddad and Marder, 2018; Rosenbaum and Marder, 2018). Therefore, in order to include the largest number of experiments in our analysis, we chose to characterize the dynamics of the LP and PD neurons.

**Nonlinear dimensionality reduction allows for the visualization of diverse pyloric circuit dynamics.** The regular pyloric rhythm involves out-of-phase bursts of spikes between LP and PD, and is observed under baseline conditions (Figure B.2 a1-3). Perturbations such as the removal of descending neuromodulatory inputs, changes in temperature, or changes in pH can qualitatively alter the rhythm, leading to a large variety of hard-to-characterize spiking patterns (Figure B.2 a4-6). Because these irregular states may lose the strong periodicity found in the canonical motor pattern, burst metrics such as burst period or phase offsets between bursts that work well to characterize the regular rhythm perform poorly. Efforts to characterize and quantify these atypical spike patterns must overcome the slow timescales in observed dynamics, the large quantity of data, and

irregularity and variability in observed spike trains. Previous work used ad hoc categorization systems to assign observations of spike trains into one of a few groups (Haddad and Marder, 2018; Haley et al., 2018), but these categorization methods scaled poorly and relied on subjective annotations.

We sought instead to visualize the totality of pyloric circuit dynamics under all conditions using a method that did not rely on a priori identification of (non)canonical dynamic patterns. Such a data visualization method, while descriptive, would generate a quantitative vocabulary to catalog the diversity of spike patterns observed both when these patterns were regular and also when they were irregular and aperiodic, thus allowing for the quantitative characterization of data previously inaccessible to traditional methods (Börner et al., 2005; Nguyen and Holmes, 2019).

The visualization was generated as follows: time-binned spike trains were converted into their equivalent interspike interval (ISI) and phase representations (Figure B.2 b, Materials and methods). For all analyses, we consider nonoverlapping 20 s time bins. We chose this time bin following inspection of circuit dynamics across many conditions in several animals. Because there can be an arbitrary number of spikes in a bin, there are an arbitrary number of ISIs and phases. This makes it challenging to find a basis to represent the entire dataset. Ideally, we want to represent the spike pattern in each 20 s bin with a point in some space of high but fixed dimensionality. To convert this into a vector of fixed length, we measured percentiles of ISIs and phases (Figure B.2 c). Together with other metrics (like ratios of ISIs, measures that capture discontinuities in ISI distributions, see Materials and methods for details), these percentiles were assembled into a fixed-length vector and each dimension was z -scored across the entire dataset (Figure

B.2 d). A collection of spike trains from an arbitrary number of neurons has thus been reduced to a matrix where each row consists of z -scored percentiles of ISIs and other metrics. This matrix can be visualized using a nonlinear dimensionality reduction technique such as t -distributed stochastic neighbor embedding (t-SNE) (Van der Maaten and Hinton, 2008), which can generate a two-dimensional representation of the full dataset (Figure B.2 e).

In this representation, each dot corresponds to a single time bin of spike trains from both neurons. We found by manual inspection that spike trains that are visually similar (Figure B.2 a1-3) tend to occur close to each other in the embedding (Figure B.2 e1-3). Spike patterns that are qualitatively different from each other (Figure B.2 a4-6) tended to occur far from each other, often in clusters separated by regions of low data density (Figure B.2 e4-6, Supplementary file 1).

How useful is such a visualization and does it represent the variation in spike patterns in the data in a reasonable manner? We colored each point by classically defined features such as the burst period or the phase (Figure B.2—figure supplement 1). We found that the embedding arranges data so that differences between clusters and within clusters had interpretable differences in various burst metrics. For example, clusters on the left edge of the map tended not to have defined LP phases, typically due to silent or very sparse LP firing (Figure B.2—figure supplement 1b). Location of data in the largest cluster was correlated to firing rate in the PD neuron (Figure B.2—figure supplement 1c). We observed that burst metrics, when they were defined, tended to vary smoothly across the map. To quantify this observation, we built a Delaunay triangulation (Materials and methods) on the embedded data and measured the triadic differences between PD burst periods and PD

duty cycles (Figure B.2—figure supplement 3). Triadic differences in these metrics were significantly smaller in the map than triadic differences in a projection of the first two principal components or a shuffled map ($p<0.0001$, Kolmogorov–Smirnv test), suggesting that the t-SNE cost function generates a useful embedding where spike features vary smoothly within clusters. Finally, to validate our approach, we generated a synthetic dataset with different classes of spike patterns (Materials and methods) and analyzed it similarly. Coloring points in the t-SNE embedding by the original class revealed that clusters in the t-SNE map corresponded to different classes in the synthetic data, suggesting that this method can identify and recover stereotyped spike patterns in neural data (Figure B.2—figure supplement 5).

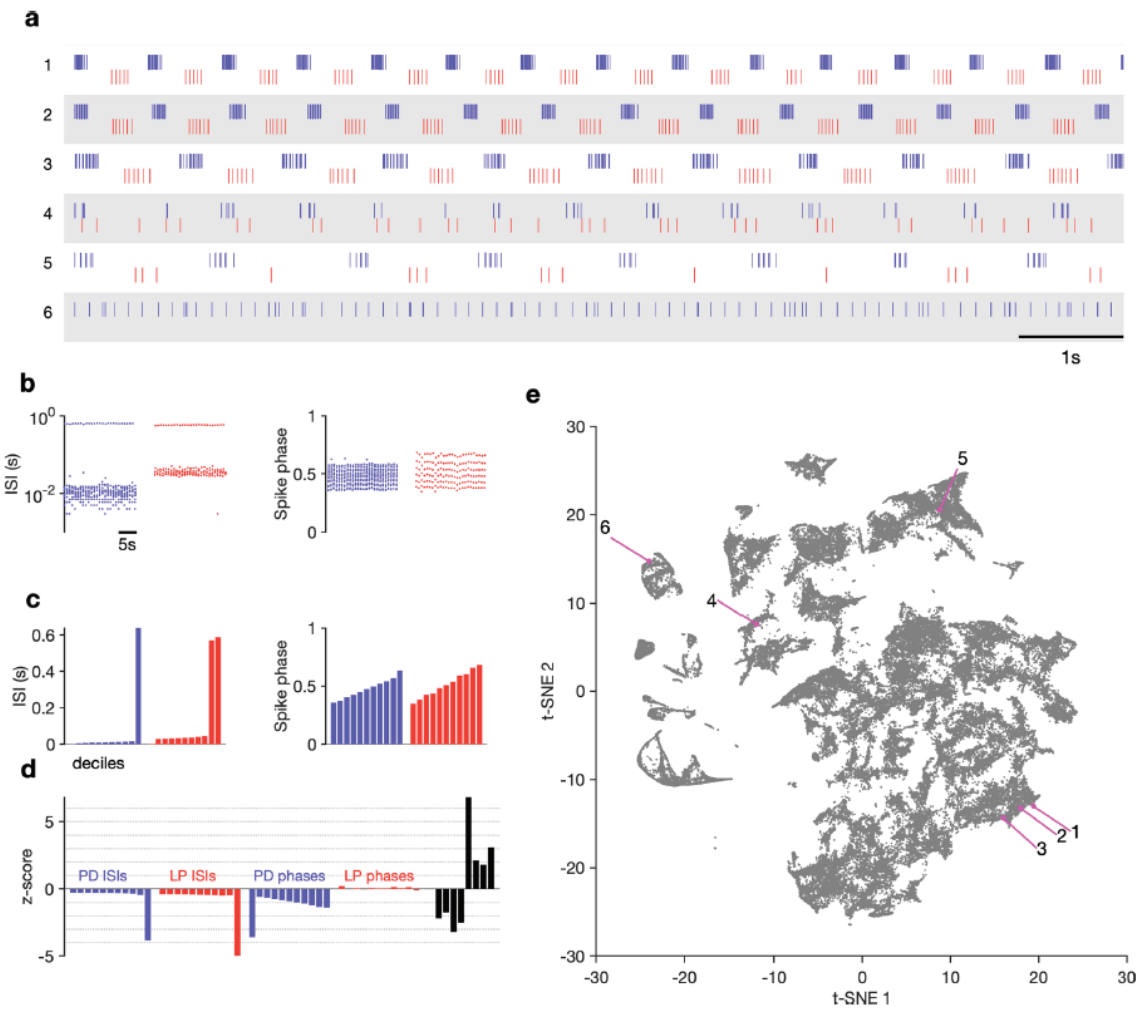


**Figure B.2** Visualization of diverse neural circuit dynamics. (a) Examples of canonical (1–3) and atypical (4–6) spike patterns of pyloric dilator (PD; blue) and lateral pyloric (LP; red) neurons. Rasters show 10 s of data. (b–d) Schematic of data analysis pipeline. (b) Spike rasters in (a2) can be equivalently represented by interspike intervals (ISIs) and phases. 20 s bins shown. Each 20 s bin contains a variable number of spikes/ISIs. (c) Summary statistics of ISI and phase sets in (d), showing tenth percentiles. Using percentiles converts the variable length sets in (b) to vectors of fixed length. (d) z -scored data assembled into a single vector, together with some additional measures (Materials and methods). (e) Embedding of data matrix containing all vectors such as the one shown in (d) using t-distributed stochastic neighbor embedding (t-SNE). Each dot in this image corresponds to a single 20 s spike train from both LP and PD. Example spike patterns shown in (a) are highlighted in the map. n = 94, 844 points from N = 426 animals. In (a–d), features derived from LP spike times are shown in red, and features derived from PD spike times are shown in blue. The online version of this article includes the following figure supplement(s) for figure B.2: Figure supplement 1. Burst metrics smoothly vary in map. Figure supplement 2. Principal components analysis (PCA) and k-means to find clusters in feature vectors. Figure supplement 3. Embedding arranges data so that neighbors tend to be similar. Figure supplement 4. Effect of varying perplexity in t-distributed stochastic neighbor embedding (t-SNE) embedding. Figure supplement 5. Validation of method using synthetic data.

**Visualization of Circuit Dynamics Allows Manual Labeling and Clustering of Data.** Previous studies have shown that regular oscillatory bursting activity of the pyloric circuit can qualitatively change on perturbation. Circuit dynamics can be highly variable and has been categorized into various states such as 'atypical firing,' 'LP-01 spikes,' or 'atypical' (Haddad and Marder, 2018; Haley et al., 2018). Both the process of constructing these categories and the process of classifying data into these categories are typically done manually, and therefore requires expert knowledge that is not explicitly captured and is impossible to reproduce. Because the embedding distributed data into clusters, we hypothesized that clusters corresponded to stereotyped dynamics that were largely similar, and different clusters represented the qualitatively different circuit dynamics identified by earlier studies.

We therefore manually inspected circuit dynamics at randomly chosen points in each apparent cluster and generated labels to describe the dynamics in that region (Figure B.3). This process colored the map and segmented it into distinct regions that broadly followed, and were largely determined by, the distribution of the data in the embedding (Figure B.3 a). Most of the data (57%) were assigned the regular label, where both PD and LP neurons burst regularly in alternation with at least two spikes per burst, and all identified regular states occurred in a single contiguous region in the map (blue). In the LP-weak-skipped state, PD bursts regularly, but LP does not burst every cycle, or only fires a single spike per burst. Irregular-bursting states showed bursting activity on both neurons, which were interrupted or otherwise irregular. In contrast, the irregular state showed spiking that was more variable and did not show strong signs of bursting at any point. LP-silent-PD-bursting states had regular bursting on PD, with no spikes on LP, while LP-silent states

also had no spikes on LP, but activity on PD was more variable, and did not show regular bursting.

The time evolution of the pyloric dynamics of every preparation constitutes a trajectory in the map, and every point in the map is therefore associated with an instantaneous speed of motion in the map. We hypothesized that instantaneous speed could vary across the map, with points labeled regular moving more slowly through the map than points with labels corresponding to atypical states such as irregular because regular rhythms would vary less over time. Consistent with this, we found that points in the regular cluster tended to have smaller speeds than points in other clusters (Figure B.3—figure supplement 1a). Speeds in the regular state were significantly lower than every other state except PD-silent-LP-bursting ($p<0.004$, permutation test), suggesting that atypical states were associated with increased variability in circuit dynamics (Figure B.3—figure supplement 1b).

Do the clusters we see in the data, and the resultant categorization of the data, depend strongly on the details of the dimensionality reduction method we used (t-SNE)? We used an entirely different embedding algorithm (Uniform Manifold Approximation and Projection [uMAP], McInnes et al., 2018) to embed the feature vectors in two-dimensional space. The map generated by uMAP preserved the coarse feature of the t-SNE embedding, suggesting that the features in the map reflected the features of the distribution of the data more strongly than details of the dimensionality reduction method. Coloring points in the uMAP embedding (Figure B.3—figure supplement 3) revealed a roughly similar

organization of data in the embedding space, suggesting that our categorization method did not strongly depend on the details of the dimensionality reduction.

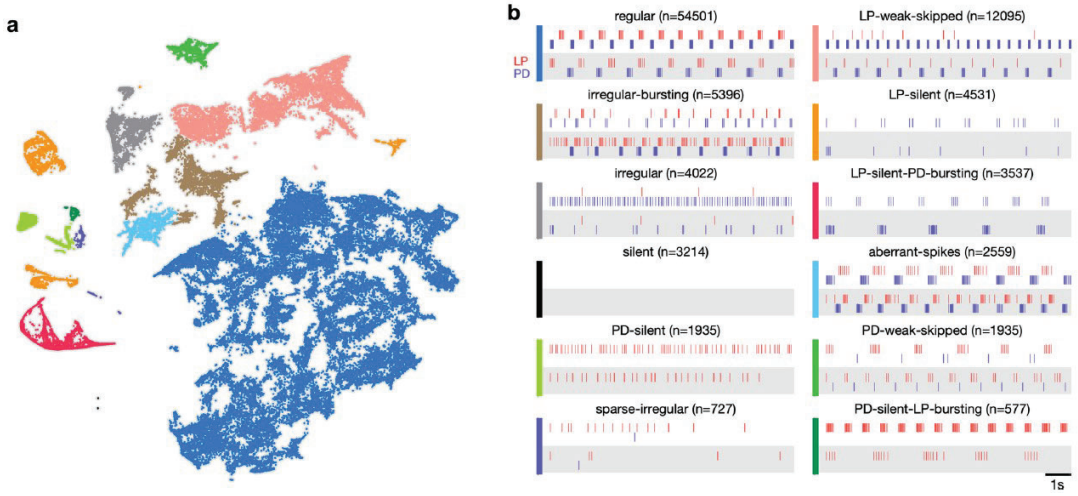


**Figure B.3** Map allows identification of distinct spiking dynamics. (a) Map of all pyloric dynamics in dataset where each point is colored by manually assigned labels. Each point corresponds to a 20 s paired spike train from lateral pyloric (LP) and pyloric dilator (PD) neurons. Each panel in (b) shows two randomly chosen points from that class. The number of points in each class is shown in parentheses above each panel. n = 94, 844 points from N = 426 animals. Labels are ordered by likelihood in the data. The online version of this article includes the following figure supplement(s) for figure 3: Figure supplement 1. Speed of trajectories through map. Figure supplement 2. Embeddings with different initializations. Figure supplement 3. Using Uniform Manifold Approximation and Projection (uMAP) instead of t-distributed stochastic neighbor embedding (t-SNE).

**Variability in Baseline Circuit Dynamics Across a Population of Wild-caught Animals.** Work on the pyloric circuit has used a wild-caught crustacean population. This uncontrolled environmental and genetic variability serves as a window into the extant variability of a functional neural circuit in a wild population of animals. In addition, experimental and computational work has shown that similar rhythms can be generated by a wide variety of circuit architectures and cellular parameters (Prinz et al., 2003; Hamood and Marder, 2014; Alonso and Marder, 2019). We therefore set out to study the variability

in baseline circuit dynamics in the 346 pyloric circuits recorded under baseline conditions in this dataset.

The burst period of the pyloric circuit in the lobster can vary two- to threefold under baseline conditions at 11°C across animals (Bucher et al., 2005). Despite this sizable variation, other burst metrics, such as the phase onset of follower neurons, or the duty cycles of individual neurons, are tightly constrained (Bucher et al., 2005), likely related to the fact that these circuits are under activity-dependent feedback regulation (Turrigiano et al., 1995; O'Leary et al., 2014; Gorur-Shandilya et al., 2020) as they develop and grow. Activity-dependent regulation of diverse pyloric circuits could constrain variability in a single circuit across time to be smaller than variability across the population.

To test this hypothesis, we measured a number of burst metrics such as burst period and the phases and duty cycles of the two neurons across these 346 preparations in baseline conditions (Figure B.4) when data are labeled regular because metrics are well-defined in this state. The mean values of each of these metrics were unimodally distributed (Figure B.4 a) and the coefficient of variation (CV) for all metrics was approximately 0.1 (Figure B.4 b). Using the mean CV in each individual as a proxy for the within-animal variability, and the CV of the individual means as a proxy for the across-animal variability, we found that every metric measured was more variable across animals than within animals (Figure B.4 c). Shuffling experimental labels generated null distributions for excess variability across animals and showed that across-animal variability was significantly greater than within-animal variability (Figure B.4 d, $p<0.007$, permutation test, Table 1).

It is reasonable to suppose that all baseline data exist in the regular cluster. While most baseline data are confined to the regular cluster ( ~ 80% , Figure B.4—figure

supplement 1a), the remaining data, nominally recorded under baseline conditions, contains atypical circuit dynamics (Figure B.4—figure supplement 1b and c). What causes these atypical circuit dynamics in this large, unbiased survey of baseline pyloric activity? One possibility could be inadvertent damage to the preparation caused by dissection and preparation of the circuit for recording. Consistent with this, we found that the probability of observing regular states was significantly reduced when cells were recorded from intracellularly (Figure B.4—figure supplement 2), which may be due to increase in leak currents owing to impaling cells with sharp electrodes (Cymbalyuk et al., 2002) or due to cell dialysis (Hooper et al., 2015). No significant correlation was observed between sea surface temperatures (a proxy for environmental conditions for these wild-caught animals) and burst metrics (Figure B.4—figure supplement 3a–c) or the probability of observing a regular state (Figure B.4—figure supplement 3d). Taken together, these results underscore the importance of verifying that baseline or control data does not include uncontrolled technical variability that could mask biological effects of interest.

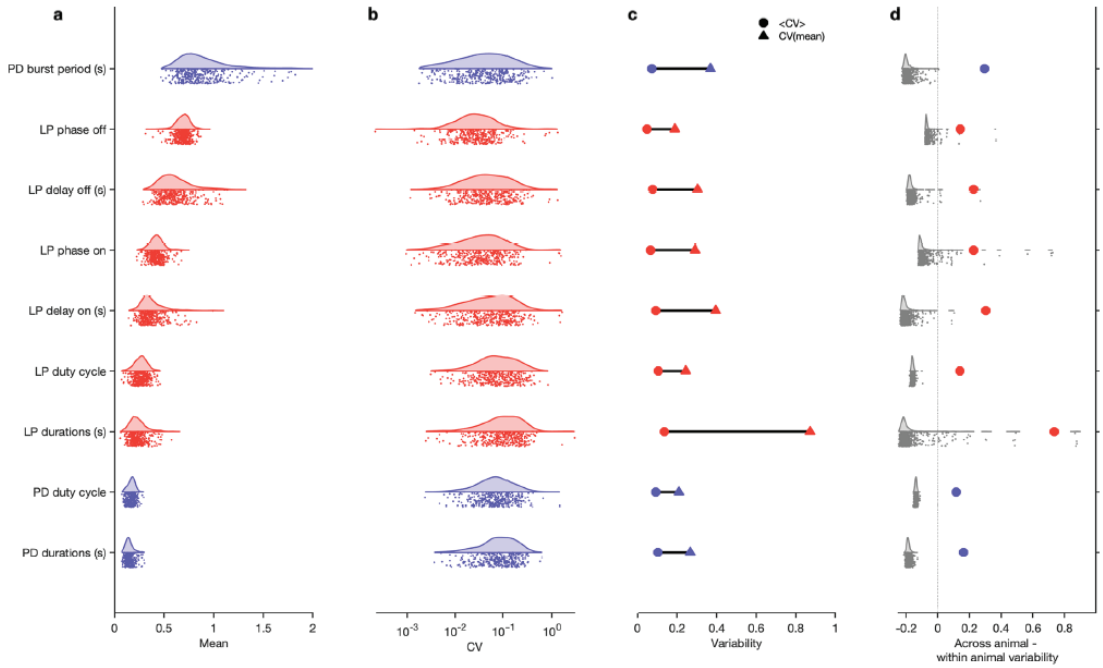


**Figure B.4** Variability of burst metrics under baseline conditions. (a) Variability of burst metrics in pyloric dilator (PD) and lateral pyloric (LP) neurons across a population of wild-caught animals. Metrics are only computed under baseline conditions and in the regular cluster. (b) Distribution of coefficient of variation (CV) of metrics in each animal across all data from that animal. In (a, b), each dot is from a single animal, and distributions show variability across the entire population. (c) Across-animal variability (CV of individual means, Δ) is greater than within-animal variation (mean of CV in each animal, O) for every metric. (d) Difference between across-animal variability and within-animal variability (colored dots). For each metric, gray dots and distribution show differences between across-animal and within-animal variability for shuffled data. n = 18, 336 points from N = 346 animals. The online version of this article includes the following figure supplement(s) for figure B.4: Figure supplement 1. State distribution under baseline conditions. Figure supplement 2. Recording condition alters regular state probability. Figure supplement 3. Effect of sea surface temperature on baseline circuit dynamics.

**Table B.1**. ANOVA Results and Power Analysis for Figure B.4

ANOVA results for burst metrics in baseline conditions. For each metric, each animal is treated as a group and the variability (mean square difference) is compared within and across group. F is the ratio of across-animal to within-animal mean square differences. $N_{.99}$ is the estimate of the sample size required to reject the null hypothesis with a probability of 0.99 when the alternative hypothesis is true. N = 346 animals.

| Metric | Across-animal MS | Within-animal MS | F | $N_{.99}$ |
|---|---|---|---|---|
| LP delay off (s) | 1.1391 | 0.010 956 | 103.97 | 6 |
| LP delay on (s) | 0.616 47 | 0.0111 | 55.54 | 6 |
| LP durations (s) | 0.363 86 | 0.012 366 | 29.424 | 4 |
| LP duty cycle | 0.159 86 | 0.001 309 3 | 122.09 | 10 |
| LP phase off | 0.234 06 | 0.007 227 9 | 32.383 | 11 |
| LP phase on | 0.216 55 | 0.008 811 5 | 24.576 | 9 |
| PD burst period (s) | 3.557 | 0.036 872 | 96.469 | 4 |
| PD durations (s) | 0.079 397 | 0.000 549 44 | 144.5 | 6 |
| PD duty cycle | 0.053 472 | 0.000 413 23 | 129.4 | 16 |

LP: lateral pyloric; PD: pyloric dilator.MS: mean square.

**Perturbation Modality Alters State Probability.** The pyloric circuit and other circuits in the crab must exhibit robustness to the environmental perturbations that these animals are likely to encounter. Previous studies have characterized the ability of crustacean circuits to be robust to environmental perturbations such as pH (Haley et al., 2018; Ratliff et al., 2021; Qadri et al., 2007), temperature (Tang et al., 2010; Tang et al., 2012; Rinberg et al., 2013; Haddad and Marder, 2018; Kushinsky et al., 2019), oxygen levels (Clemens et al., 2001), and changes in extracellular ionic concentrations (He et al., 2020). Robustness to these perturbations exists up to a limit, likely reflecting the bounds of the natural variation in these quantities that these circuits are evolved to function in. When challenged with extremes of any of these perturbation modalities, the pyloric rhythm breaks down, displaying irregular or aberrant states, and may even cease spiking entirely. Such states are commonly referred to as 'crashes' and can have many flavors (Haddad and Marder, 2018;

Tang et al., 2010; Tang et al., 2012) and involve the loss of the characteristic antiphase activity in the LP and PD neurons.

It remains unclear if extreme perturbations of different modalities share common pathways of destabilizing and disrupting the pyloric rhythm (Ratliff et al., 2021). In principle, these environmental perturbations can disrupt neuron and circuit function in qualitatively different ways: for example, changes in extracellular potassium concentration can alter the reversal potential of potassium (He et al., 2020) vs. changes in temperature can have varied effects on the timescales and conductances of all ion channels (Tang et al., 2010; Caplan et al., 2014). Because prior work was focused on studying the limits of robustness and lacked a detailed quantitative description of irregular behavior, the fine structure of the transition between functional dynamics and silent or 'crashed' states remain poorly characterized (Ratliff et al., 2021). We therefore set out to measure how pH, temperature, and extracellular potassium perturbations alter circuit state probability.

Where in the map are data under extreme environmental perturbations? Circuit spike patterns under high pH (>9.5), high temperature (>25°C), and high extracellular potassium ($2.5 \times [K^+]$ ) are distributed across a wide region of the map, spanning both regions in the regular cluster and other nonregular clusters (Figure B.5 a). Spike patterns observed under high-temperature conditions in the regular region were clustered in the lower extremity, in the region containing high firing rates and small burst periods of PD (Figure B.2—figure supplement 1), consistent with earlier studies showing that elevated temperatures tend to speed up the pyloric rhythm (Tang et al., 2010; Tang et al., 2012). Subjecting the pyloric circuit to extremes of pH, temperature, and extracellular potassium altered the distribution of observed states (Figure B.5 c). In all cases, the probability of

observing regular was significantly reduced ($p<0.001$, paired permutation test), and a variety of nonregular states were observed. We observed that high pH (>9.5) did not silence the preparation, but silent states were observed in low pH (<6.5), consistent with previously published manual annotation of this data (Haley et al., 2018). Silent states were also observed in $2.5 \times [K^+]$ , as reported earlier by He et al., 2020. Previous work has shown that the isolated pacemaker kernel (AB and PD neurons) has a stereotyped trajectory from bursting through tonic spiking to silence when subjected to pH perturbations (Ratliff et al., 2021), but moves through a different trajectory (bursting to weak bursting to silence) during temperature perturbations. Do pathways to silent states share similarities across perturbation modality in intact circuits? To answer this, we plotted the probability of observing states conditioned on the transition to silence in low pH, high temperature, and $2.5 \times [K^+]$ (Figure B.5 d). In the ~ 2000 transitions between states detected, we never observed a transition from regular to silent, suggesting that the timescales of silencing are slow, longer than the width of one data bin (20 s). Trajectories to silent states always transition through a few intermediate states such as sparse-irregular, LP-silent, or PD-silent (Figure B.5 d).

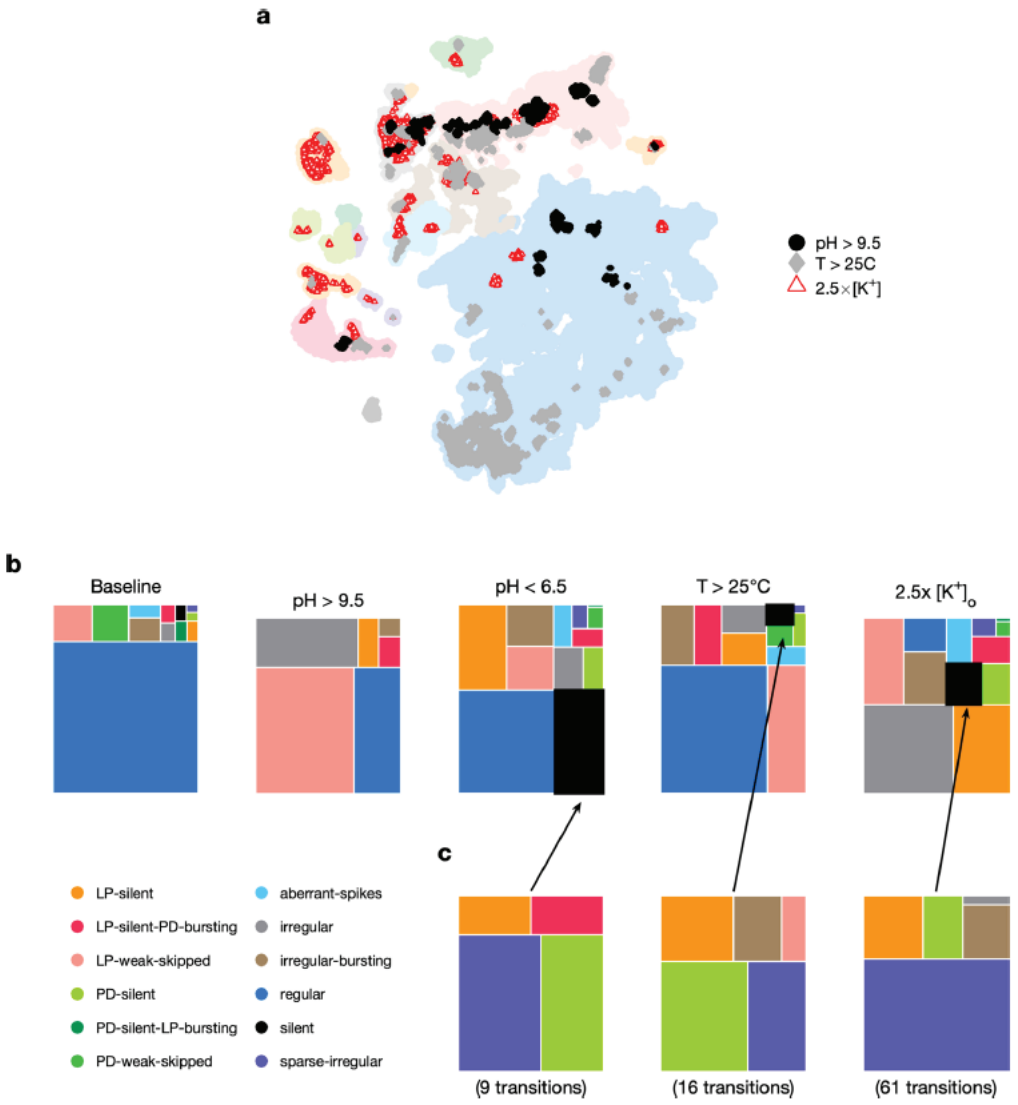


**Figure B.5** Effect of three different environmental perturbations. (a) Map showing regions that are more likely to contain data recorded under extreme environmental perturbations. (b) Treemaps showing probability distributions of states under baseline and perturbed conditions. (c) Probability distribution of states preceding silent state under perturbation. pH perturbations: n = 4023 from 6 animals; $[K^+]$ perturbations: n = 5526 from 20 animals; temperature perturbations: n = 80, 470 from 414 animals. The online version of this article includes the following figure supplement(s) for figure B.5: Figure supplement 1. Preparation-by- preparation response to pH perturbations.

**Transitions Between States During Environmental Perturbations**. Changes in temperature, pH, and [$K^+$] have different effects on the cells in the pyloric circuit and therefore can destabilize the rhythm in different ways. Increasing the extracellular [$K^+$] changes the reversal potential of K+ ions, altering the currents flowing through potassium channels, and typically depolarizes the neuron (He et al., 2020). Ion channels can be differentially sensitive to changes in temperature or pH, and changes in these variables can have complex effects on ionic currents in neurons (Tang et al., 2010; Tang et al., 2012; Haley et al., 2018). We therefore asked if different environmental perturbations changed the way in which regular rhythms destabilized.

Our analysis mapped a time series of spike times from PD and LP neurons to a categorical time series of labels such as regular. We therefore could measure the transitions between states during different environmental perturbations (Materials and methods). We found that transition matrices between states shared commonalities across environmental perturbations (Figure B.6 a), such as likely transitions between regular and LP-weak-skipped states. PD-silent-LP-bursting states tended to be followed by PD-silent states, in which the LP neuron is spiking, but not bursting regularly. The LP neuron becomes less regular in both transitions, contributing to the loss of regular rhythms. We never observed a transition from regular rhythms LP-silent or PD-silent states, suggesting slow (>20 s) time scales of rhythm collapse. In high pH, every transition away from the regular state was to the LP-weak- skipped state, hinting at increased sensitivity of the LP neuron to high pH. High pH perturbations also never silenced the circuit, as previously reported (Haley et al., 2018), and showed fewer and less varied transitions than other perturbations. Are some transitions over- or underrepresented in the transition matrix? To determine this, we

constructed a null model where transitions occurred with probabilities that scaled with the marginal probability of final states (Materials and methods). Transitions that occurred significantly more often than predicted by the null model are shown with black borders and those that occurred significantly less often than predicted are shown with filled circles (Figure B.6 a). Transitions that never occurred but occurred at significantly nonzero rates in the null model are indicated with diamonds.

Earlier work has shown that transitions from regular bursting are preceded by an increase in variability in the voltage dynamics of bursting in PD neurons pharmacologically isolated from most of the pyloric circuit (Ratliff et al., 2021). Can we detect similar signatures of destabilization before transitions from regular states in the intact circuit? We measured the CV of the burst periods of PD and LP neurons in regular states just before transitions away from regular (Figure B.6 b). Because we restricted our measurement of variability to regular states, we could disambiguate true cycle-to- cycle jitter in the timing of bursts from the apparent variability in cycle period due to alternations between bursting and nonbursting dynamics. We found that transitions away from regular were correlated with a steady and almost monotonic increase in variability in PD and LP burst periods for low pH and high [$K^+$] perturbations, but not for high pH and high-temperature perturbations (Spearman rank correlation test). This suggests mechanistically different underpinnings to the pathways of destabilization between these sets of perturbations and is consistent with previous work showing that robustness to perturbations in pH only moderately affects temperature robustness in the same neuron (Ratliff et al., 2021).

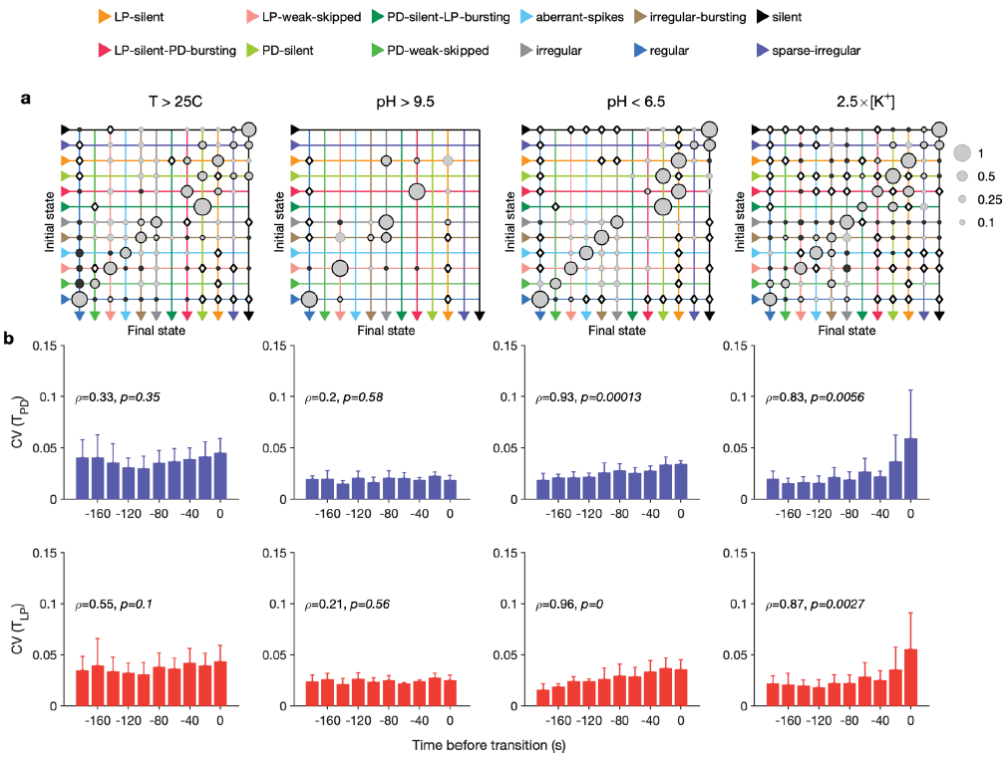


**Figure B.6** Effect of environmental perturbations on transitions between states. (a) Transition matrix between states during environmental perturbations. Each matrix shows the conditional probability of observing the final state in the next time step given an observation of the initial state. Probabilities in each row sum to 1. Size of disc scales with probability. Discs with dark borders are transitions that are significantly more likely than the null model (Materials and methods). Dark solid discs are transitions with nonzero probability that are significantly less likely than in the null model. ◊ are transitions that are never observed and are significantly less likely than in the null model. States are ordered from regular to silent. (b) Coefficient of variation (CV) of burst period of pyloric dilator (PD) (purple) and lateral pyloric (LP) (red) vs. time before transition away from the regular state. ρ, p are from Spearman test (on binned data, as plotted) to check if variability increases significantly before transition. Temperature perturbations: n = 1035 transitions in 61 animals; pH perturbations: n = 90 transitions in 6 animals; [$K^+$] perturbations: n = 271 transitions in 20 animals.

**Decentralization Elicits Variable Circuit Dynamics.** The pyloric circuit is modulated by a large and chemically diverse family of neuromodulators that it receives via the stomatogastric (stn) nerve (Marder, 2012). Decentralization, or the removal of this neuromodulatory input via transection and/or chemical block of the stn, has been shown to affect the pyloric rhythm in a number of ways (Russell, 1976). Decentralization can stop the rhythm temporarily, which can recover after a few days (Golowasch et al., 1999; Thoby-Brisson and Simmers, 1998). Decentralization slows down the pyloric rhythm (Eisen and Marder, 1982; Rosenbaum and Marder, 2018) and makes the rhythm more variable (Hamood and Marder, 2014; Hamood et al., 2015). Decentralization can evoke variable circuit dynamics, sometimes with slow timescales (Figure B.7— figure supplement 1) and can lead to changes in ion channel expression (Mizrahi et al., 2001).

The variability in circuit dynamics elicited by decentralization and the animal-to-animal variability in response to decentralization have made a quantitative analysis of the effects of decentralization difficult. We therefore set about to characterize the variable and invariant features of the changes in circuit spiking dynamics on removal of descending neuromodulation across a large ( $N = 141$ ) population.

We first asked where in the map decentralized data were (Figure B.7 a). A large fraction ( $\sim 30\%$ ) of the data was found outside the regular cluster, suggesting the existence of atypical circuit dynamics on decentralization. Decentralization also changed probabilities of observing many states. The regular state was significantly less likely on decentralization, and several atypical states were significantly more likely (Figure B.7 b and c, Table B.2, Figure B.7—figure supplement 2).

How do preparations switch between different states when decentralized? The transition matrix during decentralization revealed many transitions between diverse states (Figure B.7 d), with the most likely transitions being significantly overrepresented compared to the null model ($p<0.05$, Materials and methods). Transitions away from regular included significantly more likely transitions into states where one of the neurons was irregular such as LP-weak-skipped and PD-weak-skipped. Similar to rhythm destabilization in high $[K^+]$ or low pH, transitions away from regular were associated with a near-monotonic increase in the variability of PD and LP burst periods before the transitions (Figure B.7 e, ~ .8 , $p<0.006$, Spearman rank correlation test).

The time series of identified states on a preparation-by-preparation basis showed striking variability in the responses to decentralization (Figure B.7—figure supplement 3a), with the probability of observing regular states decreasing immediately after decentralization (Figure B.7—figure supplement 3b). What causes the observed animal-to-animal variability in circuit dynamics on decentralization? One possibility is that seasonal changes in environmental conditions alter the sensitivity of the pyloric circuit to neuromodulation. We tested this hypothesis by measuring the correlation between measures such as the probability of observing the regular state, the change in burst period, and the change in firing rate on decentralization and the sea surface temperature at the approximate location of these wild-caught animals (Figure B.7—figure supplement 4). None of these measures was significantly correlated with sea surface temperature ($p>0.07$, Spearman rank correlation test).

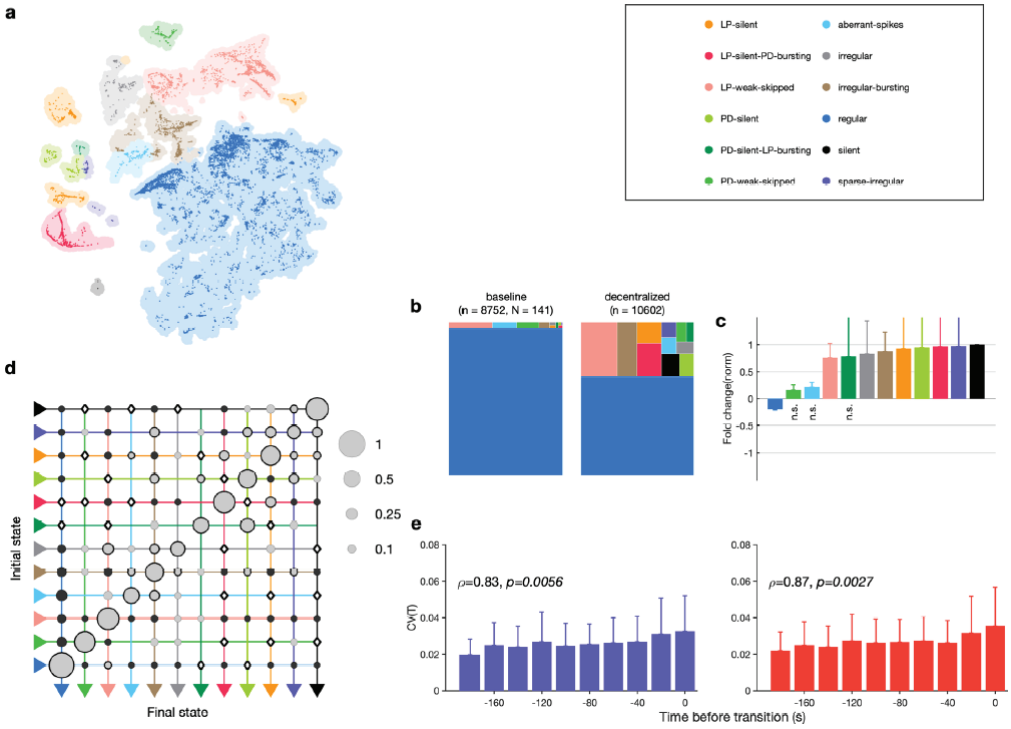


**Figure B.7** Effect of decentralization. (a) Map occupancy conditional on decentralization. Shading shows all data, and bright colored dots indicate data when preparations are decentralized. (b) State probabilities before and after decentralization. (c) Fold change in state probabilities on decentralization. States marked n.s. are not significantly more or less likely after decentralization. All other states are (paired permutation test, $p<0.00016$). (a,b) n = 10, 602 points from N = 141 animals. (d) Transition matrix during decentralization. Probabilities in each row sum to 1. Size of disc scales with probability. Discs with dark borders are transitions that are significantly more likely than the null model (Materials and methods). Dark solid discs are transitions with nonzero probability that are significantly less likely than in the null model. ◊ are transitions that are never observed and are significantly less likely than in the null model. States are ordered from regular to silent. n = 1933 transitions. (e) Coefficient of variation of pyloric dilator (PD, purple) and lateral pyloric (LP; red) burst periods before transition away from regular states. ρ, p from Spearman test. n = 1332 points from N = 79 animals. The online version of this article includes the following figure supplement(s) for figure B.7: Figure supplement 1. Decentralization evokes variable dynamics. Figure supplement 2. Effects of decentralization on state probabilities. Figure supplement 3. Time course of effects of decentralization. Figure supplement 4. Effects of decentralization do not correlate with seasonal effects.

**Table B.2** State Counts Before and After Decentralization for the Data Shown in Figure B.7

| State | $n_{control}$ | $n_{dec.}$ | $p$ | $\Delta P(state)$ |
|---|---|---|---|---|
| Regular | 7,967 | 5,791 | $lt_{0.001}$ | -0.308 77 |
| LP-silent | 22 | 724 | $lt_{0.001}$ | 0.030 65 |
| LP-silent-PD-bursting | 14 | 577 | $lt_{0.001}$ | 0.045 926 |
| PD-silent | 11 | 140 | 4 | 0.018 51 |
| PD-silent-LP-bursting | 20 | 18 | 0.469 59 | 0.000 188 91 |
| Aberrant-spikes | 111 | 168 | 0.300 37 | 0.003 285 3 |
| LP-weak-skipped | 317 | 1,628 | $lt_{0.001}$ | 0.099 875 |
| PD-weak-skipped | 142 | 118 | 0.292 19 | 0.003 453 8 |
| Sparse-irregular | 4 | 154 | $lt_{0.001}$ | 0.013 263 |
| Irregular | 13 | 116 | 0.000 23 | 0.010 877 |
| Silent | 0 | 321 | $lt_{0.001}$ | 0.024 825 |
| Irregular-bursting | 72 | 753 | $lt_{0.001}$ | 0.057 913 |

LP: lateral pyloric; PD: pyloric dilator.

**Stereotyped Effects of Decentralization on Burst Metrics.** Despite the animal to animal variation in responses to decentralization, are there stereotyped responses to decentralization? Decentralization removes some unknown mixture of modulators that are released by the stn, which can vary from animal to animal. Previous work has shown that decentralization typically slows down the pyloric rhythm (Eisen and Marder, 1982; Rosenbaum and Marder, 2018) and (Figure B.8—figure supplement 1), but a finer-grained analysis of rhythm metrics was confounded by the irregular dynamics that can arise when preparations are decentralized. For example, alteration between regular and atypical states could bias estimates of burst metrics that are not defined in atypical states. Because our analysis allows us to identify the subset of data where pyloric circuit dynamics are regular enough that burst metrics are well-defined, we measured the changes in a number

of burst metrics like the burst period, duty cycle, and phases on decentralization (Figure B.8 a). Every metric measured was significantly changed except the phase at which LP bursts start ($p<0.007$, paired permutation test). Consistent with earlier studies, we found that the CV in every metric increased following decentralization (Figure B.8 b).

What are the dynamics of changes in burst metrics on decentralization? Firing rates of both LP and PD neurons decreased immediately on decentralization, roughly halving their pre-decentralized values (Figure B.8 c). This occurred together with a doubling of PD burst periods (Figure B.8 d), suggesting that the entire rhythm is slowing down. Intriguingly, decentralization led to significant advance in the phase of LP burst ends, but not starts (Figure B.8 e), leading to a large decrease in the duty cycle of the LP neuron (Figure B.8 f) that was significantly more than the decrease in PD's duty cycle ($p<10^{-8}$, paired t-test).

The stereotyped slowing of the rhythm on decentralization can also be quantified by looking at the distribution of the data in the regular cluster before and after decentralization (Figure B.8—figure supplement 2). Data are concentrated in the upper-left edge of the regular cluster when decentralized, where burst periods are large and firing rates low (Figure B.2—figure supplement 1a and c), suggesting that decentralization could elicit a more stereotyped rhythm for circuits that continue to burst regularly, because circuits that do so tend to share a common, slow bursting dynamics. Counterintuitively, it may appear that regular rhythms in baseline conditions are more variable than regular rhythms after decentralization. To test this hypothesis, we measured the dispersion of each preparation in the map (Figure B.8—figure supplement 2b) before and after decentralization. Dynamics before decentralization were significantly more dispersed in

the regular cluster than dynamics after decentralization (Figure B.8—figure supplement 2c, p = 0.0016 , paired t-test) because they then tended to be concentrated in the upper-left edge of that cluster. To first approximation, our analysis shows that there are many ways to manifest a regular rhythm under baseline conditions, but regular rhythms on decentralization are typically slow, and stereotyped in comparison.

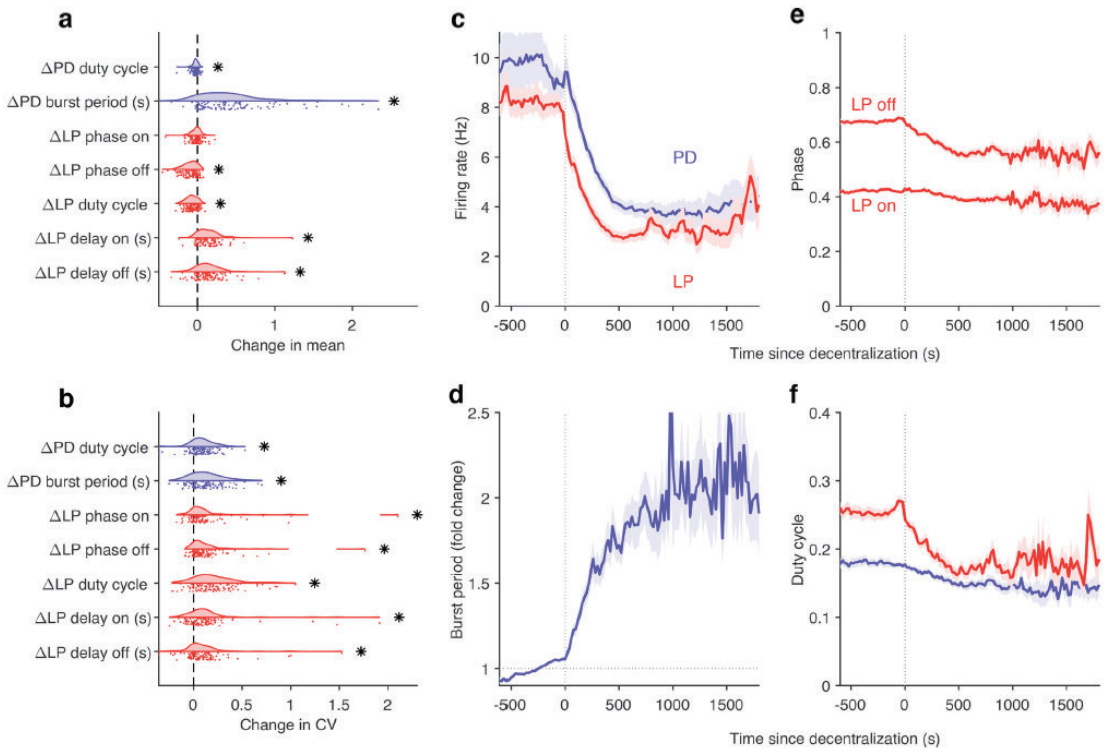


**Figure B.8** Effects of decentralization on burst metrics. (a) Change in mean burst metrics on decentralization. (b) Change in coefficient of variation of burst metrics on decentralization. In (a) and (b), each dot is a single preparation; * indicate distributions whose mean is significantly different from zero ($p<0.007$, paired permutation test). Firing rates (c), burst period (d), lateral pyloric (LP) phases (e), and duty cycles (f) vs. time since decentralization. In (c–f), thick lines indicate population means, and shading indicates the standard error of the mean. n = 13, 898 points from N = 141 preparations. The online version of this article includes the following figure supplement(s) for figure 8: Figure supplement 1. Example rasters showing effect of decentralization. Figure supplement 2. Effects of decentralization on regular rhythms.

**Neuromodulators Differentially Affect State Probabilities.** The crustacean STG is modulated by more than 30 substances (Harris-Warrick and Marder, 1991; Marder, 2012) that tune neuronal properties at an intermediate timescale between feedback homeostasis and intrinsic cellular properties (Daur et al., 2016). Earlier work has focused on understanding the effect modulators have on restoring (or destabilizing) the canonical rhythm, in part because the restoration of regular oscillatory dynamics is a common feature of neuromodulator action. Other effects that neuromodulators might have on pyloric circuit dynamics are harder to investigate and are hindered by the difficulty in characterizing circuit dynamics when nonregular. Here, we set out to systematically characterize the effects of neuromodulators on dynamic states identified in the full space of circuit behaviors (Figure B.3).

We focused our analysis on the effect of four neuromodulators: red pigment-concentrating hormone (RPCH), proctolin, oxotremorine, and serotonin. In the experiments analyzed, these neuromodulators were added to decentralized preparations so that endogenous effects of these (and other) neuromodulators were minimized. We therefore first characterized the distribution of states in decentralized preparations where neuromodulators were subsequently added (Figure B.9 a).

RPCH is a neuropeptide that targets a number of cells in the circuit (Nusbaum and Marder, 1988; Swensen and Marder, 2001) and has been shown to increase the number of spikes per burst in PD and LP (Dickinson et al., 2001; Thirumalai and Marder, 2002), though it has little effect on the pyloric period (Thirumalai et al., 2006). RPCH increased the probability of the regular state, suggesting stabilization of the triphasic rhythm, and decreased the probability of most other atypical states (Figure B.9 b, Table B.3, $p<0.004$,

paired permutation test). Consistent with earlier studies that reported that RPCH can activate rhythms in silent preparations (Nusbaum and Marder, 1988), the probability of observing the silent state was driven to 0 in the presence of RPCH, together with other atypical states such as LP-silent and LP-silent-PD-bursting (Figure B.9 b).

Proctolin also targets a number of cells in the circuit (Swensen and Marder, 2001) and strengthens the pyloric rhythm through various mechanisms: by increasing the amplitude of slow oscillations in AB and LP (Hooper and Marder, 1987; Nusbaum and Marder, 1989), depolarizing the LP neuron (Golowasch and Marder, 1992; Turrigiano and Marder, 1993), and increasing the number of spikes per burst in LP and PD (Hooper and Marder, 1987; Marder et al., 1986; Hooper and Marder, 1984). Oxotremorine, a muscarinic agonist, has also been shown to enhance the robustness of the pyloric rhythm (Bal et al., 1994; Haddad and Marder, 2018; Rosenbaum and Marder, 2018). Similar to RPCH, both proctolin and oxotremorine significantly increase the probability of the regular state (Figure B.9 b, Table B.3, $p<0.004$, paired permutation test), and the regular state is the only one significantly more likely when the neuromodulator is added. The strengthening effects of RPCH and oxotremorine are also manifested in the significantly lower probabilities of observing atypical and dysfunctional states such as silent, LP-silent, PD-silent, and sparse-irregular (Table B.3).

Serotonin can have variable effects on the pyloric circuit, varying from animal to animal, and can either speed up or slow down the rhythm (Beltz et al., 1984; Spitzer et al., 2008). In *Panularis*, serotonin depolarizes LP in culture, but hyperpolarizes LP in situ, unlike other neuromodulators that typically have the same effect in situ and in culture (Turrigiano and Marder, 1993). Consistent with earlier work in *C. borealis* showing that

serotonin destabilizes the rhythm in decentralized preparations (Haddad and Marder, 2018), we found that the probability of regular states was significantly lower on addition of serotonin (Figure B.9 b, Table B.3, $p<0.004$, paired permutation test), together with a significantly higher probability of atypical dysfunctional states such as LP-silent, aberrant-spikes, PD-silent-LP-bursting, and irregular, suggesting loss of coordination between the many neurons in the pyloric circuit with serotonin receptors (Clark et al., 2004).

Do these modulators share common features in how they (de)stabilize the rhythm? We computed the probability distribution of states conditional on transitions to the regular state for RPCH, proctolin, and oxotremorine, and conditional on transitions from the regular state for serotonin (Figure B.9 c). For all four neuromodulators, the conditional state distribution predominantly comprised these three states: LP-weak-skipped, irregular-bursting, and aberrant-spikes, suggesting that trajectories of recovery or destabilization of the regular rhythm share common features. Serotonin destabilizes the rhythm, decreasing the likelihood of observing regular states, similar to environmental perturbations (Figure B.5) and decentralization (Figure B.7).

Different neuromodulators activate different forms of the rhythm (Marder and Weimann, 1992; Marder et al., 1985; Marder, 2012), partly because different neuron types express different receptors to varying extents (Garcia et al., 2015). Moreover, similar rhythmic motor patterns can be produced by qualitatively different mechanisms, such as one that depends on voltage-gated sodium channel activity, and one that can persist in their absence (Harris-Warrick and Flamm, 1987; Epstein and Marder, 1990; Rosenbaum and Marder, 2018). To determine if different neuromodulators elicit regular rhythms that occupy different parts of the map, we plotted the location of data elicited by various

neuromodulators in the full map (Figure B.9—figure supplement 2). Regular data elicited by different neuromodulators tended to lie in clusters, whose distribution in the map was significantly different between serotonin and CCAP (Crustacean cardioactive peptide), and proctolin and every other neuromodulator tested ($p<0.05$, two-dimensional Kolmogorov–Smirnov test, using the method of Peacock, 1983). The differential clustering of regular states in the map with neuromodulator suggests that neuromodulators can elicit characteristic, distinct rhythms.

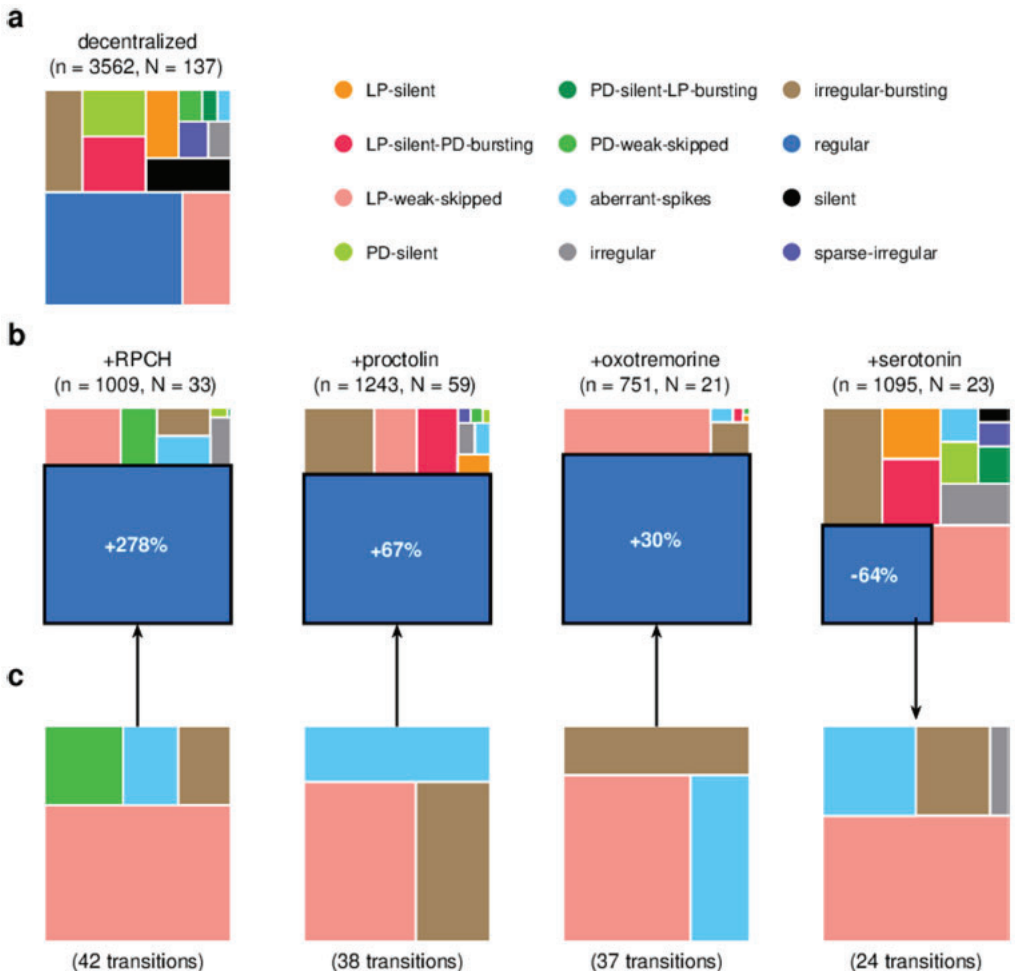


**Figure B.9** Effect of bath-applied modulators. (a) State distribution in decentralized preparations. (b) State distribution in bath application of neuromodulators. Change percentages show difference in probability of regular state from decentralized to addition of neuromodulator. (c) Probability distribution of states conditional on transition to (for red pigment-concentrating hormone [RPCH], proctolin, and oxotremorine) or from (for serotonin) the regular state. n is the number of data points, and N is the number of animals. The online version of this article includes the following figure supplement(s) for figure B.9: Figure supplement 1. Raw traces during proctolin application. Figure supplement 2. Neuromodulators affect map occupancy.

**Table B.3** Probability Distribution of States During Modulator Application, as Shown in Figure B.9

| State | Decentralized | RPCH | Proctolin | Oxotremorine | Serotonin |
|---|---|---|---|---|---|
| Regular | 0.39 | 0.73 | 0.69 | 0.78 | 0.27 |
| LP-silent | 0.06 | 0 | 0.02 | 0 | 0.07 |
| LP-silent-PD-bursting | 0.09 | 0 | 0.07 | 0 | 0.1 |
| PD-silent | 0.07 | 0 | 0 | 0 | 0.04 |
| PD-silent-LP-bursting | 0.01 | 0 | 0 | 0 | 0.03 |
| Aberrant-spikes | 0.01 | 0.04 | 0.01 | 0.01 | 0.03 |
| LP-weak-skipped | 0.14 | 0.11 | 0.07 | 0.17 | 0.19 |
| PD-weak-skipped | 0.02 | 0.05 | 0 | 0 | 0 |
| Sparse-irregular | 0.03 | 0 | 0.01 | 0 | 0.02 |
| Irregular | 0.02 | 0.02 | 0.01 | 0 | 0.07 |
| Silent | 0.07 | 0 | 0 | 0 | 0.01 |
| Irregular-bursting | 0.1 | 0.04 | 0.11 | 0.03 | 0.17 |

LP: lateral pyloric; PD: pyloric dilator.

**Neuromodulators Differentially Affect Transition Between States.** RPCH, proctolin, and oxotremorine activate a common voltage-dependent modulatory current, $I_{MI}$ (Swensen and Marder, 2001), but can differentially affect neurons in the STG because different cell types express receptors to these modulators to different degrees. For example, RPCH activates $I_{MI}$ strongly in LP neurons, but the effects of oxotremorine and proctolin are more broadly observed in the circuit (Swensen and Marder, 2000; Swensen and Marder, 2001). Though these three modulators strengthen the slow-wave oscillations in pyloric neurons, only oscillations elicited by oxotremorine and RPCH persist in tetrodotoxin, and proctolin rhythms do not, hinting that qualitatively different mechanisms underlie the generation of these seemingly similar oscillations (Rosenbaum and Marder, 2018). We therefore measured the transition rates between states during neuromodulator application to how similar or different trajectories towards recovery were.

In RPCH, proctolin, and oxotremorine application, ~100 transitions were observed between states (Figure B.10). Transitions could not always be predicted by a null model assuming that transition probabilities scaled with the conditional probability of observing states after a transition. For example, some transitions, such as the transition from irregular to regular, were never observed in RPCH, a significant deviation from the expected number of transitions given the likelihood of observing regular states after transitions (Materials and methods). Others, such as the transition LP-silent to LP-silent-PD-bursting in proctolin and oxotremorine, were observed at rates significantly higher than expected from the null model. Transitions into regular state are distributed across aberrant-spikes, LP-weak-skipped, and irregular-bursting states for all three, but no invariant feature emerges in the rest of the transition matrix.

Serotonin destabilizes the rhythm in decentralized preparations, and the transition matrix under serotonin reveals several features of the irregularity behavior observed under serotonin (Figure B.10). A number of irregular and low-firing states from silent to irregular never transition into the regular state, which is unlikely in the null model ($p<0.05$, Materials and methods). Transitions between pairs of states are symmetric and occur at rates significantly larger than in the null model, such as between LP-silent and LP-silent-PD-bursting. Intriguingly, destabilizing transitions from regular to LP-weak- skipped, aberrant-spikes, and irregular-bursting are observed at rates significantly higher than in the null model. These three abnormal states are also observed immediately preceding regular states in RPCH, proctolin, and oxotremorine (Figure B.9 c), suggesting that the mechanisms for both stabilization and destabilization of the rhythm share stereotyped trajectories.

Are transitions away from regular states also associated with increases in variability of burst periods? Similar to preparations in high [$K^+$] and low pH, and when decentralized, transitions away from regular states in serotonin were associated with significantly rising variability in the burst periods of PD and LP neurons (Figure B.10, $p<0.05$, Spearman rank correlation test).

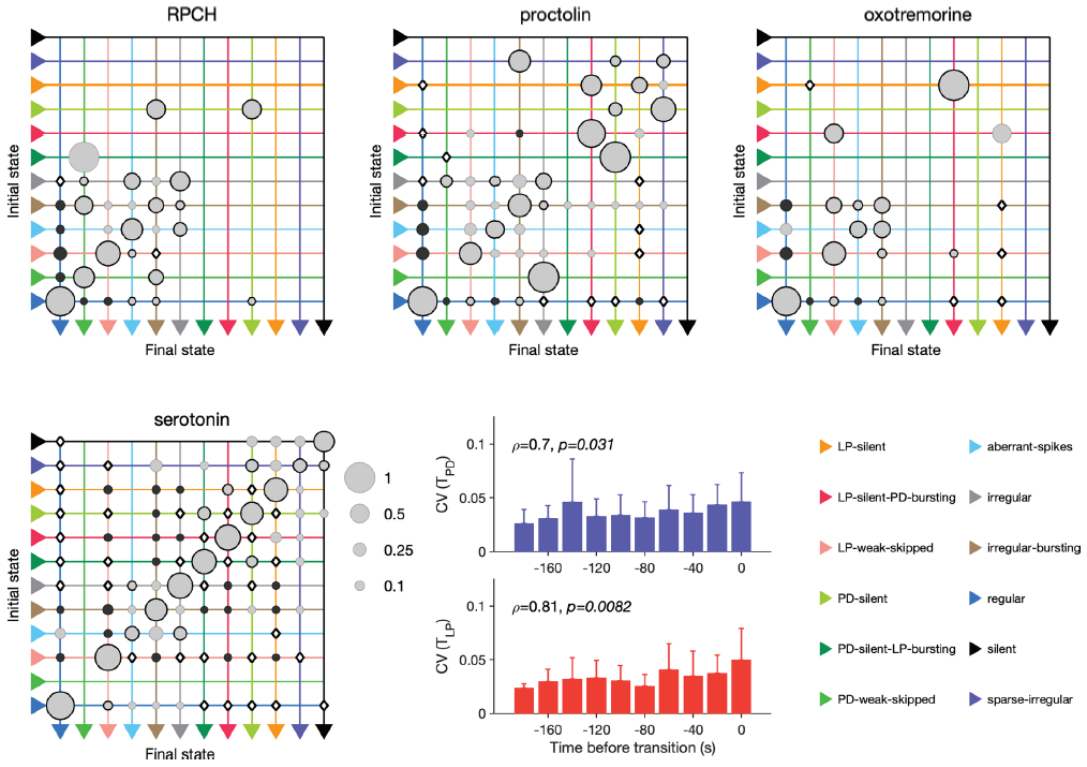


**Figure B.10** Effect of red pigment-concentrating hormone (RPCH), proctolin, oxotremorine, and serotonin on transition probabilities. Each matrix shows the conditional probability of observing the final state in the next time step given an observation of the initial state during bath application of that neuromodulator. Probabilities in each row sum to 1. Size of disc scales with probability. Discs with dark borders are transitions that are significantly more likely than the null model (Materials and methods). Dark solid discs are transitions with nonzero probability that are significantly less likely than in the null model. ◊ are transitions that are never observed and are significantly less likely than in the null model. States are ordered from regular to silent. Bar graphics show the coefficient of variability (CV) of pyloric dilator (PD) and lateral pyloric (LP) burst periods before transition away from regular states. ρ, p from Spearman rank correlation test. RPCH: n = 148 transitions in N = 33 animals; proctolin: n = 155 transitions in N = 59 animals; oxotremorine: n = 102 transitions in N = 21 animals; serotonin: n = 263 transitions in N = 23 animals. Bar graphs show the CV of burst periods of PD and LP vs. time before a transition away from regular states during serotonin application. ρ, p from Spearman rank correlation test.

## B.3 Discussion

Advances in neural recording technology have made it possible to generate increasingly large datasets, and an ongoing challenge is in developing computational tools to find structure in the neural haystack (Pachitariu et al., 2016). Nonlinear dimensionality reduction algorithms such as t-SNE can create a useful representation of datasets that are too large to visualize in their entirety using traditional methods. We combined domain-specific expert knowledge with an unsupervised dimensionality reduction process (t-SNE) by manually segmenting and labeling clusters of dynamics representing biologically significant behavior. This approach conferred two advantages: it allowed for a more accurate measure of traditional metrics such as burst phases in large datasets (Figures B.4 and B.8), and it allowed for the analysis of irregular dynamics that are typically intractable with conventional analysis methods (e.g., Figure B.9), with the disadvantage of not being fully automated, and requiring human intervention to inspect data in the embedding and draw cluster boundaries. Our work hints at a possibility to characterize nonregular spike patterns in small neural circuits and can thus provide a deeper understanding of circuit activity under baseline conditions and in response to perturbations. Our approach makes limited assumptions of the dynamics of the circuit, yet provides a formal framework based on domain-specific knowledge for characterizing circuit activity. Additionally, this way of analyzing neural spike data can readily be adapted to other circuits and systems.

**Reliable Identification of Regular Rhythms Allows for Accurate, Interpretable Analysis of Rhythm Metrics.** Characterizing the statistics of neural oscillations has several subtle challenges. For example, variations in cycle period arising from cycle to

cycle fluctuations are not distinguished from those arising from alteration between epochs of regular oscillations interrupted by spans of irregular activity where metrics like cycle period are undefined. One way to disambiguate the two is to construct elaborate checks to make sure that the spike pattern being measured meets certain criteria. However, edge cases abound, and this is a challenging and subjective approach. A fortuitous consequence of the embedding method we used is to reliably identify when rhythms were regular, and we found that burst metrics were well defined for this subset of data (blue region in Figure B.3). We were therefore able to measure the mean and variability of various burst metrics (Figure B.4) only in stretches of data where it made sense to do so, and thus the measured variability stemmed almost entirely from cycle-to-cycle variations.

Consistent with previous studies (Bucher et al., 2005; Hamood and Marder, 2014; Hamood et al., 2015), our results (Figure B.4) show that within-animal variability in pyloric burst metrics is lower than across-animal variability. Our results are from an analysis of data from several experimenters from different laboratories, collected over a span of 10 years. It is therefore an ideal dataset in which to measure variability. We find that the CV of all burst metrics measured is ~ 0.1 (Figure B.4 b), which can now be used as a standard for regular baseline pyloric oscillations. Measuring burst metrics on decentralization (Figure B.8) also allowed us to characterize how regular rhythms change, while still being recognizably regular. In addition to recapitulating well-understood phenomena such as the slowing down and increased variability in rhythms, we found that the phase of LP burst onset did not change significantly, but the phase of LP burst termination did, suggesting that features of the rhythm are differentially robust to the removal of neuromodulation.

Earlier work categorized the varied dynamics of the pyloric circuit during perturbations (Haddad and Marder, 2018; Haley et al., 2018; Ratliff et al., 2021). In those studies, categories were typically constructed by hand and were not rigorously shown to be mutually exclusive. Categories in this work, while manually chosen, emerge naturally from the distribution of the data in the reduced space (Figure B.3) and no segment of data can have more than one label because it can exist only at a single point in the map. For instance, earlier work categorized rhythms that were labeled regular into two categories, 'normal triphasic' and 'normal triphasic slow' (Haddad and Marder, 2018), while we did not observe a distinctly bimodal distribution of burst periods. In contrast, the catch-all 'atypical firing' state was separated here into a number of states (irregular, irregular-bursting, sparse-irregular) that span several well-separated clusters in the map (Figure B.3). In summary, this work recapitulates every label constructed to categorize spike patterns from PD and LP neurons in earlier work, and additionally finds new spike patterns that were either not detected or not identified as distinct because they are hard to detect by manual inspection.

**Diversity and Stereotypy in Trajectories from Functional to Crash States.** Are there preferred paths to go from regular rhythms to crash? Diversity in the solution space of functional circuits, and the varied effects of perturbations on these circuits, argues for an assortment of trajectories from functional dynamics to irregular or silent states. While transition matrices measured during different perturbations were varied (Figure B.6), we did observe universal features in transition matrices measured during environmental perturbations, decentralization, and addition of neuromodulators (Figures B.6, B.7 and B.10). The destabilizing transition from regular → LP-weak-skipped was overrepresented

in every transition matrix, suggesting that the weakening of the LP neuron is a crucial step in the trajectories towards destabilization, perhaps because there is only one copy of LP in the circuit. Earlier work studying trajectories of destabilization of regular bursting in the isolated pacemaker kernel also found a conserved motif in trajectories towards destabilization: from regular bursting to tonic spiking to silence in response to pH perturbations, and another conserved motif (bursting to weak bursting to silence) in response to temperature perturbations (Ratliff et al., 2021). Transitions away from regular rhythms were also associated with increased variability in burst periods during all perturbations except high temperature and low pH (Figures B.6, B.7 and B.10). An increase in variability in PD voltage dynamics before transitions from regular bursting has been observed in the isolated pacemaker kernel (Ratliff et al., 2021), similar to the effect we observed in the intact circuit.

The structure of the transitions between states also hints at features of the circuit that are critical for rhythm (de)stabilization. Unsurprisingly, PD-silent states precede silent states in low pH, high temperature, and high $[K^+]$ perturbations (Figure B.6). This makes sense because PD cells are electrically coupled to the endogenous burster AB in the pacemaker kernel, and silencing the pacemaker kernel can cause the circuit to go silent. Though the states are determined purely from clusters in the embedding (FigureB.2), and thus from statistical features of spike times, some states may be identified predominantly with cell-specific features (e.g., LP-weak-skipped where the LP neuron fails to burst regularly, but the PD neurons continue to burst regularly), or with circuit-level features (e.g., aberrant-spikes where one or both neurons fire spikes outside the main burst, which may be caused by incomplete inhibition). Decentralization elicits the largest number of

transition types, with ~ 80% of all transition types observed, which could be a consequence of the complex change in the neuromodulator milieu following transection of descending nerves.

**Linking Circuit Output to Circuit Mechanisms.** A large body of work has shown that there is more than one way to make a neural circuit with similar patterns of activity (Prinz et al., 2003; Prinz et al., 2004; Gutierrez et al., 2013). Several combinations of circuit parameters such as synapse strengths, ion channel conductances, and network topology can be found in circuits that generate similar emergent collective dynamics (Gonçalves et al., 2020). The dimensionality of the space of neuronal and synaptic parameters in a neural circuit is much larger than the dimensionality of the circuit output (Marder and Bucher, 2007). This disparity in dimensionality leads to an inherently many-to- one mapping from the space of circuit architecture to the space of circuit dynamics. Circuits can therefore exhibit 'cryptic' architectural variability (Haddad and Marder, 2018), where the diversity of topologies and neuronal parameters is masked by the relatively low- dimensional nature of the observed circuit outputs. However, perturbations can reveal differences between seemingly identical circuits. For instance, current injections in an oscillator network can shift phases, thus revealing connection weights between individual neurons (Timme, 2007). This work reveals a path towards analysis that can reveal cryptic variability and build mechanistic links from circuit architecture to function. By characterizing the totality of circuit dynamics under a variety of conditions, our framework provides a way to fit biophysically detailed models of the pyloric circuit to diverse circuit dynamics under baseline conditions and perturbations. From the large diversity of neuron and circuit parameters that can reproduce a snapshot of activity, only a subset of models could

potentially recapitulate the diverse irregular behavior seen under extreme perturbations. Recent work that reproduced how circuits change cycle periods with temperature (Alonso and Marder, 2020) can be extended to find parameter sets that also generate the irregular states characterized in this study at the rates observed in the data. Crucially, the characterization of the pyloric circuit dynamics in this work can be used to rule out models and parameter sets that generate irregular activity that is qualitatively dissimilar to any of the irregular states observed in the pyloric circuit. Future experimental work can pair data analysis methods such as this work with quantitative measurements of cellular and circuit parameters using emerging techniques (Schulz et al., 2006; Schulz et al., 2007; Tobin et al., 2009) to find parameter sets that generate robust rhythms and irregular states.

**Applicability to Other Systems.** The analysis method in this study is well-suited for large datasets of neural recordings from identified neurons. Data where the identity of each neuron is not or cannot be known, such as large-scale mammalian brain recordings, would require modifications to the analysis pipeline described in Figure B.2. First, it would no longer be possible to construct a data vector of fixed length because ordering of the different neurons would not be meaningful. Each data point would instead be an unordered set of spike times from each neuron, and a distance function that operated on spike times (Christen et al., 2006; Victor and Purpura, 2009; Schreiber et al., 2003; van Rossum, 2001) could be used to generate a distance matrix between raw data points, which would be the input to the embedding algorithm. In our analysis, we included features such as the 'spike phase' (Figure B.2 b and c) because the neurons in this circuit interact with one another strongly in each cycle of oscillations. The analysis of neural circuits that do not show such

strong intrinsically phase-controlled behavior could use other features more suitable to those systems.

**Comparison With Other Methods.** Visualization and other forms of analysis of large neural datasets rely on dimensionality reduction (Nguyen and Holmes, 2019). Here, we used the t-SNE algorithm as a core method to reduce the dimensionality of the dataset and visualize our data. t-SNE has been widely used in the unsupervised analysis of many types of biological data (Berman et al., 2014; Kollmorgen et al., 2020; Chen et al.,2021; Macosko et al., 2015; Kobak and Berens, 2019; Leelatian et al., 2020), including neural recordings (Dimitriadis et al., 2018). t-SNE is a technique that allows high-dimensional data to be visualized in a lower-dimensional space (Van der Maaten and Hinton, 2008; Linderman and Steinerberger, 2019), and works by preserving pairwise distances between points in the high-dimensional space and the low-dimensional embedding, within a certain neighborhood. This feature makes t-SNE an attractive tool to try to visualize large, structured datasets, such as those examined in this study, because it can demonstrate how similar spike patterns are to each other (Dimitriadis et al., 2018). t-SNE has been shown rigorously to be capable of recovering well-separated data clusters (Linderman and Steinerberger, 2019). In our application, t-SNE generated embeddings where spike patterns in different regions could be described as qualitatively different. For example, spike patterns in the top-most cluster (colored green in Figure B.3) all had weak PD spiking, but regular and strong LP spiking. This was qualitatively different from the two closest clusters LP-weak-skipped and irregular. In regions of the map where clusters were not cleanly separated (e.g., in the connection between the regular and irregular-bursting clusters), manual inspection revealed a number of intermediate states. The clustered or not-clustered

regions of the map are therefore informative of the underlying distribution of spike patterns and emerge robustly from the embedding.

t-SNE is widely used in the analysis and visualization of high-dimensional data, but is important to acknowledge its limitations. t-SNE can generate embeddings that appear to have clusters from purely randomly distributed data, can distort sizes of clusters, and can fail to preserve large-scale topological features of the data in some embeddings (Wattenberg et al., 2016). The visualization we generated was useful in that it guided manual clustering and made feasible a previously intractable task, that of classifying hundreds of hours of spike patterns from hundreds of animals.

A variety of other dimensional reduction techniques, including multidimensional scaling (Cox and Cox, 2008), convolutional non-negative matrix factorization (Mackevicius et al., 2019) and their extensions (Williams et al., 2020), tensor component analysis (Williams et al., 2018), and dynamical component analysis (Clark et al., 2019), have been developed that aid in visualizing and analysis of large neural datasets. Methods based on neural networks offer powerful tools to analyze unstructured neural data by modeling the data with a recurrent neural net and then analyzing that model (Vyas et al., 2020). Topological autoencoders are one such technique that combine autoencoders with methods from topological data analysis to produce representation in lower-dimensional spaces (Moor et al., 2019). These methods are similar in spirit to the analysis presented here, but use sophisticated neural nets whose parameters yield the lower-dimensional representation. Other analysis methods include SOM-VAE, which combines self-organizing maps (SOMs) and variational auto-encoders (VAEs) (Fortuin et al., 2018) to analyze high-dimensional time series and find transitions between states, and deep

temporal clustering, which combines dimensionality reduction and temporal clustering (Madiraju et al., 2018).

**Technical Considerations.** In this study, we have used the activity of the LP and PD neurons as a proxy for the pyloric circuit. However, the pyloric circuit contains other neurons: AB (which is electrically coupled to PD neurons), PY neurons (which are anti-phase to both PD and LP), and VD and IC neurons. A richer description of the dynamics of the pyloric circuit would include spikes from these neurons, and the methods we have described here can be scaled up to include these neurons. It is likely that we are underestimating the number of states, and thus, transitions between states, because we do not have access to the dynamics of these neurons. Datasets that contain recordings from all pyloric neurons as preparations are subjected to the perturbations studied here and are not available for large numbers of animals. We therefore chose to focus on the functional antagonists LP and PD. Additionally, neurons in the pyloric circuit are coupled using graded synapses, and the circuit can generate coordinated activity even when spiking is abolished (Rosenbaum and Marder, 2018), suggesting that subthreshold oscillations may be an important feature we are not measuring by only recording spikes. However, the data required necessitates substantially harder to perform experiments because intracellular electrodes must be used. Furthermore, the signal to the muscles – arguably the physiologically and functionally relevant signal – is the spike signal, suggesting that spike patterns from the pyloric circuit are a useful feature to measure.

The unit of data we operated on was a time series of spikes from the LP and PD neurons. In order to describe what the dynamics of these neurons is at a given point in time, we chose to look at a neighborhood in time. In this article, we chose 20 s nonoverlapping

bins, based on inspection of the data by eye. Choosing a time bin imposes certain tradeoffs in the analysis of time series: changes in dynamics on timescales smaller than the bin are counted as different states, and changes in dynamics on timescales longer than the bin size are counted as transitions between states. The statistics of the transitions we measure are therefore dependent on the bin size we chose. We note that dwell times in each state are almost always in excess of null model predictions generated by shuffling states (transition matrices in Figures B.6, B.7 and B.10), supporting the validity of our choice of 20 s bins.

**Conclusion and Outlook.** Our work provides a way to characterize nonregular spike patterns in small neural circuits. It thus provides a bridge between experimental or simulation work grounded in the biophysical detail of ion channels and synaptic currents; and the rich body of observations of circuits under baseline and perturbed conditions. The methods we have employed can easily be adapted to other circuits and systems, make limited assumptions of the dynamics of the circuit, yet provide a robust framework on which to hang a large volume of previously ineffable expert domain knowledge.

Prior to this work, crashes in the pyloric circuit and irregular dynamics in a normally regular circuit were difficult to characterize. We present a method to tame the complexity of the distribution of irregular states by exploiting the fact that pyloric dynamics are not unbounded even in their irregularity. By using a t-SNE in conjunction with manual inspection of reduced data and manual clustering, we have made this previously intractable problem feasible and found undiscovered spike patterns and transitions. Our approach was successful because we used a dataset with long recordings from identified neurons in a circuit that can be subjected to many different perturbations, which is one of the advantages of using the STG system. It will be interesting to see if this

can be applied to other systems with identified neurons in a functional circuit to characterize their function and failure modes.

In intact pyloric circuits, and in the presence of modulatory input from the stn, almost all networks are ‘normal’ and exhibit regular rhythms. Decentralization can generate more variable dynamics, presumably because the underlying differences in network structure that were compensated by modulator action now manifest as different collective dynamics in the network. Although it may appear that modulators can have similar effects when added to a decentralized network, they are in fact distinguishable when looking at how they influence the totality of circuit dynamics, not just the regular state.

A major unanswered question was whether crashes triggered by different perturbations share dynamical mechanisms and common pathways. Earlier work looking at a simpler subset of the pyloric circuit argued that different perturbations led to stereotyped but diverse transitions before crash, and we have extended this result in the intact circuit. We show that different perturbations can have different trajectories to crash, but the stereotypy observed in the simpler system was not observed, presumably due to the larger number of pathways accessible to the intact circuit. The new insight from this work stems from the fact that this is the first time transitions through multiple physiological conditions in so many modalities have been characterized and shows that there are many paths through possible circuit dynamical states from canonical states to crash. Several studies focus on one perturbation at a time. By studying a number of perturbations together, we compare responses to different kinds of perturbations on the same physiological network.

## B.4 Materials and Methods

**Animals and Experimental Methods.** Adult male Jonah crabs (*C. borealis*) were obtained from Commercial Lobster (Boston, MA), Seabra's Market (Newark, NJ), and Garden Farm Market (Newark, NJ). Dissections were carried out as previously described (Gutierrez and Grashow, 2009). Decentralization was carried out either by cutting the stn or by additionally constructing a well on the stn and adding sucrose and TTX (tetrodotoxin) as described in Haddad and Marder, 2018. Temperature was controlled as described in Tang et al., 2010; Tang et al., 2012; Haddad and Marder, 2018. Extracellular potassium concentrations were varied as described in He et al., 2020. pH perturbations are described in Haley et al., 2018.

**Data Selection and Curation.** Our goal was to include as much data as possible to create as complete a description of pyloric dynamics as possible. Following our strategy of including only the LP and PD neurons, we used every available dataset that recorded from these neurons from the Marder lab. We also included available datasets from the Nadim and Bucher labs. No dataset was explicitly excluded for reasons linked to the activity of the pyloric circuit in those datasets. Data where crucial metadata was not recorded (e.g., if the temperature of the preparation was not recorded) was excluded. Data where only lvn was recorded from was only included in cases of exceptional data quality, where it was judged that PD and LP could be reliably identified.

**Spike identification and sorting.** Spikes are identified from extracellular recordings of motor nerves or from intracellular recordings. LP spikes were identified from intracellular recordings, lvn, lpn, and gpn nerves (in descending order of likelihood). PD spikes were identified from pdn, intracellular recordings, and lvn. We used a custom-designed spike

identification and sorting software (called 'crabsort') that we have made freely available https://github.com/sg-s/crabsort (Gorur-Shandilya, 2021), previously described in Powell et al., 2021. Spikes are identified using a fully connected neural network that learns spike shapes from small labeled datasets. A new network is typically initialized for every preparation. Predictions from the neural network also indicate the confidence of the network in these predictions, and uncertain predictions are inspected and labeled and the neural network learns from these using an active learning framework (Settles, 2009).

**Data Curation and Data Model.** Each file was split into 20 s nonoverlapping bins, and spike times, together with metadata, were assembled into a single immutable instance of a custom-built class (embedding.DataStore). The data store had the following attributes:

- *Spike times* containing LP and PD spike times.
- *ISIs* containing ISIs and spike phases
- *Labels* categorical data containing manually generated labels from Figure B.3
- *Metadata* such as concentration of modulators, pH, temperature, whether the preparation was decentralized or not, etc.

Using an immutable data structure, reduced risks of accidental data alteration during analysis. Every attribute was defined for every data point.

**Embedding.** ISI and phase representation (Figure B.2 b)**.** Each data point is a 20 s bin containing spike times from LP and PD neurons (Figure B.2 a). For each data point, spike times are converted into ISIs. A set of spike times uniquely identifies a set of (ordered) ISIs. The set of LP spike times generates a set of LP ISIs, and the set of PD spike times generates a set of PD ISIs (Figure B.2 b).

For every spike in PD or LP, a 'spike phase' can be calculated as follows. Spike phases are not defined when either LP or PD are silent in that data point, or for LP/PD

spikes with no spikes from the other neuron before or after that spike. Thus, the 'spike phase' of the *i*th spike on neuron X w.r.t. neuron Y is given by

$$\frac{t_i^X - t_{i,-}^Y}{t_{i,+}^Y - t_{i,-}^Y} \in [0, 1$$

where $t^X_i$ is the time of the *i*th spike on neuron $X$, $t^Y_i,-$ is the time of the last spike on $Y$ before $t^X_i$, and $t^Y_i,+$ is the time of the first spike after $t^X_i$. Note that this definition can be generalized to $N$ neurons, though the number of spike phases grows combinatorially with $N$.

**Construction of vectorized data frame (Figure B.2 c and d).** Each data point can contain an arbitrary number of spikes, and thus an arbitrary number of ISIs and spike phases. Ideally, each data point is a data frame of fixed length (a point in some fixed high-dimensional space). To do so, we computed percentiles ISIs and spike phases (Figure B.2 c). We chose 10 bins per ISI type (deciles). The end result is not strongly dependent on the number of bins chosen as long as there are sufficiently many bins to capture the distinctly bimodal distribution in ISIs during bursting.

We included four other features to help separate spike patterns that appeared qualitatively different. First, firing rates of LP and PD neurons. Second, the ratios of second-order to first-order ISIs, defined as

$$\frac{\max I^{(2)}}{\max I^{(1)}}$$

where $I^{(n)}$ is the nth order set ofISIs computed as the time between n spikes. $I^{(1)}$ is the simple set of ISIs defined between subsequent spikes. This measure is included because it captures the difference between single spike bursts and normal bursts well. Third, the ratio between the largest and second-largest ISIs for each neuron.

Finally, we also included a metric defined as follows:

$$\frac{\max \text{diff}(\mathbf{s})}{s_{max}}$$

where **s** is a vector of sorted ISIs, and $s_{max}$ is the sorted ISI for which the difference between it and the previous sorted ISI is maximum. This metric was included as it captures to a first approximation how 'burst-like' a spike train is. Intuitively, this metric is high for spike trains with bimodal ISI distributions, as is the case during bursts.

All these features were combined into a single data frame and z -scored (Figure B.2 d).

In some cases, these features were not defined, for example, when there are no spikes on either neuron, the concepts of spike phases or ISIs are meaningless. In these cases, 'filler' values were used that were located well off the extremes of the distribution of the metric when defined. For example, ISIs were filled with values of 20 s (the size of the bin) when no spikes were observed. The overall results and shape of the embedding did not depend sensitively on the value of the filler values used.

These features were chosen to capture various modes of spiking and bursting that have been previously identified by manual inspection (Haddad and Marder, 2018; Tang et al., 2012; Haley et al., 2018). Other features may be more appropriate in other systems where spike patterns span different axes of variability. However, we note that these features while being appropriate for this data were not 'fine-tuned' to specialize in features that are exclusively found in spike patterns from the pyloric circuit. For example, these features do not explicitly measure bursting, the dominant feature of the pyloric rhythm, but instead use distributions of ISIs that are sufficiently descriptive to capture the variability in bursting and transitions from bursting to other spiking.

**Embedding using t-SNE.** So far, we have described how we converted a 20 s snippet containing spike times from LP and PD into a data frame (a vector). We did this for every 20 s snippet in the dataset. Data that did not fit into any bin was discarded (e.g., data at the trailing end of an experiment shorter than 20 s). Thus, our entire dataset is represented by $M \times N$ matrix, where $M$ is the number of features in the data frame and $N$ is the number of data points.

We used the t-SNE algorithm (Van der Maaten and Hinton, 2008) to visualize the vectorized data matrix in two dimensions. Our dataset contained ~ 105 points and was therefore too large for easy use of the original t-SNE algorithm. We used the FI-t-SNE approximate algorithm (Linderman et al., 2019) to generate these embeddings. We used a perplexity of $P = 100$ to generate these embeddings. Varying perplexity caused the embedding to change in ways consistent with what is expected for t-SNE embeddings, and the coarse features of the embedding did not sensitively depend on this choice of perplexity (Figure B.2—figure supplement 4). t-SNE is often used with random initialization, and

different random initializations can lead to different embeddings with clusters located at different positions in the map. The importance of meaningful initializations has recently been highlighted (Kobak and Linderman, 2021), and we used a fixed initialization where the x-axis corresponded to the shortest ISI in each data point and the y-axis corresponded to the maximum ratio of second-order to first-order ISI ratios (described above). For completeness, we also generated embeddings using other initializations (Figure B.3—figure supplement 2). For both random initializations (Figure B.3—figure supplement 2a–d) and initializations based on ISIs (Figure B.3—figure supplement 2e and f), we observed that regular states tended to occur in a single region, surrounded by clusters that were dominated by a single color corresponding to irregular states. Thus, the precise location of different clusters can vary with the initialization, but the overall structure of the embedding, and the identity of points that tend to co-occur in a cluster, does not vary substantially with initialization.

**Manual clustering and annotation of data.** Once the feature vectors were embedded using t-SNE, we manually inspected these points to get a sense of the spike patterns in each point cloud. To do so, we built an interactive tool that visualized spike patterns that corresponded to each point when clicked on. Random points within regions of high density were sampled to check that interior points had similar spike patterns. Points were assigned labels by drawing boundaries around them and labeling all points within that boundary. Finally, we generated plots of ISIs and rasters from points in clusters to ensure that patterns of spiking were visually similar.

**Triangulation and triadic differences (Figure B.2—figure supplement 3).** The output of the embedding algorithm is a set of points in two dimensions. We built a Delaunay

triangulation on these points. For each triangle in the triangulation, we computed the maximum difference between some burst metric (e.g., burst period of PD neurons) across the three vertices of that triangle. These triadic differences are represented colored dots, where the dots are located at the incenters of each triangle in the triangulation.

**Time-series analysis.**

**Measuring burst metrics (Figure B.4).** Burst metrics were measured following previous definitions (Prinz et al., 2004; Bucher et al., 2005). Briefly, bursts were identified by observing that ISI distributions were bimodal, with smaller ISIs corresponding to ISIs within a burst, and longer ISIs corresponding to inter-burst intervals. This allowed us to threshold ISIs, and this identifies burst starts and burst ends. From here, burst periods could be calculated, which allowed us to measure phases and delays relative to the start of the PD burst.

**Measuring transition matrices (Figures B.6, B.7 and B.10).** The transition matrix is a square matrix of size $N$ that describes the probability of transitioning from one to another of $N$ possible states. The transition matrix we report is the right stochastic matrix, where rows sum to 1. Each element of the matrix $T_{ij}$ corresponds to the conditional probability that we observe state $j$ given state . To compute this, we iterate over the sequence of states and compare the current state to the state in the next state. Breakpoints in the sequence are identified by discontinuities in the timestamps of that sequence and are ignored. We then zeroed the diagonal of the matrix and normalized each row by the sum.

**Measuring variability before transitions away from regular states (Figures B.6 and B.7).** We first identified continuous segments that corresponded to uninterrupted recordings from the same preparation at the appropriate condition. For each segment, we

found all transitions away from the regular state. We therefore computed a vector as long as the segment containing the time to the next transition. We then collected points corresponding to time to next transition ranging from $t = -200s$ to $t = 0s$ . For each time bin, we measured the CV of the burst period by dividing the standard deviation of the burst period in that datum by the mean in that datum.

**Data visualization**

**Raincloud plots (Figure B.4).** Raincloud plots (Allen et al., 2019) are used to visualize a univariate distribution. Individual points are plotted as dots, and a shaded region indicates the overall shape of the distribution. This shape is obtained by estimating a kernel smoothing function estimate over the data. Individual points are randomly jittered along the vertical axis for visibility.

**Occupancy maps (Figures B.5 and B.7).** To visualize where in the map data from a certain condition occurred, the full embedding is first plotted with colors corresponding to the state each point belongs to. The full dataset is made semi-transparent and plotted with larger dots to emphasize the data of interest. Data in the condition of interest is then plotted as usual. Each bright point in these plots corresponds to a 20 s snippet of data in the condition indicated.

**Treemaps (Figures B.7 and B.9).** Treemaps (Shneiderman and Wattenberg, 2001) were used to visualize state probabilities in a given experimental condition. For each preparation, the probability of each state was computed, and the mean probability of a given state was computed by averaging across all preparations. Thus, each preparation contributes equally. The area of the region in the treemap scales with the probability of that state.

**Transition matrices (Figures B.6, B.7 and B.10).** Transition matrices were visualized as in Corver et al., 2021. Initial states are shown along the left edge, and final states are shown along the bottom edge of each matrix. Lines are colored by origin (horizontal lines) or destination (vertical) states. The size of each disc at the intersection of each line scales with the conditional probability of moving from the initial state to the final state. Note that the size of all discs is offset by a constant to make small discs visible.

**Statistics**

**Comparing within-group to across-group variability (Figure B.4).** To compare the variability of various burst metrics within each animal and across animals, we first measured the means and CVs of each burst metrics in every animal. We then used the mean of the coefficients of variations as a proxy for the within-animal variability and used the CV of the means as a proxy for the across-animal variability. Note that both measures are dimensionless. They can therefore be directly compared.

To test if the within-animal variability was significantly less than the across-animal variability, we performed a permutation test. We shuffled the labels identifying the animal to which each data point belonged to and measured a new 'within-animal' and 'across-animal' variability measure using these shuffled labels. We repeated this process 1000 times to obtain a null distribution of differences between within- and across-animal variability. Identifying where in the null distribution the data occurred allowed us to estimate a p-value for the measured difference. For example, if the measured difference between within- and across-animal variability in metric X was greater than 99% of the null distribution obtained by shuffling labels, we conclude that the p-value is 0.01. The

significance level of 0.05 was divided by the number of burst metrics we tested to determine if any one metric was significantly more or less variable across animals.

**Measuring trends in variability in regular rhythms before transitions (Figures B.6 b, B.7 f and B.9 d).** To determine if variability significantly increased in the 200 s preceding a transition away from regular, we measured the Spearman rank correlation between time before transition (x-axis) and mean variability. The Spearman rank correlation $\rho$ is 1 if quantities monotonically increase.

**Measuring transition rate significance (Figures B.6 a, B.7 e and B.10).** In the empirical transition matrices, certain transitions never occur, and certain transitions occur with relatively high probability. Each element of the transition matrix $T_{ij}$ corresponds to the conditional probability $P$(final|initial). Our null model assumes that transitions occur at random between states, and therefore the probability of observing any transition $i \rightarrow j$ scales with the marginal probability of observing state $j$ after transitions. We therefore built a null distribution of transition rates by sampling with replacement from the marginal counts of states after transitions. The fraction of this null distribution that was above or below the empirical transition rate was interpreted to be the p-value and thus determined significance.

## Code availability

Table B.4 lists the code used in this article. The code can be downloaded by prefixing https://github.com/ to the project name.

**Table B.4** Code Availability

| Project | Notes |
|---|---|
| sg-s/crabsort | Interactive toolbox to sort spikes from extracellular data |
| sg-s/stg-embedding | Contains all scripts used to generate every figure in this article |
| KlugerLab/FIt-SNE | Fast interpolation-based *t*-distributed stochastic neighbor embedding, used to make embedding |
| sg-s/SeaSurfaceTemperature | Wrapper to scrape NOAA databases |

## REFERENCES


Allen M, Poggiali D, Whitaker K, Marshall TR, Kievit RA. 2019. Raincloud plots: a multi-platform tool for robust data visualization. *Wellcome Open Research* 4:63.

Alonso LM, Marder E. 2019. Visualization of currents in neural models with similar behavior and different conductance densities. *eLife* 8:e42722.

Alonso LM, Marder E. 2020. Temperature compensation in a small rhythmic circuit. *eLife* 9:e55470.

Bal T, Nagy F, Moulins M. 1994. Muscarinic modulation of a pattern-generating network: control of neuronal properties. *The Journal of Neuroscience* 14:3019–3035.

Beltz B, Eisen JS, Flamm R, Harris-Warrick RM, Hooper SL, Marder E. 1984. Serotonergic innervation and modulation of the stomatogastric ganglion of three decapod crustaceans (Panulirus interruptus, Homarus americanus and Cancer irroratus). *The Journal of Experimental Biology* 109:35–54.

Berman GJ, Choi DM, Bialek WS, Shaevitz JW. 2014. Mapping the stereotyped behaviour of freely moving fruit flies. *Journal of the Royal Society, Interface* 11:20140672.

Börner K, Chen C, Boyack KW. 2005. Visualizing knowledge domains. *Annual Review of Information Science and Technology* 37:179–255.

Brunel N, Wang XJ. 2003. What determines the frequency of fast network oscillations with irregular neural discharges? i. synaptic dynamics and excitation-inhibition balance. *Journal of Neurophysiology* 90:415–430.

Bucher D, Prinz AA, Marder E. 2005. Animal-to-animal variability in motor pattern production in adults and during growth. *The Journal of Neuroscience* 25:1611–1619.

Caplan JS, Williams AH, Marder E. 2014. Many parameter sets in a multicompartment model oscillator are robust to temperature perturbations. *The Journal of Neuroscience* 34:4963–4975.

Chen W, Zhao Y, Chen X, Yang Z, Xu X, Bi Y, Chen V, Li J, Choi H, Ernest B, Tran B, Mehta M, Kumar P, Farmer A, Mir A, Mehra UA, Li JL, Moos M, Xiao W, Wang C. 2021. A multicenter study benchmarking single-cell RNA sequencing technologies using reference samples. *Nature Biotechnology* 39:1103–1114.

Christen M, Kohn A, Ott T, Stoop R. 2006. Measuring spike pattern reliability with the lempel–ziv-distance. *Journal of Neuroscience Methods* 156:342–350.

Clark MC, Dever TE, Dever JJ, Xu P, Rehder V, Sosa MA, Baro DJ. 2004. Arthropod 5-HT2 Receptors: A neurohormonal receptor in decapod crustaceans that displays agonist independent activity resulting from an evolutionary alteration to the dry motif. *The Journal of Neuroscience* 24:3421–3435.

Clark DG, Livezey JA, Bouchard KE. 2019. Unsupervised discovery of temporal structure in noisy data with dynamical components analysis. *ArXiv*: 1905.09944. NeurIPS 14267-14278.

Clemens S, Massabuau JC, Meyrand P, Simmers J. 2001. A modulatory role for oxygen in shaping rhythmic motor output patterns of neuronal networks. *Respiration Physiology* 128:299–315.

Corver A, Wilkerson N, Miller J, Gordus AG. 2021. Distinct movement patterns generate stages of spider web-building. *Current Biology* 31:4983-4997.

Cox MA, Cox TF. 2008. Multidimensional scaling. Cox MA (Ed). *Handbook of Data Visualization*. Springer, Berlin, Heidelberg, p. 315–347.

Cunningham JP, Yu BM. 2014. Dimensionality reduction for large-scale neural recordings. *Nature Neuroscience* 17:1500–1509.

Cymbalyuk GS, Gaudry Q, Masino MA, Calabrese RL. 2002. Bursting in leech heart interneurons: cell- autonomous and network-based mechanisms. *The Journal of Neuroscience* 22:10580–10592.

Daur N, Nadim F, Bucher D. 2016. The complexity of small circuits: the stomatogastric nervous system. *Current Opinion in Neurobiology* 41:1–7.

Dickinson PS, Hauptman J, Hetling J, Mahadevan A. 2001. Rpch modulation of a multi-oscillator network: effects on the pyloric network of the spiny lobster. *Journal of Neurophysiology* 85:1424–1435.

Dimitriadis G, Neto JP, Kampff AR. 2018. t-SNE visualization of large-scale neural recordings. *Neural Computation* 30:1750–1774.

Eisen JS, Marder E. 1982. Mechanisms underlying pattern generation in lobster stomatogastric ganglion as determined by selective inactivation of identified neurons. iii. synaptic connections of electrically coupled pyloric neurons. *Journal of Neurophysiology* 48:1392–1415.

Eisen JS, Marder E. 1984. A mechanism for production of phase shifts in a pattern generator. *Journal of Neurophysiology* 51:1375–1393.

Epstein IR, Marder E. 1990. Multiple modes of a conditional neural oscillator. *Biological Cybernetics* 63:25–34.

Fortuin V, Hüser M, Locatello F, Strathmann H, Rätsch G. 2018. SOM-VAE: Interpretable discrete representation learning on time series. arXiv:1806.02199v7.

Franci A, O'Leary T, Golowasch J. 2020. Positive dynamical networks in neuronal regulation: how tunable variability coexists with robustness. *IEEE Control Systems Letters* 4:946–951.

Garcia VJ, Daur N, Temporal S, Schulz DJ, Bucher D. 2015. Neuropeptide receptor transcript expression levels and magnitude of ionic current responses show cell type-specific differences in a small motor circuit. *The Journal of Neuroscience* 35:6786–6800.

Golowasch J, Marder E. 1992. Proctolin activates an inward current whose voltage dependence is modified by extracellular. *The Journal of Neuroscience* 12:810–817.

Golowasch J, Casey M, Abbott LF, Marder E. 1999. Network stability from activity-dependent regulation of neuronal conductances. *Neural Computation* 11:1079–1096.

Golowasch J, Goldman MS, Abbott LF, Marder E. 2002. Failure of averaging in the construction of a conductance-based neuron model. *Journal of Neurophysiology* 87:1129–1131.

Gonçalves PJ, Lueckmann JM, Deistler M, Nonnenmacher M, Öcal K, Bassetto G, Chintaluri C, Podlaski WF, Haddad SA, Vogels TP, Greenberg DS, Macke JH. 2020. Training deep neural density estimators to identify mechanistic models of neural dynamics. *eLife* 9:e56261.

Gorur-Shandilya S, Marder E, O'Leary T. 2020. Activity-dependent compensation of cell size is vulnerable to targeted deletion of ion channels. *Scientific Reports* 10:7.

Gorur-Shandilya S. 2021. crabsort. swh:1:rev:6a67e765e90caa536e6a11f67d9d4737d059af50. GitHub. https://archive.softwareheritage.org/swh:1:dir:b22b2c2456d851ffad732d42288db699d660fa7b;origin=https://github. com/sgs/crabsort;visit=swh:1:snp:da7045d992613143c796feabea2668445c8a3e6b;anchor=swh:1:rev:6a67 e765e90caa536e6a11f67d9d4737d059af50

Gutierrez GJ, Grashow RG. 2009. Cancer borealis stomatogastric nervous system dissection. *Journal of Visualized Experiments: JoVE* 25:1207.

Gutierrez GJ, O'Leary T, Marder E. 2013. Multiple mechanisms switch an electrically coupled, synaptically inhibited neuron between competing rhythmic oscillators. *Neuron* 77:845–858.

Haddad SA, Marder E. 2018. Circuit robustness to temperature perturbation is altered by neuromodulators. *Neuron* 100:609-623.

Haley JA, Hampton D, Marder E. 2018. Two central pattern generators from the crab, Cancer borealis, respond robustly and differentially to extreme extracellular pH. *eLife* 7:e41877.

Hamood AW, Marder E. 2014. Animal-to-animal variability in neuromodulation and circuit function. Cold Spring Harbor Symposia on Quantitative Biology. 21–28.

Hamood AW, Haddad SA, Otopalik AG, Rosenbaum P, Marder E. 2015. Quantitative reevaluation of the effects of short- and long-term removal of descending modulatory inputs on the pyloric rhythm of the crab, cancer borealis *ENeuro* 2:1–13.

Harris-Warrick RM, Flamm RE. 1987. Multiple mechanisms of bursting in a conditional bursting neuron. *The Journal of Neuroscience* 7:2113–2128

Harris-Warrick RM, Marder E. 1991. Modulation of neural networks for behavior. *Annual Review of Neuroscience*14:39–57.

Hartline DK, Maynard DM. 1975. Motor patterns in the stomatogastric ganglion of the lobster Panulirus argus. *The Journal of Experimental Biology* 62:405–420.

He LS, Rue MCP, Morozova EO, Powell DJ, James EJ, Kar M, Marder E. 2020. Rapid adaptation to elevated extracellular potassium in the pyloric circuit of the crab, Cancer borealis *Journal of Neurophysiology* 123:2075– 2089.

Hooper SL, Marder E. 1984. Modulation of a central pattern generator by two neuropeptides, proctolin and FMRFamide. *Brain Research* 305:186–191.

Hooper SL, Marder E. 1987. Modulation of the lobster pyloric rhythm by the peptide proctolin. *The Journal of Neuroscience* 7:2097–2112.

Hooper SL, Thuma JB, Guschlbauer C, Schmidt J, Büschges A. 2015. Cell dialysis by sharp electrodes can cause nonphysiological changes in neuron properties. *Journal of Neurophysiology* 114:1255–1271.

Kobak D, Berens P. 2019. The art of using t-SNE for single-cell transcriptomics. *Nature Communications* 10:5416.

Kobak D, Linderman GC. 2021. Initialization is critical for preserving global data structure in both t-sne and umap. *Nature Biotechnology* 39:156–157.

Kollmorgen S, Hahnloser RHR, Mante V. 2020. Nearest neighbours reveal fast and slow components of motor learning. *Nature* 577:526–530.

Kushinsky D, Morozova EO, Marder E. 2019. In vivo effects of temperature on the heart and pyloric rhythms in the crab Cancer borealis. *Journal of Experimental Biology* 222:jeb.199190.

Leelatian N, Sinnaeve J, Mistry AM, Barone SM, Brockman AA, Diggins KE, Greenplate AR, Weaver KD, Thompson RC, Chambless LB, Mobley BC, Ihrie RA, Irish JM. 2020. Unsupervised machine learning reveals risk stratifying glioblastoma tumor cells. *eLife* 9:e56879.

Linderman GC, Rachh M, Hoskins JG, Steinerberger S, Kluger Y. 2019. Fast interpolation-based t-sne for improved visualization of single-cell rna-seq data. *Nature Methods* 16:243–245.

Linderman GC, Steinerberger S. 2019. Clustering with t-SNE, provably. *SIAM Journal on Mathematics of Data Science* 1:313–332.

Mackevicius EL, Bahle AH, Williams AH, Gu S, Denisenko NI, Goldman MS, Fee MS. 2019. Unsupervised discovery of temporal sequences in high-dimensional datasets, with applications to neuroscience. *eLife* 8:e38471.

Macosko EZ, Basu A, Satija R, Nemesh J, Shekhar K, Goldman M, Tirosh I, Bialas AR, Kamitaki N, Martersteck EM, Trombetta JJ, Weitz DA, Sanes JR, Shalek AK, Regev A, McCarroll SA. 2015. Highly parallel genome-wide expression profiling of individual cells using nanoliter droplets. *Cell* 161:1202–1214.

Madiraju NS, Sadat SM, Fisher D, Karimabadi H. 2018. Deep temporal clustering: fully unsupervised learning of time-domain features. *arXiv*.

Marbán E. 2002. Cardiac channelopathies. *Nature* 415:213–218.

Marder E, Hooper SL, Marder E. 1985. Neurotransmitter modulation of the stomatogastric ganglion of decapod crustaceans. *Model Neural Networks and Behavior* 7:319–337.

Marder E, Hooper SL, Siwicki KK. 1986. Modulatory action and distribution of the neuropeptide proctolin in the crustacean stomatogastric nervous system. *The Journal of Comparative Neurology* 243:454–467.

Marder E, Weimann JM. 1992. Modulatory control of multiple task processing in the stomatogastric nervous system. *Neurobiology of Motor Programme Selection* 6:3–19.

Marder E, Bucher D. 2007. Understanding circuit dynamics using the stomatogastric nervous system of lobsters and crabs. *Annual Review of Physiology* 69:291–316.

Marder E. 2012. Neuromodulation of neuronal circuits: back to the future. *Neuron* 76:1–11.

Mariño J, Schummers J, Lyon DC, Schwabe L, Beck O, Wiesing P, Obermayer K, Sur M. 2005. Invariant computations in local cortical networks with balanced excitation and inhibition. *Nature Neuroscience* 8:194–201.

McInnes L, Healy J, Saul N, Großberger L. 2018. Umap: Uniform manifold approximation and projection. *Journal of Open Source Software* 3:861.

Memmesheimer RM, Timme M. 2006. Designing the dynamics of spiking neural networks. *Physical Review Letters* 97:18.

Miller JP, Selverston AI. 1982. Mechanisms underlying pattern generation in lobster stomatogastric ganglion as determined by selective inactivation of identified neurons. *Journal of Neurophysiology* 48:1416–1432.

Mizrahi A, Dickinson PS, Kloppenburg P, Fénelon V, Baro DJ, Harris-Warrick RM, Meyrand P, Simmers J. 2001. Long-term maintenance of channel distribution in a central pattern generator neuron by neuromodulatory inputs revealed by decentralization in organ culture. *The Journal of Neuroscience* 21:7331–7339.

Moor M, Horn M, Rieck B, Borgwardt K. 2019. Topological autoencoders. *arXiv:* 1802.01059v1

Nguyen LH, Holmes S. 2019. Ten quick tips for effective dimensionality reduction. *PLOS Computational Biology* 15:e1006907-19.

Nusbaum MP, Marder E. 1988. A neuronal role for a crustacean red pigment concentrating hormone-like peptide: Neuromodulation of the pyloric rhythm in the crab, Cancer Borealis . *Journal of Experimental Biology* 135:165–181.

Nusbaum MP, Marder E. 1989. A modulatory proctolin-containing neuron (MPN). I. Identification and characterization. *The Journal of Neuroscience* 9:1591–1599.

O'Leary T, Williams AH, Franci A, Marder E. 2014. Cell types, network homeostasis, and pathological compensation from a biologically plausible ion channel expression model. *Neuron* 82:809–821.

Pachitariu M, Stringer C, Dipoppa M, Schröder S, Rossi LF, Dalgleish H, Carandini M, Harris KD. 2016. Suite2p: Beyond 10,000 neurons with standard two-photon microscopy. *bioRxiv*.

Pang R, Lansdell BJ, Fairhall AL. 2016. Dimensionality reduction in neuroscience. *Current Biology* 26:R656–R660.

Peacock JA. 1983. Two-dimensional goodness-of-fit testing in astronomy. *Monthly Notices of the Royal Astronomical Society* 202:615–627.

Powell D, Haddad SA, Gorur-Shandilya S, Marder E. 2021. Coupling between fast and slow oscillator circuits in Cancer borealis is temperature-compensated. *eLife* 10:e60454.

Prinz AA, Billimoria CP, Marder E. 2003. Alternative to hand-tuning conductance-based models: construction and analysis of databases of model neurons. *Journal of Neurophysiology* 90:3998–4015.

Prinz AA, Bucher D, Marder E. 2004. Similar network activity from disparate circuit parameters. *Nature Neuroscience* 7:1345–1352.

Qadri SA, Camacho J, Wang H, Taylor JR, Grosell M, Worden MK. 2007. Temperature and acid–base balance in the american lobster Homarus americanus. *The Journal of Experimental Biology* 210:1245–1254.

Ratliff J, Franci A, Marder E, O'Leary T. 2021. Neuronal oscillator robustness to multiple global perturbations. *Biophysical Journal* 120:1454–1468.

Rinberg A, Taylor AL, Marder E. 2013. The effects of temperature on the stability of a neuronal oscillator. *PLOS Computational Biology* 9:e1002857.

Rosenbaum P, Marder E. 2018. Graded transmission without action potentials sustains rhythmic activity in some but not all modulators that activate the same current. *The Journal of Neuroscience* 38:8976–8988.

Russell DF. 1976. Rhythmic excitatory inputs to the lobster stomatogastric ganglion. *Brain Research* 101:582–588.

Schreiber S, Fellous JM, Whitmer D, Tiesinga P, Sejnowski TJ. 2003. A new correlation-based measure of spike timing reliability. *Neurocomputing* 52–54:925–931.

Schulz DJ, Goaillard JM, Marder E. 2006. Variable channel expression in identified single and electrically coupled neurons in different animals. *Nature Neuroscience* 9:356–362.

Schulz DJ, Goaillard JM, Marder EE. 2007. Quantitative expression profiling of identified neurons reveals cell-specific constraints on highly variable levels of gene expression. *PNAS* 104:13187–13191.

Settles B. 2009. Active learning literature survey doctoral dissertation. University of Wisconsin-Madison. Madison, Wisconsin.

Shneiderman B, Wattenberg M. 2001. Ordered treemap layouts. IEEE Symposium on Information Visualization, 2001. 73–78.

Spitzer N, Cymbalyuk G, Zhang H, Edwards DH, Baro DJ. 2008. Serotonin transduction cascades mediate variable changes in pyloric network cycle frequency in response to the same modulatory challenge. *Journal of Neurophysiology* 99:2844–2863.

Staley K. 2015. Molecular mechanisms of epilepsy. *Nature Neuroscience* 18:367–372.

Swensen AM, Marder E. 2000. Multiple peptides converge to activate the same voltage-dependent current in a central pattern-generating circuit. *The Journal of Neuroscience* 20:6752–6759.

Swensen AM, Marder E. 2001. Modulators with convergent cellular actions elicit distinct circuit outputs. *The Journal of Neuroscience* 21:4050–4058.

Tang LS, Goeritz ML, Caplan JS, Taylor AL, Fisek M, Marder E. 2010. Precise Temperature Compensation of Phase in a Rhythmic Motor Pattern. *PLOS Biology* 8:e1000469.

Tang LS, Taylor AL, Rinberg A, Marder E. 2012. Robustness of a Rhythmic Circuit to Short- and Long-Term Temperature Changes. *The Journal of Neuroscience* 32:10075–10085.

Thirumalai V, Marder E. 2002. Colocalized neuropeptides activate a central pattern generator by acting on different circuit targets. *The Journal of Neuroscience* 22:1874–1882.

Thirumalai V, Prinz AA, Johnson CD, Marder E. 2006. Red pigment concentrating hormone strongly enhances the strength of the feedback to the pyloric rhythm oscillator but has little effect on pyloric rhythm period. *Journal of Neurophysiology* 95:1762–1770.

Thoby-Brisson M, Simmers J. 1998. Neuromodulatory inputs maintain expression of a lobster motor pattern- generating network in a modulation-dependent state: evidence from long-term decentralization in vitro. *The Journal of Neuroscience* 18:2212–2225.

Timme M. 2007. Revealing network connectivity from response dynamics. *Physical Review Letters* 98:224101.

Tobin AE, Cruz-Bermúdez ND, Marder E, Schulz DJ. 2009. Correlations in ion channel mrna in rhythmically active neurons. *PLOS ONE* 4:e6742.

Turrigiano GG, Marder E. 1993. Modulation of identified stomatogastric ganglion neurons in primary cell culture. *Journal of Neurophysiology* 69:1993–2002.

Turrigiano G, Abbott LF, Marder E. 1994. Activity-dependent changes in the intrinsic properties of cultured neurons. *Science (New York, N.Y.)* 264:974–977.

Turrigiano G, LeMasson G, Marder E. 1995. Selective regulation of current densities underlies spontaneous changes in the activity of cultured neurons. *The Journal of Neuroscience* 15:3640–3652.

Van der Maaten L, Hinton G. 2008. Visualizing data using t-sne. *Journal of Machine Learning Research* 9:11.

van Rossum MC. 2001. A novel spike distance. *Neural Computation* 13:751–763.

van Vreeswijk C, Sompolinsky H. 1996. Chaos in neuronal networks with balanced excitatory and inhibitory activity. *Science (New York, N.Y.)* 274:1724–1726.

Victor JD, Purpura KP. 2009. Metric-space analysis of spike trains: theory, algorithms and application. *Network* 8:127–164.

Vyas S, Golub MD, Sussillo D, Shenoy KV. 2020. Computation through neural population dynamics. *Annual Review of Neuroscience* 43:249–275.

Wattenberg M, Viégas F, Johnson I. 2016. How to use t-sne effectively. *Distill* 1:0002.

Williams AH, Kim TH, Wang F, Vyas S, Ryu SI, Shenoy KV, Schnitzer M, Kolda TG, Ganguli S. 2018. Unsupervised discovery of demixed, low-dimensional neural dynamics across multiple timescales through tensor component analysis. *Neuron* 98:1099–1115.

Williams AH, Degleris A, Wang Y, Linderman SW. 2020. Point process models for sequence detection in high-dimensional neural spike trains. *arXiv:* 2010.04875v1

## REFERENCES


Anderson MJ (2001) Permutation tests for univariate or multivariate analysis of variance and regression. Canadian Journal of Fisheries and Aquatic Sciences 58:626-639.

Ayali A, Johnson BR, Harris-Warrick RM (1998) Dopamine modulates graded and spike-evoked synaptic inhibition independently at single synapses in pyloric network of lobster. J Neurophysiol 79:2063-2069.

Bargmann CI (2012) Beyond the connectome: how neuromodulators shape neural circuits. Bioessays 34:458-465.

Barker DL, Kushner PD, Hooper NK (1979) Synthesis of dopamine and octopamine in the crustacean stomatogastric nervous system. Brain Res 161:99-113.

Beliez L, Barriere G, Bertrand SS, Cazalets JR (2014) Multiple monoaminergic modulation of posturo-locomotor network activity in the newborn rat spinal cord. Front Neural Circuits 8:99.

Beltz B, Eisen JS, Flamm R, Harris-Warrick RM, Hooper SL, Marder E (1984) Serotonergic innervation and modulation of the stomatogastric ganglion of three decapod crustaceans (Panulirus interruptus, Homarus americanus and Cancer irroratus). J Exp Biol 109:35-54.

Blitz DM, Nusbaum MP (1997) Motor pattern selection via inhibition of parallel pathways. J Neurosci 17:4965-4975.

Blitz DM, Nusbaum MP (1999) Distinct functions for cotransmitters mediating motor pattern selection. J Neurosci 19:6774-6783.

Blitz DM, Christie AE, Coleman MJ, Norris BJ, Marder E, Nusbaum MP (1999) Different proctolin neurons elicit distinct motor patterns from a multifunctional neuronal network. J Neurosci 19:5449-5463.

Brewer JC, Olson AC, Collins KM, Koelle MR (2019) Serotonin and neuropeptides are both released by the HSN command neuron to initiate Caenorhabditis elegans egg laying. PLoS Genet 15:e1007896.

Brezina V (2010) Beyond the wiring diagram: signalling through complex neuromodulator networks. Philos Trans R Soc Lond B Biol Sci 365:2363-2374.

Brezina V, Orekhova IV, Weiss KR (2003) Neuromuscular modulation in Aplysia. I. Dynamic model. J Neurophysiol 90:2592-2612.

Brown RE, Basheer R, McKenna JT, Strecker RE, McCarley RW (2012) Control of sleep and wakefulness. Physiol Rev 92:1087-1187.

Bucher D, Prinz AA, Marder E (2005) Animal-to-animal variability in motor pattern production in adults and during growth. J Neurosci 25:1611-1619.

Carandini M (2012) From circuits to behavior: a bridge too far? Nat Neurosci 15:507-509.

Chen R, Ouyang C, Xiao M, Li L (2014) In situ identification and mapping of neuropeptides from the stomatogastric nervous system of Cancer borealis. Rapid Commun Mass Spectrom 28:2437-2444.

Christie AE, Skiebe P, Marder E (1995) Matrix of neuromodulators in neurosecretory structures of the crab Cancer borealis. J Exp Biol 198:2431-2439.

Christie AE, Stemmler EA, Dickinson PS (2010) Crustacean neuropeptides. Cell Mol Life Sci 67:4135-4169.

Cinar R, Freund TF, Katona I, Mackie K, Szucs M (2008) Reciprocal inhibition of G-protein signaling is induced by CB(1) cannabinoid and GABA(B) receptor interactions in rat hippocampal membranes. Neurochem Int 52:1402-1409.

Clark MC, Khan R, Baro DJ (2008) Crustacean dopamine receptors: localization and G protein coupling in the stomatogastric ganglion. J Neurochem 104:1006-1019.

Clark MC, Dever TE, Dever JJ, Xu P, Rehder V, Sosa MA, Baro DJ (2004) Arthropod 5-HT2 receptors: a neurohormonal receptor in decapod crustaceans that displays agonist independent activity resulting from an evolutionary alteration to the DRY motif. J Neurosci 24:3421-3435.

Cole SH, Carney GE, McClung CA, Willard SS, Taylor BJ, Hirsh J (2005) Two functional but noncomplementing Drosophila tyrosine decarboxylase genes: distinct roles for neural tyramine and octopamine in female fertility. J Biol Chem 280:14948-14955.

Conio B, Martino M, Magioncalda P, Escelsior A, Inglese M, Amore M, Northoff G (2020) Opposite effects of dopamine and serotonin on resting-state networks: review and implications for psychiatric disorders. Mol Psychiatry 25:82-93.

Daur N, Nadim F, Bucher D (2016) The complexity of small circuits: the stomatogastric nervous system. Curr Opin Neurobiol 41:1-7.

Daur N, Nadim F, Bucher D (2021) Synaptic Dynamics Convey Differential Sensitivity to Input Pattern Changes in Two Muscles Innervated by the Same Motor Neurons. eNeuro 8.

Di Pietro NC, Seamans JK (2011) Dopamine and serotonin interactively modulate prefrontal cortex neurons in vitro. Biol Psychiatry 69:1204-1211.

Dickinson PS (2006) Neuromodulation of central pattern generators in invertebrates and vertebrates. Curr Opin Neurobiol 16:604-614.

Dickinson PS, Fairfield WP, Hetling JR, Hauptman J (1997) Neurotransmitter interactions in the stomatogastric system of the spiny lobster: one peptide alters the response of a central pattern generator to a second peptide. J Neurophysiol 77:599-610.

Dickinson PS, Hauptman J, Hetling J, Mahadevan A (2001) RPCH Modulation of a Multi-Oscillator Network: Effects on the Pyloric Network of the Spiny Lobster. Journal of Neurophysiology 85:1424-1435.

Djokaj S, Cooper RL, Rathmayer W (2001) Presynaptic effects of octopamine, serotonin, and cocktails of the two modulators on neuromuscular transmission in crustaceans. J Comp Physiol A 187:145-154.

Doi A, Ramirez JM (2008) Neuromodulation and the orchestration of the respiratory rhythm. Respir Physiol Neurobiol 164:96-104.

Doyon WM, Dong Y, Ostroumov A, Thomas AM, Zhang TA, Dani JA (2013) Nicotine decreases ethanol-induced dopamine signaling and increases self-administration via stress hormones. Neuron 79:530-540.

Eriksson A, Raczkowska M, Navawongse R, Choudhury D, Stewart JC, Tang YL, Wang Z, Claridge-Chang A (2017) Neuromodulatory circuit effects on Drosophila feeding behaviour and metabolism. Sci Rep 7:8839.

Evans PD, Maqueira B (2005) Insect octopamine receptors: a new classification scheme based on studies of cloned Drosophila G-protein coupled receptors. Invert Neurosci 5:111-118.

Falk T, Kilani RK, Strazdas LA, Borders RS, Steidl JV, Yool AJ, Sherman SJ (2003) Developmental regulation of the A-type potassium-channel current in hippocampal neurons: role of the Kvbeta 1.1 subunit. Neuroscience 120:387-404.

Farooqui T (2012) Review of octopmaine in insect nervous systems. Open Access Insect Physiology 4:1-17.

Feldman JL, Kam K (2015) Facing the challenge of mammalian neural microcircuits: taking a few breaths may help. The Journal of Physiology 593:3-23.

Flamm RE, Harris-Warrick RM (1986a) Aminergic modulation in lobster stomatogastric ganglion. II. Target neurons of dopamine, octopamine, and serotonin within the pyloric circuit. J Neurophysiol 55:866-881.

Flamm RE, Harris-Warrick RM (1986b) Aminergic modulation in lobster stomatogastric ganglion. I. Effects on motor pattern and activity of neurons within the pyloric circuit. J Neurophysiol 55:847-865.

Franklin CC, Ball JM, Schulz DJ, Nair SS (2010) Generation and preservation of the slow underlying membrane potential oscillation in model bursting neurons. J Neurophysiol 104:1589-1602.

Fuxe K, Dahlstrom AB, Jonsson G, Marcellino D, Guescini M, Dam M, Manger P, Agnati L (2010) The discovery of central monoamine neurons gave volume transmission to the wired brain. Prog Neurobiol 90:82-100.

Gabriel JP, Mahmood R, Kyriakatos A, Soll I, Hauptmann G, Calabrese RL, El Manira A (2009) Serotonergic modulation of locomotion in zebrafish: endogenous release and synaptic mechanisms. J Neurosci 29:10387-10395.

Gao P, Ganguli S (2015) On simplicity and complexity in the brave new world of large-scale neuroscience. Curr Opin Neurobiol 32:148-155.

Garcia VJ, Daur N, Temporal S, Schulz DJ, Bucher D (2015) Neuropeptide receptor transcript expression levels and magnitude of ionic current responses show cell type-specific differences in a small motor circuit. J Neurosci 35:6786-6800.

Goaillard JM, Schulz DJ, Kilman VL, Marder E (2004) Octopamine modulates the axons of modulatory projection neurons. J Neurosci 24:7063-7073.

Goaillard JM, Taylor AL, Schulz DJ, Marder E (2009) Functional consequences of animal-to-animal variation in circuit parameters. Nat Neurosci 12:1424-1430.

Golowasch J, Marder E (1992a) Ionic currents of the lateral pyloric neuron of the stomatogastric ganglion of the crab. J Neurophysiol 67:318-331.

Golowasch J, Marder E (1992b) Proctolin activates an inward current whose voltage dependence is modified by extracellular Ca2+. J Neurosci 12:810-817.

Grace AA, Floresco SB, Goto Y, Lodge DJ (2007) Regulation of firing of dopaminergic neurons and control of goal-directed behaviors. Trends Neurosci 30:220-227.

Griffith LC (2013) Neuromodulatory control of sleep in Drosophila melanogaster: integration of competing and complementary behaviors. Curr Opin Neurobiol 23:819-823.

Guertin PA (2012) Central pattern generator for locomotion: anatomical, physiological, and pathophysiological considerations. Front Neurol 3:183.

Ha GE, Cheong E (2017) Spike Frequency Adaptation in Neurons of the Central Nervous System. Exp Neurobiol 26:179-185.

Haddad SA, Marder E (2018) Circuit Robustness to Temperature Perturbation Is Altered by Neuromodulators. Neuron 100:609-623 e603.

Hamood AW, Haddad SA, Otopalik AG, Rosenbaum P, Marder E (2015) Quantitative Reevaluation of the Effects of Short- and Long-Term Removal of Descending Modulatory Inputs on the Pyloric Rhythm of the Crab, Cancer Borealis. eNeuro 2.

Harris-Warrick RM (2011) Neuromodulation and flexibility in Central Pattern Generator networks. Curr Opin Neurobiol 21:685-692.

Harris-Warrick RM, Johnson BR (2010) Checks and balances in neuromodulation. Front Behav Neurosci 4.

Harris-Warrick RM, Coniglio LM, Barazangi N, Guckenheimer J, Gueron S (1995a) Dopamine modulation of transient potassium current evokes phase shifts in a central pattern generator network. J Neurosci 15:342-358.

Harris-Warrick RM, Coniglio LM, Levini RM, Gueron S, Guckenheimer J (1995b) Dopamine modulation of two subthreshold currents produces phase shifts in activity of an identified motoneuron. J Neurophysiol 74:1404-1420.

Hooper SL, DiCaprio RA (2004) Crustacean motor pattern generator networks. Neurosignals 13:50-69.

Jing J, Vilim FS, Horn CC, Alexeeva V, Hatcher NG, Sasaki K, Yashina I, Zhurov Y, Kupfermann I, Sweedler JV, Weiss KR (2007) From hunger to satiety: reconfiguration of a feeding network by Aplysia neuropeptide Y. J Neurosci 27:3490-3502.

Johnson BR, Harris-Warrick RM (1997) Amine modulation of glutamate responses from pyloric motor neurons in lobster stomatogastric ganglion. J Neurophysiol 78:3210-3221.

Johnson BR, Peck JH, Harris-Warrick RM (1995) Distributed amine modulation of graded chemical transmission in the pyloric network of the lobster stomatogastric ganglion. J Neurophysiol 74:437-452.

Johnson BR, Kloppenburg P, Harris-Warrick RM (2003) Dopamine modulation of calcium currents in pyloric neurons of the lobster stomatogastric ganglion. J Neurophysiol 90:631-643.

Johnson BR, Brown JM, Kvarta MD, Lu JY, Schneider LR, Nadim F, Harris-Warrick RM (2011) Differential modulation of synaptic strength and timing regulate synaptic efficacy in a motor network. J Neurophysiol 105:293-304.

Katz PS (1995) Neuromodulation and Motor Pattern Generation in the Crustacean Stomatogastric Nervous System. In: Neural Control of Movement (Ferrell WR, Proske U, eds), pp 277-283. Boston, MA: Springer US.

Katz PS (2016) Evolution of central pattern generators and rhythmic behaviours. Philos Trans R Soc Lond B Biol Sci 371:20150057.

Katz PS, Frost WN (1996) Intrinsic neuromodulation: altering neuronal circuits from within. Trends Neurosci 19:54-61.

Katz PS, Calin-Jageman RJ (2009) Neuromodulation. In: Encyclopedia of Neuroscience, pp 497-503: Elsevier.

Katz PS, Eigg MH, Harris-Warrick RM (1989) Serotonergic/cholinergic muscle receptor cells in the crab stomatogastric nervous system. I. Identification and characterization of the gastropyloric receptor cells. J Neurophysiol 62:558-570.

Khorkova O, Golowasch J (2007) Neuromodulators, not activity, control coordinated expression of ionic currents. J Neurosci 27:8709-8718.

Kirby MS, Nusbaum MP (2007) Peptide hormone modulation of a neuronally modulated motor circuit. J Neurophysiol 98:3206-3220.

Kitano H (2004) Biological robustness. Nat Rev Genet 5:826-837.

Kloppenburg P, Levini RM, Harris-Warrick RM (1999) Dopamine modulates two potassium currents and inhibits the intrinsic firing properties of an identified motor neuron in a central pattern generator network. J Neurophysiol 81:29-38.

Lane BJ, Kick DR, Wilson DK, Nair SS, Schulz DJ (2018) Dopamine maintains network synchrony via direct modulation of gap junctions in the crustacean cardiac ganglion. Elife 7.

Li X, Bucher D, Nadim F (2018) Distinct Co-Modulation Rules of Synapses and Voltage-Gated Currents Coordinate Interactions of Multiple Neuromodulators. J Neurosci 38:8549-8562.

Lopez HS, Brown AM (1992) Neuromodulation. Curr Opin Neurobiol 2:317-322.

Lupica CR, Bell JA, Hoffman AF, Watson PL (2001) Contribution of the hyperpolarization-activated current (I(h)) to membrane potential and GABA release in hippocampal interneurons. J Neurophysiol 86:261-268.

Luther JA, Robie AA, Yarotsky J, Reina C, Marder E, Golowasch J (2003) Episodic bouts of activity accompany recovery of rhythmic output by a neuromodulator- and activity-deprived adult neural network. J Neurophysiol 90:2720-2730.

Ma M, Wang J, Chen R, Li L (2009) Expanding the Crustacean Neuropeptidome Using a Multifaceted Mass Spectrometric Approach. Journal of Proteome Research 8:2426-2437.

MacKay-Lyons M (2002) Central pattern generation of locomotion: a review of the evidence. Phys Ther 82:69-83.

Malcangio M, Bowery NG (1999) Peptide autoreceptors: does an autoreceptor for substance P exist? Trends Pharmacol Sci 20:405-407.

Marder E (2012) Neuromodulation of neuronal circuits: back to the future. Neuron 76:1-11.

Marder E, Weimann JM (1992) Modulatory control of multiple task processing in the stomatogastric nervous system. In: Neurobiology of Motor Programme Selection: New Approaches to the Study of Behavioural Choice (Kien J, McCrohan CR, Winlow W, eds), pp 3-19: Pergamon Press.

Marder E, Bucher D (2001) Central pattern generators and the control of rhythmic movements. Curr Biol 11:R986-996.

Marder E, Thirumalai V (2002) Cellular, synaptic and network effects of neuromodulation. Neural Netw 15:479-493.

Marder E, Bucher D (2007) Understanding circuit dynamics using the stomatogastric nervous system of lobsters and crabs. Annu Rev Physiol 69:291-316.

Martinez D, Santin JM, Schulz D, Nadim F (2019) The differential contribution of pacemaker neurons to synaptic transmission in the pyloric network of the Jonah crab, Cancer borealis. J Neurophysiol 122:1623-1633.

Matsumoto M, Togashi H, Mori K, Ueno K, Miyamoto A, Yoshioka M (1999) Characterization of endogenous serotonin-mediated regulation of dopamine release in the rat prefrontal cortex. Eur J Pharmacol 383:39-48.

McCormick DA, Nusbaum MP (2014) Editorial overview: neuromodulation: tuning the properties of neurons, networks and behavior. Curr Opin Neurobiol 29:iv-vii.

Miles GB, Sillar KT (2011) Neuromodulation of vertebrate locomotor control networks. Physiology (Bethesda) 26:393-411.

Nadim F, Bucher D (2014) Neuromodulation of neurons and synapses. Curr Opin Neurobiol 29:48-56.

Nichols TE, Holmes AP (2002) Nonparametric permutation tests for functional neuroimaging: a primer with examples. Hum Brain Mapp 15:1-25.

Noudoost B, Moore T (2011) The role of neuromodulators in selective attention. Trends Cogn Sci 15:585-591.

Nusbaum MP (2002) Regulating peptidergic modulation of rhythmically active neural circuits. Brain Behav Evol 60:378-387.

Nusbaum MP, Marder E (1988) A Neuronal Role For a Crustacean Red Pigment Concentrating Hormone-Like Peptide: Neuromodulation of the Pyloric Rhythm in the Crab, Cancer Borealis. Journal of Experimental Biology 135:165-181.

Nusbaum MP, Marder E (1989) A modulatory proctolin-containing neuron (MPN). II. State-dependent modulation of rhythmic motor activity. J Neurosci 9:1600-1607.

Nusbaum MP, Beenhakker MP (2002) A small-systems approach to motor pattern generation. Nature 417:343-350.

Nusbaum MP, Blitz DM, Swensen AM, Wood D, Marder E (2001) The roles of co-transmission in neural network modulation. Trends Neurosci 24:146-154.

Oginsky MF, Rodgers EW, Clark MC, Simmons R, Krenz WD, Baro DJ (2010) D(2) receptors receive paracrine neurotransmission and are consistently targeted to a subset of synaptic structures in an identified neuron of the crustacean stomatogastric nervous system. J Comp Neurol 518:255-276.

Ormerod KG, Hadden JK, Deady LD, Mercier AJ, Krans JL (2013) Action of octopamine and tyramine on muscles of Drosophila melanogaster larvae. J Neurophysiol 110:1984-1996.

Peck JH, Nakanishi ST, Yaple R, Harris-Warrick RM (2001) Amine modulation of the transient potassium current in identified cells of the lobster stomatogastric ganglion. J Neurophysiol 86:2957-2965.

Peck JH, Gaier E, Stevens E, Repicky S, Harris-Warrick RM (2006) Amine modulation of Ih in a small neural network. J Neurophysiol 96:2931-2940.

Pena F, Ramirez JM (2002) Endogenous activation of serotonin-2A receptors is required for respiratory rhythm generation in vitro. J Neurosci 22:11055-11064.

Pena F, Ramirez JM (2004) Substance P-mediated modulation of pacemaker properties in the mammalian respiratory network. J Neurosci 24:7549-7556.

Perez DM (2006) The adrenergic receptors : in the 21st century. Totowa, N.J.: Humana Press.

Ramirez JM, Doi A, Garcia AJ, 3rd, Elsen FP, Koch H, Wei AD (2012) The cellular building blocks of breathing. Compr Physiol 2:2683-2731.

Roberts CD, Dvoryanchikov G, Roper SD, Chaudhari N (2009) Interaction between the second messengers cAMP and Ca2+ in mouse presynaptic taste cells. J Physiol 587:1657-1668.

Rodgers EW, Fu JJ, Krenz WD, Baro DJ (2011) Tonic nanomolar dopamine enables an activity-dependent phase recovery mechanism that persistently alters the maximal conductance of the hyperpolarization-activated current in a rhythmically active neuron. J Neurosci 31:16387-16397.

Roeder T (1999) Octopamine in invertebrates. Prog Neurobiol 59:533-561.

Rosenbaum P, Marder E (2018) Graded Transmission without Action Potentials Sustains Rhythmic Activity in Some But Not All Modulators That Activate the Same Current. J Neurosci 38:8976-8988.

Sabandal JM, Sabandal PR, Kim YC, Han KA (2020) Concerted Actions of Octopamine and Dopamine Receptors Drive Olfactory Learning. J Neurosci 40:4240-4250.

Salio C, Lossi L, Ferrini F, Merighi A (2006) Neuropeptides as synaptic transmitters. Cell Tissue Res 326:583-598.

Sawin ER, Ranganathan R, Horvitz HR (2000) C. elegans locomotory rate is modulated by the environment through a dopaminergic pathway and by experience through a serotonergic pathway. Neuron 26:619-631.

Selcho M, Pauls D, El Jundi B, Stocker RF, Thum AS (2012) The role of octopamine and tyramine in Drosophila larval locomotion. J Comp Neurol 520:3764-3785.

Selverston A (2017) The Stomatogastric Ganglion. In: Reference Module in Neuroscience and Biobehavioral Psychology: Elsevier.

Selverston AI, Russell DF, Miller JP (1976) The stomatogastric nervous system: structure and function of a small neural network. Prog Neurobiol 7:215-290.

Slawinska U, Miazga K, Jordan LM (2014) The role of serotonin in the control of locomotor movements and strategies for restoring locomotion after spinal cord injury. Acta Neurobiol Exp (Wars) 74:172-187.

Spitzer N, Cymbalyuk G, Zhang H, Edwards DH, Baro DJ (2008) Serotonin transduction cascades mediate variable changes in pyloric network cycle frequency in response to the same modulatory challenge. J Neurophysiol 99:2844-2863.

Stein RB, Gossen ER, Jones KE (2005) Neuronal variability: noise or part of the signal? Nat Rev Neurosci 6:389-397.

Stein W (2009) Modulation of stomatogastric rhythms. J Comp Physiol A Neuroethol Sens Neural Behav Physiol 195:989-1009.

Svensson E, Grillner S, Parker D (2001) Gating and braking of short- and long-term modulatory effects by interactions between colocalized neuromodulators. J Neurosci 21:5984-5992.

Svensson E, Apergis-Schoute J, Burnstock G, Nusbaum MP, Parker D, Schiöth HB (2019) General Principles of Neuronal Co-transmission: Insights From Multiple Model Systems. Frontiers in Neural Circuits 12.

Swensen AM, Marder E (2000) Multiple peptides converge to activate the same voltage-dependent current in a central pattern-generating circuit. J Neurosci 20:6752-6759.

Swensen AM, Marder E (2001) Modulators with convergent cellular actions elicit distinct circuit outputs. J Neurosci 21:4050-4058.

Temporal S, Desai M, Khorkova O, Varghese G, Dai A, Schulz DJ, Golowasch J (2012) Neuromodulation independently determines correlated channel expression and conductance levels in motor neurons of the stomatogastric ganglion. J Neurophysiol 107:718-727.

Thirumalai V, Marder E (2002) Colocalized neuropeptides activate a central pattern generator by acting on different circuit targets. J Neurosci 22:1874-1882.

Vaaga CE, Borisovska M, Westbrook GL (2014) Dual-transmitter neurons: functional implications of co-release and co-transmission. Curr Opin Neurobiol 29:25-32.

Viemari JC, Ramirez JM (2006) Norepinephrine differentially modulates different types of respiratory pacemaker and nonpacemaker neurons. J Neurophysiol 95:2070-2082.

Viemari JC, Tryba AK (2009) Bioaminergic neuromodulation of respiratory rhythm in vitro. Respir Physiol Neurobiol 168:69-75.

Wang SJ, Cheng LL, Gean PW (1999) Cross-modulation of synaptic plasticity by beta-adrenergic and 5-HT1A receptors in the rat basolateral amygdala. J Neurosci 19:570-577.

Weimann JM, Meyrand P, Marder E (1991) Neurons that form multiple pattern generators: identification and multiple activity patterns of gastric/pyloric neurons in the crab stomatogastric system. J Neurophysiol 65:111-122.

Weimann JM, Marder E, Evans B, Calabrese RL (1993) The effects of SDRNFLRFamide and TNRNFLRFamide on the motor patterns of the stomatogastric ganglion of the crab Cancer borealis. J Exp Biol 181:1-26.

Weimann JM, Skiebe P, Heinzel HG, Soto C, Kopell N, Jorge-Rivera JC, Marder E (1997) Modulation of oscillator interactions in the crab stomatogastric ganglion by crustacean cardioactive peptide. J Neurosci 17:1748-1760.

Werner G, Mitterauer BJ (2013) Neuromodulatory systems. Front Neural Circuits 7:36.

Wood DE, Nusbaum MP (2002) Extracellular peptidase activity tunes motor pattern modulation. J Neurosci 22:4185-4195.

Zakharov D, Lapish C, Gutkin B, Kuznetsov A (2016) Synergy of AMPA and NMDA Receptor Currents in Dopaminergic Neurons: A Modeling Study. Front Comput Neurosci 10:48.

Zhang B, Harris-Warrick RM (1994) Multiple receptors mediate the modulatory effects of serotonergic neurons in a small neural network. J Exp Biol 190:55-77.

Zhang H, Rodgers EW, Krenz WD, Clark MC, Baro DJ (2010) Cell specific dopamine modulation of the transient potassium current in the pyloric network by the canonical D1 receptor signal transduction cascade. J Neurophysiol 104:873-884.

Zhao S, Golowasch J, Nadim F (2010) Pacemaker neuron and network oscillations depend on a neuromodulator-regulated linear current. Front Behav Neurosci 4:21.

Zhao S, Sheibanie AF, Oh M, Rabbah P, Nadim F (2011) Peptide neuromodulation of synaptic dynamics in an oscillatory network. J Neurosci 31:13991-14004.